Quark-gluon plasma in strong magnetic fields

Dissertation

zur Erlangung des Doktorgrades

des Fachsbereichs Physik

der Universität Hamburg

vorgelegt von

Tigran Kalaydzhyan

aus Jerewan

Hamburg

2013

Gutachter der Dissertation:	Prof. Dr. Volker Schomerus Dr. Ingo Kirsch
	Prof. Dr. Gerrit Schierholz
Gutachter der Disputation:	Prof. Dr. Jan Louis Dr. Ingo Kirsch
Datum der Disputation:	10. April 2013
Vorsitzender des Prüfungsausschusses:	Prof. Dr. Bernd Kniehl
Vorsitzender des Promotionsausschusses:	Prof. Dr. Peter Hauschildt
Dekan der Fakultät für Mathematik, Informatik und Naturwissenschaften:	Prof. Dr. Heinrich Graener

Abstract

One of the fundamental problems in subatomic physics is the determination of properties of matter at extreme temperatures, densities and electromagnetic fields. The modern ultrarelativistic heavy-ion experiments are able to study such states (the quark-gluon plasma) and indicate that the physics at extreme conditions differs drastically from what is known from the conventional observations. Also the theoretical methods developed mostly within the perturbative framework face various conceptual problems and need to be replaced by a nonperturbative approach. In this thesis we study the physics of the strongly-coupled quark-gluon plasma in external magnetic fields as well as general electromagnetic and topological properties of the QCD and QCD-like systems. We develop and apply various nonperturbative techniques, based on e.g. gauge-gravity correspondence, lattice QCD simulations, relativistic hydrodynamics and condensed-matter-inspired models. The thesis is mainly based on our papers [1–15], with corrections and additional comments.

Zusammenfassung

Eines der fundamentalen Probleme subatomarer Physik ist die Bestimmung der Eigenschaften von Materie bei extremen Temperaturen, Dichten und elektromagnetischen Feldern. Moderne Experimente mit ultrarelativistischen Schwerionen sind in der Lage Zustände, wie das Quark-Gluon Plasma, unter diesen Verhältnissen zu untersuchen und zeigen, dass sich die Physik unter solch extremen Bedingungen drastisch vom Verhalten unter gewöhnlichen Bedingungen unterscheidet. Weiterhin sind theoretische Modelle, die auf Störungstheorie basieren, unter solchen Umständen nicht anwendbar und müssen durch nichtperturbative Methoden ersetzt werden. In dieser Arbeit untersuchen wir daher die Physik des stark gekoppelten Quark-Gluon Plasmas in externen magnetischen Feldern sowie elektromagnetische und topologische Eigenschaften von QCD und QCD-ähnlichen Systemen. Hierzu entwickeln und verwenden wir verschiedene nichtperturbative Methoden, die unter anderem auf der Gauge-Gravity-Korrespondenz, Gitter-QCD Simulationen, relativistischer Hydrodynamik und Festkörper-inspirierten Modellen basieren. Diese Arbeit basiert auf unseren Veröffentlichungen [1–15] und enthält Korrekturen sowie zusätzliche Kommentare.

Contents

1 Introduction and overview **7**

2 Gauge-gravity duality **13**

3 Non-equilibrium physics at a holographic chiral phase transition **18**
3.1 Holographic Descriptions . . . 21
3.1.1 Chiral symmetry transition . . . 21
3.1.2 A boost-invariant expanding plasma . . . 23
3.2 Out of equilibrium description of the chiral phase transition . . . 25
3.2.1 D7 flavour brane action . . . 26
3.2.2 Naive equilibrium based approximation . . . 27
3.2.3 Adiabatic dynamic D7 brane embeddings . . . 28
3.2.4 Full PDE solutions . . . 30
3.3 Dependence of the condensate on B . . . 34
3.4 Discussion . . . 36

4 Holographic dual of a boost-invariant plasma with chemical potential **38**
4.1 Late-time background in Eddington-Finkelstein coordinates . . . 39
4.1.1 Boosted black brane solution . . . 39
4.1.2 Zeroth-order solution and first-order correction . . . 40
4.1.3 Transport coefficients from the background . . . 42
4.2 Late-time solution in Fefferman-Graham coordinates . . . 44
4.2.1 General ansatz and near-boundary behaviour . . . 44
4.2.2 Late-time ansatz for the background . . . 45
4.2.3 Zeroth-order solution . . . 47
4.2.4 Fefferman-Graham vs. Eddington-Finkelstein coordinates . . . 51
4.3 Conclusions . . . 52

5 Fluid-gravity model for the chiral magnetic effect **55**
5.1 CME and CVE in hydrodynamics . . . 56
5.2 Fluid-gravity model for the CME . . . 58

6 Anisotropic hydrodynamics, holography and the chiral magnetic effect **64**
6.1 Hydrodynamics of anisotropic fluids with triangle anomalies . . . 65
6.1.1 Thermodynamics of an anisotropic fluid with chemical potential ($n = 1$) . . . 66
6.1.2 Vortical and magnetic coefficients ($n = 1$) . . . 67
6.1.3 Multiple charge case n arbitrary) . . . 68
6.1.4 Chiral magnetic and vortical effect ($n = 2$) . . . 69
6.2 Fluid-gravity model . . . 71
6.2.1 AdS black hole with multiple U(1) charges . . . 71

6.2.2 Anisotropic AdS geometry with multiple U(1) charges . . . 72
6.3 Holographic vortical and magnetic conductivities . . . 75
6.3.1 First-order corrected background . . . 75
6.3.2 Holographic conductivities . . . 76
6.3.3 Subtleties in holographic descriptions of the CME . . . 78
6.4 Conclusions . . . 78

7 Quantum Chromodynamics on a Lattice 84
7.1 Improved action . . . 84
7.2 Monte-Carlo algorithms . . . 88
7.3 Overlap fermions . . . 92

8 SU(3) quenched lattice gauge theory in magnetic fields 94
8.1 Technical details . . . 94
8.2 Chiral condensate . . . 95
8.3 Chiral magnetization and susceptibility . . . 96
8.4 Electric dipole moment . . . 98
8.5 Some evidences of the chiral magnetic effect . . . 98

9 Magnetic-Field-Induced insulator-conductor transition 100

10 Fractal dimension of the topological charge distribution 105
10.1 Technical details . . . 106
10.1.1 Ordinary IPR for zero modes. . . . 107
10.1.2 Chiral IPR for low-lying modes. First definition. . . . 107
10.1.3 Chiral IPR for zero modes. Second definition. . . . 108
10.1.4 Fractal dimension. Results and conclusions. . . . 108

11 Chiral superfluidity of the quark-gluon plasma 111
11.1 Derivation of the effective Lagrangian . . . 113
11.1.1 The functional integral . . . 113
11.1.2 Vector currents conservation . . . 114
11.1.3 Anomaly for the axial current . . . 114
11.1.4 Axionic Lagrangian . . . 116
11.1.5 Interpretation of Λ . . . 117
11.1.6 Fermionic spectrum and chirality . . . 119
11.2 Quark-gluon plasma as a two-component fluid . . . 120
11.2.1 Hydrodynamic equations . . . 121
11.2.2 Phenomenological output, possible tests of the model . . . 123
11.2.3 Change in entropy and higher order gradient corrections . . . 123
11.2.4 Preliminary estimates for the CME . . . 125
11.3 Conclusion . . . 127

12 On chromoelectric superconductivity of the Yang-Mills vacuum 128

13 Conclusions and Outlook 133

Chapter 1

Introduction and overview

The modern nuclear experiments at the Relativistic Heavy Ion Collider (RHIC, BNL) and the Large Hadron Collider (LHC, CERN) provide us with the possibility to explore new high-energy forms of matter, such as the so-called quark-gluon plasma (QGP), which can be produced in ultrarelativistic heavy-ion collisions and consists of interacting quarks and gluons out of nucleons and mesons [16–18]. Each of the collision events begins from an intense heating in the volume occupied by the overlap of the nuclei, as a large fraction of their kinetic energy is converted into a high-temperature system of quarks, antiquarks and gluons. The time between the first contact of the nuclei and the formation of QGP is called τ_f, the formation time. The temperature of QGP is estimated to be more extreme as any of the known examples in the present universe and exceeds the critical temperature $T_c \sim 170\,\mathrm{MeV}$ of the deconfinement transition. In Ref. [19] assuming the formation time $\tau_f = 0.2\,\mathrm{fm}/c$ the initial temperatures are estimated to be $T_0 \sim 330\,\mathrm{MeV}$ for $\sqrt{s} = 200\,\mathrm{GeV}$ per nucleon pair central Au-Au collisions at RHIC $T_0 \sim 610\,\mathrm{MeV}$ for $\sqrt{s} = 2.76\,\mathrm{TeV}$ central Pb-Pb collisions at LHC[1]. Suppression of $\Upsilon(1S)$ mesons in $\sqrt{s} = 2.76\,\mathrm{TeV}$ Pb-Pb collisions [21,22] according to the quarkonia thermometry [23] leads to the conclusion that the temperatures $T > 2\,T_c$ have been indeed reached at LHC.

At the next stage, the system, presumably a liquid of quarks and gluons, immediately expands and cools down, passing through the critical temperature T_c at which QGP condenses into a gas of hadrons. As expansion continues, the system reaches the "freeze-out" density, at which the hadrons no longer interact with each other and stream into detectors. Typical time and temperature scales for the RHIC and LHC collisions are shown in Table 1.0.1.

An important property extensively used in many of the phenomenological models of QGP (including our ones) is that the matter content of QGP interacts collectively and forms hydrodynamic flows. This idea goes back to the works of Landau [24] and Bjorken [25] and can be studied experimentally by the analysis of the particle distribution in the transverse (to beam) plane,

$$E\frac{\mathrm{d}N}{\mathrm{d}^3p} = \frac{1}{2\pi}\frac{\mathrm{d}^2N}{p_T\,\mathrm{d}p_T\mathrm{d}y}\left(1 + 2\sum_{n=1}^{\infty} v_n \cos[n(\varphi - \Psi_{\mathrm{RP}})]\right), \tag{1.0.1}$$

where E is the energy of the particle with momentum $\vec{p}$ and transfer momentum p_T, φ is the azimuthal angle, y the rapidity and Ψ_{RP} the reaction plane angle. The coefficients v_n are the Fourier components of the distribution, characterizing the flows. In particular, v_2 is the so-called elliptic flow coefficient [26], which is caused by the difference between pressure gradients in the initial state (see Fig. 1.3 for a schematic shape and density evolution).

[1] See also Ref. [19] for the time evolution of temperature and [20] for direct photon measurements by PHENIX collaboration.

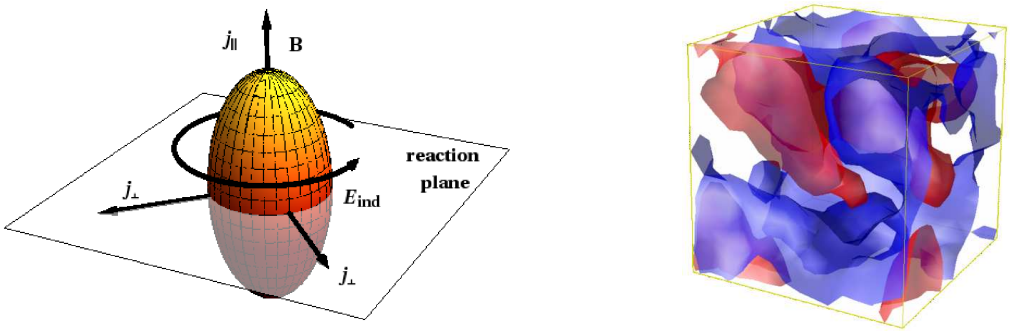

(a) (b)

Figure 1.1: (a) Geometry of the electromagnetic fields, plotted in Fig. 1.2, (b) Isosurfaces of the topological charge density (chirality) $q(x) = \pm 10^{-4}$ in QCD vacuum for a fixed time slice, corresponding to the 16^4 lattice in Chapter 10. Colors represent positive (red) and negative (blue) values, respectively. For the animation, see [27].

From a theoretical point of view, hydrodynamics corresponds to the long-wave approximation, $\lambda_H \gg l$, where λ_H is of the order of a wavelength of hydrodynamic excitations and l is a typical distance between the microscopic constituents. Hydrodynamic equations reflect the symmetries of the underlying field theory, since they are nothing but the conservation laws. In general, the fluid fluctuations are damped down on distances of order l and do not propagate further, while the only exceptional ones, which are supported by the conservation laws, will survive over a distance λ_H and larger, and contribute to the hydrodynamics. The constitutive equations are usually represented in form of a gradient expansion, i.e. in a number of derivatives of the velocity u_μ and thermodynamic quantities. In the case of approximately conserved quantities (e.g. in the case of dissipation or anomalies) one can still capture the slow variations of the quantities in the gradient expansion and use the hydrodynamic framework (see Chapter 5).

Another important issue is the presence of a strong magnetic field ($e\langle B_\parallel\rangle \equiv eB \sim m_\pi^2$), generated by the nuclei themselves in a non-central collision [28, 29]. Such a strong field may change the critical temperature of the chiral transition, several electromagnetic properties of QCD and also give rise to new phenomenological effects potentially measurable experimentally. In order to estimate the magnitude of the magnetic field, one should use the retarded Liénard-Wiechert potentials, since we deal with the ultrarelativistic kinematics. This is done in the original paper [30] and improved in [31–33]. A strong electric field E_{ind} can be "induced" by a rapidly decreasing magnetic field and calculated from the Faraday's law [34]. The spatial directions of both fields with respect to the fireball geometry are shown in Fig. 1.1(a). An estimate for the magnetic field for the impact parameter $b < 12$ fm can be extracted from Ref. [35] based on the HIJING model and is given by

$$eB = (0.3\,\mathrm{MeV})\frac{\sqrt{s}\,b}{R}\,, \tag{1.0.2}$$

temperatures	RHIC @ 200 GeV	LHC @ 2.76 TeV
$T > 2\,T_c$	–	$\tau_f < \tau < 1$
$T_c < T < 2\,T_c$	$\tau_f < \tau < 3$	$1 < \tau < 6$
$T = T_c$	$3 < \tau < 5$	$6 < \tau < 9$

Table 1.0.1: Time evolution in units fm/c for the temperatures at RHIC and LHC [19].

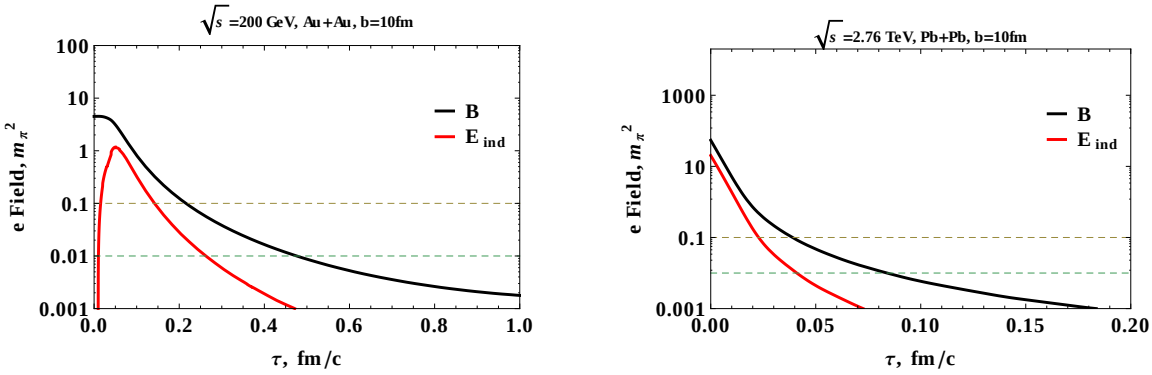

Figure 1.2: Electromagnetic fields in the fireball for RHIC (left) and LHC (right) energies and $40-50\%$ centrality. Black curves are based on the data from [35]. The moment $\tau = 0$ corresponds to the maximal overlap of the nuclei. $m_\pi^2 \sim 10^{14}$ Tesla. The QGP conductivity is not taken into account.

where $R = 1.2A^{1/3}$ fm is the radius of the nuclei. Other components of electromagnetic fields in the transverse plane are estimated to be of equal magnitude on the event-by-event basis [35, 36],

$$\langle |eB_\perp| \rangle \approx \langle |eE_\parallel| \rangle \approx \langle |eE_\perp| \rangle = \sqrt{s}\,(0.1-0.2)\,\text{MeV}\,. \tag{1.0.3}$$

The time evolution of both magnetic and concentric electric fields for the case of large centrality is shown in Fig. 1.2. Note, however, that the evolution of the magnetic field might be much slower due to a finite conductivity of the QGP [28].

One of the most prominent effects induced by the magnetic field is the so-called chiral magnetic effect (CME), which has attracted much attention in light of experimentally observed charge asymmetries in heavy-ion collisions, as seen by the STAR [37, 38], PHENIX [39] and ALICE [40] collaborations. The CME states that, in the presence of a magnetic field $\vec{B}$, an electric current is generated along $\vec{B}$ in the background of topologically nontrivial gluon fields [30, 41–43]. Analogous effects were found earlier in neutrino [44–46], electroweak [47, 48] and condensed matter physics [49, 50]. Lattice QCD results [5–7, 10, 51–54] suggest the existence of the effect, although the magnitude of the CME-induced charge asymmetry may be too small to explain the observed charge asymmetry [55].

The essential physical idea of the effect is the following. At the energy scales of the collisions, the light u and d quarks can be treated as massless chiral fermions. The magnetic moment of a chiral quark (antiquark) is always collinear to its momentum. A strong enough magnetic field forces the magnetic moment to be parallel to the direction of the field, organizing the motion of quarks along $\vec{B}$. In the equilibrium the number of left- and right-handed quarks is the same [56], so the electric currents associated with quarks compensate each other and the net current along $\vec{B}$ is zero. However, a non-trivial gluonic background $G^a_{\mu\nu}(x)$, such that

$$\int \mathrm{d}^4x\, \epsilon^{\mu\nu\alpha\beta}\, G^a_{\mu\nu}(x) G^a_{\alpha\beta}(x) \neq 0\,, \tag{1.0.4}$$

may create an imbalance between the numbers of left- and right-handed quarks, characterized by the chirality $\rho_5 = \langle \bar{q}\gamma_5 q \rangle$. A typical spatial distribution of such an imbalance is shown in Fig. 1.1(b), where the colors denote some fixed positive (red) and negative (blue) values of the chirality. This imbalance in the presence of the magnetic field creates the net current along $\vec{B}$.

In this thesis we made an attempt to explain and predict some of the properties of the strongly-coupled QGP. The text can be logically divided into three parts:

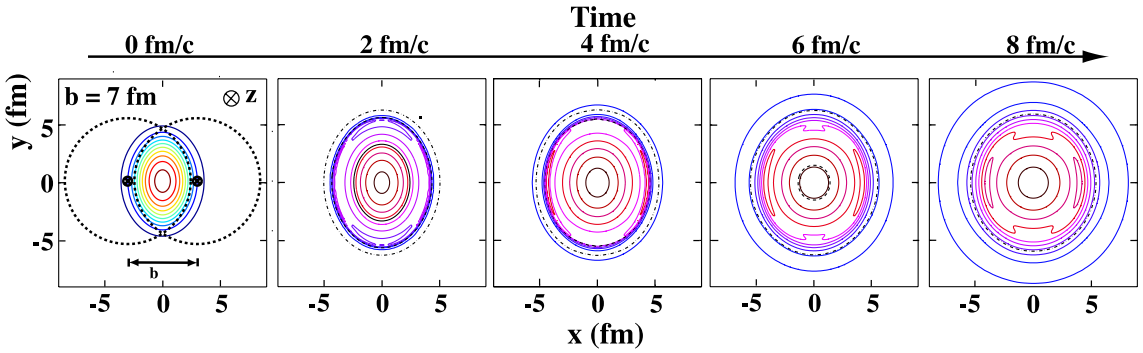

Figure 1.3: Time evolution of the fireball in a non-central collision in the transverse plane [26]. The contours denote the energy density levels.

Chapters 2 – 6 cover our studies related to the application of the gauge-gravity duality to the physics of QGP-like systems, which due to the universality of the effects (e.g. the transport properties) may take place in the real QGP. In Chapter 2 we introduce basics of the AdS/CFT-correspondence, which will be used in the main text. In Chapter 3 we study the D3/D7-brane model at finite temperature T describing a boost-invariant viscous expanding $\mathcal{N}$=2 plasma. In presence of a magnetic field B the chiral symmetry of the system is broken down and a finite chiral condensate $c(T,B)$ is formed. The value of the condensate can be read off from the profile of the probe D7-brane embeddings. The results (apart from the description of the time dynamics) are the following,

1) We observe the enhancement of the chiral symmetry breaking at $T=0$, $c(T,B)\sim B^{3/2}$.

2) The chiral condensate grows linearly at high T, $c(T,B)\sim B$.

3) The critical temperature grows with the strength of the magnetic field $T_c\sim\sqrt{B}$.

4) Viscosity changes the moment of time when the transition occurs, see the main text.

In Chapter 4 we construct a gravity dual of a boost-invariant $\mathcal{N}=4$ $SU(N)$ super Yang-Mills plasma with a chemical potential. The resulting background takes the form of a time-dependent AdS Reissner-Nordström-type black hole. We further extend this model in Chapter 5 to the case of two chemical potentials (ordinary μ and the chiral μ_5) and obtain a fluid-gravity model for certain $\mathcal{CP}$-odd transport coefficients hypothetically present in the quark gluon plasma at strong magnetic field B^μ and vorticity $\omega^\mu\equiv\frac{1}{2}\varepsilon^{\mu\nu\alpha\beta}u_\nu\partial_\alpha u_\beta$. The result is the expressions for the electric j^μ and axial j_5^μ currents in the plasma,

$$j^\mu=\rho u^\mu+\kappa_\omega\omega^\mu+\kappa_B B^\mu\,,\qquad\qquad j_5^\mu=\rho_5 u^\mu+\xi_\omega\omega^\mu+\xi_B B^\mu\,, \tag{1.0.5}$$

with coefficients

$$\kappa_\omega=2C\mu\mu_5\left(1-\frac{\mu\rho}{\epsilon+P}\right)\text{ - chiral vortical effect},\qquad \kappa_B=C\mu_5\left(1-\frac{\mu\rho}{\epsilon+P}\right)\text{ - chiral magnetic effect},$$
$$\xi_\omega=C\mu^2\left(1-2\frac{\mu_5\rho_5}{\epsilon+P}\right)\text{ - quark vortical effect},\qquad \xi_B=C\mu\left(1-\frac{\mu_5\rho_5}{\epsilon+P}\right)\text{ - chiral separation effect},$$

where u^μ is the four-velocity of the fluid (e.g. strongly-coupled plasma), ρ and ρ_5 are the densities of the electric and axial charges, respectively. $C=\frac{N_c}{2\pi^2}$ is the chiral anomaly, ϵ and P are the energy density and pressure of the plasma. For numerical estimates and time evolution of the vorticity read [57]. Finally, we study anisotropic hydrodynamics with multiple anomalous U(1) currents

(Chapter 6) and find corrections to the chiral magnetic effect due to the anisotropic expansion of QGP. We obtained the result first within the hydrodynamics and then reproduced it using our fluid-gravity model.

In **Chapters 7 – 10** we measured electromagnetic and topological properties of the QCD vacuum on the lattice. Chapter 7 covers the basics of Lattice QCD and briefly describes the methods and algorithms we used in the simulations. In Chapter 8 we study some properties of the non-Abelian vacuum induced by strong external magnetic fields, $B \gtrsim m_\pi^2$. We perform calculations in the quenched SU(3) lattice gauge theory with tadpole-improved Lüscher-Weisz action and chirally invariant lattice Dirac operator. The following results are obtained:

1) The chiral symmetry breaking is enhanced by the magnetic field. The chiral condensate is given by $\Sigma(B) = \Sigma_0 + const \cdot B^\nu$ at $T = 0$, where $\Sigma_0 = [(228 \pm 3)\,\mathrm{MeV}]^3$ and the exponent $\nu = (1.6 \pm 0.2) \approx 3/2$.

2) There is a paramagnetic polarization of the vacuum with the corresponding magnetic susceptibility $\chi = -4.2 \pm 0.2\,\mathrm{GeV}^{-2}$.

3) Magnetic field induces a local electric dipole moment of quarks $d_i(x) = \bar{\psi}(x)\sigma_{0i}\psi(x)$ along the field, which is a spin analogue of CME.

4) There are non-zero local fluctuations of the chirality $\rho_5(x)$ and electric current $J_i(x) = \bar{\psi}(x)\gamma_i\psi(x)$, both of which grow with the magnetic field strength. These fluctuations are present at all T and can be a manifestation of the chiral magnetic effect (CME).

For further lattice works we consider a similar setup but with two colors. In Chapter 9 we measure the Euclidean time correlator of two vector quark currents,

$$G_{ij}(\tau) = \int d^3\vec{x} \langle J_i(\vec{x},\tau) J_j(\vec{0},0)\rangle\,, \tag{1.0.6}$$

and extract the corresponding spectral function. The latter provides us with the value of the electric conductivity of the vacuum by means of the Kubo formula. In summary, we obtain

1) At $T > T_c$ QCD vacuum is a conductor, $\sigma = 15 \pm 2\,\mathrm{MeV}$ slightly above T_c,

2) At $T < T_c$ the vacuum is either an insulator (with $B = 0$) or an anisotropic conductor (at strong B) with a finite conductivity along the magnetic field.

Both facts are in favor of CME, allowing us to interpret the fluctuations of current J_i as a macroscopic current. The primary consequence of the second fact is that one can expect an enhancement of the dilepton and soft photon production rates in direction transverse to $\vec{B}$. Finally, in Chapter 10 we measure the Hausdorff dimension d of the chirality distribution $\rho_5(x)$ and conclude that it depends on the resolution of a measurement. Lattice calculation without cooling ("high resolution") gives us $d = 2 \div 3$, i.e. presumably the vortex/domain-wall nature of the localization. In opposite, the cooling procedure ("resolution lowering") increases the dimensionality towards $d = 4$, i.e. restore the instanton picture of the QCD vacuum.

Chapters 11 and 12 introduce a new condensed-matter-inspired treatment of the QGP dynamics, based on a straightforward calculation from the QCD Lagrangian. In Chapter 11 we argue that the sQGP can be considered as a chiral superfluid. The "normal" component of the fluid is the thermalized matter in common sense, while the "superfluid" part consists of long wavelength (chiral) fermionic states moving independently. We use several non-perturbative techniques to demonstrate that. First, we analyze the fermionic spectrum in the deconfinement phase ($T_c < T < 2\,T_c$) using lattice (overlap) fermions and observe a gap between near-zero modes and the bulk of the spectrum. Second, we use the bosonization procedure with a finite cut-off and obtain a dynamical

axion-like field out of the chiral fermionic modes. Third, we use relativistic hydrodynamics for macroscopic description of the effective theory obtained after the bosonization. Finally, solving the hydrodynamic equations in gradient expansion, we find that in presence of external electromagnetic fields the motion of the "superfluid" component gives rise to the chiral magnetic, chiral electric and dipole wave effects. Latter two effects are specific for a two-component fluid, which provides us with crucial experimental tests of the model. In Chapter 12 we study the properties of chromodynamic flux tubes populating the Yang-Mills vacuum and arrive to a conclusion that the ground state of QCD is a chromoelectric superconductor.

Chapter 2

Gauge-gravity duality

The gauge-gravity duality [58–61] is a duality between a quantum field theory and a theory of gravity (string theory) in a higher dimensional spacetime. There are many versions of the duality formulated for various limits and spaces [62, 63], and for our applications we will concentrate on the weak one, which relates classical dynamics of gravity in a $(D+1)$-dimensional manifold to the quantum physics of a strongly-coupled conformal theory on the D-dimensional boundary of this manifold. Let us begin with an intuitive argument, why this duality should take place and then proceed with a formal definition and dictionary of the correspondence. Additional information can be found in numerous reviews, read e.g. [62–66].

Intuitive arguments

Consider a field theory on a lattice with spacing a governed by a Hamiltonian,

$$H = \sum_{x,i} J_i(x)\mathcal{O}^i(x)\,, \tag{2.0.1}$$

where $\{\mathcal{O}^i(x)\}$ are operators and $\{J_i(x)\}$ are couplings or sources defined at site x. The same theory on a coarse-grained lattice (with spacing $2a$, $4a$, ...) can be obtained by averaging the multiple sites and tuning sources $\{J_i(x)\}$ so as to preserve the ground state and the physics of low-energy excitation. The latter can be done by means of the Kadanoff-Wilson Renormalization Group (RG) equation,

$$u\frac{\partial}{\partial u}J_i(x,u) = \beta_i(J_j(x,u),u)\,, \tag{2.0.2}$$

where the couplings $J_i(x,u)$ now depend on the scales $u = a$, $2a$, ... and $\beta_i(J,u)$ are the beta-functions. If we consider now a stack of coarse-grained lattices, ordered by the scale u, then one can think of $J_i(x,u)$ as of bulk fields on a one-higher-dimensional lattice, where the additional coordinate corresponds to the RG flow direction (Fig. 2.1) and the boundary value (in the UV) is defined by $J_i(x,a) \equiv J_i(x)$. One can ask, what kind of higher-dimensional field theory this can be. Any boundary QFT should include among its operators the stress-energy tensor $T_{\mu\nu}$, meaning that the bulk QFT contains the spin-2 metric field $g_{\mu\nu}$. Also the QFT's at all the layers $u' > u$ are defined from the one at a layer u via the RG evolution, meaning that the former $(D+1)$ system has the same number of degrees of freedom as the D-dimensional QFT at the layer u. This fact, very much in spirit of the holographic principle [67, 68], suggests the theory of quantum gravity as the bulk theory (see also additional arguments in [65]).

Restricting now to a D-dimensional conformal field theory (CFT) on the boundary and assuming that it is described by a $(D+1)$ gravity bulk theory (a classical one in the long wavelength

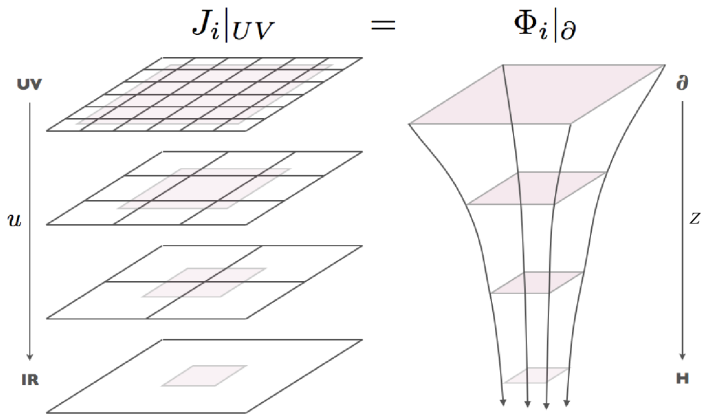

Figure 2.1: Illustration to the intuitive picture presented in the text, adapted from [65].

limit), we can deduce some of the properties of this $(D+1)$ spacetime (Fig. 2.1). The most general metric consistent with D-dimensional Poincare symmetry can be written as

$$ds^2 = \Omega^2(z)(-dx_0^2 + dx_i^2 + dz^2), \qquad i = \overline{1,\, D-1}\,, \tag{2.0.3}$$

where z is the extra (RG) spatial direction and $\Omega(z)$ is a function of z only, due to the translational symmetries in x_μ. A conformally invariant symmetry is invariant under the rescaling $x_\mu \to \Lambda x_\mu$. The coordinate z should be transformed in the same way, since it describes a length scale in the boundary theory. Therefore the warp factor should scale in that case as

$$\Omega(z) \to \Lambda^{-1}\Omega(z), \qquad z \to \Lambda z\,. \tag{2.0.4}$$

This determines Ω, such that the metric becomes

$$ds^2 = \frac{R^2}{z^2}(-dx_0^2 + dx_i^2 + dz^2), \qquad i = \overline{1,\, D-1}\,, \tag{2.0.5}$$

where R is a constant. This metric is nothing but the $(D+1)$-dimensional anti-de Sitter spacetime, AdS_{D+1} with curvature radius R (yet unfixed).

Formal definition of the AdS/CFT-correspondence

The gauge-gravity duality was initially formulated for the four-dimensional $\mathcal{N} = 4$ super-Yang-Mills (SYM) theory with $SU(N)$ gauge group and g_{YM} coupling. The theory contains a vector field, four fermions and six real scalars (all fields in the adjoint representation of the gauge group). The action of the theory can be written as

$$S_{\mathcal{N}=4} = -\frac{1}{g_{YM}^2}\int \mathrm{d}^4x\, \mathrm{Tr}\left(\frac{1}{4}F^{\mu\nu}F_{\mu\nu} + \frac{1}{2}D_\mu\Phi^i D^\mu\Phi^i + \left[\Phi^i, \Phi^j\right]^2\right) + \text{fermions}\,. \tag{2.0.6}$$

The theory has a vanishing beta-function and is a CFT. In the limit of large number of colors, i.e. $N \to \infty$, the perturbative expansion is controlled by the 't Hooft coupling $\lambda = g_{YM}^2 N$, and the Feynman graphs become organized by their topologies [69].

On the gravity side we have Type IIB superstring theory with string coupling g_s on $AdS_5 \times S^5$, with both AdS and 5-sphere having the same radius R and with an integer flux of the self-dual

RR 4-form[1] ($N_{\rm flux} = \int_{S^5} F_5^+$). The duality fixes the following relations between the string theory and $\mathcal{N} = 4$ SYM parameters,

$$g_{YM}^2 = 4\pi g_s, \qquad N = N_{\rm flux}, \qquad g_{YM}^2 N = \frac{R^4}{l_s^4}\,, \tag{2.0.7}$$

where l_s is the string length ($l_s^2 \equiv \alpha'$). The weak form of the conjecture mentioned above corresponds to the limit $\lambda = g_s N \to \infty$, $N \to \infty$ and $g_s \to 0$. The gravity side in this case is reduced to the Type IIB supergravity (SUGRA) on $AdS_5 \times S^5$, while the CFT is strongly-coupled and the duality can be formulated at the level of partition functions for both theories,

$$\left\langle \exp\left\{ -i \sum_i \int \mathrm{d}^4x\, J_i(x) \mathcal{O}^i(x) \right\} \right\rangle = \exp\left\{ -i S_{min}[AdS_5 \times S^5]_{J_i(x,\,z)|_{z=0} = J_i(x)} \right\}, \tag{2.0.8}$$

where the average is taken at the CFT side and $J_i(x,\,z)$ are, as before, classical solutions for the SUGRA action S_{min} matched with couplings/sources $J_i(x)$ on the boundary. This recalls the intuitive arguments above: *the bulk fields are the couplings promoted to dynamical fields on the RG-extended spacetime*.

The example above is one of the best established (but still unproved) dualities between a QFT and a theory of gravity. In order to apply this duality to QCD (or to a QCD-like system) one should consider a deformation of the quantum theory and hence a modification of the duality. There are two ways to do this: so-called top-down models and bottom-up models. The former corresponds to the models derived directly from the string theory constructions, while the latter refers to giving a gravity dual by hand. In the following chapters we use both approaches. In the case of the bottom-up models we usually do not know the microscopic content of the CFT, but require it to have suitable properties relevant to the real QCD phenomena (e.g. a QFT with electric charges, quantum anomalies, etc.). The main method we rely on in this case is the so-called holographic renormalization [70, 71], which links the boundary sources and expectation values of the boundary operators with the near-boundary expansion of the bulk fields.

Holographic renormalization

Let us consider an asymptotic AdS_{D+1} bulk gravity solution of the Einstein equations with cosmological constant $\Lambda = -\frac{D(D-1)}{2}$ written in Fefferman-Graham coordinates[2],

$$ds^2 = g_{MN}(x,z) dx^M dx^N = \frac{g_{\mu\nu}(x) dx^\mu dx^\nu + dz^2}{z^2}\,, \tag{2.0.9}$$

where $g_{MN}(x,z)$ has the following near-boundary expansion,

$$g(x,z) = g^{(0)}(x) + g^{(2)}(x)\, z^2 + ... + g^{(D)}(x)\, z^{(D)} + h^{(D)}(x)\, z^{(D)} \log z^2 + \mathcal{O}(z^{D+1})\,. \tag{2.0.10}$$

The log-term appears only in even dimensions [70, 71], also only even powers of r appear up to the order $r^{\lfloor D-1 \rfloor}$. It is a remarkable fact that the solution of the Einstein equations has an integration constant $g^{(D)}$, which can be fixed using the CFT data on the boundary, i.e. from the VEV of the energy-momentum tensor

$$\langle T_{\mu\nu} \rangle = \frac{D}{16\pi G_N} g_{\mu\nu}^{(D)} + ...\,, \tag{2.0.11}$$

[1] The form comes from the $D3$-brane solution, from which the $AdS_5 \times S^5$ originates, consult with e.g. [63].
[2] We use for simplicity the units, where $R = 1$.

where ellipses denote a non-universal part depending on the spacetime dimension. In a relevant for our studies case $D = 4$ one has [70, 71]

$$\langle T_{\mu\nu}\rangle = \frac{1}{4\pi G_N}\left\{ g^{(4)}_{\mu\nu} - \frac{1}{8} g^{(0)}_{\mu\nu}[(\mathrm{Tr}\, g^{(2)})^2 - \mathrm{Tr}\, {g^{(2)}}^2] - \frac{1}{2}({g^{(2)}}^2)_{\mu\nu} + \frac{1}{4} g^{(2)}_{\mu\nu} \mathrm{Tr}\, g^{(2)} \right\}, \tag{2.0.12}$$

which in a case of CFT on the 4D Minkowski boundary simplifies drastically,

$$\langle T_{\mu\nu}\rangle_{CFT} = \frac{1}{4\pi G_N} g^{(4)}_{\mu\nu}\,, \qquad \text{and so} \qquad g_{\mu\nu}(x,z) = \eta_{\mu\nu} + 4\pi G_N \langle T_{\mu\nu}(x)\rangle\, z^4 + ... \tag{2.0.13}$$

The same can be repeated for all other bulk fields, if present, giving similar expansions for scalar and vector fields, i.e. involving both the boundary values of the fields and expectation values of the corresponding operators $\langle \mathcal{O}_i \rangle$.

Black holes

While the *AdS* space is a ground state for gravity, finite-temperature states correspond to an *AdS* black hole solution. The Hawking temperature, associated with the black hole (or, more generally, black brane), is identified with the temperature of the gauge theory. The simplest asymptotically-*AdS* black hole is the Schwarzschild AdS black brane,

$$ds^2 = \frac{1}{z^2}\left(-f(z)\, dt^2 + d\vec{x}^2 + \frac{1}{f(z)} dz^2 \right) \tag{2.0.14}$$

with factor

$$f(z) = 1 - \left(\frac{z}{z_H}\right)^D. \tag{2.0.15}$$

Near the asymptotic boundary $z \to 0$, $f \to 1$ and the metric is asymptotically AdS_{D+1}. Coordinate z_H is the position of horizon, a zero of the function $f(z)$. The Hawking temperature T, energy density ϵ and entropy density s are given by [72, 73]

$$T \equiv -\frac{f'(z_H)}{4\pi} = \frac{D}{4\pi z_H}, \qquad \epsilon = \frac{D-1}{16\pi G_N z_H^D}, \qquad s = \frac{1}{4 G_N z_H^{D-1}}\,. \tag{2.0.16}$$

Let us turn now to the charged (Reissner-Nordström) *AdS* black hole, which plays a significant role in the AdS/CFT-applications and will be used by us in the next chapters. The Reissner-Nordström *AdS* black hole is a solution of the Einstein-Maxwell equation, corresponding to the action

$$S_{EM} = \frac{1}{16\pi G_N}\int d^{D+1}x\, \sqrt{-g}\left(R - 2\Lambda - \frac{1}{4} F^{MN} F_{MN} \right), \tag{2.0.17}$$

where F_{MN} is the field stress tensor for the vector field $A_M(z, t, \vec{x})$. The solution can written in analogy with (2.0.14),

$$ds^2 = \frac{1}{z^2}\left(-f(z)\, dt^2 + d\vec{x}^2 + \frac{1}{f(z)} dz^2 \right), \qquad A = A_t(z)\, dt \tag{2.0.18}$$

with factors

$$f(z) = 1 - \left(1 + \frac{z_H^2 \mu^2}{\mathfrak{z}^2}\right)\left(\frac{z}{z_H}\right)^D + \left(\frac{z_H^2 \mu^2}{\mathfrak{z}^2}\right)\left(\frac{z}{z_H}\right)^{2(D-1)}, \quad A_t(z) = \mu\left(1 - \left(\frac{z}{z_H}\right)^{D-2}\right). \tag{2.0.19}$$

In the last expression we defined $\mathfrak{z}^2 = \frac{2(D-1)}{D-2}$. The prefactor μ is the difference between the scalar potential at the horizon and at the boundary and plays the role of the chemical potential. The Hawking temperature is given now by [72]

$$T = \frac{D}{4\pi z_H}\left(1 - \frac{D-2}{\mathfrak{z}^2 D}\mu^2 z_H^2\right), \tag{2.0.20}$$

and the energy, entropy, charge densities by

$$\epsilon = \frac{D-1}{16\pi G_N z_H^D}\left(1 + \frac{z_H^2\mu^2}{\mathfrak{z}^2}\right), \qquad s = \frac{1}{4G_N\, z_H^{D-1}}, \qquad \rho = \frac{D-1}{\mathfrak{z}^2 8\pi G_N}\frac{\mu}{z_H^D}. \tag{2.0.21}$$

One can easily check, that these variables satisfy the first law of thermodynamics, $d\epsilon = T\, ds + \mu\, d\rho$.

Fluid-gravity duality

One of the particular cases of the duality is the case, when the boundary CFT obeys a set hydrodynamic equations and can be mapped to a black brane solution of the Einstein equations in one higher dimension (see e.g. [74–77]). This situation is called "fluid-gravity correspondence" and can be used for a phenomenological description of the strongly-coupled QGP, since the latter is a nearly-perfect quantum liquid. As a simple example we can consider the AdS black hole solution (2.0.14, 2.0.15) with $D = 4$ and change the variables,

$$z \to \frac{\tilde{z}}{\sqrt{1 + \tilde{z}^4/\tilde{z}_H^4}}, \qquad z_H \to \tilde{z}_H/\sqrt{2}, \tag{2.0.22}$$

such that the metric becomes

$$ds^2 = -\frac{(1 - \tilde{z}^4/\tilde{z}_H^4)^2}{(1 + \tilde{z}^4/\tilde{z}_H^4)\tilde{z}^2}\, dt^2 + (1 + \tilde{z}^4/\tilde{z}_H^4)\,\frac{d\vec{x}^2}{\tilde{z}^2} + \frac{d\tilde{z}^2}{\tilde{z}^2}. \tag{2.0.23}$$

This form is suitable for the holographic renormalization (2.0.13) and gives us

$$\langle T_{\mu\nu}\rangle = \frac{1}{4\pi G_N} g^{(4)}_{\mu\nu} = \frac{1}{16\pi G_N}\,\mathrm{diag}\left(\frac{3}{z_H^4}, \frac{1}{z_H^4}, \frac{1}{z_H^4}, \frac{1}{z_H^4}\right) = \mathrm{diag}\left(\epsilon, \frac{\epsilon}{3}, \frac{\epsilon}{3}, \frac{\epsilon}{3}\right), \tag{2.0.24}$$

where in the last step we used the expression (2.0.16) for the energy density. One can notice that the obtained energy-momentum tensor is nothing but the one for a conformal ideal fluid at rest ($\epsilon = 3P$). We can go further and boost the black hole solution (2.0.14) along u_μ, which will result in the covariant energy-momentum tensor of an ideal fluid,

$$T^{\mu\nu} = (\epsilon + P)\, u^\mu u^\nu + P g^{\mu\nu}. \tag{2.0.25}$$

In a relativistic setup, which we consider in the next chapters, one can then systematically correct it by including higher-order gradient terms (corresponding to e.g. dissipative effects). One should also mention, that such gradient series do not converge and is an example of asymptotic series [78].

Chapter 3

Non-equilibrium physics at a holographic chiral phase transition

Thermal phase transitions are a crucial aspect of the evolution of the Universe after the Big Bang and also in the physics of heavy ion collisions. We have traditionally lacked tools to study these transitions though in strongly coupled systems such as QCD. The AdS/CFT correspondence [59–61], which gives a weakly coupled string/gravity description of a class of strongly coupled gauge theories, offers the chance to study similar transitions in detail.

In this chapter we study a simple dual of a theory with gauge fields and quarks which has (in the presence of a magnetic field) a first order chiral symmetry restoring phase transition as it is heated. Previous analysis of this gauge theory (using probe branes in an AdS-Schwarzschild black hole geometry) has explored the first order transition for equilibrium (time independent) configurations. The heating or cooling of the system can be studied thanks to the boost-invariant expanding or contracting plasma geometry of Janik and Peschanski [74]. That geometry, which we will review below, has a moving black hole horizon describing the changing temperature in the gauge theory. We will study probe branes in this geometry to learn more about the first order phase transition out of equilibrium.

The particular duality we concentrate on is the simplest example of holography with fundamental quark fields [79–84]. We do not consider the specific degrees of freedom of the theory too crucial - it is some strongly coupled gauge theory that displays a chiral phase transition. We hope, in the spirit of AdS/QCD models [85, 86], that it reflects broad aspects of many strongly coupled systems. The specific gauge theory is constructed from the D3/D7 system in type IIB string theory which we will describe further below. The theory is the large N_c $\mathcal{N} = 4$ $U(N_c)$ gauge theory with a small number of quark hypermultiplets. We will work in the quenched approximation [81] (appropriate when $N_f \ll N_c$) which on the gravity dual side corresponds to treating the D7 branes as probes in the metric generated by the D3 branes. There is a $U(1)$ chiral symmetry (a remnant of the $SU(4)$ R-symmetry of the $\mathcal{N} = 4$ theory) which is broken when a quark condensate forms [83, 87, 88]. Several mechanisms for triggering this condensation have been explored. The cleanest is when a background magnetic field is introduced [89–97] so we will use that mechanism here. The reader might want to loosely view the B field as simply the introduction of a conformal symmetry and supersymmetry breaking parameter that triggers the strong dynamics to cause the symmetry breaking. Physically, magnetic fields may be strong during structure formation in the early universe, in particular during the epoch of the QCD primordial phase transition, and in non-central high-energy heavy-ion collisions studied at RHIC. Running of the coupling in the holographic dual also causes quark condensation as has been shown in back-reacted dilaton flow geometries [83, 98] and models with a phenomenologically imposed dilaton profile [99]. The quark

condensate can be determined in these models and an effective IR quark mass is generated. The theories display a massless pion-like Goldstone field and a massive sigma field (since we are at large N_c it is stable) that is the effective Higgs particle.

The equilibrium finite temperature behaviour of the theory with a magnetic field has been studied in [89–91, 96, 97]. Finite temperature can be included through the presence of an AdS Schwarzschild black hole. At a critical temperature the D7 embedding flips from a chiral symmetry breaking embedding away from the horizon to a symmetry preserving embedding that enters the horizon. The transition is therefore also associated with meson melting [100–102] - for embeddings away from the horizon there are regular linearized fluctuations describing the meson spectrum of the theory. For the embedding that enters the horizon there are only in-falling quasi-normal modes describing unstable plasma fluctuations. In terms of the quarks of the theory the high temperature phase is analogous to the quark gluon plasma phase in QCD whilst the low energy phase is more akin to the hadronic phase of QCD. It should be noted though that the gluonic degrees of freedom deconfine at any finite temperature so the analogy is imperfect.

The crucial extra ingredient we shall add to this story in this chapter is provided by the boost-invariant expanding or contracting plasma geometry of Janik and Peschanski [74]. This geometry has a black hole whose horizon moves away from the boundary in time as the $\mathcal{N} = 4$ plasma it describes expands and cools. The time reversed solution at zero viscosity describes a heating plasma and we will find it useful to discuss that scenario too below. The geometry is a late time expansion (when the black hole is small) in powers of inverse time. However, by controlling the strength of the magnetic field on the D7 probes, felt by the quarks, we can arrange to place the chiral phase transition at any point in the evolution so the expansion is sufficient to fully study the transition.

We will place a D7 brane[1] into the expanding plasma geometry and determine the partial differential equation (PDE) that describes the time dependence of its embedding. A good first approximation to the transition behaviour is provided by the equilibrium results with the temperature replaced by the temperature as a function of time from the moving background. In fact we will see that that is an extremely good approximation when talking about the slow or adiabatic heating or cooling of vacuum configurations at temperatures even close to the phase transition. If the chiral symmetry breaking embedding is heated though, the local minima in the effective potential associated with that embedding is eventually lost and the configuration becomes an out of equilibrium configuration. The equilibrium results can not describe the subsequent evolution. Similarly excited vacuum states must be studied through the full PDE system.

We first turn to an approximation to the PDE. The solution can be power expanded in inverse powers of time. This reduces the PDE to a system of ordinary differential equations (ODEs) that are much easier to solve. This analysis was first done in [105] where the time evolution of the high temperature phase of the pure $\mathcal{N} = 2$ theory was studied. Using this technique we solve the ODE system and find the moving D7 solution. This method assumes that the initial vacuum state is exactly a maximum or minimum of the zero temperature effective potential. Again the heating is essentially adiabatic in nature. The expansion breaks down if the super-heated state ceases to be an extrema of the effective potential. This method allows us to confirm the success of the equilibrium derived results although in fact the expansion breaks down before the equilibrium results deviate from the full PDE solutions.

The most interesting out of equilibrium questions lie beyond the adiabatic approximation though. In a physical first order transition quantities such as the condensate do not jump but the vacuum state instead performs a fast roll from one configuration to another. The timing of that transition can and most likely will be spatially dependent *i.e.* bubbles of the true vacuum will form and grow. We turn to solving the full PDEs to study these phenomena (with care this

[1] By placing a fundamental string, which corresponds to a heavy quark, into the expanding plasma geometry, the diffusion constant [103] and drag force [104] was computed.

can be done using in built PDE solvers in for example Mathematica). For example we are able to watch the super-heated chiral symmetry breaking phase roll to the symmetric phase. We can also simulate initial conditions with some extra energy (which might for example come from thermal fluctuations) and see such configurations transition away from the super-heated vacuum before the meta-stable vacuum has disappeared in the effective potential. This allows us to confirm some elements of the transition such as the length of time in which there is a mixed phase. We also are effectively watching a very large bubble form.

Our main result then is to have developed numerical techniques that let us reproduce the phase structure using the PDE solutions and to describe non-equilibrium physics that is necessarily present in the first order transition.

In our final section we also analyze the ODE expansion approximation to the PDE solutions for the D7 embedding to make clear the full dependence of the solutions on the magnetic field value. In that case the dependence is available analytically. We also show the effects of the viscosity.

3.1 Holographic Descriptions

In this section we review the $\mathcal{N} = 2$ gauge theory with a magnetic field and its holographic description. We discuss the theory's finite temperature *chiral phase transition* in an equilibrium description. We then review how to study flavour physics in a *nonequilibrium* set-up using holography.

3.1.1 Chiral symmetry transition

We will study the D3/D7 brane model at finite temperature and with a magnetic field [89–91,96,97]. The magnetic field, which causes chiral symmetry breaking, competes with the temperature that prefers to restore chiral symmetry. Consequently there is a first order phase transition.

The $\mathcal{N} = 4$ $SU(N)$ gauge theory at finite temperature has a holographic description in terms of an AdS_5 black hole geometry which can be written as

$$ds^2 = \frac{w^2}{R^2}(-g_t dt^2 + g_x d\vec{x}^2) + \frac{R^2}{w^2}(d\rho^2 + \rho^2 d\Omega_3^2 + dL^2 + L^2 d\phi^2) \ , \tag{3.1.1}$$

where ϕ is a $U(1)$ angle and $w = \sqrt{\rho^2 + L^2}$, $\rho = w \sin\phi$, $L = w\cos\phi$ and

$$g_t = \frac{(w^4 - w_H^4)^2}{2w^4(w^4 + w_H^4)} \ , \qquad g_x = \frac{w^4 + w_H^4}{2w^4} \ . \tag{3.1.2}$$

Note $R^4 = 4\pi g_s N \alpha'^2$, and the temperature is given by $w_H = \pi R^2 T$.

Quenched ($N_f \ll N$) $\mathcal{N}$=2 quark superfields can be included in the $\mathcal{N} = 4$ $SU(N)$ gauge theory through probe D7 branes in the geometry [81]. The D7 probe can be described by its Dirac-Born-Infeld (DBI) action

$$S_{DBI} = -T_{D7} \int d^8\xi \sqrt{-\det(P[G]_{ab} + 2\pi\alpha' F_{ab})} \ , \tag{3.1.3}$$

where $P[G]_{ab}$ is the pullback of the metric and F_{ab} is the gauge field living on the D7 world volume. We will use F_{ab} to introduce a constant magnetic field [89–91],

$$F_{12} = -F_{21} = B/(2\pi\alpha') \ . \tag{3.1.4}$$

We embed the D7 brane assuming only ρ dependence: $L(\rho)$ at constant ϕ. The full DBI action we will consider is then

$$S_{DBI} = \int d\xi^8 \mathcal{L}(\rho) = \left(\int_{S^3} \epsilon_3 \int dt d\vec{x}\right) \int d\rho \ \mathcal{L}(\rho) \ , \tag{3.1.5}$$

where ϵ_3 is a volume element on the 3-sphere and

$$-\mathcal{L} \equiv \widetilde{\Omega} \equiv N_f T_{D7} (R\sqrt{B})^4 \widetilde{\rho}^3 \left(1 - \frac{\widetilde{w}_H^4}{\widetilde{w}^4}\right) \sqrt{\left(1 + \widetilde{L}'^2\right)} \sqrt{\left(\left(1 + \frac{\widetilde{w}_H^4}{\widetilde{w}^4}\right)^2 + \frac{1}{\widetilde{w}^4}\right)} \tag{3.1.6}$$

with the dimensionless variables defined as

$$(\widetilde{w}, \widetilde{L}, \widetilde{\rho}) = \left(\frac{w}{R\sqrt{2B}}, \frac{L}{R\sqrt{2B}}, \frac{\rho}{R\sqrt{2B}}\right) \ . \tag{3.1.7}$$

Note that we can use the magnetic field value as the intrinsic scale of conformal symmetry breaking in the theory - that is we can rescale L and ρ by B. The Euclidean on-shell Lagrangian ($-\mathcal{L}$) is interpreted as the free energy density ($\widetilde{\Omega}$).

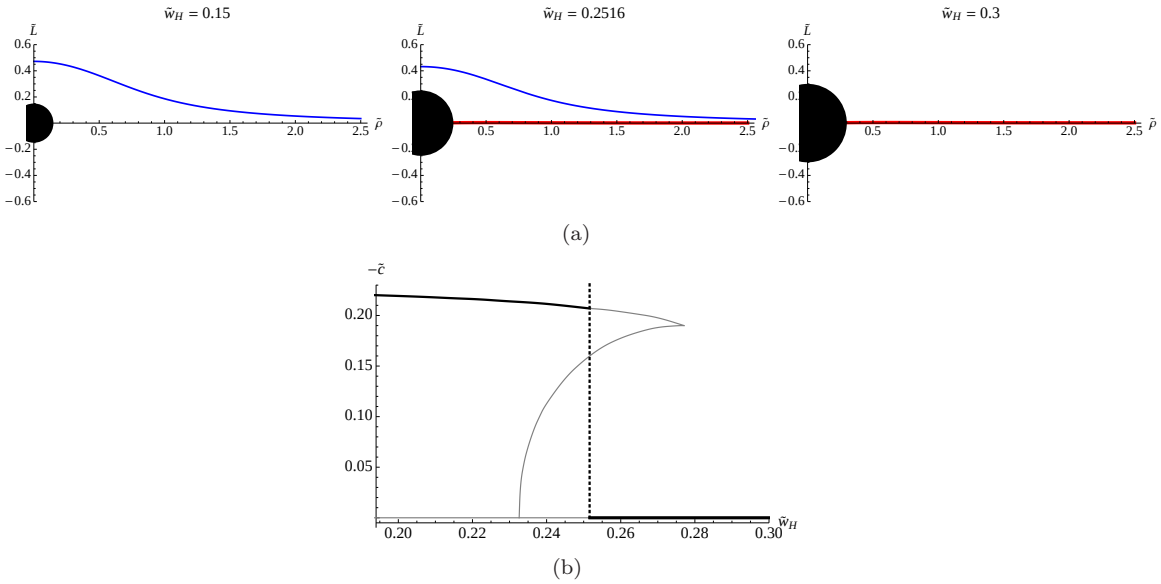

Figure 3.1: The equilibrium description of the first order chiral phase transition in the $\mathcal{N} = 2$ gauge theory with a magnetic field: (a) The D7 brane embedding profiles $\widetilde{L}(\widetilde{\rho})$ as a function of temperature $\widetilde{w}_H$. The low temperature symmetry breaking embedding is shown on the left whilst the symmetric flat embedding on the right is preferred at high temperature. (b) A plot of the chiral condensate as a function of the temperature with the dotted line indicating the position of the first order transition.

In all cases the embeddings become flat at large ρ taking the form

$$\widetilde{L}(\widetilde{\rho}) \sim \widetilde{m} + \frac{\widetilde{c}}{\widetilde{\rho}^2} \ , \quad \widetilde{m} = \frac{2\pi\alpha' m_q}{R\sqrt{2B}} \ , \quad \widetilde{c} = \langle \bar{q}q \rangle \frac{(2\pi\alpha')^3}{(R\sqrt{2B})^3} \ , \tag{3.1.8}$$

where $\widetilde{m}$ and $\widetilde{c}$ are identified with the quark mass and the quark condensate, respectively. Since we are interested in spontaneous symmetry breaking we impose $\widetilde{m} = 0$ in the UV ($\widetilde{\rho} \to \infty$). Then the value of $\widetilde{c}$ is determined by requiring regularity in the IR ($\widetilde{\rho} \ll 1$). If there is more than one solution then we choose the one giving the minimum free energy.

The results are displayed in Fig. 3.1. At low temperatures $T \ll B$, the black hole is small and the embeddings are repelled from the origin of the $\widetilde{L} - \widetilde{\rho}$ plane (Fig. 3.1 (left)). This behaviour is a result of the inverse powers of $\widetilde{w}^4$, when $\widetilde{w}_H \ll 1$, in the last term of the Lagrangian (3.1.6), which causes the action to grow if the D7 approaches the origin. Consequently $\widetilde{c}$ is non-zero and chiral symmetry is broken. If the temperature is allowed to rise sufficiently then the black hole horizon grows to mask the area of the plane in which the inverse $\widetilde{w}^4$ terms in the Lagrangian are large. At a critical value of T ($\tilde{w}_H = 0.2516$, Fig. 3.1 (middle)) the benefit to the $\widetilde{m} = 0$ embedding of curving off the axis becomes disfavoured and it instead lies along the $\tilde{\rho}$ axis - chiral symmetry breaking switches off. This transition is first order since the condensate vanishes discontinuously, which corresponds to the embedding change from the blue to the red one. At higher temperatures (Fig. 3.1 (right)), the embedding stays flat, $\widetilde{c} = 0$, as expected in the chirally symmetric phase. The corresponding condensate vs. temperature ($-\tilde{c}$-$\tilde{w}_H$) plot is shown in Fig. 3.1 (bottom).

3.1.2 A boost-invariant expanding plasma

The geometry (3.1.1) is dual to a system in thermodynamical equilibrium and therefore not suitable for the description of the chiral phase transition in a rapidly expanding plasma, in which the transition is basically a non-equilibrium process. Boost-invariant expanding $\mathcal{N}=4$ $SU(N)$ plasmas out of equilibrium can however be described by the time-dependent background found in [74] (see [106] for a review). In the following we review the basic features of this background and discuss the embedding of probe D7 branes dual to quenched flavours ("quarks") in the plasma.

The boost-invariant geometry is a 5D spacetime with coordinates $\{\tau, y, x_\perp(=x^1,x^2), z\}$, which, apart from the holographic direction z, parameterise the 4D spacetime on the boundary. The longitudinal position plane is parameterised by the proper time τ and rapidity y (related to $x^{0,3}$ as $x^0=\tau\cosh y,\ x^3=\tau\sinh y$), the transverse coordinates are collected in $x_\perp$. We also add a five-sphere to obtain a full type IIB supergravity background. The metric is then of the form

$$\frac{ds^2}{R^2}=\frac{1}{z^2}\left(-e^{a(\tau,z)}d\tau^2+e^{b(\tau,z)}\tau^2dy^2+e^{c(\tau,z)}dx_\perp^2\right)+\frac{dz^2}{z^2}+d\Omega_5^2\ , \tag{3.1.9}$$

where R is the radius of the AdS_5 space. At late times, the coefficients can be expanded to first order as [74, 107, 108]

$$\begin{aligned}
a(\tau,z)&=\ln\left(\frac{(1-v^4/3)^2}{1+v^4/3}\right)+2\eta_0\frac{(9+v^4)v^4}{9-v^8}\left[\frac{1}{(\varepsilon_0^{3/8}\tau)^{2/3}}\right]+\mathcal{O}\left[\frac{1}{\tau^{4/3}}\right],\\
b(\tau,z)&=\ln(1+v^4/3)+\left(-2\eta_0\frac{v^4}{3+v^4}+2\eta_0\ln\frac{3-v^4}{3+v^4}\right)\left[\frac{1}{(\varepsilon_0^{3/8}\tau)^{2/3}}\right]+\mathcal{O}\left[\frac{1}{\tau^{4/3}}\right],\\
b(\tau,z)&=\ln(1+v^4/3)+\left(-2\eta_0\frac{v^4}{3+v^4}-\eta_0\ln\frac{3-v^4}{3+v^4}\right)\left[\frac{1}{(\varepsilon_0^{3/8}\tau)^{2/3}}\right]+\mathcal{O}\left[\frac{1}{\tau^{4/3}}\right],
\end{aligned} \tag{3.1.10}$$

with

$$v\equiv\frac{z}{\tau^{1/3}\varepsilon_0^{1/4}}\ ,\qquad \eta_0=\frac{1}{2^{1/2}3^{3/4}}\ . \tag{3.1.11}$$

ε_0 is a free parameter of mass dimension 8/3 and is related to the energy density, while η_0 is related to the shear viscosity. v is a scaling parameter valid at large τ. Note that $a(\tau,z), b(\tau,z)$ and $c(\tau,z)$ are expanded around $\tau=\infty$ in powers of $1/\tau^{2/3}$ as [74, 107, 108]

$$a(\tau,z)=\sum_{n=0}^{\infty}a_n(v)\left(\frac{1}{\varepsilon_0^{3/8}\tau}\right)^{\frac{2}{3}n}\ , \tag{3.1.12}$$

and similarly for $b(\tau,z)$ and $c(\tau,z)$. The coefficients are functions of a scaling parameter v only. Due to this scaling behaviour the complicated PDE Einstein equations can be reduced to an ODE system, which allows analytic solutions. At early time $\tau\ll 1$ there is no scaling behaviour and we should solve the full PDEs.

To find which gauge theory state corresponds to this bulk metric according to the AdS/CFT dictionary let us expand the metric around $z=0$,

$$\begin{aligned}
g_{\tau\tau}&\equiv -e^{a(\tau,z)}=-1+\frac{2\pi^2}{N_c^2}z^4\left[\bar{\varepsilon}-\frac{2\eta}{\tau}\right]+\mathcal{O}(z^6),\\
g_{yy}&\equiv \tau^2e^{b(\tau,z)}=\tau^2+\frac{2\pi^2}{N_c^2}z^4\left[\tau^2\left(\frac{\bar{\varepsilon}}{3}-\frac{2\eta}{\tau}\right)\right]+\mathcal{O}(z^6),\\
g_{11}(=g_{22})&\equiv e^{c(\tau,z)}=1+\frac{2\pi^2}{N_c^2}z^4\left[\frac{\bar{\varepsilon}}{3}\right]+\mathcal{O}(z^6)\ ,
\end{aligned} \tag{3.1.13}$$

where [2]

$$\bar{\varepsilon} \equiv \frac{N_c^2}{2\pi^2}\frac{\varepsilon_0}{\tau^{4/3}} , \qquad \eta \equiv \frac{N_c^2}{2\pi^2}\frac{\eta_0 \varepsilon_0^{3/4}}{\tau} . \tag{3.1.15}$$

The leading terms (of order $\mathcal{O}(z^0)$) of the metric elements (3.1.13) is simply the Minkowski metric in the $\tau - y$ coordinate system, and the subleading terms (of order $\mathcal{O}(z^4)$) correspond to the expectation value of the energy-momentum tensor, *i.e.*

$$\langle T_{00}\rangle = \bar{\varepsilon} - \frac{2\eta}{\tau} , \quad \langle T_{yy}\rangle = \tau^2\left(\frac{\bar{\varepsilon}}{3} - \frac{2\eta}{\tau}\right) , \quad \langle T_{11}\rangle = \langle T_{22}\rangle = \frac{\bar{\varepsilon}}{3} . \tag{3.1.16}$$

This energy-momentum tensor is precisely that of a longitudinal viscous boost-invariant $\mathcal{N} = 4$ SYM conformal plasma with finite η.

In $g_{\tau\tau}$ we recover a time-dependent emblackening factor, which describes a moving horizon. The size of the horizon determines the time-dependence of the 'temperature' as [105, 107]

$$T(\tau) = \frac{\sqrt{2}}{\pi R^2} r_H = \left(\frac{4\varepsilon_0}{3}\right)^{1/4} \frac{1}{\pi\tau^{1/3}}\left(1 - \frac{\eta_0}{2\varepsilon_0^{1/4}\tau^{2/3}}\right) . \tag{3.1.17}$$

If we assume that the time-dependent entropy density $s(\tau)$ has the same form as in the static case, $s(\tau) = (\pi^2/2)N_c^2 T(\tau)^3$, then the ratio η/s can be computed as [108]

$$\frac{\eta}{s} = \frac{1}{4\pi} + \mathcal{O}(\tau^{2/3}) , \tag{3.1.18}$$

which at large τ agrees with the known static bound. Note that the numerical value of η_0 in (3.1.11) is crucial to get $1/4\pi$.

Finally we note the uniqueness of the gravity solution. There is a potential singularity at $v = 3^{1/4}$ in (3.1.10). The curvature invariant, $R_{\mu\nu\rho\sigma}R^{\mu\nu\rho\sigma} = R_0(v) + R_1(v)\tau^{-2/3} + R_2(v)\tau^{-3/4} + \cdots$ is only regular at each order if one makes the specific choices above. We must choose $-1/3$ for the power of τ in (3.1.11) to make R_0 regular [74]. We must also choose (3.1.10) with the specific choice of the numerical value η_0 as in (3.1.11) to make R_2 regular [108]. (R_1 is always regular and does not give any constraint.)

Flavours in this background were first studied in [105]. Knowing the explicit background geometry (3.1.9) we can study flavour physics using the D7 brane DBI action. The action schematically reads

$$S \sim \int d^8\xi \sqrt{-\det(P[G]_{ab})} \sim \int d\tau d\rho\, \tau\rho^3 \mathbb{A}\sqrt{1 + (\partial_\rho L)^2 - \mathbb{B}\frac{(\partial_\tau L)^2}{(\rho^2 + L^2)^2}} , \tag{3.1.19}$$

where $\mathbb{A}$ and $\mathbb{B}$ are complicated but known functions of τ and ρ, see (3.2.5) and (3.2.6) in the next section. $L = L(\tau, \rho)$ is the embedding profile of the D7 brane and is assumed to be a function of τ and ρ.

The equation of motion coming from (3.1.19) is a non-linear PDE. However it can be semi-analytically solved by the late-time expansion

$$L(\tau, \rho) = m + \sum_{i=1}^{\infty} f_i(\rho)\tau^{-\frac{i}{3}} . \tag{3.1.20}$$

[2] Here $\frac{2\pi^2}{N_c^2}$ has been factored out to apply the AdS/CFT dictionary

$$\langle T_{\mu\nu}\rangle = \frac{N_c^2}{2\pi^2}\lim_{z\to 0}\frac{1}{z^4}(g_{\mu\nu} - \eta_{\mu\nu}) . \tag{3.1.14}$$

This expansion inherently assumes that the late time configuration is precisely the equilibrium vacuum and when we heat it there is no excess energy. This leads to an adiabatic approximation. The fraction 1/3 is chosen because all exponents of τ in $\mathbb{A}$ and $\mathbb{B}$ are integer multiples of 1/3 and the constant m reflects the fact that the embeddings get flat at large τ. Here we only consider a large bare quark mass ($m \gg 1$) and Minkowski embeddings, *i.e.* D7 configurations which end well above the black hole horizon.

This reduces the partial differential equation to an infinite set of ordinary differential equations given by

$$\rho^{-3}\partial_\rho\left(\rho^3 f_i'(\rho)\right) = \frac{8m\varepsilon_0^2}{9(m^2+\rho^2)^5} I_i \ , \tag{3.1.21}$$

$$I_8 = 1 \ , \quad I_{10} = -4\eta_0\varepsilon_0^{-1/4} \ , \quad \text{otherwise} \ \ I_{i\leq 13} = 0 \ , \tag{3.1.22}$$

where we do not consider terms with $i > 13$ since they are beyond the validity regime of our approximation of the boost-invariant metric. The asymptotic solution at large ρ is

$$f_i \sim m_i + \frac{c_i}{\rho^2} \, . \tag{3.1.23}$$

We set $m_i = 0$ so the bare quark mass is zero and not time-dependent. We also impose the condition $f_i'(0) = 0$ for regularity. With these boundary conditions, we find $f_i = 0$ except for f_8, f_{10}. As a result, one gets

$$L(\tau,\rho) = m + c(\tau)\frac{\rho^4 + 3\rho^2 m^2 + 3m^4}{(m^2+\rho^2)^3} \, , \tag{3.1.24}$$

where

$$c(\tau) = -\frac{\epsilon_0^2}{54m^5}\left(\tau^{-8/3} - 4\eta_0\epsilon_0^{-1/4}\tau^{-10/3} + \cdots\right) \ . \tag{3.1.25}$$

The condensate approaches zero as $\sim -\tau^{-8/3}$ and the viscosity has a "dragging" effect $\sim +\tau^{-10/3}$.

We close this section with some technical remarks on black hole embeddings. In the Fefferman-Graham (FG) coordinate system (3.1.9) one cannot approach the horizon for fixed τ as in the Schwarzschild black hole metric. There is also an extended background written in terms of Eddington-Finkelstein (EF) coordinates, where the spacetime is well defined across the horizon [109, 110] and black hole embeddings may be described more consistently there. However we have found that the embedding configuration is not easy to handle in those coordinates. Below, to enable us to study black hole embeddings, we use FG coordinates but with a cut-off slightly above the horizon. Since the FG coordinate system is a good patch near the horizon at large τ, by restricting ourselves to large τ, we may capture the essential physics of the embedding. This will allow us to go beyond the results in [105].

3.2 Out of equilibrium description of the chiral phase transition

In the previous section we reviewed the holographic description of dynamical flavours in an expanding plasma [105]. A boost-invariant background with embedded D7 branes is however not sufficient to study the chiral transition. In that case the D7 embeddings are always flat in the chiral limit ($m \to 0$) and the system is always in the chiral symmetric phase with vanishing quark condensate. In order to describe the transition to the chiral broken phase, we need a *repulsive* effect to compete against the attractive force of the black hole. As in the static case reviewed in section

3.1.1, this can be achieved by turning on a magnetic field. In this section, we will therefore consider D7 branes with a world-volume magnetic field in the dual geometry of an expanding plasma. In this way we will find the holographic dual of a chiral transition and deduce the dynamic effective potential for the time-dependent quark condensate.

3.2.1 D7 flavour brane action

The background metric for a boost-invariant expanding plasma can be written as

$$ds^2 = \frac{r^2}{R^2}(-e^{a(\tau,r)}d\tau^2 + e^{b(\tau,r)}\tau^2 dy^2 + e^{c(\tau,r)}dx_\perp^2) + \frac{R^2}{r^2}(d\rho^2 + \rho^2 d\Omega_3^2 + dL^2 + L^2 d\phi^2) \quad (3.2.1)$$

where $r^2 \equiv \rho^2 + L^2$. The S^5 part is written as in (3.1.1) and the AdS_5 part follows from (3.1.9) with a change $z \to R^2/r$, *i.e.* $a(\tau, r) \equiv a(\tau, z \to R^2/r)$ in (3.1.10) and similarly for $b(\tau, r)$ and $c(\tau, r)$.

We are interested in time-dependent D7 brane embeddings of the type $L = L(\tau, \rho)$. The corresponding DBI action is

$$S_{DBI} = -T_{D7}\int d^8\xi \sqrt{-\det(P[G]_{ab} + 2\pi\alpha' F_{ab})}\ , \quad (3.2.2)$$

where we turn on a constant magnetic field [89–91],

$$F_{12} = -F_{21} = B/(2\pi\alpha')\ , \quad (3.2.3)$$

in order to induce the chiral symmetry breaking.

More explicitly, the D7-brane action reads

$$S = \mathbb{N}\int d\tau d\rho\, \tau\rho^3 \mathbb{A}\sqrt{\left(1 + \mathbb{C}\frac{R^4B^2}{(\rho^2+L^2)^2}\right)\left(1 + L'^2 - \mathbb{B}\frac{R^4\dot{L}^2}{(\rho^2+L^2)^2}\right)} \quad (3.2.4)$$

$$\mathbb{A} \equiv \left(1 - \frac{v^8}{9}\right)\exp\left[4\eta_0\varepsilon_0^{-1/4}\frac{v^8}{9-v^8}\tau^{-2/3}\right]\ , \quad (3.2.5)$$

$$\mathbb{B} \equiv \frac{1 + \frac{v^4}{3}}{\left(1 - \frac{v^4}{3}\right)^2}\exp\left[-2\eta_0\varepsilon_0^{-1/4}v^4\frac{9+v^4}{9-v^8}\tau^{-2/3}\right]\ , \quad (3.2.6)$$

$$\mathbb{C} \equiv \frac{9}{(3+v^4)^2}\exp\left[4\eta_0\varepsilon_0^{-1/4}\left(\frac{v^4}{3+v^4} - \mathrm{Coth}^{-1}\left(\frac{3}{v^4}\right)\right)\tau^{-2/3}\right]\ , \quad (3.2.7)$$

$$v \equiv \frac{\varepsilon_0^{1/4}R^2}{\tau^{1/3}\sqrt{\rho^2+L^2}}\ , \quad \mathbb{N} \equiv N_f T_{D7}\int \epsilon_3 \int dy d^2x_\perp\ , \quad (3.2.8)$$

where $\mathbb{A} = e^{a/2+b/2+c}$, $\mathbb{B} = e^{-a}$, $\mathbb{C} = e^{-2c}$, $\eta_0 = 1/(2^{1/2}3^{3/4})$ as in (3.1.11), and ϵ_3 is the volume form of the three-sphere. For vanishing B, the action reduces to that in (3.1.19).

It turns out to be convenient to work with the rescaled variables

$$\rho \equiv \sqrt{B}R\widetilde{\rho}\ , \quad L \equiv \sqrt{B}R\widetilde{L}\ , \quad \tau \equiv \frac{R}{\sqrt{B}}\widetilde{\tau}\ , \quad \varepsilon_0 \equiv B^{4/3}R^{-8/3}\widetilde{\varepsilon}_0\ . \quad (3.2.9)$$

For $R = 1$ the action then reads

$$S = \mathbb{N}B\int d\widetilde{\tau}d\widetilde{\rho}\,\widetilde{\tau}\widetilde{\rho}^3\mathbb{A}\sqrt{\left(1 + \mathbb{C}\frac{1}{(\widetilde{\rho}^2+\widetilde{L}^2)^2}\right)\left(1 + \widetilde{L}'^2 - \mathbb{B}\frac{\dot{\widetilde{L}}^2}{(\widetilde{\rho}^2+\widetilde{L}^2)^2}\right)}\ , \quad (3.2.10)$$

with $\mathbb{A}, \mathbb{B}, \mathbb{C}$ as in (3.2.5)-(3.2.7) but now expressed in terms of $\widetilde{\tau}, \widetilde{\varepsilon}_0, \widetilde{\rho}$, and $\widetilde{L}$.

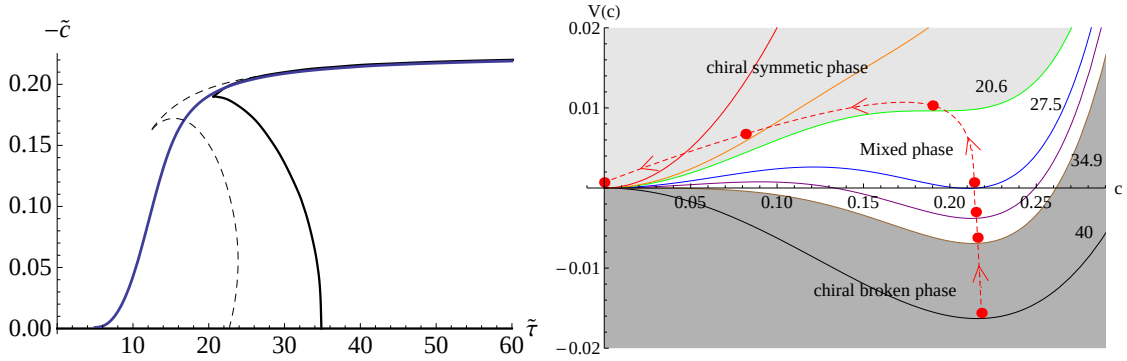

(a) (b)

Figure 3.2: A summary of our main results showing the first order phase transition in our various approaches. (a) The condensate $\widetilde{c}(\widetilde{\tau})$ in the equilibrium (black), adiabatic (dashed) and non-equilibrium (blue) approaches. In the equilibrium description, the different branches correspond to the extrema of the potential $V(c)$ (b). The complete potential is obtained by a $U(1)$ rotation around the vertical axis. The dashed red curve schematically shows the path of the adiabatic heating evolution.

3.2.2 Naive equilibrium based approximation

An obvious first approximation to understanding the time dependent chiral phase transition in this set up is to use the equilibrium results from section 2.1. There we described how the D7 embedding behaved in the background of a fixed size black hole and determined the quark condensate as a function of temperature. In the cooling plasma geometry of section 2.2 the black hole horizon moves as a function of time $\widetilde{\tau}$ as

$$\tilde{r}_H = \frac{\tilde{\varepsilon}_0^{1/4}}{3^{1/4}\widetilde{\tau}^{1/3}}\left(1 - \frac{\eta_0}{2\tilde{\varepsilon}_0^{1/4}\tilde{\tau}^{2/3}}\right) . \tag{3.2.11}$$

If this heating were very slow (as it is at large $\widetilde{\tau}$) we would expect to be able to plot the quark condensate against $\widetilde{\tau}$ by simply substituting for the temperature T in the equilibrium results. We show that plot in Fig. 3.2a (black solid curve) which follows directly from the c-T plot in Fig. 3.1.

We can recast the $\widetilde{c}$ vs. $\widetilde{\tau}$ plot schematically as a time dependent effective potential by fitting it at each value of $\widetilde{\tau}$ to a potential of the form

$$V = m^2\widetilde{c}^2 + \lambda\widetilde{c}^4 + \lambda'\widetilde{c}^6 \tag{3.2.12}$$

using the values of $\widetilde{c}$ at the extrema to fix the parameters (the overall scale is not set but the figure is intended to only be schematic). We plot this in Fig. 3.2b. This is the standard picture of a first order transition.

It is important to interpret these plots correctly. Firstly note that there is a $\widetilde{c} = 0$ solution for all $\widetilde{\tau}$. If we begin at high temperature with the symmetric flat embedding and cool slowly or adiabatically (*i.e.* move to large $\widetilde{\tau}$) then we can remain in that embedding for all $\widetilde{\tau}$. Above the time $\widetilde{\tau}_a = 20.6$ two extra solutions for the condensate develop and these, as we will discuss, trigger the first order transition. At large $\widetilde{\tau}$ the $\widetilde{c} = 0$ flat embedding becomes a local maximum of the effective potential. To stay in the flat embedding for all $\widetilde{\tau}$ is the extreme limit of super-cooling the high temperature phase into an unstable vacuum state.

The top trajectory in the $\widetilde{c}$ vs. $\widetilde{\tau}$ plot is best thought about in the time reversed solution that is heating up. At early times (large $\widetilde{\tau}$ in the plot) the solution is the $T = 0$ symmetry breaking

D7 embedding vacuum. Now as we heat adiabatically the condensate tracks along the trajectory to smaller $\widetilde{\tau}$. The solution ceases to exist at $\widetilde{\tau}_a$, where the cusp in the (black) curve is, indicating that the minimum of the effective potential corresponding to this solution has ceased to exist at $\widetilde{\tau}_a$. At this point the brane will move quickly, as an out of equilibrium configuration, ending as the flat embedding or oscillating about it. The real-time evolution of the configuration is represented by the path of red dots in Fig. 2b. Starting from the global minimum with $c \neq 0$, the minimum is lifted up and the configuration moves adiabatically. At $\widetilde{\tau}_a$ the minimum disappears and the system roles down the potential to the true vacuum with $c = 0$. The equilibrium results can not tell us about this motion.

Now we also see the role of the middle arc in the plot - these solutions are symmetry breaking embeddings that end on the horizon and they are a local maximum of the potential lying between the two minima (the embeddings of the top trajectory and the flat embedding).

In fact the first order transition point between the symmetry preserving and the symmetry breaking embeddings can be computed from the free energy in the equilibrium computation. This transition occurs at $\widetilde{\tau}_c = 27.5$, where the local and the global minimum in the effective potential interchange their roles, *i.e.* for $\widetilde{\tau}_c \geq 27.5$ the symmetry breaking vacuum (with $c \neq 0$) becomes the global minimum. Another important time determined by the equilibrium computation is $\widetilde{\tau}_b = 34.9$ where the mixed phase ends at large $\widetilde{\tau}$.

Our first task in solving the PDEs for the D7 brane motion that result from (3.2.4) is to demonstrate that this description is essentially correct - we will see that it is. We will try to find confirmation of the times $\widetilde{\tau}_{a-c}$ of these events. The more interesting task is that we will be able to follow the evolution of a particular initial condition through the phase transition. Of course in the first order transition the brane configuration does not discontinuously leap between the symmetry breaking embedding to the flat embedding but evolves continuously. We will provide solutions for this evolution.

Another interesting phenomena associated with a first order transition is bubble formation. In real systems thermal energy will lead to volumes of space which have more energy than an equilibrium like state in a local minimum of the potential at any particular time. These volumes may "climb" over the potential hill to the other local minimum during the mixed phase period shown in Fig. 3.2. These bubbles then grow or contract triggering the phase transition around $\widetilde{\tau}_c$ ending any super-heated or cooled phase. We will not look at (x_3) spatial dependent brane embeddings. However, we can inject kinetic energy in the holographic directions of our description into the brane configuration before we heat or cool it to see the configurations moving more quickly between the two local minima than the lowest energy configuration. This will allow us to test the time period in which the mixed phase exists in the out of equilibrium problem.

3.2.3 Adiabatic dynamic D7 brane embeddings

Our first study of the PDEs describing the D7 embedding in the expanding plasma geometry will be to study adiabatic expansion. The non-linear partial differential equations resulting from (3.2.10) can again be transformed into a set of second-order ordinary differential equations as we reviewed for the case with no symmetry breaking in section 2.2. For that, we use the late-time expansion

$$\widetilde{L}(\widetilde{\tau},\widetilde{\rho}) = f_0(\widetilde{\rho}) + \sum_{i=1}^{\infty} f_i(\widetilde{\rho})\widetilde{\tau}^{-\frac{i}{3}}\,. \tag{3.2.13}$$

Thus we will be following the evolution of the symmetry breaking embedding as τ decreases. There is also the solution $f_i = 0$ which corresponds to the symmetric embedding. Note that, contrary to (3.1.20), a nontrivial asymptotic embedding $f_0(\widetilde{\rho})$ is assumed because of the repelling effect of the magnetic field. The equations for every $f_i(\widetilde{\rho})$ can be obtained order by order in $\tau^{-\frac{1}{3}}$, which will be solved recursively. Unlike (3.1.21) these equations are quite lengthy and will not be presented here.

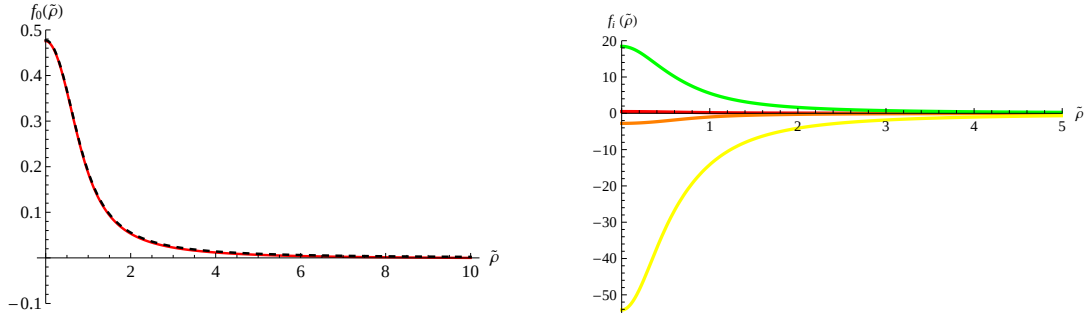

(a) (b)

Figure 3.3: Solutions of the ODEs in the adiabatic approximation - $f_{0,4,8,10}(\widetilde{\rho})$ for $\widetilde{\varepsilon}_0 = 1$. (a) f_0 (red) compared to the dashed curve which is the profile obtained in the static case at $T = 0$. (b) f_0 (red), f_4 (orange), f_8 (yellow), f_{10} (green).

They do not allow for an analytic solution such as (3.1.24) but can be numerically solved without any difficulty. As in the static case [83], there are expected to be two types of brane solutions, Minkowski and black hole embeddings, depending on whether the brane ends on or above the horizon.

For Minkowski embeddings, the boundary conditions are

$$f_i'(0) = 0 \qquad \text{and} \qquad f_i(\infty) = 0\,, \tag{3.2.14}$$

as before. With these boundary conditions, we find non-trivial profiles $f_i = f_i(\widetilde{\rho})$ for $i = 0, 4, 8, 10$, and $f_i = 0$ otherwise. A general dynamical embedding function is therefore of the form

$$\widetilde{L}(\widetilde{\tau}, \widetilde{\rho}) = f_0(\widetilde{\rho}) + \frac{f_4(\widetilde{\rho}; \widetilde{\varepsilon}_0)}{\widetilde{\tau}^{4/3}} + \frac{f_8(\widetilde{\rho}; \widetilde{\varepsilon}_0)}{\widetilde{\tau}^{8/3}} + \frac{f_{10}(\widetilde{\rho}; \widetilde{\varepsilon}_0, \eta_0)}{\widetilde{\tau}^{10/3}}\,, \tag{3.2.15}$$

where we neglect terms with $i > 11$ since they are beyond the validity regime of our approximation of the boost-invariant metric.[3] The numerical plots of the non-trivial profiles f_i $(i = 0, 4, 8, 10)$ are shown in Fig. 3.3.

These profiles have the following qualitative properties. As compared to the solution (3.1.24) for $B = 0$, there are additional non-trivial profiles, f_0 and f_4. The profile f_0 agrees with that in the static case ($\widetilde{\tau} \to \infty$) [89–91] (dashed curve in Fig. 3.3a) We found that the equation for f_0 is independent of $\widetilde{\varepsilon}_0$ and η_0, which is natural since at $\widetilde{\tau} \to \infty$ the system achieves equilibrium at low temperature and will not depend on the non-equilibrium dynamics (η_0) or specific initial conditions ($\widetilde{\varepsilon}_0$) anymore. The profiles f_4 and f_8 depend on $\widetilde{\varepsilon}_0$ and have a negative sign, which reflects the attraction of the D7 brane to the black hole. f_{10} is the first profile which depends on η_0. In contrast to f_4 and f_8, f_{10} has a positive sign showing the dragging effect, as in the zero B case around (3.1.25). The big amplitudes of f_4, f_8, and f_{10} will be suppressed at large $\widetilde{\tau}$ by negative powers of $\widetilde{\tau}$. For self-consistency we will only consider the $\widetilde{\tau}$ region where all the sub-leading terms are well dominated by the leading terms, *i.e.* $f_0 \gg f_4\widetilde{\tau}^{-3/4} \gg \cdots$. Some of the final embedding profiles $\widetilde{L}(\widetilde{\tau}, \widetilde{\rho})$ are shown in Fig. 3.4, where the green lines are plotted by plugging the numerical data of Fig. 3.3 into (3.2.15).

We would not expect this expansion approach to work beyond the point where the symmetry breaking embedding ceases to be even a local minimum because higher order terms will grow. One can nevertheless plot solutions using $f_0 - f_{10}$ that reach down all the way to the horizon. We will

[3] In principle there may be a finite f_{12}, but we will ignore it since it is a higher order term.

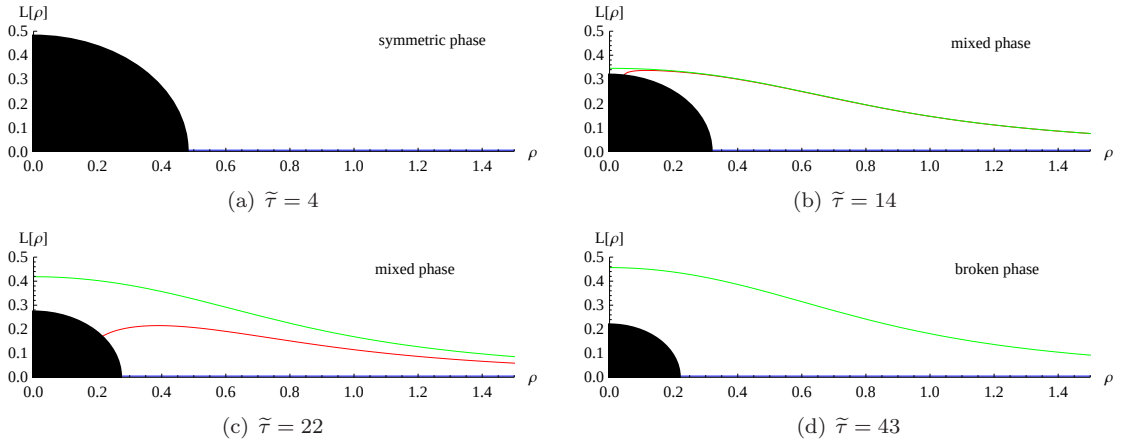

(a) $\widetilde{\tau} = 4$ (b) $\widetilde{\tau} = 14$

(c) $\widetilde{\tau} = 22$ (d) $\widetilde{\tau} = 43$

Figure 3.4: Embedding profiles $L(\widetilde{\tau}, \widetilde{\rho})$ obtained from the adiabatic ODE expansion method for $\widetilde{\varepsilon}_0 = 1, \eta_0 = 0.3102$ before (a), during (b,c) and after the phase transition (d): Minkowski embedding (green), black hole embedding (red), flat embeddings (blue).

use the full PDE solutions in the next section to test the point where the expansion has broken down.

In fact early in our studies we tried to use the expansion even for black hole embeddings. The ODEs for the f_i do not contain the horizon however. We attempted to put the horizon in by hand by imposing boundary conditions relevant to a black hole. For each point in the $L - \rho$ plane if we assume a horizon is present we can deduce the value of τ from (3.2.11) - one can impose some boundary condition such as orthogonality to the posited horizon and seek solutions for each f_i. This correctly gives one massless solution at each $\widetilde{\tau}$ and they look very similar to the equilibrium black hole embeddings. In fact though on solving the full PDEs we realize that this is far beyond the point where the expansion method has collapsed! We will include some of the resulting curves below though as evidence of the break down of the ODE approximation.

Fig. 3.4 shows the embedding profiles at various stages of the evolution of the expanding plasma. The black hole horizon (3.2.11) is indicated by a black quarter circle in the figure. Its size decreases with time corresponding to a cooling and expanding plasma. Fig. 3.4 reflects the division of the quark-gluon plasma into the three phases described above.

The quark condensate as a function of time can be read form the asymptotic form of the solutions

$$\widetilde{L}(\widetilde{\tau}, \widetilde{\rho}) \sim \frac{\widetilde{c}(\widetilde{\tau})}{\widetilde{\rho}^2} \ . \tag{3.2.16}$$

We plot these results in Fig. 3.2a (the dashed lines) for comparison to the equilibrium inspired results. The main result here is that the late time behaviour is indeed just the equilibrium expectations. Where the curved line deviates from the equilibrium results is in fact a sign that the expansion used in this section has broken down, the configuration is out of equilibrium and adiabatic behaviour is no longer possible. Full solutions of the PDEs will show this in the next section.

3.2.4 Full PDE solutions

In the previous section we interpreted our solution obtained from the ordinary differential system as the evolution of extremum states in the potential. This evolution also reflects the real time

dynamics of the plasma whenever there is a unique deep global minimum for the vacuum state, because the embedding time dynamics is expected to be well localized around the minimum. This is the case in the chiral symmetric phase at early times and in the broken phase at late times. In the mixed phase at intermediate times there appears also a local minimum in addition to the global minimum. The small potential barrier separating these minima is potentially easily overcome by a fluctuation. The path of the local maximum seen in the adiabatic approach will not be realized as a dynamical solution since it is unstable. Further below the critical time $\widetilde{\tau}_a$ where the symmetry breaking minimum disappears a heating vacuum will be left in a very non-equilibrium state that again can not be followed using the expansion technique of section 3.2.3.

To find the real time evolution of the chiral transition out of equilibrium, we need to solve the PDE directly and compare the solution with our previous approximate solutions. In practice it is more convenient to consider a heating process than a cooling one[4] because we can use a well defined starting configuration at large $\widetilde{\tau}$ as an initial condition of our partial differential equation, *i.e.*

$$\widetilde{L}(\widetilde{\tau}\to\infty,\widetilde{\rho}) = f_0 \ , \qquad \partial_{\widetilde{\tau}}\widetilde{L}(\widetilde{\tau}\to\infty,\widetilde{\rho}) = 0 \ , \tag{3.2.17}$$

with f_0 as in (3.2.15). For simplicity, we impose only Neumann boundary conditions at $\widetilde{\rho}=0$ associated to Minkowski embeddings and a zero bare quark mass condition at $\widetilde{\rho}\to\infty$ to study the spontaneous symmetry breaking,

$$\partial_{\widetilde{\rho}}\widetilde{L}(\widetilde{\tau},\widetilde{\rho}=0) = 0 \ , \qquad \widetilde{L}(\widetilde{\tau},\widetilde{\rho}\to\infty) = 0 \, . \tag{3.2.18}$$

The conditions (3.2.17) and (3.2.18) completely determine the dynamics with the partial differential equation derived by varying the action (3.2.10). Again, the actual expression of the equation of motion is lengthy and will not be shown here.

Numerically we solve the equation using Mathematica's inbuilt PDE solvers. These are somewhat temperamental and one needs to spend considerable time adjusting precision tolerances in order to find smooth solutions in sensible periods of computer time. When we have such solutions we test their stability to changes in precision settings to ensure they are reliable.

With the boundary conditions above we can run our simulations until the embeddings touch the black hole. Beyond that one needs dynamic boundary conditions along the black hole surface. At least in the coordinates we use here this is a hard problem. We have found a simple trick that seems to produce sensible black hole embeddings though. After the D7 has touched the horizon at $\widetilde{\rho}=0$ we artificially hold the embedding at the top of the horizon. The large $\widetilde{\rho}$ evolution of the D7 is local and relatively unaffected by this incorrect embedding at small $\widetilde{\rho}$. Further, as has been observed before, solutions shooting from the black hole horizon experience a numerical attraction onto the unique regular black hole embedding ending at a given point on the horizon. The result is that we get numerical solutions like those shown in Fig. 3.5 (*e.g.* the red, blue, or orange curve) where the D7 follows the horizon before shooting out to large $\widetilde{\rho}$. We believe that these represent very good approximations to the large $\widetilde{\rho}$ embeddings solutions. Since we extract the condensate $\widetilde{c}$ at large $\widetilde{\rho}$ we will live with the improper near horizon behaviour. It would of course be interesting to try to improve on this with dynamic boundary conditions in the future.

As a first example of a solution we will study the super-heated symmetry breaking vacuum. At large $\widetilde{\tau}$ we use the leading terms in the expansion from Section 3.2 to find the UV configuration - one needs to use several terms in the expansion to find the embedding with no extra energy. We then solve for the evolution to low $\widetilde{\tau}$. In Fig. 3.5 we show plots of the embedding $\tilde{L}(\widetilde{\rho})$ for different $\widetilde{\tau}$ with the black hole's position for each $\widetilde{\tau}$ also shown. We expect that the near horizon behaviour is not correct but the far UV embedding should approximate the solution we seek well. In the 3d

[4] In principle, time reversed heating is justified only at zero viscosity since a finite viscosity results in decreasing entropy. However, we keep a finite viscosity in our numerics since it has a negligible effect and the results are relevant to the cooling case.

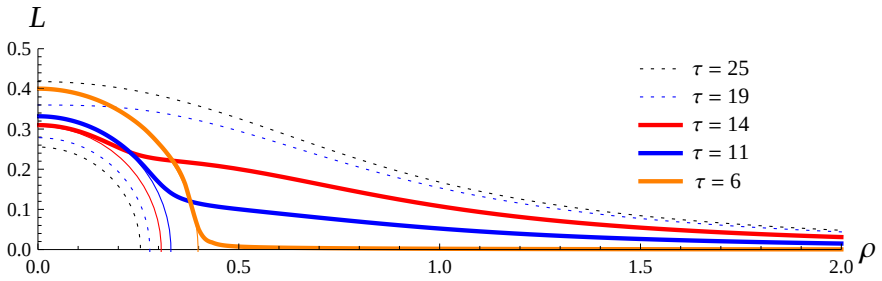

Figure 3.5: The embedding profiles $\tilde{L}(\widetilde{\tau},\widetilde{\rho})$ from the full PDE solution for a solution starting in the low temperature symmetry breaking vacuum ($\kappa = 1$).

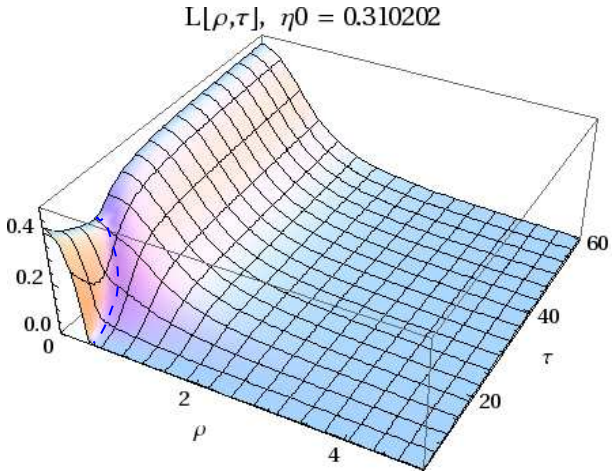

Figure 3.6: 3D plot of the embedding profile $\tilde{L}(\widetilde{\tau},\widetilde{\rho})$.

plot of $\widetilde{L}(\widetilde{\tau},\widetilde{\rho})$ shown in Fig. 3.6 this corresponds to excising the interior of the region indicated by the dashed blue line.

A smooth evolution is apparent. To compare this to our various approximations above we also plot the condensate as a function of time in Fig. 3.2a (blue curve). Again the solution follows the equilibrium estimate and the expansion solution at large $\widetilde{\tau}$. In the period $\widetilde{\tau}_{a-c}$ it follows the equilibrium result not the ODE expansion results showing that expansion had broken down before the brane left the mixed phase. The success of the equilibrium approximation suggests we should take its estimate of the transition points $\widetilde{\tau}_a$ (where the local symmetry breaking minimum vanishes) and $\widetilde{\tau}_c$ (where the two minima of the mixed phase are degenerate in energy) as correct. The full PDE solutions allow us to know in addition the behaviour of the condensate when we have heated above the temperature where the super-heated phase has stopped having a local minima (beyond $\widetilde{\tau}_a$). This is the main result of our analysis here.

It would be nice to test the equilibrium configurations estimate for the length of time in which the mixed phase exists ($\widetilde{\tau}_b - \widetilde{\tau}_a$ which is about 10 units of $\widetilde{\tau}$). This we can do by looking at some simple out of equilibrium configurations. For the plots so far shown we computed $\dot{\tilde{L}}(\widetilde{\rho})$ at some large $\widetilde{\tau}$ from the f_4 term in the expansion for $\widetilde{L}(\widetilde{\rho},\widetilde{\tau})$. We can give the configuration more energy by simply multiplying that $\dot{\tilde{L}}(\widetilde{\rho})$ by a numerical factor, κ [5]. One might think of these initial states as

[5]In practice, we fix some $\widetilde{\tau}_{\max}$ and modify the initial conditions (3.2.17) as $L(\widetilde{\tau}\to\widetilde{\tau}_{\max},\widetilde{\rho}) = L^{ODE}(\widetilde{\tau}_{\max},\widetilde{\rho})$ and $\dot{L}(\widetilde{\tau}\to\widetilde{\tau}_{\max},\widetilde{\rho}) = \kappa * \dot{L}^{ODE}(\widetilde{\tau}_{\max},\widetilde{\rho})$, where L^{ODE} is given by (3.2.15).

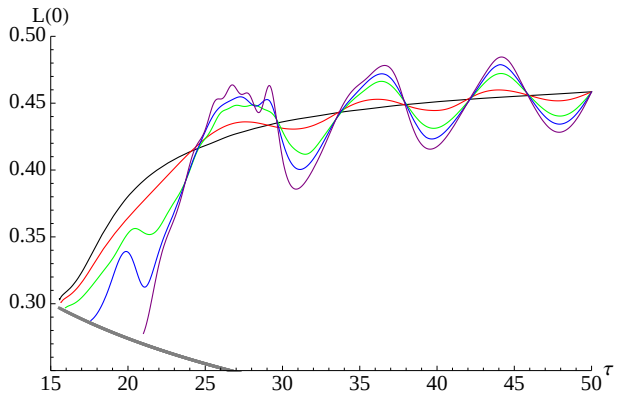

Figure 3.7: Plots of the IR position of the D7 brane against time for a number of large time initial conditions with different energy. Initial velocities: black ($\kappa = 1$), red ($\kappa = 10$), green ($\kappa = 30$), blue ($\kappa = 40$), purple ($\kappa = 50$). The thick black line is the horizon.

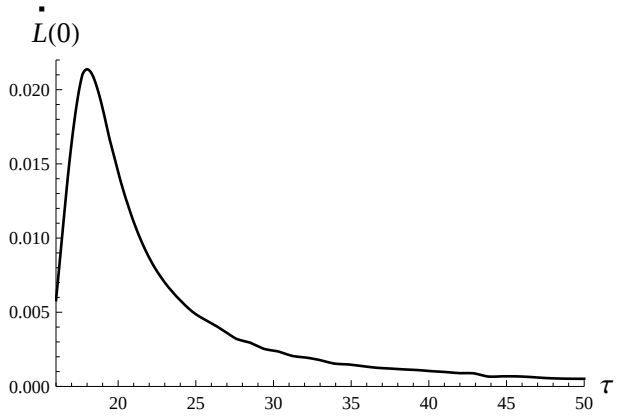

Figure 3.8: The IR speed of the D7 brane against time for the $\kappa = 1$ initial condition.

thermally excited versions of the asymptotic vacuum. In Fig. 3.7 we plot the evolution of $\widetilde{L}(\widetilde{\rho} = 0)$ as a function of $\widetilde{\tau}$ for a number of such states. At large $\widetilde{\tau}$ when the theory is cold the unique vacuum is the symmetry breaking one and with extra energy the configuration oscillates about that minimum. The motion is simple harmonic as can be seen from the independence of the period on the amplitude of the oscillations. As the solutions approach $\widetilde{\tau}_c$ the different solutions begin to diverge. The solution with $\kappa = 10$ lies close to the equilibrium curve - the oscillations about the minimum are small and the state stays super-heated. When $\kappa = 30, 40$ $\widetilde{L}(0)$ falls more quickly suggesting that at least some of the brane's length in ρ has escaped the local potential minimum. The upwards wiggles suggest that some of the length is still repelled back into the well though. Finally though by $\kappa = 50$ the brane has ridden over the potential barrier and escaped the local minimum. The difference in arrival times at the horizon for these configurations (about 6 units of $\widetilde{\tau}$) is a rough estimate of the period of the mixed phase. It seems to broadly match the equilibrium inspired picture again.

In Fig. 3.8 we plot the motion of the IR $\rho = 0$ end point of the brane with time for a low energy configuration ($\kappa \simeq 1$). The brane certainly seems localized in a minimum down to a time of order $\widetilde{\tau} = 27$ (compare to the equilibrium estimate that the mixed phase begins at $\widetilde{\tau}_b = 34.9$ and becomes meta-stable at $\widetilde{\tau}_c = 27.5$). Further the steepest period of acceleration is below $\widetilde{\tau} = 22$

(to be compared with the equilibrium estimate for when the metastable vacuum ceases to exist $\widetilde{\tau}_a = 20.6$). We conclude that this system is indeed a super-heated state that survives in the local minimum until very close to the equilibrium estimate for $\widetilde{\tau}_a$. Note the other obvious feature in the plot is the deceleration just below $\widetilde{\tau} = 20$. This corresponds to where in our simulation the D7 first impacts on the black hole - at smaller $\widetilde{\tau}$ we hold the D7 at the horizon as discussed above so this behaviour is an artefact. A full solution would continue to accelerate along the horizon.

These configurations with excess $\dot{L}$ are also very much linked to bubble formation. A bubble forms in the mixed phase when a volume of space has excess energy due to a thermal fluctuation and escapes the local minima early. Here by treating the whole space as one we are essentially describing the formation of a large homogeneous bubble. It would be interesting in the future to try to study x dependent initial conditions to understand how quickly or slowly bubbles grow.

3.3 Dependence of the condensate on B

In the previous section we focused on the chiral transition induced by a magnetic field, which simply played the role of an intrinsic symmetry breaking scale. In this section we turn to the physics depending on B more quantitatively.

To make analytic progress we will concentrate on the adiabatic (ODE) approach in which we rescaled all variables by some power of B, see (3.2.9). In order to study the dependence of the quark condensate on B, we use the original parameters, in terms of which the condensate can be expanded as

$$c(\tau, B) = B^{3/2}\left(c_0 + \frac{1}{B^{2/3}}\frac{c_4(B^{-4/3}\varepsilon_0)}{\tau^{4/3}} + \frac{1}{B^{4/3}}\frac{c_8(B^{-4/3}\varepsilon_0)}{\tau^{8/3}} + \frac{1}{B^{5/3}}\frac{c_{10}(B^{-4/3}\varepsilon_0, \eta_0)}{\tau^{10/3}}\right). \tag{3.3.1}$$

Note that c_0 is independent of ε_0, η_0 and η_0 enters only in c_{10}. The B dependence of the leading term agrees with that in the static (zero temperature) case [89–91], *i.e.* it scales as $B^{3/2}$. The first subleading term ($\sim \tau^{-4/3}$) may be compared to the finite temperature case [89–91, 96, 97]. In the adiabatic approximation, where $T \sim \tau^{-1/3}$, this term scales approximately like $T^4 B^{-5/6}$. However, due to the B dependence of c_4, this scaling is not exact. In general, the effect of the subleading terms is to lower the exponent in $c(\tau, B) \sim B^\nu$ to a value $\nu < 3/2$. The scaling of the total condensate $c(\tau, B)$ with B will again be determined numerically.

Fig. 3.9a shows our results for the condensate for various values of the magnetic field. We have only plotted the condensates associated with the Minkowski embeddings, which exist for some time $\tau > \tau_*(B)$. Here τ_* is defined as the time, when the Minkowski solution meets the black hole solution (This corresponds to the cusp in the dashed curve in Fig. 3.2a). We take τ_* to mark the time of the phase transition. As can be seen from Fig. 3.2a the early time behaviour is an imperfect approximation to the full PDE solutions but the later time solutions are consistent with the solutions. We find that for fixed τ, or equivalently for fixed temperature, the condensate grows with increasing magnetic field. In the limit $\tau \to \infty$ (*i.e.* at zero temperature), we find the following dependence on B:

$$\lim_{\tau\to\infty} c(\tau) = c_0 B^{3/2} = 0.223 B^{3/2}, \tag{3.3.2}$$

which is in agreement with the zero temperature result [89–91]. For earlier times, the dependence on B is shown in Fig. 3.9b. We find numerically that $c(\tau, B) \sim B^\nu$ where the power ν decreases from 1.5 at large τ to approximately 1.0 at small τ. In other words, the dependence on B tends to become linear at high temperatures. Our results hold for sufficiently strong magnetic fields. At small B the system is in the symmetric phase ($c = 0$).

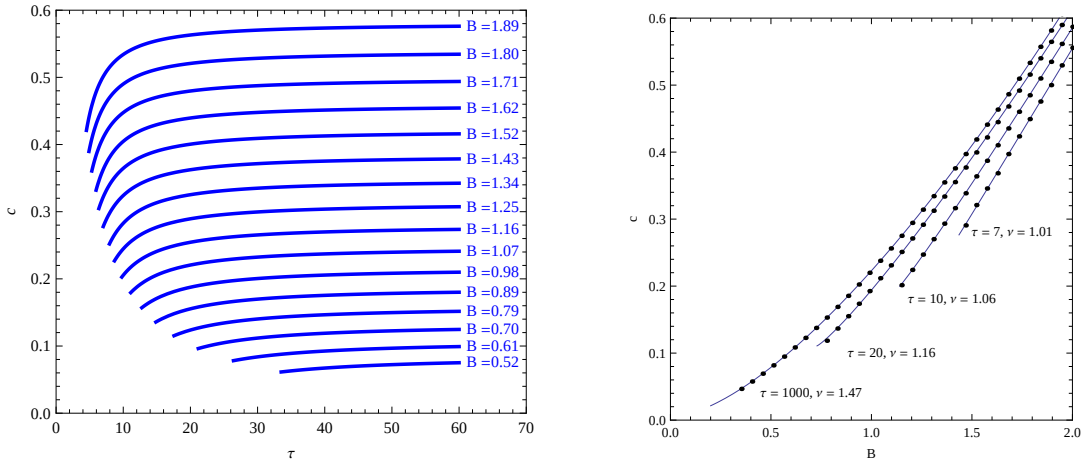

(a) (b)

Figure 3.9: The condensate $c(\tau, B)$ ($\varepsilon_0 = 1$) from the ODE adiabatic approximation results. (a) condensate $c(\tau)$ for various B. (b) showing $c(B) \propto B^{\nu}$ for $\tau = 7, 10, 20, 1000]$

The tendency for the condensate to increase with B is in qualitative agreement with observations in chiral perturbation theory [111, 112] ($\propto B^{3/2}$ for strong fields, $\propto B$ for weak fields), in the Nambu-Jona-Lasinio model [113] ($\propto B^2$), in a confining deformation of the holographic Karch-Katz model [114] ($\propto B^2$), and in SU(2) [115] ($\propto B$) and SU(3) [6, 7] lattice calculations ($\propto B^{1.6\pm0.2}$). The dependence on B typically ranges from linear to quadratic behaviour, *i.e.* the powers of B are in the range $1 \leq \nu \leq 2$.

We may also study the effect of B on the time of the chiral transition which is marked by τ_*. From the D-brane picture we expect that τ_* decreases with B. For large B, the repelling force caused by the B-field is much stronger than the attractive force of the black hole. Even at early times, Minkowski embeddings, associated to stable mesons, are therefore favoured over black hole embeddings, which implies that the meson melting process sets in at some earlier time, *i.e.* at higher temperatures.

Fig. 3.10 shows τ_* as a function of B. We find that τ_* indeed decreases with increasing B as $\tau_*(B) \sim B^{-1.55}$. The numerically found exponent -1.55 for the scaling of B is close to -1.5 for the case of vanishing shear viscosity, which can be explained as follows. At $\widetilde{\tau} = \widetilde{\tau}_*$ and $\eta = 0$, the horizon is located at

$$\tilde{r}_* = \frac{\widetilde{\varepsilon}_0^{1/4}}{3^{1/4}\widetilde{\tau}_*^{1/3}} = \frac{\varepsilon_0^{1/4}}{3^{1/4}\sqrt{B}}\tau_*^{-1/3} = \frac{1}{3^{1/4}(12.45)^{1/3}} \ , \tag{3.3.3}$$

where the last equality is from the numerical value of $\tilde{r}_*$ at $\widetilde{\varepsilon}_0 = 1$. Thus

$$\tau_* = 12.45 B^{-1.5} \, , \tag{3.3.4}$$

where for the numerical analysis we chose $\varepsilon_0 = 1$. The deviation from -1.5 is due to the effect of the shear viscosity. We also numerically confirmed that the exponent is 1.5 without viscosity.

This scaling of τ_* may be compared to results for the critical temperature T_c of the phase transition in the static case. In the adiabatic approximation (when $\eta_0 = 0$), $T \sim \tau^{-1/3}$, which implies $T_* \sim B^{1/2}$. This square root behaviour is in agreement with the result for the critical temperature T_c in the static approach [96, 97] and with [112] for strong magnetic fields. It is also in qualitative agreement with studies in QCD [116, 117].

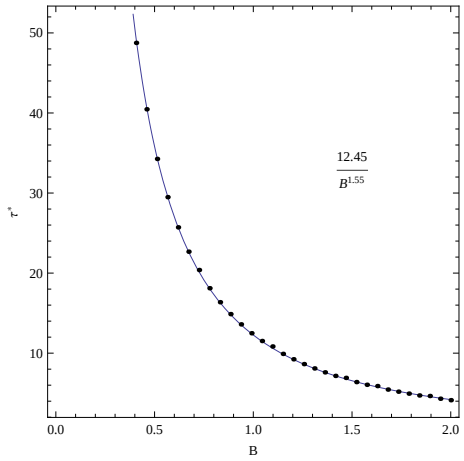

Figure 3.10: τ_* as a function of B ($\varepsilon_0 = 1$) from the ODE adiabatic approximation results.

Finally we consider the effect of changing the viscosity. The viscosity effect is very small, since it is doubly suppressed by both large $\widetilde{\tau}$ and small η_0. This can also be seen in Fig. 3.11, where the condensate is plotted for four cases: the green is the leading term, the blue includes the subleading term, the red includes up to the third term and the black is the full expression. The viscosity effect is then the difference between the red and black curves. There is a small visible difference only at small $\widetilde{\tau}$.

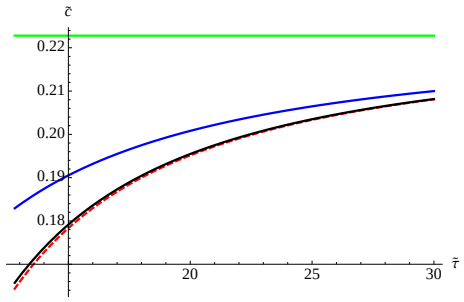

Figure 3.11: The condensate $\widetilde{c}(\widetilde{\tau})$. The green curve is the leading term, the blue is up to subleading term, the red is up to third term and the black is the whole expression.

3.4 Discussion

We have analyzed the first order chiral and meson melting phase transition in a warming or cooling strongly coupled gauge theory with quarks using the AdS/CFT Correspondence. We have developed numerical techniques to study the PDE that describes the motion of a D7 brane in a time dependent geometry. In particular this allows us to explicitly find smooth solutions of the non-equilibrium configurations that are necessarily part of the transition. These results confirm the equilibrium analysis of the transition but also go beyond them. For example we have described the formation of large homogeneous bubbles in the mixed phase of the transition. In the future it would be interesting to study spatially inhomogeneous bubbles to understand their growth although this would require the solution of a 2+1 dimensional PDE which is potentially more numerically tricky.

To keep our problem a simpler 1+1 dimensional PDE we also restricted motion of the D7 brane to the holographic coordinates L and ρ. There could also of course be fluctuations in the holographic angular direction ϕ which we have not described. Such configurations might be useful in the study, for example, of disordered chiral condensates [118]. We may also consider the finite density case by turning on the time component of the $U(1)$ gauge field on the probe brane [96, 97, 119, 120].

We hope that the system we have studied can shed some light on first order transitions in a range of strongly coupled gauge theories including perhaps QCD. The $\mathcal{N} = 4$ background, however, does deconfine in the presence of an infinitesimal temperature, which is not expected in simple QCD. We note though that there are several arguments in favour of a possible splitting of the deconfinement and chiral transitions in QCD in the presence of a strong magnetic field [116]. While the temperature of the chiral transition increases [116, 121], the temperature of the deconfining transition either decreases with increasing magnetic field [122] or increases but much slower than the chiral transition [116]. Both transitions become first-order transitions and a new phase with broken chiral symmetry and deconfinement appears for sufficiently strong magnetic fields. So, it is the region of the T-B phase diagram with strong magnetic fields and above the deconfinement temperature in which our model might be qualitatively compared with QCD.

Chapter 4

Holographic dual of a boost-invariant plasma with chemical potential

In the recent years, the application of the AdS/CFT correspondence [59–61] to the quark-gluon plasma (QGP) has become a very active research area. One line of research within such holographic studies was initiated by Janik and Peschanski [74] who established a time-dependent gravity dual of the boost-invariant flow of an $\mathcal{N} = 4$ plasma. This geometry has mainly been studied in the regime of large proper time, when the system is near equilibrium and approaches the hydrodynamic regime (see however [123,124]). In [75,107–110,125–127] higher-order corrections to this late-time background were constructed and found to be equivalent to a gradient expansion of hydrodynamics, see [106] for a review.

An important aspect of the plasma which has not yet received much attention in a time-dependent gravity background is the effects of chemical potentials, even though an asymptotic boost-invariant geometry (*without* corrections) dual to an $\mathcal{N} = 4$ plasma with $U(1)$ R-charge is known for quite some time [128]. Also the transport coefficients of plasmas with $U(1)$ currents have already been holographically computed in [76,77,129–131] (up to second order). Such currents are generated, for instance, shortly after the collision of two heavy ions, when the two sheets of color glass condensates have passed through each other and longitudinal color electric and magnetic flux tubes are produced between the sheets [132]. This gives rise to a large topological charge density $F^{\mu\nu}_a \tilde{F}^a_{\mu\nu}$, which in turn leads to an imbalance of the number of quarks with left- and right-handed chirality and chemical potentials μ_R and μ_L. In addition to the usual baryon chemical potential $\mu = \frac{\mu_R+\mu_L}{2}$, one may therefore also consider a chiral chemical potential $\mu_5 = \frac{\mu_R-\mu_L}{2}$ which mimics the effect of an imbalanced chirality.

In this chapter we will construct a modification of the Janik-Peschanski background, which will additionally include a time-dependent $U(1)$ gauge field. The bulk theory will be five-dimensional Einstein-Maxwell gravity with a negative cosmological constant and a Chern-Simons term. As in the case without chemical potential, it appears to be difficult to find an analytic solution for all times and we will restrict to solving the equations of motion at late times. As a further simplification, we seek for a solution in which only the time-component of the $U(1)$ gauge field dual to the chemical potential is non-vanishing (the spatial components are set to zero). Asymptotically, at large proper time τ, we may expand the late-time geometry in powers of $\tau^{-2/3}$. Employing both Eddington-Finkelstein and Fefferman-Graham coordinates we present the late-time solution up to first order (in $\tau^{-2/3}$). The resulting background will essentially take the form of a time-dependent AdS_5 Reissner-Nordström solution whose inner and outer horizon move into the bulk of the AdS

space. This background can be extended to a full type IIB supergravity solution (by taking the product with an S^5) and is dual to a strongly-coupled $\mathcal{N}=4$ $SU(N)$ supersymmetric-Yang-Mills plasma with a non-vanishing chemical potential.

4.1 Late-time background in Eddington-Finkelstein coordinates

In this section we are interested in finding a late-time gravity dual of an expanding $\mathcal{N}=4$ viscous plasma with non-vanishing chemical potential.

The relevant five-dimensional Einstein-Maxwell-Chern-Simons action is given by

$$S=\frac{1}{16\pi G_5}\int d^5x\,\sqrt{-g_5}\left(R+12-F_{\alpha\beta}F^{\alpha\beta}+\frac{4\kappa}{3}\epsilon^{\sigma\alpha\beta\gamma\delta}A_\sigma F_{\alpha\beta}F_{\gamma\delta}\right), \tag{4.1.1}$$

where $\alpha,\beta,...$ denote the 5D bulk coordinates. The cosmological constant is $\Lambda=-6$ and the Chern-Simons parameter is fixed as $\kappa=-1/(2\sqrt{3})$. Also, $1/(16\pi G_5)=N_c^2/(8\pi^2)$ for an $\mathcal{N}=4$ plasma [76]. The corresponding equations of motion are given by the combined system of Einstein-Maxwell equations,

$$R_{\alpha\beta}-\frac{1}{2}g_{\alpha\beta}R-6g_{\alpha\beta}+2\left(F_\alpha{}^\gamma F_{\gamma\beta}-\frac{1}{4}g_{\alpha\beta}F^2\right)=0\,, \tag{4.1.2}$$

and covariant Maxwell equations (with Chern-Simons-term),

$$\nabla_\beta F^{\beta\alpha}+\kappa\epsilon^{\alpha\beta\gamma\delta\sigma}F_{\beta\gamma}F_{\delta\sigma}=0\,. \tag{4.1.3}$$

$F^{\alpha\beta}$ is the field strength of the $U(1)$ gauge field A_α we wish to introduce in the background.

4.1.1 Boosted black brane solution

Our starting point for the construction of a time-dependent solution is the *static* AdS_5 Reissner-Nordström (RN) black-hole solution [73]. Using ingoing Eddington-Finkelstein coordinates, we may write the RN metric and gauge field as

$$ds^2=-r^2(1-\frac{m}{r^4}+\frac{q^2}{r^6})dv^2+2dvdr+r^2d\vec{x}^2\,, \tag{4.1.4}$$

$$A=-\frac{\sqrt{3}q}{2r^2}d\widetilde{\tau}\,, \tag{4.1.5}$$

with mass m and charge q. Here v is a time-like coordinate (not to be mixed up with the scaling variable v introduced below), $\vec{x}$ are the spatial coordinates on the boundary, and r parameterizes the holographic direction. The location of the outer horizon $r_+=r_+(m,q)$ is given by the largest real positive root of $V(r_+)=r_+^6-mr_+^2+q^2=0$.

A charged black hole is dual to a fluid at finite temperature T and chemical potential μ. Both the Hawking temperature and the chemical potential are given in terms of r_+ by [73]

$$T=-\frac{1}{4\pi}g'_{vv}(r_+)\,,\qquad \mu=\frac{\sqrt{3}q}{2r_+^2}\,. \tag{4.1.6}$$

These relations can be inverted to give m and q as functions of T and μ [76],

$$m=r_+^4\frac{3\gamma-1}{\gamma+1}\,,\qquad q=\frac{2\mu}{\sqrt{3}}r_+^2\,, \tag{4.1.7}$$

with

$$r_+ = \frac{\pi T}{2}(\gamma+1)\,, \qquad \gamma = \sqrt{1+\frac{8\mu^2}{3\pi^2 T^2}}\,. \tag{4.1.8}$$

Following [75, 109], we now consider the corresponding five-dimensional boosted charged black brane solution given by

$$\begin{aligned} ds^2 &= -2u_\mu dx^\mu dr - r^2\left(1-\frac{m}{r^4}+\frac{q^2}{r^6}\right)u_\mu u_\nu dx^\mu dx^\nu + r^2 P_{\mu\nu}dx^\mu dx^\nu\,,\\ A &= \frac{\sqrt{3}q}{2r^2}u_\mu dx^\mu\,, \qquad P_{\mu\nu} = \eta_{\mu\nu}+u_\mu u_\nu\,, \end{aligned} \tag{4.1.9}$$

where u^μ is the boost velocity along x^μ ($\mu = 0,1,2,3$), and $m = m(\mu,T)$ and $q = q(\mu,T)$ as given by (4.1.7). From this solution we may deduce a time-dependent solution by choosing the frame $u^\mu = (1,0,0,0)$ and introducing an Eddington-Finkelstein proper time-like coordinate $\tilde\tau$ and rapidity-like coordinate y. We also substitute the asymptotic late-time behaviour of T [25] and μ,

$$T = \Lambda\widetilde\tau^{-1/3} \qquad \text{and} \qquad \mu = \widetilde\mu_0\widetilde\tau^{-1/3}\,, \qquad \Lambda, \widetilde\mu_0 = const.\,, \tag{4.1.10}$$

into the explicit expressions for m and q. Here we assumed $\mu \propto T$, as one would expect for a perfect fluid, such that the quotient $\mu/T = \widetilde\mu_0/\Lambda = const.$ is independent of time. This leads to the following metric[1]

$$\begin{aligned} ds^2 &= -r^2(1-\frac{m(\widetilde\tau)}{r^4}+\frac{q(\widetilde\tau)^2}{r^6})d\widetilde\tau^2 + 2d\widetilde\tau dr + (1+r\widetilde\tau)^2 dy^2 + r^2 dx_\perp^2\,,\\ A &= -\frac{\sqrt{3}q}{2r^2}d\widetilde\tau\,, \end{aligned} \tag{4.1.11}$$

with coefficients

$$m(\widetilde\tau) = b(\widetilde\tau)^{-4} \equiv r_+(\widetilde\tau)^4\frac{3\gamma-1}{\gamma+1}\,, \quad q(\widetilde\tau) = \frac{2\widetilde\mu_0}{\sqrt{3}\widetilde\tau^{1/3}}r_+(\widetilde\tau)^2\,, \tag{4.1.12}$$

$$r_+(\widetilde\tau) = \frac{\pi\Lambda}{2\widetilde\tau^{1/3}}(\gamma+1)\,, \quad \gamma = \sqrt{1+\frac{8\widetilde\mu_0^2}{3\pi^2\Lambda^2}}\,. \tag{4.1.13}$$

For $q = 0$ (or $\widetilde\mu_0 = 0$), this metric reduces to the uncharged (zeroth-order) late-time solution in Eddington-Finkelstein coordinates found in [109, 110, 127] ($m = b^{-4} = \pi^4\Lambda^4\widetilde\tau^{-4/3}$ there). Note that the size of the outer (and inner) horizon r_+ (r_-) decreases with time.

4.1.2 Zeroth-order solution and first-order correction

The boosted metric (4.1.11) is not an exact solution of the Einstein-Maxwell equations. It is a good approximation of the boost-invariant solution at large $\widetilde\tau$ though. At smaller $\widetilde\tau$, it receives subleading corrections corresponding to higher-order gradient corrections to the energy-momentum tensor and $U(1)$ current, which will be discussed in section 4.1.3. These corrections to the metric (4.1.11) can be found by choosing the following metric ansatz for the time-dependent solution:[2]

$$\begin{aligned} ds^2 &= -r^2 e^{a(\widetilde\tau,r)}d\widetilde\tau^2 + 2d\widetilde\tau dr + (1+r\widetilde\tau)^2 e^{b(\widetilde\tau,r)}dy^2 + r^2 e^{c(\widetilde\tau,r)}dx_\perp^2\,,\\ A &= d(\widetilde\tau,r)d\widetilde\tau\,. \end{aligned} \tag{4.1.14}$$

[1] There is an additional 1 in the factor $(1+r\widetilde\tau)^2$ in front of dy^2 which is not expected from the boosted solution (4.1.11). This is to ensure an asymptotic AdS space in the limit $\Lambda \to 0$, see [110] for details.

[2] For this particular ansatz, the Maxwell equation reduces to $\frac{1}{\sqrt{-g}}\partial_\beta(\sqrt{-g}F^{\beta\alpha}) = 0$. The Chern-Simons term is absent, since only $F_{r\widetilde\tau}$ and $F_{\widetilde\tau r}$ are non-vanishing.

As in the case without chemical potential, we may introduce the scaling variable $v = r\widetilde{\tau}^{1/3}$ and expand the metric coefficients in powers of $\widetilde{\tau}^{-2/3}$,

$$e^{a(\widetilde{\tau},r)} = A(v) + a_1(v)\widetilde{\tau}^{-2/3} + \dots\,, \tag{4.1.15}$$

$$e^{b(\widetilde{\tau},r)} = B(v)\exp(b_1(v)\widetilde{\tau}^{-2/3} + \dots)\,, \tag{4.1.16}$$

$$e^{c(\widetilde{\tau},r)} = C(v)\exp(c_1(v)\widetilde{\tau}^{-2/3} + \dots)\,. \tag{4.1.17}$$

Similarly, for the coefficient of the gauge field we choose

$$d(\widetilde{\tau},r) = D(v)\widetilde{\tau}^{-1/3}\exp(d_1(v)\widetilde{\tau}^{-2/3} + \dots)\,. \tag{4.1.18}$$

Note that the gauge field has an overall factor $\widetilde{\tau}^{-1/3}$. The existence of a late-time scaling variable v will be shown in section 4.2.2.

The system of Einstein-Maxwell equations (4.1.2) and Maxwell equations (4.1.3) can then be solved order by order in $\widetilde{\tau}^{-2/3}$. At zeroth-order in $\widetilde{\tau}^{-2/3}$, we find the coefficients

$$A(v) = 1 - \frac{m_0}{v^4} + \frac{\tilde{q}_0^2}{v^6}\,, \qquad B(v) = C(v) = 1\,, \qquad D(v) = -\frac{\sqrt{3}\tilde{q}_0}{2v^2}\,, \tag{4.1.19}$$

where we defined the time-independent variables

$$m_0 = b_0^{-4} \equiv \widetilde{\tau}^{4/3} m(\widetilde{\tau})\,, \qquad \tilde{q}_0 = \widetilde{\tau} q(\widetilde{\tau}) \tag{4.1.20}$$

with $m(\widetilde{\tau})$ and $q(\widetilde{\tau})$ as in (4.1.12). In the same way, we also define the variable

$$\zeta_+ = r_+(\widetilde{\tau})\widetilde{\tau}^{1/3} \tag{4.1.21}$$

from the (outer) horizon r_+ as given by (4.1.13). $A(v), ..., D(v)$ are in agreement with the metric (4.1.11) deduced from the boosted black brane.

At first order in $\widetilde{\tau}^{-2/3}$, we find the coefficients

$$\begin{aligned}
a_1(v) &= -\frac{4q_0^2}{3v^7} + \frac{2m_0}{3v^5} + \frac{C_2}{v^4}\,,\\
b_1(v) &= -2c_1(v) = -\frac{4}{3v} + C_3 + \frac{1}{6}\sum_{i=1}^{6}\frac{3C_1\log[v-\zeta_i] - 4\log[v-\zeta_i]\zeta_i^3}{3\zeta_i^4 - m_0}\,,\\
d_1(v) &= -\frac{2}{3v} + \frac{1}{2}v^2 C_1\,,
\end{aligned} \tag{4.1.22}$$

where ζ_i are the solutions of

$$\zeta_i^6 - m_0\zeta_i^2 + \tilde{q}_0^2 = 0\,. \tag{4.1.23}$$

The resulting expression for $b_1(v)$ is real, even though we need to consider all six roots of (4.1.23) including the imaginary ones. Explicit expressions for these roots can be found in appendix 4.3. Note that one of the six roots of this equation corresponds to the outer horizon ζ_+. In Reissner-Nordström solutions there is always an upper bound on the charge $\tilde{q}_0$, at which the discriminant of the equation (4.1.23) vanishes,

$$\tilde{q}_0 \leq \tilde{q}_0^{extr.} = \sqrt[4]{\frac{4}{27}m_0^3}\,. \tag{4.1.24}$$

For larger values of $\tilde{q}_0$, there would be a naked singularity at the origin. Remarkably, this bound is satisfied for any value of the quotient $\widetilde{\mu}_0/\Lambda$ and saturated in the limit $\widetilde{\mu}_0/\Lambda \to \infty$, as can be seen by substituting (4.1.20) with (4.1.12) into the bound (4.1.24). In other words, there is *no* bound on the chemical potential. Nevertheless, let us assume that $\widetilde{\mu}_0 \ll \Lambda$ in order to avoid potential stability problems [133], which arise when the black hole is close to extremality.

We still need to fix the integration constants $C_{1,2,3}$. C_1 can be found by requiring regularity of the first-order solution (4.1.22) at the outer horizon, *i.e.* C_1 should be a function of the positive root ζ_+. More precisely, by choosing

$$C_1 = \frac{4}{3}\zeta_+^3\,, \tag{4.1.25}$$

we cancel the $\log[v-\zeta_+]$ terms in $b_1(v)$, which are singular at $v=\zeta_+$. The metric then still contains singularities but they are hidden behind the outer horizon.

The constant C_3 is fixed by the requirement that the metric reduces to a pure AdS space in the limit $\Lambda \to 0$. This simply sets C_3 to zero,

$$C_3 = 0\,. \tag{4.1.26}$$

There is one remaining integration constant C_2 which can not be fixed at first order. Note that, in general, at each order k there is one integration constant which can only be fixed by regularity at order $k+1$ [109], C_2 in our case. Nevertheless, we may guess the correct value for C_2 by comparing with the uncharged solution [109, 110, 127], in which $C_2 = \frac{2}{3}\zeta_H^3 = \frac{2}{3}\pi^3\Lambda^3$. As for C_1, it seems natural to replace the horizon ζ_H of the uncharged solution by the outer horizon ζ_+ of the charged solution such that

$$C_2 = \frac{2}{3}\zeta_+^3\,. \tag{4.1.27}$$

Later in section 4.1.3 we will justify this value again. It will turn out to correctly reproduce the expected transport coefficients.

We have checked that for $\tilde{q}_0 = 0$ (or, equivalently, $\widetilde{\mu}_0 = 0$) the metric reduces to the first-order corrected uncharged solution found in [109, 110, 127]. Moreover, for the Kretschmann scalar we find

$$\begin{aligned} R^2_{\mu\nu\rho\sigma} = {} & \frac{4(127\tilde{q}_0^4 - 90 m_0 \tilde{q}_0^2 v^2 + 18 m_0^2 v^4 + 2\tilde{q}_0^2 v^6 + 10 v^{12})}{v^{12}} \\ & + \frac{8(254\tilde{q}_0^4 - 150 m_0 \tilde{q}_0^2 v^2 + 24 m_0^2 v^4 + 2\tilde{q}_0^2 v^6 - 45\tilde{q}_0^2 v^3 C_2 + 18 m_0 v^5 C_2)}{v^{13}} \widetilde{\tau}^{-2/3} + \dots\,, \end{aligned} \tag{4.1.28}$$

which is only singular at $v=0$. In the limit $\tilde{q}_0 \to 0$, we have $m_0 \to \pi^4\Lambda^4$ and $R^2_{\mu\nu\rho\sigma}$ reduces to the corresponding expression in the uncharged case, see [110].

We have thus constructed a natural extension of the first-order corrected boost-invariant plasma geometry of [109, 110, 127] to the corresponding one with non-trivial $U(1)$ gauge field.

4.1.3 Transport coefficients from the background

In the hydrodynamic approximation, the energy-momentum and $U(1)$ current are given by

$$\langle T_{\mu\nu}\rangle = \frac{\varepsilon}{3}(4u_\mu u_\nu + \eta_{\mu\nu}) + \Pi_{\mu\nu}\,, \qquad \langle J_\mu\rangle = \rho u_\mu + \Upsilon_\mu\,, \tag{4.1.29}$$

where the first terms on the right hand side correspond to a perfect fluid with chemical potential. Since the velocity field u^μ, energy density ε and charge density ρ vary slowly with the spacetime

coordinates, the energy-momentum tensor and current receive higher-order gradient corrections given by (up to first order)

$$\Pi_{\mu\nu} = -\eta\sigma_{\mu\nu}\,, \qquad \Upsilon_\mu = -\sigma P_\mu{}^\alpha \partial_\alpha \frac{\mu}{T} + \xi \epsilon_\mu{}^{\rho\sigma\tau} u_\rho \partial_\sigma u_\tau\,, \tag{4.1.30}$$

where η, σ and ξ denote the viscosity, conductivity and vorticity coefficient, respectively. The corrections satisfy $u^\nu \Upsilon_\nu = 0$ and $u^\nu \Pi_{\mu\nu} = 0$. The transport coefficients of the fluid entering these corrections were holographically computed in [76, 77, 129] (up to second order) by slowly varying u^μ, q and m in the boosted solution (4.1.9) with the space-time coordinates x^μ. In this way the hydrodynamic equations are obtained from AdS/CFT without constructing an explicit solution.

In the following we will compute the first-order corrections directly from our time-dependent solution using holographic renormalization techniques [70, 71]. Recently, a rigorous holographic renormalization of the Einstein-Maxwell-Chern-Simons theory, including the full back-reaction of the gauge field, has been performed in [134]. The energy-momentum tensor can be obtained from

$$\langle T_{\mu\nu}\rangle = \lim_{r\to\infty}\left[\frac{N_c^2}{4\pi^2} r^2 \left(K_{\mu\nu} - K\gamma_{\mu\nu} - 3\gamma_{\mu\nu} + \frac{1}{2}G_{\mu\nu}\right)\right]\,, \tag{4.1.31}$$

where $\gamma_{\mu\nu}$ is the induce metric on a constant-r hypersurface, which regularizes the boundary. $K_{\mu\nu}$ is the extrinsic curvature of on this hypersurface, K the corresponding scalar $K = K_{\mu\nu}\gamma^{\mu\nu}$ and $G_{\mu\nu}$ the boundary Einstein tensor with respect to the metric $\gamma_{\mu\nu}$. Substituting our explicit first-order solution into (4.1.31), we find the time-dependent energy density[3]

$$\varepsilon(\widetilde{\tau}) = \frac{\varepsilon_0}{\widetilde{\tau}^{4/3}} - \frac{2\eta_0}{\widetilde{\tau}^2}\,, \tag{4.1.32}$$

with

$$\varepsilon_0 \equiv \frac{3N_c^2}{8\pi^2 b_0^4}\,, \qquad \eta_0 \equiv \frac{3N_c^2}{16\pi^2} C_2 = \frac{N_c^2}{8\pi^2}\zeta_+^3\,, \tag{4.1.33}$$

and $b_0 = b\widetilde{\tau}^{-1/3}$ as in (4.1.20), see appendix 4.3 for more details on the computation. The first term in $\varepsilon(\widetilde{\tau})$ is the zeroth-order energy density and is in agreement with that in [76], see Eq. (20a) therein. The second term is the first-order correction and formally agrees with that in the uncharged case [109, 110, 127] but now with a more general shear viscosity $\eta_0 = \eta_0(\widetilde{\mu}_0, \Lambda)$.[4] This correction is also in exact agreement with the first-order gradient correction to the energy-momentum tensor computed in [76]. There [76], the viscosity was found to be

$$\eta = \frac{s}{4\pi} = \frac{N_c^2}{8\pi^2} r_+^3 = \frac{N_c^2}{8\pi^2}\zeta_+^3 \widetilde{\tau}^{-1}\,, \tag{4.1.34}$$

with r_+ as in (4.1.8) (The $\mathcal{N} = 4$ plasma saturates the KSS bound [135–138]). Here we have already substituted the asymptotic behaviour $T = \Lambda\widetilde{\tau}^{-1/3}$ and $r_+ = \zeta_+\widetilde{\tau}^{-1/3}$. Given that η_0 is defined as $\eta_0 = \eta\widetilde{\tau}$, we get the same η_0 as in (4.1.33) and thus agreement with [76].

Similarly, the expectation value of the R-charge current can be computed from

$$\langle J^\mu\rangle = \frac{N_c^2}{4\pi^2}\left(\eta^{\mu\rho}A_\rho^{(2)} - \frac{\kappa}{2}\epsilon^{\mu\nu\sigma\rho}A_\nu^{(0)}F_{\sigma\rho}^{(0)}\right)\,, \tag{4.1.35}$$

[3] Asymptotically, $\widetilde{\tau}$ can be identified with the proper time τ, $\widetilde{\tau} \approx \tau$, see section 4.2.4 below.

[4] In order to check η_0 in the limit of vanishing chemical potential, we note that the viscosity is differently normalised in [110]. Consider $\frac{\eta_0}{\varepsilon_0} = \frac{1}{3}\zeta_+^3 b_0^4 \to \frac{1}{3\pi\Lambda}$ for $\widetilde{\mu}_0 = 0$. This is identical with $\eta_0^{KMNO} = \frac{1}{3w}$ found in [110] since $\pi\Lambda = w$ there.

where $A_\rho^{(n)}$ is the r^{-n} coefficient of the large-r expansion of the gauge field A_ρ. Since the spatial components of the gauge field are zero, the second term proportional to κ is absent in our case. Substituting the solution for the gauge field into (4.1.35), we read off the $U(1)$ charge density

$$\rho(\widetilde{\tau}) = \frac{N_c^2}{4\pi^2}\frac{\sqrt{3}\tilde{q}_0}{2}\frac{1}{\widetilde{\tau}} \tag{4.1.36}$$

with $\tilde{q}_0 = q\widetilde{\tau}$ as in (4.1.20). Recalling $\sqrt{3}q/2 = \mu r_+^2$, we find agreement with the zeroth-order charge density in [76], see Eq. (20b) therein. The asymptotic $1/\widetilde{\tau}$ behaviour of the charge density was also found in [128]. There are no first-order corrections to the charge density in our case.

More generally, for gauge fields with vanishing spatial components, there are no higher-order gradient corrections. This follows directly from the relation $u^\nu \Upsilon_\nu = 0$. The corrections Υ_ν are orthogonal to u^ν and cannot come from the near boundary expansion of a gauge field proportional to u^ν.

4.2 Late-time solution in Fefferman-Graham coordinates

In this section we seek for a time-dependent solution of the Einstein-Maxwell equations (4.1.2) and (4.1.3) in Fefferman-Graham coordinates.

4.2.1 General ansatz and near-boundary behaviour

In Fefferman-Graham coordinates, we choose the same metric ansatz as in the uncharged case [74] given by

$$ds^2 = \frac{1}{z^2}\left(-e^{a(\tau,z)}d\tau^2 + e^{b(\tau,z)}\tau^2 dy^2 + e^{c(\tau,z)}dx_\perp^2 + dz^2\right). \tag{4.2.1}$$

Of course, the warp factors $a(\tau,z)$, $b(\tau,z)$ and $c(\tau,z)$ will be modified due to the effects from the back-reaction of the gauge field. As before, we set the spatial components of the gauge field to zero and assume a non-vanishing time-component,

$$A_0 = -d(\tau,z)\,, \qquad A_y = A_z = A_{x_\perp} = 0\,. \tag{4.2.2}$$

Let us first study the general behaviour of the solution near the boundary at $z=0$. Following [123], we choose the small-z expansions

$$\begin{aligned} a(\tau,z) &= -\varepsilon(\tau)z^4 + a_6(\tau)z^6 + a_8(\tau)z^8 + \dots\,,\\ b(\tau,z) &= b_4(\tau)z^4 + b_6(\tau)z^6 + b_8(\tau)z^8 + \dots\,,\\ c(\tau,z) &= c_4(\tau)z^4 + c_6(\tau)z^6 + c_8(\tau)z^8 + \dots \end{aligned} \tag{4.2.3}$$

and

$$d(\tau,z) = \rho(\tau)z^2 + d_4(\tau)z^4 + d_6(\tau)z^6 + \dots \tag{4.2.4}$$

Here the lowest coefficients are determined by the energy and charge density, respectively. For instance, solving the Einstein-Maxwell equations to lowest order in z, we obtain

$$b_4(\tau) = -\left(\varepsilon(\tau) + \tau\varepsilon'(\tau)\right), \quad c_4(\tau) = \varepsilon(\tau) + \tfrac{1}{2}\tau\varepsilon'(\tau)\,, \tag{4.2.5}$$

as in [123]. There is no back-reaction of the gauge field on the geometry at this order ($\rho(\tau)$ does neither appear in $b_4(\tau)$ nor $c_4(\tau)$). Likewise, the metric does not enter the Maxwell equations at this order. However, other than the energy density $\varepsilon(\tau)$, which can be freely chosen (at least

at early times), the charge density $\rho(\tau)$ is uniquely fixed by the z-component of the Maxwell equations,

$$-\frac{2\rho(\tau)}{\tau} - 2\rho'(\tau) = 0\,, \tag{4.2.6}$$

which is solved by

$$\rho(\tau) = \frac{q_0}{\tau}\,, \tag{4.2.7}$$

$q_0 = const.$ Any dependence on the warp factors has dropped out in the Maxwell equations such that $\rho(\tau)$ is independent of $\varepsilon(\tau)$. The result (4.2.7) for the charge density holds for all times $\tau > 0$. Remarkably, the charge density diverges at $\tau = 0$.[5]

Solving the system of equations (4.1.2) and (4.1.3) order by order, we find the solution up to order z^8,

$$\begin{aligned} a(\tau,z) = &-\varepsilon(\tau)z^4 + \left(-\frac{\varepsilon'(\tau)}{4\tau} - \frac{\varepsilon''(\tau)}{12} + \frac{10\rho(\tau)^2}{9}\right) z^6 \\ &- \left(\frac{1}{6}\varepsilon(\tau)^2 + \frac{1}{6}\tau\varepsilon'(\tau)\varepsilon(\tau) + \frac{1}{16}\tau^2\varepsilon'(\tau)^2 - \frac{\varepsilon'(\tau)}{128\tau^3} + \frac{\varepsilon''(\tau)}{128\tau^2}\right. \\ &\left. + \frac{\varepsilon^{(3)}(\tau)}{64\tau} + \frac{1}{384}\varepsilon^{(4)}(\tau) + \frac{\rho(\tau)^2}{36\tau^2}\right) z^8 + \dots\,, \\ d(\tau,z) = &\,\rho(\tau)\left(z^2 - \frac{\varepsilon(\tau)}{3}z^6 + \left(\frac{2\rho(\tau)^2}{9} - \frac{\varepsilon'(\tau)}{16\tau} - \frac{\varepsilon''(\tau)}{48}\right) z^8 + \dots\right) \end{aligned} \tag{4.2.8}$$

and similar expressions for $b(\tau,z)$ and $c(\tau,z)$. These expressions for the warp factors generalise the corresponding ones for $q_0 = 0$ found in [123]. They describe the all-time near boundary behaviour of the background as a function of the energy and charge density.

4.2.2 Late-time ansatz for the background

A full analytical all-time solution is difficult to find, even in the uncharged case ($q_0 = 0$). It is however possible to find a late-time solution. The general late-time behaviour of the energy and charge densities can be found as follows (For the energy density the derivation is very similar to that in [74,107]). In the local rest frame the energy-momentum tensor is diagonal with elements $T_{\tau\tau}$, T_{yy} and $T_{xx} = T_{x_2x_2} = T_{x_3x_3}$ and the current has only a time-component J_τ while $J_y = J_{x_2} = J_{x_3} = 0$. Moreover, we assume that these components depend only on τ.

Using proper time and rapidity coordinates in flat Minkowski spacetime, defined by $x_0 = \tau\cosh y$ and $x_1 = \tau\sinh y$,

$$ds^2 = -d\tau^2 + \tau^2 dy^2 + dx_\perp^2\,, \tag{4.2.9}$$

the tracelessness condition $T^\nu{}_\nu = 0$, energy-momentum conservation $T^{\mu\nu}{}_{;\nu} = 0$ and charge conservation $J^\nu{}_{;\nu} = 0$ have the form

$$-T_{\tau\tau} + \frac{1}{\tau^2}T_{yy} + T_{xx} = 0\,, \tag{4.2.10}$$

$$\tau\partial_\tau T_{\tau\tau} + T_{\tau\tau} + \frac{1}{\tau^2}T_{yy} = 0\,, \tag{4.2.11}$$

$$\tau\partial_\tau J_\tau + J_\tau = 0\,. \tag{4.2.12}$$

[5] Generic solutions of viscous fluid dynamics are not expected to be regular in the infinite past (see footnote 4 in [76] in this context): The volume element on the boundary at constant proper time scales linearly with τ. Integrating the charge density ($\propto 1/\tau$) over this volume element ($\propto \tau$) yields a constant total charge. Thus, even though the charge density is divergent, the total charge is regular, even at $\tau = 0$, ensuring the validity of the hydrodynamic approximation.

Here we assumed that the anomaly in the $U(1)$ current is absent, which is true for our simple ansatz of the gauge field.

Comparing with the zeroth-order energy-momentum tensor and current given in (4.1.29), in the frame $u^\nu = (1, 0, 0, 0)$ we obtain

$$\varepsilon(\tau) = \frac{\varepsilon_0}{\tau^{4/3}}\,, \qquad \rho(\tau) = \frac{q_0}{\tau}\,. \tag{4.2.13}$$

We observe that the asymptotic charge density (4.2.13) is in exact agreement with the expression (4.2.7) for the charge density, which is valid for all times. In other words, the late time charge density (4.2.13) does not receive any higher-order gradient corrections, in agreement with our findings in the previous section.

Substituting the asymptotic behaviour (4.2.13) into the general solution (4.2.8) and expanding the resulting expressions for large τ, we get ($\varepsilon_0 = 1$)

$$a(\tau, z) = -\frac{z^4}{\tau^{4/3}} + \frac{2 + 30{q_0}^2\tau^{4/3}}{27\tau^{10/3}}z^6 + \frac{10 - 27{q_0}^2\tau^{4/3} - 54\tau^{8/3}}{972\tau^{16/3}}z^8 + \cdots\,, \tag{4.2.14}$$

$$b(\tau, z) = \frac{z^4}{3\tau^{4/3}} - \frac{14 + 18\tau^{4/3}q_0^2}{81\tau^{10/3}}z^6 + \frac{-130 + 243\tau^{4/3}q_0^2 - 162\tau^{8/3}}{2916\tau^{16/3}}z^8 + \cdots\,, \tag{4.2.15}$$

$$c(\tau, z) = \frac{z^4}{3\tau^{4/3}} + \left(\frac{4}{81\tau^{10/3}} - \frac{2q_0^2}{9\tau^2}\right)z^6 + \frac{50 - 81\tau^{4/3}q_0^2 - 162\tau^{8/3}}{2916\tau^{16/3}}z^8 + \cdots\,, \tag{4.2.16}$$

$$d(\tau, z) = \frac{q_0}{\tau}z^2 - \frac{q_0}{3\tau^{7/3}}z^6 + \left(\frac{q_0}{54\tau^{13/3}} + \frac{2{q_0}^3}{9\tau^3}\right)z^8 + \cdots\,. \tag{4.2.17}$$

We find that the dominant terms at large τ scale as

$$a_n(\tau)z^n \sim \frac{z^n}{\tau^{n/3}}\,, \qquad d_n(\tau)z^n \sim \frac{1}{\tau^{1/3}}\frac{z^n}{\tau^{n/3}}\,, \tag{4.2.18}$$

and similarly $b_n(\tau)z^n$ and $c_n(\tau)z^n$. As in [74], it is therefore useful to introduce the scaling variable[6]

$$v = \frac{z}{\tau^{1/3}}\,. \tag{4.2.19}$$

This suggests the following ansatz at late times,

$$\begin{aligned} a(\tau, z) &= a_0(v) + a_1(v)\frac{1}{\tau^{2/3}} + ... \\ d(\tau, z) &= \tau^{-1/3}\left(d_0(v) + d_1(v)\frac{1}{\tau^{2/3}} + ...\right) \end{aligned} \tag{4.2.20}$$

and similarly for $b(\tau, z)$ and $c(\tau, z)$. Inserting the ansatz (4.2.1) and (4.2.2) with (4.2.20) into the combined system of Einstein-Maxwell and covariant Maxwell equations (4.1.2) and (4.1.3) will turn the equation of motions into a system of nonlinear ordinary differential equations for the coefficients $a_i, ..., d_i$ ($i \geq 0$). In principle, this system can then be solved order by order in $\tau^{-2/3}$.

[6] With hindsight, this justifies the introduction of the scaling variable $v = r\widetilde{\tau}^{1/3}$ in the previous section for the late-time solution in Eddington-Finkelstein coordinates.

4.2.3 Zeroth-order solution

In the following we restrict to give an exact solution for the zeroth-order coefficients $a_0(v), ..., d_0(v)$. The non-vanishing components of the Einstein-Maxwell equations are

$$\begin{aligned}
(\tau\tau): \quad & 4e^{-a_0(v)}v^3 {d_0}'(v)^2 = 6{b_0}'(v) - v{b_0}'(v)^2 + 12{c_0}'(v) \\
& \quad - 2v{b_0}'(v){c_0}'(v) - 3v{c_0}'(v)^2 - 2v{b_0}''(v) - 4v{c_0}''(v)\,, \\
(yy): \quad & 4e^{-a_0(v)}v^3 {d_0}'(v)^2 = -6{a_0}'(v) + v{a_0}'(v)^2 - 12{c_0}'(v) \\
& \quad + 2v{a_0}'(v){c_0}'(v) + 3v{c_0}'(v)^2 + 2v{a_0}''(v) + 4v{c_0}''(v)\,, \\
(\perp\perp): \quad & 4e^{-a_0(v)}v^3 {d_0}'(v)^2 = -6{a_0}'(v) + v{a_0}'(v)^2 - 6{b_0}'(v) + v{a_0}'(v){b_0}'(v) + v{b_0}'(v)^2 \\
& \quad - 6{c_0}'(v) + v{a_0}'(v){c_0}'(v) + v{b_0}'(v){c_0}'(v) + v{c_0}'(v)^2 \\
& \quad + 2v{a_0}''(v) + 2v{b_0}''(v) + 2v{c_0}''(v)\,, \\
(zz): \quad & 4e^{-a_0(v)}v^3 {d_0}'(v)^2 = 6a_0'(v) + 6b_0'(v) - va_0'(v)b_0'(v) \\
& \quad + 12c_0'(v) - 2va_0'(v)c_0'(v) - 2vb_0'(v)c_0'(v) - vc_0'(v)^2\,, \\
(z\tau): \quad & 6a_0'(v) - 4b_0'(v) - va_0'(v)b_0'(v) + vb_0'(v)^2 + 4c_0'(v) \\
& \quad - 2va_0'(v)c_0'(v) + 2vc_0'(v)^2 + 2vb_0''(v) + 4vc_0''(v) = 0\,.
\end{aligned} \tag{4.2.21}$$

At zeroth order, the z- and τ-components of the Maxwell equation both lead to the same equation,

$$\big(2 + v{a_0}'(v) - v{b_0}'(v) - 2v{c_0}'(v)\big)\, {d_0}'(v) = 2v{d_0}''(v)\,. \tag{4.2.22}$$

The other components are zero.

These equations can be simplified a lot. Note that only four out of the five plus one equations are independent. We also find from a linear combination of the $\tau\tau$- , zz- and $z\tau$-components of the Einstein-Maxwell equations that $b_0(v) = c_0(v)$. Next, the Maxwell equation (4.2.22) can be solved for $d_0(v)$,

$$d_0(v) = S_4 \int_0^v \tilde{v} e^{\frac{1}{2}(a_0(\tilde{v}) - b_0(\tilde{v}) - 2c_0(\tilde{v}))}\, d\tilde{v}, \tag{4.2.23}$$

where S_4 is some integration constant which will be fixed below.

Substituting this back into the Einstein equations, the two remaining independent equations are given by the $\tau\tau$- and zz-components. The first one $(\tau\tau)$ is an equation for $b_0(v)$,

$$3vb_0''(v) + 3v(b_0'(v))^2 - 9b_0'(v) + 8q_0^2 v^5 e^{-3b_0(v)} = 0\,. \tag{4.2.24}$$

while the second one (zz),

$$a_0'(v) = -v\frac{(b_0'(v))^2 + 2b_0''(v)}{2 - vb_0'(v)}\,, \tag{4.2.25}$$

can be used to find $a_0(v)$ as soon as a solution for $b_0(v)$ is known. Our primary goal will be to solve (4.2.24) for $b_0(v)$. $a_0(v)$ and $d_0(v)$ can then easily be obtained from (4.2.25) and (4.2.23).

Later, in order to fix some integration constants, we will need the asymptotic solution close to

the boundary which can be expanded in powers of v as (here we present it up to $\mathcal{O}(v^{10})$)

$$\begin{aligned} a_0(v) &= -\varepsilon_0 v^4 + \frac{10{q_0}^2}{9}v^6 - \frac{\varepsilon_0^2}{18}v^8 - \frac{2{q_0}^2\varepsilon_0}{45}v^{10} + \cdots , \\ b_0(v) = c_0(v) &= \frac{\varepsilon_0}{3}v^4 - \frac{2{q_0}^2}{9}v^6 - \frac{\varepsilon_0^2}{18}v^8 + \frac{14{q_0}^2\varepsilon_0}{135}v^{10} + \cdots , \\ d_0(v) &= q_0 v^2 - \frac{q_0\varepsilon_0}{3}v^6 + \frac{2q_0^3}{9}v^8 + \frac{q_0\varepsilon_0^2}{9}v^{10} + \cdots . \end{aligned} \tag{4.2.26}$$

It shows us that the solution exists and is uniquely fixed by parameters ε_0 and q_0. Comparing the expression (4.2.23) with the boundary behaviour (4.2.26), we may immediately fix the integration constant S_4 as

$$S_4 = 2q_0 \,. \tag{4.2.27}$$

We now solve (4.2.24) for $b_0(v)$. By setting

$$b_0(v) = \log(\beta(v)) \,, \tag{4.2.28}$$

we simplify this equation to the form

$$v\beta'' - 3\beta' + \frac{8}{3}q_0^2 v^5 \beta^{-2} = 0 \,, \tag{4.2.29}$$

which turns out to be the modified Emden-Fowler equation [139]. Its solution can be written in the parametric form

$$\beta(v) = pS_3^2 \exp\left\{ S_2 \int_{p_+}^{p} \left(\frac{\tilde{p}^2}{4} + S_1 + \frac{q_0^2}{3}\frac{1}{\tilde{p}} \right)^{-1/2} d\tilde{p} \right\} \tag{4.2.30}$$

and

$$v = S_3 \exp\left\{ \frac{S_2}{2} \int_{p_+}^{p} \left(\frac{\tilde{p}^2}{4} + S_1 + \frac{q_0^2}{3}\frac{1}{\tilde{p}} \right)^{-1/2} d\tilde{p} \right\} . \tag{4.2.31}$$

Here S_1, S_2, S_3 and p_+ are some integration constants. One can in principle absorb p_+ in S_3 but we separate them for the moment. There are two useful expressions for $\beta(v)$ and $\beta'(v)$,

$$\beta(v) = pv^2 \tag{4.2.32}$$

and

$$\frac{d\beta(v)}{dv} = \frac{2v}{S_2}\sqrt{\frac{p^2}{4} + S_1 + \frac{q_0^2}{3}\frac{1}{p}} + 2pv \,. \tag{4.2.33}$$

From (4.2.26), we get the near-boundary conditions

$$\beta(v) = 1 + O(v^4) \,, \qquad \beta'(v) = \frac{4\varepsilon_0}{3}v^3 + O(v^5) \,, \tag{4.2.34}$$

which will be used to fix the integration constants S_1 and S_2.

Comparing (4.2.32) with (4.2.34), we find that near the boundary v should behave as

$$v \approx \frac{1}{\sqrt{p}}\,, \tag{4.2.35}$$

which is small if p is large. This should be compared with the general large-p behaviour

$$v = S_3 \exp\left\{\frac{S_2}{2}\int_{p_+}^{p}\left(\frac{\tilde{p}}{2}+\cdots\right)^{-1} d\tilde{p}\right\} \approx const.\ p^{S_2}\,. \tag{4.2.36}$$

This fixes S_2 as

$$S_2 = -\frac{1}{2}\,. \tag{4.2.37}$$

Substituting (4.2.35) into (4.2.34), we extract the expected asymptotics for $\beta'(v)$ as a function of p,

$$\beta'(v) \approx \frac{4\varepsilon_0}{3}\frac{1}{p^{3/2}}\,. \tag{4.2.38}$$

Generically, at large p, (4.2.33) is approximated by

$$\beta'(v) = -4v\sqrt{S_1 + \frac{p^2}{4} + \cdots} + 2pv \approx -\frac{4S_1}{p^{3/2}}\,, \tag{4.2.39}$$

which fixes S_1 as

$$S_1 = -\frac{\varepsilon_0}{3}. \tag{4.2.40}$$

Remarkably both constants S_1 and S_2 do not depend on q_0.

Let us now relate S_3 and p_+ by setting $S_3 = v_+$ with $v_+ \equiv v(p_+)$. v_+ will be fixed by the requirement that the outer horizon of the geometry is located at $v = v_+$. Formally, the horizon v_+ is defined as the largest zero of the denominator on the right hand side of (4.2.25),

$$2 - v_+\frac{\beta'(v_+)}{\beta(v_+)} = 0\,. \tag{4.2.41}$$

This can be rewritten in terms of p_+. Using (4.2.33), (4.2.32) and the expressions for S_1 and S_2, we get the condition

$$p_+^3 - \frac{4\varepsilon_0}{3}p_+ + \frac{4q_0^2}{3} = 0\,, \tag{4.2.42}$$

which can be solved by Cardano's formula. The largest solution of this equation is[7]

$$p_+ = \left(\frac{2}{3}\right)^{1/3}\left(\left(-q_0^2 + \sqrt{q_0^4 - \frac{16}{81}\varepsilon_0^3}\right)^{1/3} + \left(-q_0^2 - \sqrt{q_0^4 - \frac{16}{81}\varepsilon_0^3}\right)^{1/3}\right)\,. \tag{4.2.43}$$

The last step is to fix v_+ in (4.2.31). This can be done by substituting the p_+ solution (4.2.43) (and all the constants $S_{1,2,3}$) back into (4.2.31) and expand $v(p)$ for large p. In this way we

[7] In order to extract the roots correctly we use the following standard convention:
$a_+a_- = \left(\frac{2}{3}\right)^{4/3}\varepsilon_0$, where $a_\pm = \left(-q_0^2 \pm \sqrt{q_0^4 - \frac{16}{81}\varepsilon_0^3}\right)^{1/3}$.

determine the constant on the right hand side of (4.2.36) as a function of v_+. Since this constant must be one, we get

$$v_+(\varepsilon_0, q_0) = \exp\left\{\frac{1}{2}\lim_{p\to\infty}\left[\int_{p_+}^{p}\frac{d\tilde{p}}{\sqrt{4U(\tilde{p})}} - \log p\right]\right\}, \tag{4.2.44}$$

where $U(\tilde{p})$ is defined as

$$U(\tilde{p}) = \frac{\tilde{p}^2}{4} - \frac{\varepsilon_0}{3} + \frac{q_0^2}{3\tilde{p}}. \tag{4.2.45}$$

For $q_0 = 0$, the integral can be performed analytically and v_+ reduces to the well-known result for the horizon [74],

$$v_+(\varepsilon_0, q_0)|_{_{q_0\to 0}} = \sqrt[4]{\frac{3}{\varepsilon_0}}. \tag{4.2.46}$$

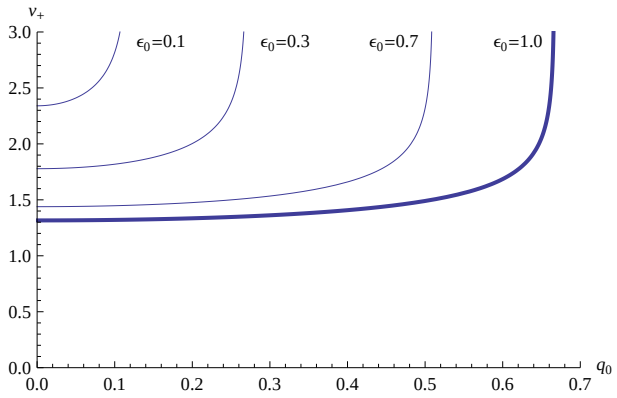

Figure 4.1: The outer horizon $v_+ = v_+(\varepsilon_0, q_0)$.

For general q_0, this integral can in principle be written as a lengthy expression of elliptic integrals of the first and third kind, $F(\phi, k)$ and $\Pi(n; \phi|m)$, respectively, which we will not do here. Instead, in Fig. 4.1 we show the dependence of v_+ on the charge q_0 for some particular choices of ε_0. We note that for each ε_0 there is some maximal allowed value of the charge at which the black hole becomes extremal. This value can be found from the condition that the discriminant Δ of (4.2.42) vanishes,

$$\Delta = \left(-\frac{4}{9}\varepsilon_0\right)^3 + \left(-\frac{2}{3}q_0^2\right)^2 = 0, \tag{4.2.47}$$

which leads to the bound

$$q_0 \le q_0^{extr.} = \frac{2}{3}\varepsilon_0^{3/4}. \tag{4.2.48}$$

In Fig. 4.2 we present some plots of the exact solution and compare them with the power expansions (4.2.26). For the particular choice $\varepsilon_0 = 1$ and $q_0 = 0.6 \lesssim q_0^{extr.}$ the difference between both curves is clearly visible. The function $a_0(v)$ by definition has a singularity on the horizon, as can be seen in Fig. 4.2(a). The other functions $b_0(v)$, $c_0(v)$ and $d_0(v)$ are regular on the horizon

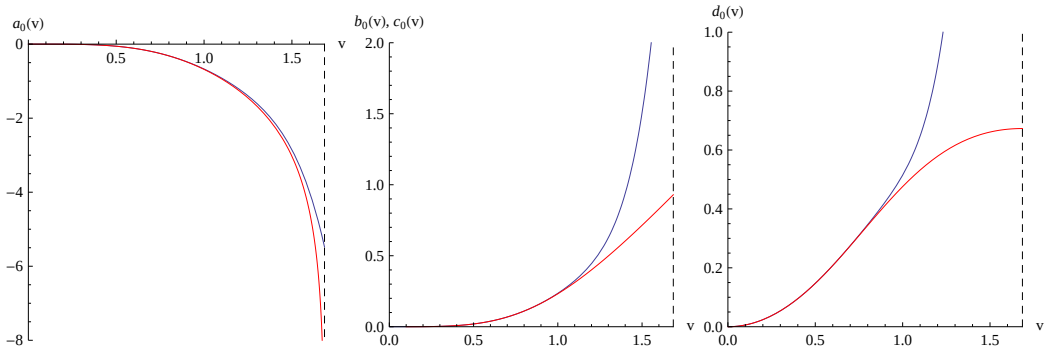

Figure 4.2: Exact solutions (red curves) and their near-boundary power expansions (blue curves) for $\varepsilon_0 = 1$ and $q_0 = 0.6 \lesssim q_0^{extr.}$. The black dashed lines correspond to the horizon $v_+(\varepsilon_0, q_0) \simeq 1.685$.

and their power expansions are valid up to $v \lesssim 1$. Note also that $d_0(v)$ grows quadratically near the boundary, which reflects the Coulomb law in $D = 5$ dimensions. Near the horizon it approaches some finite constant value μ_0 related to the chemical potential as

$$\mu = A_0|_{boundary} - A_0|_{horizon} = \frac{d_0(v_+) - d_0(0)}{\tau^{1/3}} = \frac{\mu_0}{\tau^{1/3}}\,, \tag{4.2.49}$$

which confirms the scaling behaviour (4.1.10).

In summary, the zeroth-order solution $b_0(v)$ is given by

$$\begin{aligned} e^{b_0(v)} &= p v_+^2 \exp\big(-\frac{1}{2}\int_{p_+}^{p} U(\tilde{p})^{-1/2} d\tilde{p}\big)\,, \\ v &= v_+ \exp\big(-\frac{1}{4}\int_{p_+}^{p} U(\tilde{p})^{-1/2} d\tilde{p}\big)\,, \end{aligned} \tag{4.2.50}$$

with v_+ and $U(\tilde{p})$ given by (4.2.44) and (4.2.45), respectively. $a_0(v)$ and $d_0(v)$ are obtained by substituting $b_0(v)$ in (4.2.25) and (4.2.23).

4.2.4 Fefferman-Graham vs. Eddington-Finkelstein coordinates

The zeroth-order solution in Fefferman-Graham (FG) coordinates can be related to that in Eddington-Finkelstein (EF) coordinates by the coordinate transformation

$$\tilde{\tau} = \tau\,, \qquad r = \frac{1}{z} e^{b(\tau,z)/2}\,. \tag{4.2.51}$$

Transforming the Eddington-Finkelstein metric (4.1.14)-(4.1.18) and comparing the result with the power expansion (4.2.26), we find

$$q_0 = \frac{\sqrt{3}}{2}\tilde{q}_0. \tag{4.2.52}$$

Comparing also the bound (4.2.48) with that in Eddington-Finkelstein coordinates given by (4.1.24), we find some relation between ε_0 and m_0 using (4.2.52):

$$\varepsilon_0 = \frac{3}{4} m_0\,. \tag{4.2.53}$$

For $q_0 = 0$ this relation can be easily checked by our solution with the general form of the metric in [74, 107, 127]. In this case, we find that our solution (4.2.50) reduces to

$$e^{b_0(v)} = 1 + \frac{\varepsilon_0}{3} v^4 \,, \tag{4.2.54}$$

and similarly $a_0(v)$, such that

$$ds^2\big|_{q_0=0} = \frac{1}{z^2}\left[dz^2 - \frac{(1-\frac{m_0}{4}v^4)^2}{1+\frac{m_0}{4}v^4} d\tau^2 + \tau^2\left(1+\frac{m_0}{4}v^4\right)dy^2 + \left(1+\frac{m_0}{4}v^4\right)dx_\perp^2\right] . \tag{4.2.55}$$

We also note that the transformation (4.2.51) relates the outer horizons, ζ_+ in EF coordinates and p_+ in FG coordinates, as $\zeta_+ = \sqrt{p_+}$. The chemical potential μ_0 can therefore be written as a function of ε_0 and q_0. Using (4.1.12) and (4.2.52), we find

$$\mu_0(\varepsilon_0, q_0) = \widetilde{\mu}_0 = \frac{\sqrt{3}}{2}\frac{\tilde{q}_0}{\zeta_+^2} = \frac{q_0}{p_+(\varepsilon_0, q_0)} \,. \tag{4.2.56}$$

This dependence is shown in Fig. 4.3 for some particular values of ε_0.

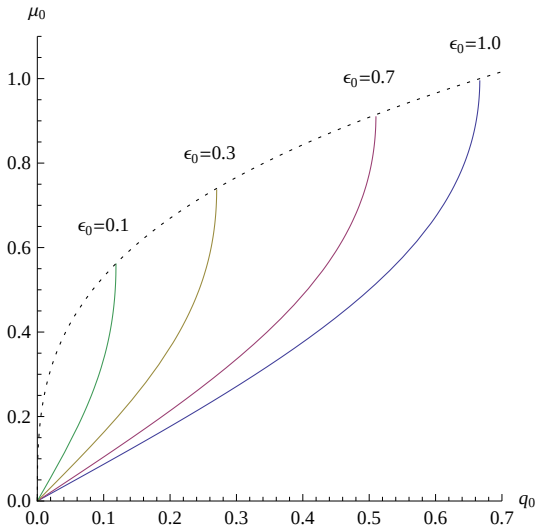

Figure 4.3: The chemical potential $\mu_0 = \mu_0(\varepsilon_0, q_0)$. The dotted line corresponds to the upper bound for μ_0.

Using this expression with the definition (4.2.42) for p_+ and substituting there the maximal value for q_0 (4.2.48) we find the following bound for the chemical potential:

$$\mu_0(\varepsilon_0, q_0) \leq \mu_0^{extr.} = \left(\frac{3}{2} q_0^{extr.}\right)^{1/3} = \varepsilon_0^{1/4} \,. \tag{4.2.57}$$

This is not in contradiction with our earlier statement that the disappearance of the horzion does not impose a bound on $\tilde{\mu}_0/\Lambda$. Note that if we identify ε_0 with m_0 as in (4.2.53), then ε_0 explicitly depends on $\tilde{\mu}_0 = \mu_0$ and therefore (4.2.57) is not a bound on $\tilde{\mu}_0/\Lambda$.

4.3 Conclusions

We constructed a natural extension of the late-time boost-invariant background found in [74] (and [75,107–110,125–127]) to a background dual to an expanding $\mathcal{N} = 4$ plasma *with* chemical potential.

The solution we found depends on two parameters, the chemical potential $\widetilde{\mu}_0$ and temperature scale Λ, which are encoded in the mass parameter m_0 and charge $\tilde{q}_0$ of a time-dependent AdS Reissner-Nordström-like solution. In Eddington-Finkelstein coordinates the first-order solution is given by the expansion (4.1.14)–(4.1.18), with the zeroth-order and first-order coefficients given by (4.1.19) and (4.1.22), respectively. We showed that the viscosity of the boundary theory computed from the time-dependent solution is in agreement with that in [76]. We also constructed a zeroth-order solution in Fefferman-Graham coordinates, which we presented in parametric form, see the general ansatz (4.2.1) and (4.2.2) with (4.2.50). FG coordinates may be the preferred choice, when strings [103] or branes [1, 105] are embedded into the geometry. Finally, we found the coordinate transformation which maps the zeroth-order solution in FG coordinates to that in EF coordinates.

We argued in several ways that the charge density behaves like τ^{-1} at all times. Unlike the energy density, it can not be chosen freely at early times. This is basically because the charge density behaves like τ^{-1} at large τ, see e.g. (4.1.36) or (4.2.13), and higher-order corrections are absent. It also follows directly from the equations of motion, see (4.2.7) which holds for all times. Naive extrapolation to early times shows a singularity in the gauge field at $\tau = 0$. However, this does not signal a breakdown of the hydrodynamic approximation since the total charge is constant at all times and therefore regular even at $\tau = 0$ (see footnote 5 on p. 45).

A possible application of the background, when appropriately modified and extended, could be the chiral magnetic effect (CME) [30, 41–43], see the Chapter 5.

Finally, it would be interesting to find a numerical solution of our background *à la* Chesler and Yaffe [124] which would hold beyond the hydrodynamic regime.

Appendix A. Roots of (4.1.23)

For completeness, we present the six roots of (4.1.23) in this appendix. The equation (4.1.23) is depressed bicubic in ζ_i and, therefore, can be solved by Cardano's formula. It has six solutions, which can be expressed as

$$\zeta_i \in \left\{ \pm\sqrt{\alpha_+ + \alpha_-}, \pm\sqrt{-\frac{\alpha_+ + \alpha_-}{2} - i\frac{\alpha_+ - \alpha_-}{2}\sqrt{3}}, \pm\sqrt{-\frac{\alpha_+ + \alpha_-}{2} + i\frac{\alpha_+ - \alpha_-}{2}\sqrt{3}} \right\} , \quad (4.3.1)$$

where

$$\alpha_\pm^3 = -\frac{\tilde{q}_0^2}{2} \pm \sqrt{\frac{\tilde{q}_0^4}{4} - \frac{m_0^3}{27}} . \quad (4.3.2)$$

Here we use the standard convention $\alpha_+\alpha_- = m_0/3$. One can recognize the outer horizon $\zeta_+ \equiv r_+\tau^{1/3}$ in the first pair of solutions and the inner horizon $\zeta_- \equiv r_-\tau^{1/3}$ in the second one.

Appendix B. The energy-momentum tensor (4.1.31)

In this appendix we introduce the geometric quantities used for the computation of the energy-momentum tensor (4.1.31). Here we consider an $r = const.$ four-dimensional surface with induced metric $\gamma_{\mu\nu}$ on it:[8]

$$\gamma_{\mu\nu} = g_{\mu\nu} - n_\mu n_\nu , \quad (4.3.3)$$

where $g_{\mu\nu}$ is the 5-metric and n^μ is the outward-pointing unit normal vector to the surface. For our ansatz (4.1.14) it is given by

[8] Here and after all Greek letters denote a 5-index.

$$n_\mu = \left(0,0,0,0,\frac{1}{\sqrt{-g_{\tilde{\tau}\tilde{\tau}}}}\right) , \tag{4.3.4}$$

where $g_{\tilde{\tau}\tilde{\tau}} = -r^2 e^{a(\tilde{\tau},r)}$. The indices of the induced metric can be raised and lowered by means of the 5-metric $g_{\mu\nu}$,

$$\gamma_\mu{}^\nu = \gamma_{\mu\alpha} g^{\alpha\nu} . \tag{4.3.5}$$

The surface extrinsic curvature is given by

$$K_{\mu\nu} \equiv -\frac{1}{2}({}^{(4)}\nabla_\alpha n_\beta + {}^{(4)}\nabla_\beta n_\alpha) = -\frac{1}{2}\gamma_\mu{}^\alpha \gamma_\nu{}^\beta \left(\nabla_\alpha n_\beta + \nabla_\beta n_\alpha\right) , \tag{4.3.6}$$

where we put ${}^{(4)}$ to covariant derivatives associated with the induced metric, while the derivatives on the right-hand side are defined with respect to the 5-metric. We also define a scalar $K = K_{\mu\nu} g^{\mu\nu} = K_{\mu\nu}\gamma^{\mu\nu}$, which is used in the Gibbons-Hawking-York part of (4.1.31).

The Einstein tensor on the surface is defined as

$$G_{\mu\nu} = {}^{(4)}R_{\mu\nu} - \frac{1}{2}\gamma_{\mu\nu}{}^{(4)}R , \tag{4.3.7}$$

where the 4-tensors can be expressed through the 5-tensors (defined with respect to $g_{\mu\nu}$) by the Gauss equations:

$$\begin{aligned}
{}^{(4)}R^\alpha{}_{\mu\beta\nu} &= R^\kappa{}_{\lambda\rho\sigma}\gamma^\alpha{}_\kappa \gamma_\mu{}^\lambda \gamma_\beta{}^\rho \gamma_\nu{}^\sigma + K^\alpha{}_\beta K_{\mu\nu} - K_{\mu\beta}K^\alpha{}_\nu , && (4.3.8)\\
{}^{(4)}R_{\mu\nu} &= {}^{(4)}R^\alpha{}_{\mu\beta\nu}\gamma_\alpha{}^\beta = \gamma_\kappa{}^\lambda \gamma_\mu{}^\rho \gamma_\nu{}^\sigma R^\kappa{}_{\rho\lambda\sigma} + K K_{\mu\nu} - K_{\mu\alpha}K^\alpha{}_\nu , && (4.3.9)\\
{}^{(4)}R &= {}^{(4)}R_{\mu\nu}\gamma^{\mu\nu} = R - n^\alpha n^\beta R_{\alpha\beta} + K^2 - K_{\alpha\beta}K^{\alpha\beta} , && (4.3.10)
\end{aligned}$$

where the raising/lowering rule is given by $K_\nu{}^\mu = K_{\nu\alpha}\gamma^{\alpha\mu} = \gamma_{\nu\alpha}K^{\alpha\mu}$.

Chapter 5

Fluid-gravity model for the chiral magnetic effect

In the past few years, the chiral magnetic effect (CME) [30, 41–43] has received much attention in lattice QCD [5, 10, 51–54], hydrodynamics [130, 140–143] and holographic models [93, 144–154]. The CME states that, in the presence of a magnetic field $\mathbf{B}$, an electric current of the type

$$\mathbf{J} = C\mu_5\mathbf{B}\,, \qquad C = \frac{N_c}{2\pi^2} \tag{5.0.1}$$

is generated in the background of topologically nontrivial gluon fields. This could possibly contribute to the charge asymmetry observed in heavy-ion collisions at RHIC and LHC [37–40].

A hydrodynamic description of the CME has recently been found in [140,141], using techniques developed in [130]. This model contains two $U(1)$ currents, an axial and a vector one, which are assumed to be conserved, at least in the absence of electric fields. This allows us to introduce the corresponding chemical potentials μ and μ_5, and the CME was shown to arise as a first-order transport coefficient κ_B in the constitutive equation for the electromagnetic current $\Delta j^\mu = \kappa_B B^\mu$ with $\kappa_B = C\mu_5$.

There have also been several proposals for a holographic description of the CME. In the early works [144, 145], the axial anomaly was not realized in covariant form and the electromagnetic current was not strictly conserved. Aiming at restoring the conservation of the electromagnetic current, Ref. [148] introduced the Bardeen counterterm into the action. However, as shown in [146,148] for some standard AdS/QCD models, this typically leads to a vanishing electromagnetic current.

In [146, 147] the problem was traced back to the difficulty of introducing a chemical potential conjugated to a nonconserved charge. Reference [146] therefore suggested a modification of the action in which the axial charge is conserved. This charge is, however, only gauge invariant when integrated over all space in homogeneous configurations [147], while the charge separation in heavy-ion collisions is clearly inhomogeneous. In contrast, Ref. [147] introduced a chiral chemical potential dual to a gauge invariant current, despite it being anomalous. This required a singular bulk gauge field at the horizon, a phenomenon which seems to be generic in AdS black hole models of the CME.

In this chapter, we propose a different approach which is based on the fluid-gravity correspondence [75] rather than a static (AdS/QCD) model. The fluid-gravity duality is more flexible since the hydrodynamic gradient expansion captures (small) deviations from equilibrium. This includes the CME and the change of the chiral charge density due to the anomaly $E \cdot B$ as first- and second-order effects, respectively. This allows us to introduce chemical potentials even for anomalous currents.

Our main goal is to construct a holographic dual of the hydrodynamic two-charge model of Ref. [140]. We will start from the three-charge STU model [155] which we take as a prototype of an AdS black hole background with several $U(1)$ charges. We consider it as a *phenomenological* model of a strongly coupled plasma with multiple chemical potentials; *i.e.*, we prescind from the strict string theory interpretation of the three $U(1)$'s as R charges inside the $SO(6)_R$ R symmetry of $\mathcal{N}=4$ super-Yang-Mills theory. This allows us to interpret one of them as an axial $U(1)$ charge and the other two as a single vector $U(1)$ charge. These charges are dual to μ and μ_5 required in the hydrodynamic description [140].

We proceed as follows. First, we show that the two-charge model of [140] can be considered as a special case of the hydrodynamic three-charge model of [130,131]. Next, we reproduce the relevant magnetic conductivities in this three-charge model from the dual STU model (plus background gauge fields), using fluid-gravity duality [75]. We then reduce the model to two charges and recover the CME (*i.e.* κ_B of [140]) as well as other related effects. Finally, we present a time-dependent version of the STU model dual to a boost-invariant expanding plasma.

5.1 CME and CVE in hydrodynamics

Hydrodynamics of a $U(1)^3$ plasma. The hydrodynamic regime of relativistic quantum gauge theories with triangle anomalies has been studied in [130, 131]. The anomaly coefficients are usually given by a totally symmetric rank-3 tensor C^{abc} and the hydrodynamic equations are

$$\partial_\mu T^{\mu\nu} = F^{a\nu\lambda} j^a_\lambda \,, \qquad \partial_\mu j^{a\mu} = C^{abc} E^b \cdot B^c \,, \tag{5.1.1}$$

where $E^{a\mu} = F^{a\mu\nu} u_\nu$, $B^{a\mu} = \frac{1}{2}\epsilon^{\mu\nu\alpha\beta} u_\nu F^a_{\alpha\beta}$ $(a = 1,2,3)$ are electric and magnetic fields, and $F^a_{\mu\nu} = \partial_\mu A^a_\nu - \partial_\nu A^a_\mu$ denotes the gauge field strengths. The stress-energy tensor $T^{\mu\nu}$ and $U(1)$ currents $j^{a\mu}$ are

$$\begin{aligned} T^{\mu\nu} &= (\epsilon + P) u^\mu u^\nu + P g^{\mu\nu} + \tau^{\mu\nu} \,, \\ j^{a\mu} &= \rho^a u^\mu + \nu^{a\mu} \,, \end{aligned} \tag{5.1.2}$$

where $\tau^{\mu\nu}$ and $\nu^{a\mu}$ denote higher-gradient corrections. ρ^a, ϵ, and P denote the charge densities, energy density and pressure, respectively.

In the presence of E and B fields the first-order correction of the $U(1)$ currents is given by

$$\nu^{a\mu} = \xi^a_\omega \omega^\mu + \xi^{ab}_B B^{b\mu} + \dots \,, \tag{5.1.3}$$

where $\omega^\mu \equiv \frac{1}{2}\epsilon^{\mu\nu\lambda\rho} u_\nu \partial_\lambda u_\rho$ is the vorticity. The ellipses indicate further terms involving electric fields. The conductivities ξ^a_ω and ξ^{ab}_B were first introduced in [76, 130] and are given by [131] (see also [130, 156])

$$\xi^a_\omega = C^{abc}\mu^b\mu^c - \frac{2}{3}\rho^a C^{bcd}\frac{\mu^b\mu^c\mu^d}{\epsilon + P} \,, \tag{5.1.4}$$

$$\xi^{ab}_B = C^{abc}\mu^c - \frac{1}{2}\rho^a C^{bcd}\frac{\mu^c\mu^d}{\epsilon + P} \,, \tag{5.1.5}$$

where μ^a are the three chemical potentials. These conductivities are specific for relativistic quantum field theories with quantum anomalies and do not appear in nonrelativistic theories [130].

Magnetic and vortical Effects. For the hydrodynamical description of the chiral magnetic effect, we only need an axial and a vector chemical potential, μ_5 and μ. The three-charge model

can be reduced to one with two charges by choosing the following identifications[1],

$$\begin{aligned} A^A_\mu &= A^1_\mu\,, \qquad A^V_\mu = A^2_\mu = A^3_\mu\,, \\ \mu_5 &= \mu^1\,, \qquad \mu = \mu^2 = \mu^3\,, \\ j^\mu_5 &= j^{1\mu}\,, \qquad j^\mu = j^{2\mu} + j^{3\mu}\,, \end{aligned} \tag{5.1.6}$$

and $C^{123} = C^{(123)} = \frac{C}{2}$. In the absence of axial gauge fields A^A_μ (which are not required), (5.1.1) simplifies to[2]

$$\partial_\mu T^{\mu\nu} \simeq F^{V\nu\lambda} j_\lambda\,, \quad \partial_\mu j^\mu_5 = C E^\lambda B_\lambda\,, \quad \partial_\mu j^\mu \simeq 0\,, \tag{5.1.7}$$

where $E^\mu \equiv F^{V\mu\nu} u_\nu$, $B^\mu \equiv \frac{1}{2}\epsilon^{\mu\nu\alpha\beta} u_\nu F^V_{\alpha\beta}$. The symbol "$\simeq$" indicates that the equation only holds for $A^A_\mu = 0$.

Let us also define

$$\begin{aligned} &\rho_5 = \rho^1\,, \quad \rho = \rho^2 + \rho^3\,, \\ &\kappa_\omega = \xi^2_\omega + \xi^3_\omega\,, \quad \kappa_B = \xi^{22}_B + \xi^{23}_B + \xi^{32}_B + \xi^{33}_B\,, \\ &\xi_\omega = \xi^1_\omega\,, \quad \xi_B = \xi^{12}_B + \xi^{13}_B\,. \end{aligned} \tag{5.1.8}$$

Then from (5.1.2)–(5.1.5) we get the constitutive equations

$$\begin{aligned} j^\mu &= \rho u^\mu + \kappa_\omega \omega^\mu + \kappa_B B^\mu\,, \\ j^\mu_5 &= \rho_5 u^\mu + \xi_\omega \omega^\mu + \xi_B B^\mu\,, \end{aligned} \tag{5.1.9}$$

with coefficients

$$\begin{aligned} &\kappa_\omega = 2C\mu\mu_5 \left(1 - \frac{\mu\rho}{\epsilon + P}\right), \quad \kappa_B = C\mu_5 \left(1 - \frac{\mu\rho}{\epsilon + P}\right), \\ &\xi_\omega = C\mu^2 \left(1 - 2\frac{\mu_5\rho_5}{\epsilon + P}\right), \;\; \xi_B = C\mu \left(1 - \frac{\mu_5\rho_5}{\epsilon + P}\right), \end{aligned} \tag{5.1.10}$$

which to leading order are in agreement with [140].

The leading term in κ_B is nothing but the *chiral magnetic effect* (CME) [30, 41–43], $\kappa_B = C\mu_5$. There is a second effect given by the term $\kappa_\omega = 2C\mu\mu_5$ which has recently been termed *chiral vortical effect* (CVE) [157]. The CVE states that, if the liquid rotates with some angular velocity $\vec{\omega}$, an electromagnetic current is induced along $\vec{\omega}$ – there are analogous effects in the axial current j^μ_5. The leading term in ξ_B, $\xi_B = C\mu$, generates an axial current parallel to the magnetic field, while $\xi_\omega = C\mu^2$ describes chirality separation through rotation. These two effects are usually refered as the *chiral separation effect* (CSE) [130, 158–160].

We may also shift all anomalies in (5.1.1) entirely into the current $j^{1\mu}$ ($= j^\mu_5$) by adding Bardeen currents,

$$\begin{aligned} j'^\mu &\equiv j^\mu + j^\mu_B\,, \qquad j'^\mu_5 \equiv j^\mu_5 + j^\mu_{5,B}\,, \\ j^\mu_B &= c_B \varepsilon^{\mu\nu\lambda\rho} (A^V_\nu F^A_{\lambda\rho} - 2A^A_\nu F^V_{\lambda\rho})\,, \\ j^\mu_{5,B} &= c_B \varepsilon^{\mu\nu\lambda\rho} A^V_\nu F^V_{\lambda\rho}\,, \end{aligned} \tag{5.1.11}$$

with $c_B = -C/2$ such that (5.1.1) becomes ($C' = 3C$)

$$\partial_\mu T^{\mu\nu} \simeq F^{V\nu\lambda} j'_\lambda\,, \quad \partial_\mu j'^\mu_5 = C' E^\lambda B_\lambda\,, \quad \partial_\mu j'^\mu = 0\,.$$

This is formally identical to (5.1.7), leading again to (5.1.10).

[1] Two of three U(1) charges are chosen to be identical and corresponding to the electric charge.

[2] For the sake of simplicity, we consider only a part of the chiral anomaly corresponding to the triangle diagram with two vector legs. This leads to the absence of the subleading μ_5^2 and μ_5^3 terms in (5.1.10). For a full treatment, involving also the second diagram with three axial legs, see Chapter 6.

5.2 Fluid-gravity model for the CME

Three-charge STU model with external fields. In the following we propose the three-charge STU model [155] as a holographic dual gravity theory for the (chiral) magnetic and vortical effects in a relativistic fluid. We begin by showing that the first-order transport coefficients (5.1.4) and (5.1.5) of the $U(1)^3$ theory can be reproduced from the STU model [155]. Subsequently, we will reduce it to a two-charge model and recover the conductivities (5.1.10).

The Lagrangian of the STU-model is given by [155]

$$\begin{aligned}\mathcal{L} = R - \frac{1}{2}G_{ab}F^a_{MN}F^{bMN} - G_{ab}\partial_M X^a \partial^M X^b + 4\sum_{a=1}^{3}\frac{1}{X^a} \\ + \frac{1}{24}\sqrt{-g_5}\epsilon^{MNPQR}S_{abc}F^a_{MN}F^b_{PQ}A^c_R\,,\end{aligned} \tag{5.2.1}$$

where

$$G_{ab} = \frac{1}{2}\delta_{abc}(X^c)^{-2}, \qquad X^1X^2X^3 = 1\,. \tag{5.2.2}$$

g_{MN}, X^a and A^a_M $(M,N = 0,1,...,4,\ a,b,c = 1,2,3)$ denote the metric, three scalars and $U(1)$ gauge fields, respectively.

The boosted black brane solution corresponding to the three-charge STU model is given by [155]

$$\begin{aligned} ds^2 &= -H^{-\frac{2}{3}}(r)f(r)u_\mu u_\nu dx^\mu dx^\nu - 2H^{-\frac{1}{6}}(r)u_\mu dx^\mu dr \\ &\quad + r^2 H^{\frac{1}{3}}(r)\left(\eta_{\mu\nu} + u_\mu u_\nu\right)dx^\mu dx^\nu\,, \\ A^a &= \left(A^a_0(r)\,u_\mu + \mathcal{A}^a_\mu\right)dx^\mu\,, \quad X^a = \frac{H^{\frac{1}{3}}(r)}{H_a(r)}\,, \end{aligned} \tag{5.2.3}$$

where $(\mu,\nu = 0,1,2,3)$

$$\begin{aligned} f(r) &= -\frac{m}{r^2} + r^2 H(r)\,, \quad H(r) = \prod_{a=1}^{3} H^a(r)\,, \\ H^a(r) &= 1 + \frac{q^a}{r^2}\,, \qquad A^a_0(r) = \frac{\sqrt{mq^a}}{r^2+q^a}\,, \end{aligned} \tag{5.2.4}$$

and u_μ is the four-velocity of the fluid with $u_\mu u^\mu = -1$. Following [130], we have formally introduced constant background gauge fields $\mathcal{A}^a_\mu$, which are necessary for the computation of the transport coefficients ξ^{ab}_B.

We now use the standard procedure [75] to holographically compute the transport coefficients ξ^a_ω and ξ^{ab}_B. We closely follow [129] which has already determined ξ^a_ω from the STU-model (but not ξ^{ab}_B relevant for the CME). Working in the frame $u_\mu = (-1,0,0,0)$ (at $x^\mu = 0$), we slowly vary u_μ and $\mathcal{A}^a_\mu$ up to first order as

$$u_\mu = (-1, x^\nu\partial_\nu u_i), \qquad \mathcal{A}^a_\mu = (0, x^\nu\partial_\nu\mathcal{A}^a_i)\,. \tag{5.2.5}$$

We may also vary m and q in this way, but it turns out that varying these parameters has no influence on the transport coefficients ξ^a_ω and ξ^{ab}_B.

As a consequence, the background (5.2.3) is no longer an exact solution of the equations of motion but receives higher-order corrections. The corrected metric and gauge fields can be rewritten

in Fefferman-Graham coordinates and expanded near the boundary (at $z = 0$) as

$$\begin{aligned} ds^2 &= \frac{1}{z^2}\left(g_{\mu\nu}(z,\,x)\,dx^\mu dx^\nu + dz^2\right)\,, \\ g_{\mu\nu}(z,x) &= \eta_{\mu\nu} + g^{(2)}_{\mu\nu}(x)\,z^2 + g^{(4)}_{\mu\nu}(x)\,z^4 + \dots\,, \\ A^a_\mu(z,\,x) &= A^{a(0)}_\mu(x) + A^{a(2)}_\mu(x)\,z^2 + \dots\,. \end{aligned} \tag{5.2.6}$$

The first-order gradient corrections of the energy-momentum tensor and $U(1)$ currents (5.1.2) are then read off from [70, 71, 134]

$$T_{\mu\nu} = \frac{g^{(4)}_{\mu\nu}(x)}{4\pi G_5} + c.t.\,, \quad j^\mu_a = \frac{\eta^{\mu\nu}A^{(2)}_{a\nu}(x)}{8\pi G_5} + \hat{j}^\mu_a\,, \tag{5.2.7}$$

$$\hat{j}^\mu_a = -\frac{S_{abc}}{32\pi G_5}\epsilon^{\mu\nu\rho\sigma}A^{(0)}_{b\nu}(x)\partial_\rho A^{(0)}_{c\sigma}(x)\,, \tag{5.2.8}$$

where $c.t.$ denotes diagonal corrections to the energy-momentum tensor due to counterterms. The term $\hat{j}^\mu_a$ will be discussed below around (5.2.13).

The computation of the corrected metric and gauge fields is very similar to that in [129]. At zeroth order, we get the same expressions for the pressure P and charge densities ρ_a as in [129], $P \equiv m/16\pi G_5$ and $\rho_a \equiv \sqrt{mq_a}/8\pi G_5$, which may be combined to give

$$\frac{\sqrt{mq^a}}{2m} = \frac{\rho^a}{\epsilon + P} \qquad (\epsilon = 3P)\,. \tag{5.2.9}$$

At first order, the transport coefficients ξ^a_ω and ξ^{ab}_B are read off from the near boundary behavior of A^a_μ via (5.2.7),

$$\xi^a_\omega = \frac{1}{16\pi G_5}\left(S^{abc}\mu^b\mu^c - \frac{\sqrt{mq^a}}{3m}S^{bcd}\mu^b\mu^c\mu^d\right), \tag{5.2.10}$$

$$\xi^{ab}_B = \frac{1}{16\pi G_5}\left(S^{abc}\mu^c - \frac{\sqrt{mq^a}}{4m}S^{bcd}\mu^c\mu^d\right), \tag{5.2.11}$$

with $\mu^a \equiv A^a_0(r_H) - A^a_0(\infty)$. Using a standard relation between the anomaly coefficients C_{abc} and the Chern-Simons parameters S_{abc}, $C_{abc} = S_{abc}/16\pi G_5$, as well as (5.2.9), we find that the holographically computed transport coefficients (5.2.10) and (5.2.11) coincide exactly with those found in hydrodynamics, (5.1.4) and (5.1.5).

Holographic magnetic and vortical effects. In order to obtain the holographic versions of the magnetic and vortical effects (5.1.10), we reduce the STU model to a two-charge model using the same identities as in hydrodynamics, (5.1.6) and (5.1.8). In particular, we define (vector and axial) gauge fields A^V_μ and A^A_μ, chemical potentials μ and μ_5, and currents j^μ and j^μ_5 as in (5.1.6) but now with $\mu^a \equiv A^a_0(r_H) - A^a_0(\infty)$, and A^a and j^μ_a as in (5.2.3) and (5.2.7), respectively. Moreover, we set $S_{abc} = S/2$ with $S = 16\pi G_5 C$ and keep S_{abc} general, as in [130].

Using also the identifications (5.1.8), but now for the holographically computed transport coefficients (5.2.10) and (5.2.11), we get

$$\begin{aligned} \kappa_\omega &= 2C\mu\mu_5\left(1 - \mu\sqrt{\frac{q}{m}}\right), \quad \kappa_B = C\mu_5\left(1 - \mu\sqrt{\frac{q}{m}}\right), \\ \xi_\omega &= C\mu^2\left(1 - \mu_5\sqrt{\frac{q_5}{m}}\right), \quad \xi_B = C\mu\left(1 - \frac{\mu_5}{2}\sqrt{\frac{q_5}{m}}\right), \end{aligned}$$

in agreement with (5.1.10). This shows that the CME, CVE, etc. are realized in the STU-model, when appropriately reduced to a two-charge model.

Comments. To get an anomaly free three-point function for j^μ, we also need to add the Bardeen currents (5.1.11). As in hydrodynamics, this does not change the structure of the transport coefficients. Note however that, together with (5.2.8), the Bardeen term gives rise to additional contributions of the type

$$\begin{aligned}\Delta j^\mu &= \hat{j}^{2\mu} + \hat{j}^{3\mu} + j_B^\mu \\ &\supset \varepsilon^{\mu\nu\rho\sigma}(\mathcal{A}^A_\nu(x)\mathcal{F}^V_{\rho\sigma}(x) - \mathcal{A}^V_\nu(x)\mathcal{F}^A_{\rho\sigma}(x))\,. \end{aligned} \tag{5.2.12}$$

If we choose $\mathcal{A}^A_\nu = \alpha^A u_\nu$ (at $x=0$) with some constant $\alpha^A \neq 0$, we get terms of the type $\mathcal{A}^A_0 B^\mu$ which are forbidden by electromagnetic gauge invariance [146]. As in [146, 147], we are therefore forced to switch off the axial background gauge field $\mathcal{A}^A_\mu$ completely[3], $\alpha^A = 0$. This corresponds to a nonvanishing gauge field at the horizon, as in [147]. There is also an additional term in j^μ_5,

$$\Delta j^\mu_5 = \hat{j}^\mu_5 + j^\mu_{5,B} \propto \epsilon^{\mu\nu\rho\sigma}\mathcal{A}^V_\nu(x)\mathcal{F}^V_{\rho\sigma}(x)\,, \tag{5.2.13}$$

which is of second order, as can be seen by substituting $\mathcal{A}^V_\nu(x) = (0, x^\nu\partial_\nu\mathcal{A}^V_i)$. For instance, choosing $\mathcal{A}^V_\mu = (0, -x_2 B, 0, -tE)$, *i.e.* constant E and B fields along x^3, the charge density $\rho_5 \equiv j^0_5$ changes linearly in time, $\Delta\rho_5 \sim S\epsilon^{0321}\mathcal{A}^V_3\partial_2\mathcal{A}^V_1 \sim tCEB$, as expected. Thus, holographic renormalization perfectly takes into account changes of hydrodynamic currents due to the anomaly, showing that fluid-gravity duality is consistent even for nonconserved currents. [The effects enter via the Chern-Simons parameters $S^{abc} \propto C^{abc}$ in (5.2.8).]

Holographic time-dependent model for the CME. – It is well known that the hydrodynamic gradient expansion of a fluid is also realized in the late-time evolution of a boost-invariant expanding plasma *à la* [74]. Recently, a time-dependent Reissner-Nordström-type solution was found in [2] which describes the late-time evolution of an expanding $\mathcal{N}=4$ super Yang-Mills plasma with a single chemical potential. Similarly, we now construct a late-time solution from the boosted black brane solution (5.2.3) (dual to three chemical potentials). Proceeding as in [2], we assume the late-time behavior $m = \tilde{\tau}^{-4/3}m_0$, $q^a = \tilde{\tau}^{-2/3}q^a_0$ for the parameters m and q^a and find the zeroth-order solution ($v = \tilde{\tau}^{1/3}r$)

$$\begin{aligned} ds^2 &= -H^{-\frac{2}{3}}(v)f(v)d\widetilde{\tau}^2 + 2H^{-\frac{1}{6}}(v)d\widetilde{\tau}dr \\ &\quad + H^{\frac{1}{3}}(v)\left((1+r\widetilde{\tau})^2dy^2 + r^2dx_\perp^2\right)\,, \\ A^a &= -A^a_0(v)d\widetilde{\tau} + \mathcal{A}^a_\mu dx^\mu\,, \quad X^a = \frac{H^{\frac{1}{3}}(v)}{H_a(v)}\,, \\ f(v) &= r^2\left(-\frac{m_0}{v^4} + H(v)\right)\,, \quad H(v) = \prod_{a=1}^3 H^a(v)\,, \\ H^a(v) &= 1 + \frac{q^a_0}{v^2}\,, \qquad A^a_0(v) = \frac{1}{\tilde{\tau}^{1/3}}\frac{\sqrt{m_0 q^a_0}}{v^2+q^a_0}\,. \end{aligned} \tag{5.2.14}$$

This background is a good approximation of the full time-dependent solution at large $\widetilde{\tau}$ (as we have explicitly checked using computer algebra for $\mathcal{A}^1_\mu = 0$, $\mathcal{A}^{2,3}_\mu = (0, -x_2B, 0, 0)$). At smaller $\widetilde{\tau}$, it receives subleading corrections in $\widetilde{\tau}^{-2/3}$ corresponding to higher-order gradient corrections. It has been shown many times that first-order transport coefficients appear in the first correction in $\widetilde{\tau}^{-2/3}$. It therefore follows from the above discussion that the conductivities ξ^{ab}_B, relevant for the CME, appear in the first-order correction to the solution (5.2.14).

[3] Another reason is that $\alpha^A \neq 0$ introduces an additional source for the chirality, which we already mimic by μ_5. With $\alpha^A \propto \mu_5$ this may lead to the cancellation of CME

Appendix A. Details on the computation of ξ^a_ω and ξ^{ab}_B

The computation of the magnetic transport coefficients ξ^{ab}_B is quite similar to the computation of ξ^a_ω in [129]. We work in the static frame $u_\mu = (-1,0,0,0)$ and consider vanishing background fields $\mathcal{A}^a_\mu$ (at $x^\mu = 0$). We then slowly vary the velocity u_μ and the background fields $\mathcal{A}^a_\mu$ up to first order as

$$u_\mu = (-1, x^\nu \partial_\nu u_i)\,, \qquad \mathcal{A}^a_\mu = (0, x^\nu \partial_\nu \mathcal{A}^a_i)\,. \tag{5.2.15}$$

As explained above, we do not consider variations of m and q.

We denote the first-order corrections to the fields by

$$\tilde{g}_{MN} = \tilde{g}_{MN}(r), \quad \tilde{A}^a_M = \tilde{A}^a_M(r), \quad \tilde{X}^a = \tilde{X}^a(r) \tag{5.2.16}$$

and, as in [129], choose the gauge

$$\tilde{g}_{rr} = 0, \quad \tilde{g}_{r\mu} \sim u_\mu, \quad \tilde{A}^a_r = 0, \quad \sum_{i=1}^{3} \tilde{g}_{ii} = 0\,. \tag{5.2.17}$$

The first-order corrected metric is then

$$\begin{aligned} ds^2 = &\left(-H^{-\frac{2}{3}} f(r) + \tilde{g}_{tt}\right) dt^2 + 2\left(H^{-\frac{1}{6}} + \tilde{g}_{tr}\right) dt dr \\ &+ r^2 H^{\frac{1}{3}} (dx^i)^2 + \tilde{g}_{ij} dx^i dx^j - 2H^{-\frac{1}{6}} x^\nu \partial_\nu u_i dr dx^i \\ &+ 2\left(\left(H^{\frac{2}{3}} f(r) - r^2 H^{\frac{1}{3}}\right) x^\nu \partial_\nu u_i + \tilde{g}_{ti}\right) dt dx^i\,, \end{aligned} \tag{5.2.18}$$

the gauge fields become

$$\begin{aligned} A^a = &\left(-\frac{\sqrt{m q_a}}{r^2 + q_a} + \tilde{A}^a_t\right) dt \\ &+ \left(\frac{\sqrt{m q_a}}{r^2 + q_a} x^\nu \partial_\nu u_i + x^\nu \partial_\nu \mathcal{A}^a_i + \tilde{A}^a_i\right) dx^i\,, \end{aligned} \tag{5.2.19}$$

and the scalars are

$$X^a = \frac{H^{\frac{1}{3}}}{H_a} + \tilde{X}^a\,. \tag{5.2.20}$$

Let us denote the Nth component of the Maxwell equation (which can be obtained from (5.2.1)) by M^a_N and the components of the Einstein equation by E_{NP}. Then, from $g^{rt} M^a_t + g^{rr} M^a_r = 0$ and $g^{rt} E_{ti} + g^{rr} E_{ri} = 0$ we find $\partial_i u_i = 0$ and $\partial_t u_i = 0$, respectively. In this case E_{tt} is equivalent to E_{rt} and E_{ti} is equivalent to E_{ri}. E_{tt}, E_{rt}, E_{rr}, E_{tt}, M^a_t, M^a_r and the scalar field equations are trivially solved by

$$\tilde{g}_{tr} = \tilde{g}_{tt} = \tilde{A}^a_t = \tilde{X}^a = 0\,. \tag{5.2.21}$$

The remaining equations are E_{ij}, E_{ti}, M^a_i.

From E_{ij} we get

$$-\partial_r\left(r^3 f(r) \partial_r\left(\frac{\tilde{g}_{ij}}{r^2 H^{\frac{1}{3}}}\right)\right) = \partial_r\left(r^3 H^{\frac{1}{2}}\right)\left[\partial_i u_j + \partial_j u_i\right]\,. \tag{5.2.22}$$

From E_{ti} we get

$$-\frac{f(r)}{2r^3H}\partial_r\left(r^5H\partial_r\left(\frac{\tilde{g}_{ti}}{r^2H^{\frac{1}{3}}}\right)\right)=\sum_{a=1}^{3}\frac{f(r)\sqrt{mq_a}}{r^3H}\partial_r\tilde{A}_i^a\,. \tag{5.2.23}$$

From M_i^a we get

$$\begin{aligned}&\frac{1}{r}\partial_r\left(\frac{rf(r)\left(H_a\right)^2}{H}\partial_r\tilde{A}_i^a\right)+\frac{2\sqrt{mq_a}}{r}\partial_r\left(\frac{\tilde{g}_{ti}}{r^2H^{\frac{1}{3}}}\right)\\&=\frac{1}{r}\partial_r\left(\frac{1}{2}S_{abc}\frac{\sqrt{mq_b}\sqrt{mq_c}}{(r^2+q_b)(r^2+q_c)}\epsilon^{ijk}\left(\partial_j u_k\right)+S_{abc}\frac{\sqrt{mq_b}}{(r^2+q_b)}\epsilon^{ijk}\left(\partial_j\mathcal{A}_k^c\right)\right)\equiv\frac{1}{r}\partial_r Q_i^a(r)\,.\end{aligned} \tag{5.2.24}$$

Eq. (5.2.22) depends only on $\tilde{g}_{ij}$ and can easily be solved. Integration of (5.2.24) leads to

$$\frac{rf(r)\left(H_a\right)^2}{H}\partial_r\tilde{A}_i^a+2\sqrt{mq_a}\left(\frac{\tilde{g}_{ti}}{r^2H^{\frac{1}{3}}}\right)=Q_i^a(r)-Q_i^a(r_H)+\frac{2\sqrt{mq_a}}{r_H^2H^{\frac{1}{3}}(r_H)}C_i\,, \tag{5.2.25}$$

where C_i are some integration constants. Using this expression we replace $\partial_r\tilde{A}_i^a$ in (5.2.23) and solve the resulting equation for $\tilde{g}_{ti}$,

$$\tilde{g}_{ti}(r)=\frac{f(r)}{H^{\frac{2}{3}}(r)}\int_\infty^r dr'\,\frac{H(r')}{r'\left(f(r')\right)^2}\left(\int_{r_H}^{r'}dr''\,\mathcal{I}_i(r'')-\frac{r_Hf'(r_H)}{H^{\frac{1}{3}}(r_H)}C_i\right)\,, \tag{5.2.26}$$

where

$$\mathcal{I}_i(r'')=\sum_{a=1}^{3}\frac{-2\sqrt{mq_a}}{(r'')^3\left(H_a(r'')\right)^2}\Big(Q_i^a(r'')-Q_i^a(r_H)+\frac{2\sqrt{mq_a}}{r_H^2H^{\frac{1}{3}}(r_H)}C_i\Big)\,. \tag{5.2.27}$$

In the Landau frame we require $u_\mu\tilde{T}^{\mu\nu}=0$, which in particular implies the absence of corrections to T^{ti}. Following the renormalization procedure (5.2.7), we conclude that

$$\lim_{r\to\infty}r^2\,\tilde{g}_{ti}(r)=0\,. \tag{5.2.28}$$

Let us demonstrate how this constraint fixes the integration constant C_i. For $r\to\infty$ one derives the asymptotics

$$f(r)=r^2+O(1),\qquad H(r)=1+O(\frac{1}{r^2}),\qquad \int_{r_H}^{r}dr'\,I(r')=O(1)$$

and from (5.2.28) we obtain the following equation on C_i,

$$\begin{aligned}\frac{r_Hf'(r_H)}{H^{\frac{1}{3}}(r_H)}C_i&=\int_{r_H}^{\infty}dr'\sum_{a=1}^{3}\frac{-2\sqrt{mq_a}}{(r')^3\left(H_a(r')\right)^2}\left(Q_i^a(r')-Q_i^a(r_H)+\frac{2\sqrt{mq_a}}{r_H^2H^{\frac{1}{3}}(r_H)}C_i\right)\\&=\mathcal{I}_1+\mathcal{I}_2\cdot C_i\,,\end{aligned} \tag{5.2.29}$$

where we define the integrals

$$\begin{aligned}\mathcal{I}_1&\equiv\int_{r_H}^{\infty}dr'\sum_{a=1}^{3}\frac{-2\sqrt{mq_a}}{(r')^3\left(H_a(r')\right)^2}\left(Q_i^a(r')-Q_i^a(r_H)\right)\\&=\frac{1}{3}S_{abc}\frac{\sqrt{mq_a}\sqrt{mq_b}\sqrt{mq_c}}{(r_H^2+q_a)(r_H^2+q_b)(r_H^2+q_c)}\epsilon^{ijk}\left(\partial_j u_k\right)+\frac{1}{2}S_{abc}\frac{\sqrt{mq_a}\sqrt{mq_b}}{(r_H^2+q_a)(r_H^2+q_b)}\epsilon^{ijk}\left(\partial_j\mathcal{A}_k^c\right)\end{aligned} \tag{5.2.30}$$

and

$$\mathcal{I}_2 \equiv \int_{r_H}^{\infty} dr' \sum_{a=1}^{3} \frac{-2\sqrt{mq_a}}{(r')^3 \left(H_a(r')\right)^2} \left(\frac{2\sqrt{mq_a}}{r_H^2 H^{\frac{1}{3}}(r_H)} \right) = \frac{2m}{r_H^2 H^{\frac{1}{3}}(r_H)} \left(-3 + \sum_{a=1}^{3} \frac{1}{H_a(r_H)} \right) \tag{5.2.31}$$

So, moving the terms proportional to C_i to the left part of (5.2.29) we come to the final answer:

$$\begin{aligned} C_i = & \frac{r_H^2 H^{\frac{1}{3}}(r_H)}{4m} \\ & \times \left(\frac{1}{3} S_{abc} \frac{\sqrt{mq_a}\sqrt{mq_b}\sqrt{mq_c}}{(r_H^2+q_a)(r_H^2+q_b)(r_H^2+q_c)} \epsilon^{ijk} \left(\partial_j u_k\right) + \frac{1}{2} S_{abc} \frac{\sqrt{mq_a}\sqrt{mq_b}}{(r_H^2+q_a)(r_H^2+q_b)} \epsilon^{ijk} \left(\partial_j \mathcal{A}_k^c\right) \right), \end{aligned} \tag{5.2.32}$$

where we used the identity $m = r_H^4 H(r_H)$ to simplify it.

We now rewrite the obtained quantities in a covariant form out of the static frame. Then the first order correction to the current will be

$$\tilde{J}^{a\mu} = \lim_{r\to\infty} \frac{r^2}{8\pi G_5} \eta^{\mu\nu} \tilde{A}_\nu^a(r) = \frac{1}{16\pi G_5} \left(Q_\mu^a(r_H) - \frac{2\sqrt{mq_a}}{r_H^2 H^{\frac{1}{3}}(r_H)} C_\mu \right). \tag{5.2.33}$$

Comparing this with the general expansion

$$\begin{aligned} \tilde{J}^{a\mu} &= \xi^a \, \omega^\mu + \xi_B^{ab} \, B^{b\mu} \\ &= \xi^a \, \frac{1}{2} \epsilon^{\nu\rho\sigma\mu} u_\nu \partial_\rho u_\sigma + \xi_B^{ab} \epsilon^{\nu\rho\sigma\mu} u_\nu \partial_\rho \mathcal{A}_\sigma^b \,, \end{aligned} \tag{5.2.34}$$

we finally obtain the coefficients (5.2.10) and (5.2.11).

Chapter 6

Anisotropic hydrodynamics, holography and the chiral magnetic effect

In a recent experiment [161], the charge separation is measured as a function of the elliptic flow coefficient v_2. The data is taken from (rare) Au+Au collisions with $20-40\%$ centrality but different v_2. In this way v_2 is varied while at the same time the number of participating nucleons (and therefore the magnetic field) is kept almost constant. The plots in [161] suggest that the charge separation is proportional to v_2. If this holds true, the charge separation will depend on the event anisotropy.

In this chapter we address the question of whether and how the CME depends on the elliptic flow v_2, which is a crucial step before we can interpret the experimental data. We study this both in hydrodynamics and in terms of a holographic gravity dual. The hydrodynamical approach to the CME and CME-related phenomena was proposed in [3,130,131,140–143,156]. There, the CME appears in form of a nonvanishing transport coefficient in the electric current, $\vec{j} = \kappa_B \vec{B}$, which measures the response of the system to an external magnetic field [76,130]. In the previous chapter the chiral magnetic conductivity in an isotropic fluid was determined as

$$\kappa_B = C\mu_5 \left(1 - \frac{\mu\rho}{\epsilon + P}\right). \tag{6.0.1}$$

The first term is the standard term for the CME and depends only on the axial anomaly coefficient C and the axial chemical potential μ_5. The second term proportional to the factor $\frac{\rho}{\epsilon+P}$ depends on the dynamics of the fluid and has a chance to depend on v_2 in the anisotropic case.

In the first part of the chapter we study this in a hydrodynamic model for an *anisotropic* fluid with multiple anomalous $U(1)$ charges (This model extends those in [163–165]). We compute the CME coefficient κ_B and express the result in terms of the momentum anisotropy ε_p [166] defined as

$$\varepsilon_p = \frac{\langle P_T - P_L \rangle}{\langle P_T + P_L \rangle}, \tag{6.0.2}$$

where P_T and P_L are the pressures in the plane transverse to the beam line (In our conventions the indices L and T refer to the longitudinal and transverse direction with respect to an anisotropy vector v_μ normal to the reaction plane, see Fig. 6.1). A sketch of ε_p as a function of the proper time τ is shown in Fig. 6.1. ε_p describes the build-up of the elliptic flow in off-central collisions.

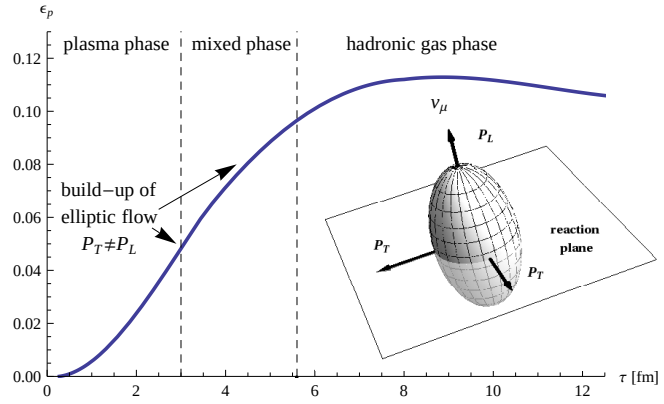

Figure 6.1: Sketch of the time evolution of the momentum anisotropy ε_p (based on [162]). The small figure shows the orientation of P_L and P_T with respect to the reaction plane.

Our model describes a state after thermalization with unequal pressures $P_T \neq P_L$. At freeze-out ε_p roughly equals v_2, and we find that for small anisotropies the CME-coefficient κ_B increases linearly with v_2.

In the second part of the chapter we perform a holographic computation of κ_B in the dual gravity model. In the anisotropic case, we first need to construct an appropriate gravity background. As an ansatz, we choose a multiply charged AdS black hole solution with some additional functions w_L and w_T inserted which will make the background anisotropic and ε_p-dependent. Since analytical solutions for charged anisotropic backgrounds are notoriously difficult to find, we will use shooting techniques to find a numerical solution. Other AdS backgrounds dual to anisotropic fluids are constructed in [167–171].

As the AdS solution in [171], the background is static and does not describe the process of isotropization. Even though such models have some limitations [171], they are nevertheless useful for the computation of transport coefficients. We show this, following [3], by determining κ_B from the first-order corrections to this background using the fluid-gravity duality [75]. For small anisotropies, we find numerical agreement with the hydrodynamic result for κ_B. Other (dissipative) transport coefficients in strongly-coupled anisotropic plasmas are discussed in [172–174].

The chapter is organized as follows. In Sec. 6.1 we review the hydrodynamics of an anisotropic relativistic fluid with several $U(1)$ charges and triangle anomalies. We then compute the vortical and magnetic conductivities of such a fluid by extending the method of Son and Surowka [130] to the anisotropic case. In Sec. 6.2 we construct the dual gravity background and present a numerical solution for its gauge field and metric functions. In Sec. 6.3 we use this background to perform a holographic computation of the vortical and magnetic conductivities.

6.1 Hydrodynamics of anisotropic fluids with triangle anomalies

The hydrodynamic regime of isotropic relativistic fluids with triangle anomalies has been studied in [130,131,140–142,156], and much can be taken over to the anisotropic case. Such fluids typically contain n anomalous $U(1)$ charges which commute with each other. The anomaly coefficients are given by a totally symmetric rank-3 tensor C^{abc}. The hydrodynamic equations are

$$\partial_\mu T^{\mu\nu} = F^{a\nu\lambda} j^a_\lambda \,, \qquad \partial_\mu j^{a\mu} = C^{abc} E^b \cdot B^c \,, \tag{6.1.1}$$

where $E^{a\mu} = F^{a\mu\nu}u_\nu$, $B^{a\mu} = \frac{1}{2}\epsilon^{\mu\nu\alpha\beta}u_\nu F^a_{\alpha\beta}$ $(a = 1, ..., n)$ are electric and magnetic fields, and $F^a_{\mu\nu} = \partial_\mu A^a_\nu - \partial_\nu A^a_\mu$ denotes the gauge field strengths. As in [130], we expand the constitutive equations for $T^{\mu\nu}$ and j^μ up to first order, taking $A^a_\mu \sim O(p^0)$ and $F^a_{\mu\nu} \sim O(p)$. The gauge fields A^a_μ are nondynamical.

In *anisotropic* relativistic fluids, the hydrodynamic equations are again given by (6.1.1) but the stress-energy tensor $T^{\mu\nu}$ and $U(1)$ currents $j^{a\mu}$ now have the more general form[1]

$$T^{\mu\nu} = (\epsilon + P_T)u^\mu u^\nu + P_T g^{\mu\nu} - \Delta v^\mu v^\nu + \tau^{\mu\nu}\,, \tag{6.1.2}$$

$$j^{a\mu} = \rho^a u^\mu + \nu^{a\mu}\,, \tag{6.1.3}$$

where ϵ is the energy density, ρ^a are the $U(1)$ charge densities, $\Delta = P_T - P_L$, and P_T and P_L denote the transverse and longitudinal pressures, respectively [163–165]. $g_{\mu\nu}$ is the metric with signature $(-,+,+,+)$. $\tau^{\mu\nu}$ and $\nu^{a\mu}$ denote higher-gradient corrections, for which we require $u_\mu\tau^{\mu\nu} = 0$ and $u_\mu\nu^{a\mu} = 0$.

The four-vectors u^μ and v^μ describe the flow of the fluid and the direction of the longitudinal axis, respectively. The vector v^μ is spacelike and orthogonal to u^μ,

$$u_\mu u^\mu = -1\,, \qquad v_\mu v^\mu = 1\,, \qquad u_\mu v^\mu = 0\,. \tag{6.1.4}$$

It is convenient to define the proper time τ by $\partial^\nu \ln\tau \equiv v^\mu\partial_\mu v^\nu$ [164]. In the rest frame of the fluid, $u^\mu = (1,0,0,0)$ and $v^\mu = (0,0,0,1)$, the stress-energy tensor becomes diagonal,

$$T^{\mu\nu} = \begin{pmatrix} \epsilon & 0 & 0 & 0 \\ 0 & P_T & 0 & 0 \\ 0 & 0 & P_T & 0 \\ 0 & 0 & 0 & P_L \end{pmatrix}. \tag{6.1.5}$$

In conformal fluids, the stress-energy tensor is traceless, $T^\mu{}_\mu = 0$, and $\epsilon = 2P_T + P_L$. Clearly, the isotropic case corresponds to equal pressures P_T and P_L, $P = P_T = P_L$.

For simplicity, we restrict to the case of a single charge in Secs. 6.1.1 and 6.1.2, $n = 1$. In Secs. 6.1.3 and 6.1.4 we generalize our findings to arbitrary n and discuss the case $n = 2$, which is relevant for the CME.

6.1.1 Thermodynamics of an anisotropic fluid with chemical potential $(n = 1)$

Hydrodynamic models for an anisotropic fluid (without chemical potential) have been studied in [163–165]. Following these works, we derive some thermodynamic identities, now for the case of a fluid with a chemical potential μ.

These identities can be found by computing the quantity $I_0 = u_\nu\partial_\mu T^{\mu\nu} + \mu\partial_\mu j^\mu$ at zeroth order. Since the right-hand side of (6.1.1) can be dropped at order $O(p^0)$, we have $I_0 = 0$. Using $\partial_\mu(su^\mu) = 0$, we get

$$\begin{aligned} u_\nu\partial_\mu T^{\mu\nu} &= -u^\mu\partial_\mu\epsilon - (\epsilon + P_T)\partial_\mu u^\mu - \Delta u_\nu\partial^\nu\ln\tau \\ &= -u^\mu\partial_\mu\epsilon + \frac{\epsilon + P_T}{s}u^\mu\partial_\mu s - \frac{\Delta}{\tau}u^\mu\partial_\mu\tau\,, \end{aligned} \tag{6.1.6}$$

$$\mu\partial_\mu j^\mu = \mu(\partial_\mu\rho)u^\mu - \frac{\mu\rho}{s}u^\mu\partial_\mu s\,. \tag{6.1.7}$$

[1]The symmetries allow in principle for more general currents $j^{a\mu} = \rho^a u^\mu + c^a v^\mu + \nu^{a\mu}$ with some coefficients c^a. Here we switch off all the 'electric' background currents, $c^a = 0$. One can think about v^μ as corresponding to a neutral second component of the fluid.

As in [164], we consider a generalized energy density $\epsilon = \epsilon(s, \rho, \tau)$, which depends not only on the entropy density s and particle density ρ but also on the new variable τ. Its differential is

$$d\epsilon = \left(\frac{\partial\epsilon}{\partial s}\right)_{\rho,\tau} ds + \left(\frac{\partial\epsilon}{\partial\rho}\right)_{s,\tau} d\rho + \left(\frac{\partial\epsilon}{\partial\tau}\right)_{s,\rho} d\tau\,, \tag{6.1.8}$$

with

$$\left(\frac{\partial\epsilon}{\partial s}\right)_{\rho,\tau} = T\,, \quad \left(\frac{\partial\epsilon}{\partial\rho}\right)_{s,\tau} = \mu\,, \quad \left(\frac{\partial\epsilon}{\partial\tau}\right)_{s,\rho} = -\frac{\Delta}{\tau}\,. \tag{6.1.9}$$

The temperature and the chemical potential are defined in the usual way. If we also impose $(\partial\epsilon/\partial\tau)_{s,\rho} = -\Delta/\tau$ and substitute (6.1.8) into (6.1.6), then $I_0 = 0$ implies the following thermodynamical identities for an anisotropic fluid:

$$\epsilon + P_T = Ts + \mu\rho\,, \tag{6.1.10}$$

$$dP_T = \frac{\Delta}{\tau} d\tau + sdT + \rho d\mu\,, \tag{6.1.11}$$

$$d\epsilon = Tds + \mu d\rho - \frac{\Delta}{\tau} d\tau\,, \tag{6.1.12}$$

in agreement with [164] for $\mu = 0$.

6.1.2 Vortical and magnetic coefficients $(n = 1)$

We now discuss corrections to the $U(1)$ current $j^\mu \equiv j^{1\mu}$ $(n = 1)$. In anisotropic fluids the transport coefficients are usually promoted to tensors such that one should consider first-derivative corrections of the type

$$\nu^\mu = (\xi_\omega)^\mu{}_\nu \omega^\nu + (\xi_B)^\mu{}_\nu B^\nu\,, \tag{6.1.13}$$

where $\omega^\mu = \frac{1}{2}\epsilon^{\nu\rho\sigma\mu} u_\nu \partial_\rho u_\sigma$ is the vorticity, and B^μ is an external magnetic field. In Landau frame $u_\mu \nu^\mu = 0$ and therefore $u_\mu (\xi_\omega)^\mu{}_\nu \omega^\nu = 0$ (and similar for $(\xi_B)^\mu{}_\nu$). This is satisfied *e.g.* for $(\xi_\omega)^\mu{}_\nu = \xi_\omega \delta^\mu{}_\nu$, since $u_\mu \omega^\mu = 0$ (We do not consider other components of ξ_ω here). We therefore restrict to consider corrections of the type

$$\nu^\mu = \xi_\omega \omega^\mu + \xi_B B^\mu\,, \tag{6.1.14}$$

as in the isotropic case [130]. Our goal is to compute the vortical and magnetic conductivities ξ_ω and ξ_B. These transport coefficients can be found by assuming the existence of an entropy current s^μ with a non-negative derivative, $\partial_\mu s^\mu \geq 0$. The computation closely follows that of [130].

The hydrodynamic Eqs. (6.1.1) imply that the quantity

$$I_1 = u_\nu \partial_\mu T^{\mu\nu} + \mu \partial_\mu j^\mu + E^\mu \nu_\mu - \mu C E^\mu B_\mu \tag{6.1.15}$$

vanishes at first order, $I_1 = 0$. Substituting the explicit expressions for the stress-energy tensor and $U(1)$ currents into I_1 and using the thermodynamical identities (6.1.10) and (6.1.12), we find

$$\begin{aligned}\partial_\mu \left(s u^\mu - \frac{\mu}{T}\nu^\mu\right) = &-\frac{1}{T}\partial_\mu u_\nu \tau^{\mu\nu} - \nu^\mu \left(\partial_\mu \frac{\mu}{T} - \frac{E_\mu}{T}\right) \\ &- C\frac{\mu}{T} E\cdot B\,,\end{aligned} \tag{6.1.16}$$

which is exactly the same equation for the entropy production as in the isotropic case [130].

In the following, we will need the identities

$$\partial_\mu \omega^\mu = -\frac{2}{\epsilon + P_T}\omega^\mu(\partial_\mu P_T - \Delta\partial_\mu \ln\tau - \rho E_\mu)\,, \tag{6.1.17}$$
$$\partial_\mu B^\mu = -2\omega^\mu E_\mu - \frac{B^\mu}{\epsilon + P_T}(\partial_\mu P_T - \Delta\partial_\mu \ln\tau - \rho E_\mu)\,,$$

which we derived from ideal hydrodynamics in Appendix 6.4. In deriving these identities we assumed that the fluid satisfies

$$\partial_\mu v^\mu = 0\,, \qquad v^\mu \partial_\mu \Delta = 0\,. \tag{6.1.18}$$

The first equation is basically a "continuity equation" for the vector v^μ. There are no sources for the generation of anisotropy. The second equation imposes an orthogonality relation between the gradient of the pressure difference $\Delta = P_T - P_L$ and v^μ.

As in [130], we assume a generalized entropy current of the form

$$s^\mu = su^\mu - \frac{\mu}{T}\nu^\mu + D\omega^\mu + D_B B^\mu, \tag{6.1.19}$$

where ξ_ω, ξ_B, D, and D_B are functions of T, μ and τ. We now compute $\partial_\mu s^\mu$, using (6.1.16) and (6.1.17) and impose $\partial_\mu s^\mu \geq 0$. Since the coefficients in front of ω^μ, B^μ, $\omega_\mu E^\mu$ and $E_\mu B^\mu$ inside $\partial_\mu s^\mu$ can have either sign, we require them to vanish and obtain the following four differential equations:

$$\partial_\mu D - \frac{2D}{\epsilon + P_T}(\partial_\mu P_T - \Delta\partial_\mu \ln\tau) - \xi_\omega \partial_\mu \frac{\mu}{T} = 0\,, \tag{6.1.20}$$
$$\partial_\mu D_B - \frac{D_B}{\epsilon + P_T}(\partial_\mu P_T - \Delta\partial_\mu \ln\tau) - \xi_B \partial_\mu \frac{\mu}{T} = 0\,, \tag{6.1.21}$$
$$\frac{2\rho D}{\epsilon + P_T} - 2D_B + \frac{\xi_\omega}{T} = 0\,, \tag{6.1.22}$$
$$\frac{\rho D_B}{\epsilon + P_T} + \frac{\xi_B}{T} - C\frac{\mu}{T} = 0\,. \tag{6.1.23}$$

For $\Delta = 0$, these equations reduce to those in the isotropic case [130].

In Appendix 6.4 we solve (6.1.20)–(6.1.23) for D, D_B, ξ_ω and ξ_B. As a result, we find the vortical and magnetic conductivities

$$\xi_\omega = C\left(\mu^2 - \frac{2}{3}\frac{\rho\mu^3}{\epsilon + P_T}\right) + \mathcal{O}(T^2)\,,$$
$$\xi_B = C\left(\mu - \frac{1}{2}\frac{\rho\mu^2}{\epsilon + P_T}\right) + \mathcal{O}(T^2)\,, \tag{6.1.24}$$

where $\mathcal{O}(T^2)$ denotes terms proportional to T^2, see (6.4.23) in Appendix 6.4. These terms are related to gravitational triangle anomalies [131, 175] and may, in the anisotropic case, depend on the proper time τ. In the absence of gravitational anomalies, which we do not discuss in this chapter, the conductivities do not depend on τ. Apart from these changes in $\mathcal{O}(T^2)$, the relations have the same form as in the isotropic case but with P replaced by the transverse pressure P_T.

6.1.3 Multiple charge case n arbitrary)

The generalization of the previous computation to a fluid with multiple anomalous $U(1)$ charges is straightforward, and we only state the result here. The corrections $\nu^{a\mu}$ of the currents $j^{a\mu}$ in (6.1.3) are

$$\nu^{a\mu} = \xi^a_\omega \omega^\mu + \xi^{ab}_B B^{b\mu}\,, \tag{6.1.25}$$

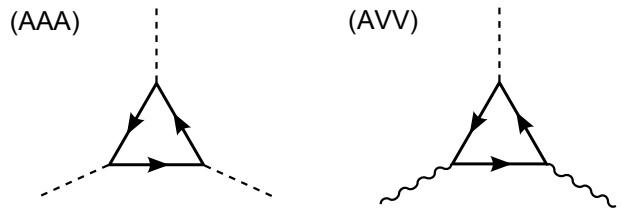

Figure 6.2: Anomalous diagrams corresponding to C^{111}(left) and to $C^{122} = C^{221} = C^{212}$ (right). Dashed (wavy) lines denote the axial (vector) currents/fields.

with [terms of order $\mathcal{O}(T^2)$ ignored]

$$\xi^a_\omega = C^{abc}\mu^b\mu^c - \frac{2}{3}\rho^a C^{bcd}\frac{\mu^b\mu^c\mu^d}{\epsilon + P_T}\,, \tag{6.1.26}$$

$$\xi^{ab}_B = C^{abc}\mu^c - \frac{1}{2}\rho^a C^{bcd}\frac{\mu^c\mu^d}{\epsilon + P_T}\,. \tag{6.1.27}$$

These are simple generalizations of the corresponding conductivities in the isotropic case [130,131].

6.1.4 Chiral magnetic and vortical effect ($n = 2$)

Physically, the most interesting case is that involving two charges ($n = 2$) [3, 140, 141]. The chiral magnetic effect [30, 41–43] can be described by one axial and one vector $U(1)$, denoted by $U(1)_A \times U(1)_V$. A convenient notation for the gauge fields and currents is $(a, b, ... = 1, 2)$

$$\begin{aligned} A^A_\mu &= A^1_\mu\,, \qquad A^V_\mu = A^2_\mu\,, \\ j^\mu_5 &= j^{1\mu}\,, \qquad j^\mu = j^{2\mu}\,. \end{aligned} \tag{6.1.28}$$

Let us now derive the chiral magnetic and vortical effects from (6.1.26) and (6.1.27). $C-$parity allows for two anomalous triangle diagrams, (AAA) and (AVV), shown in Fig. 6.2, while diagrams of the type (VVV) and (VAA) vanish. Accordingly, the anomaly coefficients are

$$\begin{aligned} &C^{121} = C^{211} = C^{112} = 0\,, && (VAA) \\ &C^{222} = 0\,, && (VVV) \\ &C^{111} \neq 0\,, && (AAA) \\ &C^{122} = C^{221} = C^{212} \neq 0\,. && (AVV) \end{aligned} \tag{6.1.29}$$

The hydrodynamic Eqs. (6.1.1) then imply nonconserved vector and axial currents

$$\begin{aligned} \partial_\mu j^\mu &= -\tfrac{1}{4}(C^{212}F^A_{\mu\nu}\tilde{F}^{V\mu\nu} + C^{221}F^V_{\mu\nu}\tilde{F}^{A\mu\nu})\,, \\ \partial_\mu j^\mu_5 &= -\tfrac{1}{4}(C^{111}F^A_{\mu\nu}\tilde{F}^{A\mu\nu} + C^{122}F^V_{\mu\nu}\tilde{F}^{V\mu\nu})\,, \end{aligned} \tag{6.1.30}$$

where we rewrote $E^b \cdot B^c = -\frac{1}{4}F^b_{\mu\nu}\tilde{F}^{c\,\mu\nu}$ (with $\tilde{F}^{a\mu\nu} = \frac{1}{2}\varepsilon^{\mu\nu\rho\sigma}F^a_{\rho\sigma}$).

To restore conservation of the vector current, we add the (topological) Bardeen term to the boundary theory,

$$S_B = c_B \int d^4x\, \epsilon^{\mu\nu\lambda\rho} A^A_\mu A^V_\nu F^V_{\lambda\rho}\,. \tag{6.1.31}$$

Combining the corresponding Bardeen currents

$$\begin{aligned} j_B^\mu &= c_B \varepsilon^{\mu\nu\lambda\rho}(A_\nu^V F_{\lambda\rho}^A - 2A_\nu^A F_{\lambda\rho}^V)\,, \\ j_{5,B}^\mu &= c_B \varepsilon^{\mu\nu\lambda\rho} A_\nu^V F_{\lambda\rho}^V\,, \end{aligned} \tag{6.1.32}$$

with the vector and axial currents,

$$j'^\mu \equiv j^\mu + j_B^\mu\,, \qquad j_5'^\mu \equiv j_5^\mu + j_{5,B}^\mu\,, \tag{6.1.33}$$

we obtain the anomaly equations

$$\begin{aligned} \partial_\mu j'^\mu &= -\left(\frac{C^{122}}{2} + c_B\right) F_{\alpha\beta}^V \tilde{F}^{A\,\alpha\beta}\,, \\ \partial_\mu j_5'^\mu &= -\frac{C^{111}}{4} F_{\alpha\beta}^A \tilde{F}^{A\,\alpha\beta} - \left(\frac{C^{122}}{4} - c_B\right) F_{\alpha\beta}^V \tilde{F}^{V\,\alpha\beta}\,. \end{aligned} \tag{6.1.34}$$

The electric current j'^μ is conserved if $c_B = -C^{122}/2$. Setting $C^{111} = C^{122} \equiv C/3$, the hydrodynamic Eqs. (6.1.1) become

$$\begin{aligned} \partial_\mu T^{\mu\nu} &= F^{V\nu\lambda} j'_\lambda + F^{A\nu\lambda} j'_{5\lambda}\,, \\ \partial_\mu j'^\mu &= 0\,, \\ \partial_\mu j_5'^\mu &= CE\cdot B + (C/3) E_5 \cdot B_5\,. \end{aligned} \tag{6.1.35}$$

Using the derivative expansion

$$j'^\mu = \rho u^\mu + \kappa_\omega \omega^\mu + \kappa_B B^\mu + \kappa_{5,B} B_5^\mu\,, \tag{6.1.36}$$

where $\kappa_\omega \equiv \xi_\omega^2$, $\kappa_B \equiv \xi_B^{22}$ and $\kappa_{5,B} \equiv \xi_B^{21}$, we obtain from (6.1.26) and (6.1.27) the conductivities ($\mu_5 \equiv \mu^1$, $\mu \equiv \mu^2$)

$$\begin{aligned} \kappa_\omega &= 2C\mu_5 \left(\mu - \frac{\rho}{\epsilon + P_T}\left[\mu^2 + \frac{\mu_5^2}{3}\right]\right), \\ \kappa_B &= C\mu_5 \left(1 - \frac{\mu\rho}{\epsilon + P_T}\right), \\ \kappa_{5,B} &= C\mu \left(1 - \frac{1}{2}\frac{\mu\rho}{\epsilon + P_T}\left[1 + \frac{\mu_5^2}{3\mu^2}\right]\right). \end{aligned} \tag{6.1.37}$$

There are analogous transport coefficients in the axial current j_5^μ [3]. The axial fields $E_{5\mu}$ and $B_{5\mu}$ are not needed and can now be switched off. The first term in κ_B and κ_ω, $\kappa_B = C\mu_5$ and $\kappa_\omega = 2C\mu\mu_5$, is the leading term in the *chiral magnetic* (CME) [30, 41–43] and *chiral vortical effect* [157], respectively.[2] They are in agreement with those found in the isotropic case [3,140,141]. The second term proportional to $\rho/(\epsilon + P_T)$ actually depends on the dynamics of the fluid[3] and therefore on ε_p.

The dependence of κ_B on ε_p can be made more visible by introducing an average pressure $\bar{P} = (2P_T + P_L)/3$ such that $\epsilon = 3\bar{P}$. Assuming ε_p to be small (see Fig. 6.1), we expand the CME-coefficient κ_B to linear order in ε_p,

$$\kappa_B \approx C\mu_5 \left(1 - \frac{\mu\rho}{\epsilon + \bar{P}}\left[1 - \frac{\varepsilon_p}{6}\right]\right). \tag{6.1.38}$$

[2] $\kappa_{5,B}$ represents another effect, which we added for completeness, but it seems not to be realized in heavy-ion collisions.

[3] In [142] this term was considered as a one-loop correction in an effective theory and $(\epsilon + P)/\rho$ was interpreted as the corresponding infrared cutoff in the energy/momentum integration.

Despite the crudeness of the model, one can assume that such an anisotropic fluid describes to some extent the anisotropic quark-gluon plasma, with our ε_p imitating the real $\varepsilon_p \approx 2v_2$ for pions [166]. Since the net chemical potential μ is quite small in current heavy-ion experiments [176], the dependence on ε_p (and hence v_2) in (6.1.38) appears to be very mild. Even though the anisotropy dependence of κ_B is very weak, (6.1.38) tells us how the CME, if present in the experimental data, can be separated from the v_2-dependent background (for one of the attempts of such a separation see [177]).

6.2 Fluid-gravity model

In this section we construct the gravity dual of a static anisotropic plasma with diagonal stress-energy momentum $T_{\mu\nu} = \mathrm{diag}(\epsilon, P_T, P_T, P_L)$ and charge densities ρ^a.

We start from a five-dimensional $U(1)^n$ Einstein-Maxwell theory in an asymptotic AdS space. The action is

$$S = \frac{1}{16\pi G_5}\int d^5x\sqrt{-g}\left[R - 2\Lambda - F^a_{MN}F^{aMN} + \frac{S_{abc}}{6\sqrt{-g}}\varepsilon^{PKLMN}A^a_P F^b_{KL}F^c_{MN}\right], \tag{6.2.1}$$

where $\Lambda = -6$ is the cosmological constant. As usual, the $U(1)$ field strengths are defined by

$$F^a_{MN} = \partial_M A^a_N - \partial_N A^a_M\,, \tag{6.2.2}$$

where $M, N, ... = 0, ..., 4$ and $a = 1, ..., n$. The Chern-Simons term $A\wedge F\wedge F$ encodes the information of the triangle anomalies in the field theory [130]. In fact, the Chern-Simons coefficients S_{abc} are related to the anomaly coefficients C_{abc} by

$$C_{abc} = S_{abc}/(4\pi G_5)\,. \tag{6.2.3}$$

The corresponding equations of motion are given by the combined system of Einstein-Maxwell and Maxwell equations,

$$G_{MN} - 6g_{MN} = T_{MN}\,, \tag{6.2.4}$$

$$\nabla_M F^{aMP} = -\frac{S_{abc}}{8\sqrt{-g}}\varepsilon^{PMNKL}F^b_{MN}F^c_{KL}\,, \tag{6.2.5}$$

where the energy-momentum tensor T_{MN} is

$$T_{MN} = -2\left(F^a_{MR}F^{aR}{}_N + \frac{1}{4}g_{MN}F^a_{SR}F^{aSR}\right). \tag{6.2.6}$$

6.2.1 AdS black hole with multiple U(1) charges

A gravity dual to an *isotropic* fluid ($\epsilon = 3P$) with multiple chemical potentials μ_a ($a = 1, ..., n$) at finite temperature T is given by an AdS black hole solution with mass m and multiple $U(1)$ charges q^a. In Eddington-Finkelstein coordinates, the metric and $U(1)$ gauge fields of this solution are

$$\begin{aligned} ds^2 &= -f(r)dt^2 + 2drdt + r^2d\vec{x}^2\,,\\ A^a &= -A^a_0(r)dt\,, \end{aligned} \tag{6.2.7}$$

where

$$f(r) = r^2 - \frac{m}{r^2} + \sum_a \frac{(q^a)^2}{r^4}\,,$$
$$A_0^a(r) = \mu_\infty^a + \frac{\sqrt{3}q^a}{2r^2}\,. \tag{6.2.8}$$

The constants μ_∞^a can be fixed such that the gauge fields vanish at the horizon. In case of a single charge ($n = 1$), the background reduces to an ordinary Reissner-Nordstrøm black hole solution in AdS_5 [73].

The temperature T and chemical potentials μ^a of the fluid are defined by

$$T = \frac{\kappa}{2\pi} = \frac{f'(r_+)}{4\pi} = \frac{2r_+^6 - \sum_a (q_a)^2}{2\pi r_+^5}\,, \tag{6.2.9}$$
$$\mu^a = A_0^a(r_+) - A_0^a(r_\infty)\,, \tag{6.2.10}$$

where r_+ is the outer horizon defined by the maximal solution of $f(r) = 0$, and r_∞ indicates the location of the boundary. The temperature of the fluid is the Hawking temperature of the black hole and is computed from the surface gravity $\kappa = \sqrt{\partial_M|\chi|\partial^M|\chi|}|_{r_+}$, where $|\chi| = (-\chi^M\chi_M)^{(1/2)}$ is the norm of the timelike Killing vector $\chi^M = \delta_0^M$ [here $|\chi| = \sqrt{f(r)}$].

6.2.2 Anisotropic AdS geometry with multiple U(1) charges

We now construct a solution for an *anisotropic* fluid ($\epsilon = 2P_T + P_L$). An ansatz for an anisotropic AdS black hole solution is given by

$$\begin{aligned} ds^2 &= -f(r)dt^2 + 2drdt \\ &\quad + r^2(w_T(r)dx^2 + w_T(r)dy^2 + w_L(r)dz^2)\,, \\ A^a &= -A_0^a(r)dt\,. \end{aligned} \tag{6.2.11}$$

The anisotropies are realized via $w_T(r)$ and $w_L(r)$, which are functions of the momentum anisotropy ε_p as defined in (6.0.2),

$$\varepsilon_p = \frac{\langle P_T - P_L\rangle}{\langle P_T + P_L\rangle}\,. \tag{6.2.12}$$

In the isotropic case ($\varepsilon_p = 0$), these functions are required to be one, $w_T(r) = w_L(r) = 1$, and the background reduces to the AdS black hole geometry (6.2.7).

An analytical solution of the type (6.2.11) is difficult to find, and we resort to numerics in the next subsection. For this, we need to know the solution close to the boundary. An asymptotic solution ($r \to \infty$) is given by the four functions

$$\begin{aligned} A_0^a(r) &= \mu_\infty^a + \frac{\sqrt{3}q^a}{2r^2} + \mathcal{O}(r^{-8})\,, \\ f(r)/r^2 &= 1 - \frac{m}{r^4} + \sum_a \frac{(q^a)^2}{r^6} + \mathcal{O}(r^{-8})\,, \\ w_T(r) &= 1 + \frac{w_T^{(4)}}{r^4} + \mathcal{O}(r^{-8})\,, \\ w_L(r) &= 1 + \frac{w_L^{(4)}}{r^4} + \mathcal{O}(r^{-8})\,, \end{aligned} \tag{6.2.13}$$

where $w_L^{(4)} = -2w_T^{(4)} = -m\zeta/2$, $\mu_\infty^a = const.$, and ζ is related to the momentum anisotropy ε_p by

$$\zeta = \frac{2\varepsilon_p}{\varepsilon_p + 3}\,. \tag{6.2.14}$$

The functions $w_T(r)$ and $w_L(r)$ have been introduced in view of the structure of the anisotropic fluid stress-energy tensor. More precisely, in (6.2.13) we fixed the r^{-4} coefficients $w_T^{(4)}$ and $w_L^{(4)}$ such that the fluid stress-energy tensor is of the diagonal form (6.1.5), $T^{\mu\nu} = \mathrm{diag}(\epsilon, P_T, P_T, P_L)$ with $\epsilon = 2P_T + P_L$. Computing the stress-energy tensor in the standard way from the asymptotic solution (6.2.13) via the extrinsic curvature, see *e.g.* [2], we find the transverse and longitudinal pressures

$$P_T = \frac{m - 4w_T^{(4)} - 4w_L^{(4)}}{16\pi G_5} = \frac{m(1+\zeta)}{16\pi G_5}\,, \tag{6.2.15}$$

$$P_L = \frac{m - 8w_T^{(4)}}{16\pi G_5} = \frac{m(1-2\zeta)}{16\pi G_5}\,. \tag{6.2.16}$$

Note that if (6.2.14) holds true, the pressures P_T and P_L satisfy (6.2.12). Likewise, the charge densities are

$$\rho^a = \frac{\sqrt{3}q^a}{4\pi G_5}\,. \tag{6.2.17}$$

From these relations, we find the useful identity

$$\frac{\rho^a}{\epsilon + P_T} = \frac{\sqrt{3}q^a}{m(1+\frac{1}{4}\zeta)}\,, \tag{6.2.18}$$

which we will need later.

Numerical solution

We now use shooting techniques to solve the system of ordinary differential equations (ODE) which follows from the equations of motion (6.2.4) and (6.2.5) upon substituting the ansatz (6.2.11). The idea is to vary the metric and gauge fields at some minimal value r_+ in the radial direction, integrate outwards and find solutions with the correct asymptotic behavior (6.2.13). A similar method was previously applied in [170].

We first need to study the asymptotic solution near r_+ and near the boundary at $r_\infty \gg r_+$ (we choose $r_\infty = 50$ in our numerics). We define r_+ by the maximal solution of

$$f(r_+) = 0 \tag{6.2.19}$$

and use scale invariance to set $r_+ = 1$. We then expand the functions in the metric and gauge fields near r_+ in powers of the parameter $\varepsilon = \frac{r}{r_+} - 1 \ll 1$ and substitute them into the equations of motion. In this way, we find that the only independent variables are $\{f'(r_+), w_T(r_+), w_L(r_+), w_L'(r_+)\}$ since the gauge field parameters $A_0^a(r_+)$ can be set to zero using gauge invariance, $A_0^a(r_+) = 0$. The other parameters at r_+ can be expressed in terms of these four parameters, *e.g.* $w_T'(r_+) = w_T(r_+)w_L'(r_+)/w_L(r_+)$.

The near-boundary solution is given by (6.2.11) with (6.2.13) and is parameterized by the values

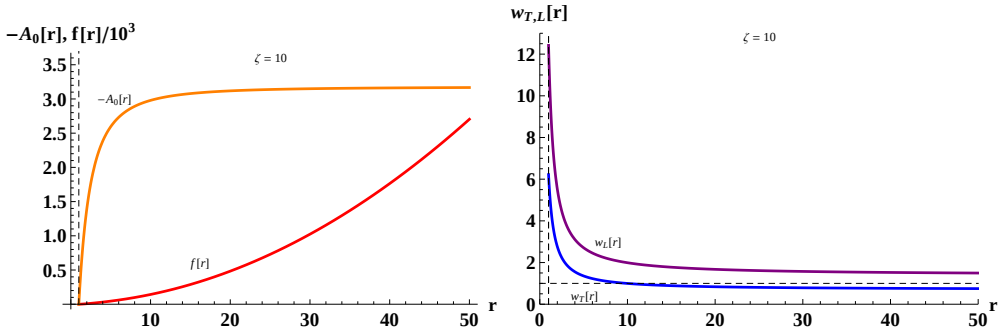

Figure 6.3: Numerical plots of $f(r)$, $A_0(r)$, $w_T(r)$ and $w_L(r)$ for $\zeta = 10$ ($r_+ = 1$). We get $w_L(r_+) = 12.42$.

$(\zeta, m, q^a, \mu^a_\infty)$. The final set of data is summarized in the following table:

$r = r_+ = 1$	$r = r_\infty \gg r_+$
$A^a_0(r_+) = 0$	μ^a_∞
$f(r_+) = 0$	$f(r_\infty)$
$f'(r_+) =$ fixed	$A^{a\prime}_0(r_\infty)$
$w_L(r_+) =$ var	$w_L(r_\infty)$
$w_T(r_+) =$ var	$w_T(r_\infty)$
$w'_L(r_+) =$ var	

Parameters not listed are related to those in the table by the equations of motion.

To integrate the equations we proceed as follows. We fix ζ and vary three parameters at r_+, namely $w_T(r_+)$, $w_L(r_+)$ and $w'_L(r_+)$, by choosing a grid with suitable number of sites (in our case $20^3 - 40^3$). The value $f'(r_+)$ can be thought of as the temperature of the system and will simply be fixed to some value. It turns out that the form of the functions $w_{L,T}(r)$ does not depend on this parameter. For each site in the grid we numerically solve the system of ODEs and determine the pair (m, q^a) from the known asymptotics of $A^{a\prime}_0(r = r_\infty)$ and $f(r = r_\infty)$. This ensures that the analytical and numerical values for these quantities coincide.

We then calculate the combined residual

$$\begin{aligned}&\mathrm{res}_\infty[w_T(r_+), w_L(r_+), w'_L(r_+))] \\ &= (w^\#_L(r_\infty) - w^*_L(r_\infty))^2 + (w^\#_T(r_\infty) - w^*_T(r_\infty))^2,\end{aligned} \tag{6.2.20}$$

where $w^\#_{L,T}(r_\infty)$ are the numerical values, and $w^*_{L,T}(r_\infty)$ are the analytical values given by (6.2.13). We interpolate the residual by a piecewise linear function and find its global minimum by the simulated annealing method [178, 179]. The result of the minimization is shown in Fig. 6.3, which depicts numerical plots of $f(r)$, $A_0(r)$, $w_T(r)$ and $w_L(r)$ for $n = 1$.

We conclude this section with a comment on r_+. In the isotropic case, r_+ is simply the size of the horizon of the AdS black hole geometry. For nonvanishing anisotropies and vanishing $U(1)$ charges, a naked singularity was found at r_+ [171], implying that the static background does not exist indefinitely. The singularity is mild in the sense that there is a notion of ingoing boundary conditions and possible instabilities are absent at the linear level in the anisotropy parameter [171]. This behavior may persist even for nonvanishing $U(1)$ charges, even though it was difficult to see the singularity in our numerics, *cf.* Figure 6.4. Despite this subtlety, we show in the next section that, at least for small anisotropies where the bulk geometry approximates a black hole solution, the singular geometry may be used to compute some transport coefficients of the fluid.

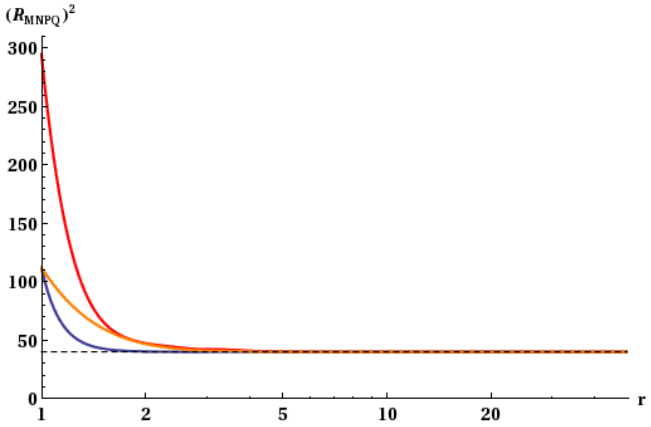

Figure 6.4: Numerical plots of $(R_{MNPQ})^2$ for $\zeta = 10$, $q \neq 0$ (red), $\zeta = 10$, $q = 0$ (orange), and $\zeta = 0$, $q = 0$ (blue).

6.3 Holographic vortical and magnetic conductivities

We will now compute the chiral vortical and magnetic conductivities ξ^a_ω and ξ^{ab}_B from first-order corrections to the numerical AdS geometry (6.2.11) using the fluid-gravity correspondence [75].

6.3.1 First-order corrected background

In order to become a dual to a multiply charged fluid, the AdS geometry (6.2.11) must be boosted along the four-velocity of the fluid u_μ ($\mu = 0, ..., 3$). The boosted version of (6.2.11) is

$$\begin{aligned} ds^2 &= \left(r^2 w_T(r) P_{\mu\nu} - f(r) u_\mu u_\nu\right) dx^\mu dx^\nu - 2u_\mu dx^\mu dr \\ &\quad - r^2 (w_T(r) - w_L(r)) v_\mu v_\nu dx^\mu dx^\nu \,, \\ A^a &= (A^a_0(r) u_\mu + \mathcal{A}^a_\mu) dx^\mu \,, \end{aligned} \tag{6.3.1}$$

where $P^{\mu\nu} = g^{\mu\nu} + u^\mu u^\nu$, and $f(r)$, $A^a_0(r)$, $w_T(r)$ and $w_L(r)$ are numerically known functions. As in hydrodynamics, the four-vector v^μ determines the direction of the longitudinal axis, cf. Sec. 2. Following [3, 130], we have formally introduced constant background gauge fields $\mathcal{A}^a_\mu$ to model external electromagnetic fields, such as the magnetic fields $B^{a\mu}$ needed for the chiral magnetic effect.

The transport coefficients ξ^a_ω and ξ^{ab}_B can now be computed using standard fluid-gravity techniques [75]. We closely follow [3, 129, 130], in which these transport coefficients were determined for an isotropic fluid with one and three charges ($n = 1, 3$). We work in the static frame $u_\mu = (-1, 0, 0, 0)$, $v_\mu = (0, 0, 0, 1)$, and consider vanishing background fields $\mathcal{A}^a_\mu$ (at $x^\mu = 0$). The transport coefficients ξ^a_ω and ξ^{ab}_B measure the response of the system to rotation and the perturbation by an external magnetic field. We therefore slowly vary the velocity u_μ and the background fields $\mathcal{A}^a_\mu$ up to first order as

$$u_\mu = (-1, x^\nu \partial_\nu u_i) \,, \qquad \mathcal{A}^a_\mu = (0, x^\nu \partial_\nu \mathcal{A}^a_i) \,. \tag{6.3.2}$$

We may also vary m and q in this way, but it turns out that varying these parameters has no influence on the transport coefficients ξ^a_ω and ξ^{ab}_B.

Because of the dependence on x^μ, the background (6.3.1) is no longer an exact solution of the equations of motion. Instead with varying parameters the solution (6.3.1) receives higher-order corrections, which are in this case of first order in the derivatives.

An ansatz for the first-order corrected metric and gauge fields is given by

$$\begin{aligned} ds^2 &= (-f(r)+\tilde{g}_{tt})\,dt^2 + 2\,(1+\tilde{g}_{tr})\,dtdr + r^2(w_T(r)dx^2 + w_T(r)dy^2 + w_L(r)dz^2) \\ &\quad + \tilde{g}_{ij}dx^i dx^j - 2x^\nu \partial_\nu u_i dr dx^i + 2\left(\left(f(r)-r^2\right)x^\nu\partial_\nu u_i + \tilde{g}_{ti}\right)dtdx^i\,, \\ A^a &= \left(-A_0^a(r)+\tilde{A}_t^a\right)dt + \left(A_0^a(r)x^\nu\partial_\nu u_i + x^\nu\partial_\nu \mathcal{A}_i^a + \tilde{A}_i^a\right)dx^i\,, \end{aligned} \tag{6.3.3}$$

where the first-order corrections are denoted by

$$\tilde{g}_{MN} = \tilde{g}_{MN}(r)\,, \quad \tilde{A}_M^a = \tilde{A}_M^a(r)\,. \tag{6.3.4}$$

As in [129], we work in the gauge

$$\tilde{g}_{rr} = 0\,, \quad \tilde{g}_{r\mu} \sim u_\mu\,, \quad \tilde{A}_r^a = 0\,, \quad \sum_{i=1}^{3}\tilde{g}_{ii} = 0\,. \tag{6.3.5}$$

The first-order corrections can be obtained by substituting the ansatz (6.3.3) into the equations of motion (6.2.4) and (6.2.5). The computation is straight-forward but lengthy and has been shifted to Appendix 6.4 [we set $\mu_\infty^a = A_0^a(r_\infty) = 0$ there, see Sec. 6.1.3 for a discussion]. As a result, we find the following corrections:

$$\tilde{g}_{tr} = \tilde{g}_{tt} = \tilde{A}_t^a = 0\,, \tag{6.3.6}$$

$$\tilde{g}_{ti}(r) = f(r)\int_\infty^r dr'\,\frac{1}{w_L(r')^{1/2}r'\left(f(r')\right)^2}\left(\int_{r_+}^{r'} dr''\,I(r'') - w_L(r_+)^{1/2}r_+ f'(r_+)C_i\right)\,,$$

$$\tilde{A}_i^a(r) = \int_\infty^r dr'\frac{1}{r'f(r')w_L(r')^{1/2}}\left[Q_i^a(r') - Q_i^a(r_+) - C_i r_+ A_0^{a\prime}(r_+)w_L(r_+)^{1/2} + r'\tilde{g}_{ti}(r')A_0^{a\prime}(r')\right]\,,$$

with

$$\begin{aligned} I(r) &= \sum_{a=1}^{n} 4A_0^{a\prime}(r)\Big(Q_i^a(r) - Q_i^a(r_+) - C_i r_+ w_L(r_+)^{1/2}A_0^{a\prime}(r_+)\Big)\,, \\ Q_a^i &\equiv \frac{1}{2}S_{abc}A_0^b A_0^c\epsilon^{ijk}\left(\partial_j u_k\right) + S_{abc}A_0^b\epsilon^{ijk}\left(\partial_j\mathcal{A}_k^c\right)\,, \\ C^i &= \frac{4c(r_+)}{w_L(r_+)^{1/2}}\left(\frac{1}{3}S_{abc}A_0^a(r_+)A_0^b(r_+)A_0^c(r_+)\epsilon^{ijk}\left(\partial_j u_k\right) + \frac{1}{2}S_{abc}A_0^a(r_+)A_0^b(r_+)\epsilon^{ijk}\left(\partial_j\mathcal{A}_k^c\right)\right)\,, \\ c(r_+) &= \frac{1}{r_+(f'(r_+) - 4\sum_a A_0^a(r_+)A_0^{a\prime}(r_+))}\,, \end{aligned}$$

and r_+ as defined around (6.2.19) [$\tilde{g}_{ij}$ can be obtained by solving (5.2.22) in Appendix 6.4 but will not be needed here].

6.3.2 Holographic conductivities

On the boundary of the asymptotic AdS space (6.3.3), the metric and gauge fields couple to the fluid stress-energy tensor and $U(1)$ currents, respectively. Holographic renormalization [70, 71] provides relations between these currents and the near-boundary behavior of their dual bulk fields. For the magnetic and vortical effects, we need the $U(1)$ currents $j^{a\mu}$, which are related to the bulk gauge fields $A^{a\mu}$ by[4] [70, 71, 134]

$$j^{a\mu} = \lim_{r\to\infty}\frac{r^2}{2\pi G_5}\eta^{\mu\nu}A_\nu^a(r)\,. \tag{6.3.7}$$

[4]We notices a few typos in [4] fixed in this section and in [12]. The final result (6.3.12, 6.3.13) is correct and is the same in all our papers.

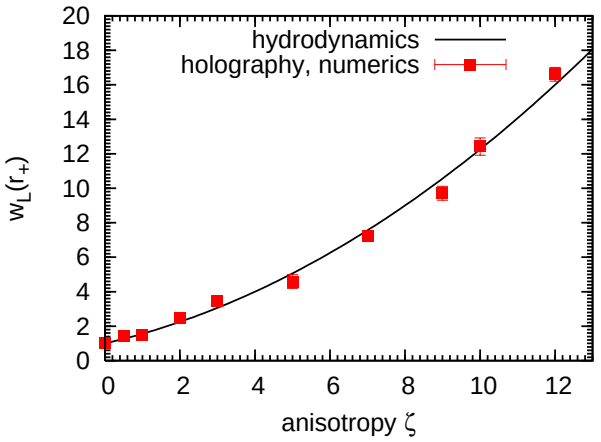

Figure 6.5: Values of $w_L(r_+)$ as a function of the anisotropy ζ. The numerically determined values for $w_L(r_+)$ lie on the solid curve, which represents the function $(1+\frac{1}{4}\zeta)^2$.

Expanding the solution in $\frac{1}{r}$ and substituting only the corrections $\tilde{A}^a_\mu$, we get the currents

$$\tilde{j}^{a\mu} = \lim_{r\to\infty} \frac{r^2}{2\pi G_5}\eta^{\mu\nu}\tilde{A}^a_\nu(r) = \frac{1}{4\pi G_5}\eta^{\mu\nu}\left(Q^a_\nu(r_+) + r_+ A_0^{a\prime}(r_+)C_\nu\right) . \tag{6.3.8}$$

Note that, in the isotropic case ($w_L = 1$, $P_T = P_L = P$), the prefactor of the second term of (6.3.8) is simply

$$r_+ A_0^{a\prime}(r_+)c(r_+) = \frac{\sqrt{3}}{4m}q^a , \tag{6.3.9}$$

as can be seen by substituting the Reissner-Nordstrøm solution (6.2.8) into the left-hand-side of this equation. In the anisotropic case, we need to show that

$$r_+ A_0^{a\prime}(r_+)c(r_+)\cdot w_L(r_+)^{-1/2} = \frac{\sqrt{3}q^a}{4m}\cdot\frac{1}{1+\frac{1}{4}\zeta} , \tag{6.3.10}$$

which, by (6.2.18), is equivalent to $\dfrac{\rho^a}{4(\epsilon+P_T)}$. This equation holds in particular if the first and second factors on both sides agree individually. The first factors correspond to (6.3.9), which is expected to hold, at least approximately for small anisotropies ζ. The second factors are identical if $w_L(r_+,\zeta) = (1+\frac{1}{4}\zeta)^2$. We find numerically (for $n=1$) that $w_L(r_+)$ indeed satisfies this equation, see Fig. 6.5. Thus (6.3.10) holds numerically, at least in the limit of small ζ.

Comparing (6.3.8) with the general expansion

$$\begin{aligned}\tilde{j}^{a\mu} &= \xi^a_\omega\,\omega^\mu + \xi^{ab}_B\,B^{b\mu} \\ &= \xi^a_\omega\,\tfrac{1}{2}\epsilon^{\nu\rho\sigma\mu}u_\nu\partial_\rho u_\sigma + \xi^{ab}_B\epsilon^{\nu\rho\sigma\mu}u_\nu\partial_\rho\mathcal{A}^b_\sigma ,\end{aligned} \tag{6.3.11}$$

we finally obtain the coefficients

$$\xi^a_\omega = \frac{1}{4\pi G_5}\left(S^{abc}\mu^b\mu^c - \frac{2}{3}\frac{\rho^a}{\epsilon+P_T}S^{bcd}\mu^b\mu^c\mu^d\right) , \tag{6.3.12}$$

$$\xi^{ab}_B = \frac{1}{4\pi G_5}\left(S^{abc}\mu^c - \frac{1}{2}\frac{\rho^a}{\epsilon+P_T}S^{bcd}\mu^c\mu^d\right) , \tag{6.3.13}$$

with $\mu^a \equiv A_0^a(r_+)$ [since $A_0^a(\infty) = 0$]. Using the relation (6.2.3), we find that the holographically computed transport coefficients (6.3.12) and (6.3.13) coincide exactly with those found in hydrodynamics, (6.1.26) and (6.1.27).

6.3.3 Subtleties in holographic descriptions of the CME

The conservation of the electromagnetic current requires the introduction of the Bardeen counterterm into the action. In AdS/QCD models of the CME, this typically leads to a vanishing result for the electromagnetic current [146,148]. The problem is related to the difficulty of introducing a chemical potential conjugated to a nonconserved chiral charge [146,147]. It is possible to modify the action to obtain a conserved chiral charge [146]. This charge is however only gauge-invariant when integrated over all space in homogeneous configurations.

In AdS black hole models of the CME, one usually introduces a chiral chemical potential dual to a gauge-invariant current, despite it being anomalous [3,147]. The prize to pay is the appearance of a singular bulk gauge field at the horizon, a phenomenon which seems to be generic in AdS black hole models of the CME.

Careful holographic renormalization shows that, in the presence of Chern-Simons terms, there is an additional term on the right-hand side of (6.3.7) [134]. This term is of the form

$$\hat{j}_a^\mu = -\frac{S_{abc}}{8\pi G_5}\epsilon^{\mu\nu\rho\sigma} A_{b\nu}^{(0)}(x)\partial_\rho A_{c\sigma}^{(0)}(x)\,, \tag{6.3.14}$$

where $A_{a\mu}^{(0)}(x)$ are the 0th-order coefficients in a $\frac{1}{r}$ expansion of the bulk gauge fields $A_{a\mu}(r,x)$. In (6.3.2) we expanded the background gauge fields $\mathcal{A}_\mu^a$ around zero and set $A_\nu^{a(0)} = \mu_\infty^a u_\nu = 0$. This allowed us to ignore terms in (6.3.7) coming from (6.3.14) (at least to first order in the derivatives).

Problems arise if $\mu_\infty^a \neq 0$. To see this, let us restrict again to two charges ($n = 2$) as in Sec. 6.1.3 and define axial and vector gauge fields by $A_\mu^A = A_\mu^1$ and $A_\mu^V = A_\mu^2$. Then $\hat{j}^\mu = \hat{j}_2^\mu$ gives rise to additional contributions of the type

$$\hat{j}^\mu \supset \varepsilon^{\mu\nu\rho\sigma} A_\nu^{A(0)}(x) F_{\rho\sigma}^{V(0)}(x)\,, \tag{6.3.15}$$

which are forbidden by electromagnetic gauge invariance [146], unless $A_\nu^{A(0)}(x) = 0$. However, in general $A_\nu^{A(0)}(x) = \mu_5^\infty u_\nu$ (at $x = 0$) with some constant μ_5^∞. We should thus set $\mu_5^\infty = 0$ [Note that this does not imply $\mu_5 = A_0^A(r_\infty) - A_0^A(r_+) = 0$]. This corresponds to a nonvanishing gauge field at the horizon, as noticed also in [3,147].

6.4 Conclusions

Our main result is (6.1.38), which gives the chiral magnetic conductivity κ_B for an anisotropic plasma. It explicitly shows the dependence on the momentum anisotropy ε_p. We also computed the CME coefficient in the holographic dual model and found numerical agreement with the hydrodynamic result for small anisotropies.

Appendix A. Computation of $\partial_\mu\omega^\mu$ and $\partial_\mu B^\mu$

In the following we will use the identities

$$u^\mu u^\lambda \partial_\mu \omega_\lambda = -\frac{1}{2}\partial_\mu \omega^\mu\,, \tag{6.4.1}$$

$$u^\mu u^\lambda \partial_\mu B_\lambda = \partial_\mu B^\mu + 2\omega^\rho E_\rho\,. \tag{6.4.2}$$

To find an explicit expression for $\partial_\mu \omega^\mu$, we compute the term $\omega_\nu \partial_\mu T^{\mu\nu}$ in two ways. First, using the hydrodynamic equations, we get

$$\omega_\nu \partial_\mu T^{\mu\nu} = \omega_\nu F^{\nu\mu} j_\mu = \rho \omega_\nu F^{\nu\mu} u_\mu = \rho \omega_\nu E^\nu \,. \tag{6.4.3}$$

Next, substituting the stress-energy tensor (6.1.2) in this expression, we find

$$\begin{aligned} \omega_\nu \partial_\mu T^{\mu\nu} &= (\epsilon + P_T) u^\mu \omega_\nu \partial_\mu u^\nu + \omega_\nu g^{\mu\nu} \partial_\mu P_T - \Delta \omega_\nu v^\mu \partial_\mu v^\nu \\ &\quad - v^\nu \omega_\nu v^\mu \partial_\mu \Delta - \Delta v^\nu \omega_\nu \partial_\mu v^\mu \\ &= -(\epsilon + P_T) u^\mu u^\nu \partial_\mu \omega_\nu + \omega^\mu \partial_\mu P_T - \Delta \omega_\nu \partial^\nu \ln \tau \\ &\quad - v^\nu \omega_\nu v^\mu \partial_\mu \Delta - \Delta v^\nu \omega_\nu \partial_\mu v^\mu \,. \end{aligned} \tag{6.4.4}$$

Using the identity (6.4.1), we find

$$\partial_\mu \omega^\mu = -\frac{2}{\epsilon + P_T} \omega^\mu (\partial_\mu P_T - \Delta \partial_\mu \ln \tau - \rho E_\mu - v_\mu v^\nu \partial_\nu \Delta - \Delta v_\mu \partial_\nu v^\nu) \,. \tag{6.4.5}$$

Similar manipulations of the term $B_\nu \partial_\mu T^{\mu\nu}$ lead to

$$B_\nu \partial_\mu T^{\mu\nu} = B_\nu F^{\nu\mu} j_\mu = \rho B_\mu E^\mu \,, \tag{6.4.6}$$

$$\begin{aligned} B_\nu \partial_\mu T^{\mu\nu} &= -(\epsilon + P_T) u^\mu u^\nu \partial_\mu B_\nu + B^\mu \partial_\mu P_T \\ &\quad - \Delta B_\nu v^\mu \partial_\mu v^\nu - B_\nu v^\nu v^\mu \partial_\mu \Delta - \Delta B_\nu v^\nu \partial_\mu v^\mu \\ &= -(\epsilon + P_T)(\partial_\mu B^\mu - 2 \omega^\mu E_\mu) - \Delta B_\mu \partial^\mu \ln \tau \\ &\quad - B_\nu v^\nu v^\mu \partial_\mu \Delta - \Delta B_\nu v^\nu \partial_\mu v^\mu \,, \end{aligned} \tag{6.4.7}$$

where we used (6.4.2). From (6.4.6) and (6.4.7) we obtain the following expression:

$$\partial_\mu B^\mu = -2 \omega^\mu E_\mu - \frac{B^\mu}{\epsilon + P_T} (\partial_\mu P_T - \Delta \partial_\mu \ln \tau - \rho E_\mu - v_\mu v^\nu \partial_\nu \Delta - \Delta v_\mu \partial_\nu v^\nu) \,. \tag{6.4.8}$$

The last two terms in (6.4.5) and (6.4.8) vanish provided the fluid satisfies

$$\partial_\mu v^\mu = 0 \,, \qquad v^\mu \partial_\mu \Delta = 0 \,. \tag{6.4.9}$$

Then (6.4.5) and (6.4.8) become identical to the expressions in (6.1.17).

Appendix B. Computation of the transport coefficients ξ_ω and ξ_B

In this appendix we compute the conductivities ξ_ω and ξ_B by solving the system of Eqs. (6.1.20)-(6.1.23). Following [130], we change variables from $\ln \tau$, μ, T to $\ln \tau$, $\bar{\mu} = \mu / T$ and P_T. From (6.1.10) and (6.1.11), we derive the thermodynamic expressions

$$\left(\frac{\partial \bar{\mu}}{\partial T} \right)_{P_T, \ln \tau} = -\frac{\epsilon + P_T}{\rho T^2} \,, \tag{6.4.10}$$

$$\left(\frac{\partial P_T}{\partial T} \right)_{\bar{\mu}, \ln \tau} = \frac{\epsilon + P_T}{T} \,, \tag{6.4.11}$$

$$\left(\frac{\partial \ln \tau}{\partial T} \right)_{\bar{\mu}, P_T} = -\frac{1}{\Delta} \frac{\epsilon + P_T}{T} \,. \tag{6.4.12}$$

Using

$$\partial_\mu D = \frac{\partial D}{\partial P_T}\partial_\mu P_T + \frac{\partial D}{\partial \bar{\mu}}\partial_\mu \bar{\mu} + \frac{\partial D}{\partial \ln\tau}\partial_\mu \ln\tau\,, \tag{6.4.13}$$

$$\partial_\mu D_B = \frac{\partial D_B}{\partial P_T}\partial_\mu P_T + \frac{\partial D_B}{\partial \bar{\mu}}\partial_\mu \bar{\mu} + \frac{\partial D_B}{\partial \ln\tau}\partial_\mu \ln\tau\,, \tag{6.4.14}$$

the first two equations, (6.1.20) and(6.1.21), can be rewritten as

$$-\xi_\omega + \frac{\partial D}{\partial \bar{\mu}} = 0\,, \qquad -\xi_B + \frac{\partial D_B}{\partial \bar{\mu}} = 0\,, \tag{6.4.15}$$

$$\frac{\partial D}{\partial P_T} - \frac{2D}{\epsilon + P_T} = 0\,, \qquad \frac{\partial D_B}{\partial P_T} - \frac{D_B}{\epsilon + P_T} = 0\,, \tag{6.4.16}$$

$$\frac{\partial D}{\partial \ln\tau} + \frac{2\Delta D}{\epsilon + P_T} = 0\,, \qquad \frac{\partial D_B}{\partial \ln\tau} + \frac{\Delta D_B}{\epsilon + P_T} = 0\,. \tag{6.4.17}$$

Note that (6.4.16) and (6.4.17) are related by the thermodynamic identities (6.4.11) and (6.4.12). Using the ansatz

$$D = T^2 d(\bar{\mu}, \ln\tau)\,, \quad D_B = T d_B(\bar{\mu}, \ln\tau)\,, \tag{6.4.18}$$

and (6.4.10), we obtain two differential equations from (6.1.22) and (6.1.23),

$$\begin{aligned} 0 &= \frac{2\rho D}{\epsilon + P_T} - 2D_B + \frac{\xi_\omega}{T} \\ &= T\left(\partial_{\bar{\mu}} d(\bar{\mu}, \ln\tau) - 2 d_B(\bar{\mu}, \ln\tau)\right)\,, \end{aligned} \tag{6.4.19}$$

$$\begin{aligned} 0 &= \frac{\rho D_B}{\epsilon + P_T} + \frac{\xi_B}{T} - C\bar{\mu} \\ &= \partial_{\bar{\mu}} d_B(\bar{\mu}, \ln\tau) - C\bar{\mu}\,. \end{aligned} \tag{6.4.20}$$

These equations can be integrated to give

$$d_B(\bar{\mu}, \ln\tau) = \frac{1}{2}C\bar{\mu}^2 + \beta(\ln\tau)\,, \tag{6.4.21}$$

$$d(\bar{\mu}, \ln\tau) = \frac{1}{3}C\bar{\mu}^3 + 2\bar{\mu}\beta(\ln\tau) + \gamma(\ln\tau)\,, \tag{6.4.22}$$

where $\beta(\ln\tau)$ and $\gamma(\ln\tau)$ are arbitrary functions of $\ln\tau$. Substituting this back into (6.1.22), (6.1.23), we get the conductivities

$$\begin{aligned} \xi_\omega &= C\left(\mu^2 - \frac{2}{3}\frac{\rho\mu^3}{\epsilon + P_T}\right) + 2T^2\beta(\ln\tau) - \frac{2\rho T^3}{\epsilon + P_T}\left(2\bar{\mu}\beta(\ln\tau) + \gamma(\ln\tau)\right)\,, \\ \xi_B &= C\left(\mu - \frac{1}{2}\frac{\rho\mu^2}{\epsilon + P_T}\right) - \frac{T^2}{\epsilon + P_T}\beta(\ln\tau)\,. \end{aligned} \tag{6.4.23}$$

The function $\gamma(\ln\tau)$ is forbidden by CPT invariance [152].

Appendix C. First-order corrected background geometry

In this appendix we compute the first-order corrections to the background (6.3.1) using the ansatz (6.3.3). The computation follows that for the three-charge STU model [155] presented in [129] and [3].

We begin by substituting the ansatz (6.3.3) into the equations of motion (6.2.4) and (6.2.5). We denote the resulting Maxwell equations, Eqs. (6.2.5) by M_N^a $(a = 1, ..., n)$ and the components of the Einstein equation, Eqn. (6.2.4) by E_{MN} $M, N = 0, ..., 4$ $[x^M = (t, x^1, x^2, x^3, r)]$. Then, from $g^{rt}E_{ti} + g^{rr}E_{ri} = 0$, we find $\partial_t u_i = 0$, and E_{tt}, E_{rt}, E_{rr}, E_{tt}, M_t^a, and M_r^a are solved by

$$\partial_i u_i = \tilde{g}_{tr} = \tilde{g}_{tt} = \tilde{A}_t^a = 0\,. \tag{6.4.24}$$

The remaining equations are E_{ij}, E_{ti}, M_i^a. From E_{ij} we get

$$-\partial_r\left(r^3 f(r)\partial_r\left(\frac{\tilde{g}_{ij}(r)}{r^2}\right)\right) = 3r^2(\partial_i u_j + \partial_j u_i)\,. \tag{6.4.25}$$

From E_{ti} we get

$$\begin{aligned}&\left[\frac{f'(r)}{f(r)}\left(\frac{2}{r} + \frac{w_T'(r)}{w_T(r)}\right) + \frac{4}{3f(r)}\left(\sum_{a=1}^n A_0^{a\prime}(r)^2 - 6\right)\right]\tilde{g}_{ti}(r)\\ &\quad + \left(\frac{1}{r} + \frac{w_L'(r)}{2w_L(r)}\right)\tilde{g}_{ti}'(r) + \tilde{g}_{ti}''(r) = 4\sum_{a=1}^n A_0^{a\prime}(r)\tilde{A}_i^{a\prime}(r)\,,\end{aligned} \tag{6.4.26}$$

where a prime denotes the partial derivative ∂_r with respect to r. From M_i^a we get

$$\begin{aligned}&\partial_r\left[w_L(r)^{1/2} r\left(f(r)\tilde{A}_i^{a\prime} - \tilde{g}_{ti}(r)A_0^{a\prime}\right)\right] = \partial_r\left(\frac{1}{2}S_{abc}A_0^b A_0^c\epsilon^{ijk}\left(\partial_j u_k\right) + S_{abc}A_0^b\epsilon^{ijk}\left(\partial_j \mathcal{A}_k^c\right)\right)\\ &\quad \equiv \partial_r Q_i^a(r)\,.\end{aligned} \tag{6.4.27}$$

Equation (6.4.25) depends only on $\tilde{g}_{ij}(r)$ and can easily be solved. The integration of (6.4.27) leads to

$$w_L(r)^{1/2}\left(rf(r)\tilde{A}_i^{a\prime}(r) - r\tilde{g}_{ti}(r)A_0^{a\prime}(r)\right) = Q_i^a(r) + C_i^a\,. \tag{6.4.28}$$

Here C_i^a are some integration constants, which can be fixed as

$$C_i^a = -Q_i^a(r_+) - C_i w_L(r_+)^{1/2} r_+ A_0^{a\prime}(r_+)\,, \tag{6.4.29}$$

with r_+ as in (6.2.19) and $C_i = \tilde{g}_{ti}(r_+)$. This can be solved for $\tilde{A}_i^a(r)$,

$$\tilde{A}_i^a(r) = \int_\infty^r dr' \frac{1}{r' f(r') w_L(r')^{1/2}}\Big[Q_i^a(r') - Q_i^a(r_+) - C_i r_+ A_0^{a\prime}(r_+) w_L(r_+)^{1/2} + r'\tilde{g}_{ti}(r')A_0^{a\prime}(r')\Big]\,. \tag{6.4.30}$$

We still need to determine the constants C_i. Using (6.4.28), we replace $\tilde{A}_i^{a\prime}$ in (6.4.26) and obtain

$$\begin{aligned}&\left[\frac{f'(r)}{f(r)}\left(\frac{2}{r} + \frac{w_T'(r)}{w_T(r)}\right) - \frac{8}{3f(r)}\left(\sum_{a=1}^n A_0^{a\prime}(r)^2 + 3\right)\right]\tilde{g}_{ti}(r)\\ &\quad + \left(\frac{1}{r} + \frac{w_L'(r)}{2w_L(r)}\right)\tilde{g}_{ti}'(r) + \tilde{g}_{ti}''(r) = \frac{1}{w_L(r)^{1/2} r f(r)} I(r)\,,\end{aligned} \tag{6.4.31}$$

where

$$I(r) = \sum_{a=1}^n 4A_0^{a\prime}(r)\Big(Q_i^a(r) - Q_i^a(r_+) - C_i r_+ w_L(r_+)^{1/2} A_0^{a\prime}(r_+)\Big)\,. \tag{6.4.32}$$

A homogeneous solution of this equation $\tilde{g}_{ti}(r) = g_{tt}^{(0)}(r) = f(r)$ can be generated by the infinitesimal coordinate transformation

$$dt \to dt - \epsilon(dx + dy + dz)\,, \quad dz \to dz + \epsilon\frac{dr}{r^2 w_L}\,,$$
$$dx \to dz + \epsilon\frac{dr}{r^2 w_T}\,, \quad dy \to dy + \epsilon\frac{dr}{r^2 w_T}\,. \tag{6.4.33}$$

Then, using this homogeneous solution and Appendix 6.4 [$P(r) = f(r)$ and $E(r) = r w_L(r)^{1/2}$ there], we bring (6.4.31) to the integrable form

$$\partial_r\left(w_L(r)^{1/2} r f^2(r)\partial_r\left(\frac{\tilde{g}_{ti}(r)}{f(r)}\right)\right) = I(r)\,. \tag{6.4.34}$$

Solving this equation for $\tilde{g}_{ti}(r)$ and fixing the integration constants at r_+, we get

$$\tilde{g}_{ti}(r) = f(r)\int_\infty^r dr'\,\frac{1}{w_L(r')^{1/2} r'\,(f(r'))^2}\Big(\int_{r_+}^{r'} dr''\,I(r'') - w_L(r_+)^{1/2} r_+ f'(r_+) C_i\Big)\,. \tag{6.4.35}$$

In the Landau frame we require $u_\mu \tau^{\mu\nu} = 0$, which in particular implies the absence of corrections to T^{ti}. Holographic renormalization [70,71] translates this into a constraint for the r^{-2} coefficient of $\tilde{g}_{ti}(r)$ which is proportional to the first correction of T^{ti},

$$\lim_{r\to\infty} r^2\,\tilde{g}_{ti}(r) = 0\,. \tag{6.4.36}$$

In the limit $r \to \infty$, we have the asymptotics

$$f(r) = O(r^2)\,, \qquad w_L(r) = O(1)\,, \qquad \int_{r_+}^r dr'\,I(r') = O(1)\,, \tag{6.4.37}$$

and, from the vanishing of the r^{-2}-coefficient of $\tilde{g}_{ti}(r)$, we obtain the following equation for C_i:

$$w_L(r_+)^{1/2} r_+ f'(r_+) C_i = \int_{r_+}^\infty dr'\,I(r') \equiv \mathcal{I}_1 + \mathcal{I}_2 \cdot C_i\,, \tag{6.4.38}$$

where we defined the integrals

$$\begin{aligned}\mathcal{I}_1 &\equiv 4\int_{r_+}^\infty dr' \sum_{a=1}^n A_0^{a\prime}(r')\,(Q_i^a(r') - Q_i^a(r_+)) \\ &= \frac{4}{3} S_{abc} A_0^a(r_+) A_0^b(r_+) A_0^c(r_+)\epsilon^{ijk}\,(\partial_j u_k) + 2\,S_{abc} A_0^a(r_+) A_0^b(r_+)\epsilon^{ijk}\,(\partial_j \mathcal{A}_k^c)\end{aligned} \tag{6.4.39}$$

and

$$\begin{aligned}\mathcal{I}_2 &\equiv 4\int_{r_+}^\infty dr' \sum_{a=1}^n A_0^{a\prime}(r')\left(-w_L(r_+)^{1/2} r_+ A_0^{a\prime}(r_+)\right) \\ &= 4\,w_L(r_+)^{1/2} r_+ \sum_{a=1}^n A_0^a(r_+) A_0^{a\prime}(r_+)\,.\end{aligned} \tag{6.4.40}$$

Solving this for C_i, we eventually get

$$\begin{aligned}C^i = &\frac{4}{r_+(f'(r_+) - 4\sum_a A_0^a(r_+) A_0^{a\prime}(r_+))}\cdot\frac{1}{w_L(r_+)^{1/2}} \\ &\times\left(\frac{1}{3} S_{abc} A_0^a(r_+) A_0^b(r_+) A_0^c(r_+)\epsilon^{ijk}\,(\partial_j u_k) + \frac{1}{2} S_{abc} A_0^a(r_+) A_0^b(r_+)\epsilon^{ijk}\,(\partial_j \mathcal{A}_k^c)\right).\end{aligned} \tag{6.4.41}$$

Appendix D. Integrable form of a linear ordinary differential equation

In this appendix we present a method to bring an arbitrary linear ODE of second order to an integrable form. Let us consider a general form of this equation

$$G(g'', g', g, r) \equiv g''(r) + a(r)g'(r) + b(r)g(r) = c(r). \tag{6.4.42}$$

If we know a homogeneous solution $P(r)$ of this equation, *i.e.*

$$G(P'', P', P, r) = 0\,, \tag{6.4.43}$$

then we can make the substitution

$$g(r) \to P(r)Q(r), \quad Q'(r) \to u(r) \tag{6.4.44}$$

and lower the order of the differential operator (6.4.42)

$$\begin{aligned} G &= P(r)\left(u'(r) + \left[a(r) + 2\frac{P'(r)}{P(r)}\right]u(r)\right) \\ &\equiv P(r)(u'(r) + F(r)u(r))\,. \end{aligned} \tag{6.4.45}$$

The term in the brackets can be represented as

$$u'(r) + F(r)u(r) = \frac{1}{A(r)}\partial_r\left(A(r)u(r)\right)\,, \tag{6.4.46}$$

where

$$A(r) = \exp\left\{\int F(r)dr\right\} = P(r)^2\,\exp\left\{\int a(r)dr\right\}\,. \tag{6.4.47}$$

Taking into account (6.4.44), we finally bring (6.4.42) to the following integrable form

$$\frac{1}{P(r)E(r)}\partial_r\left(P(r)^2E(r)\partial_r\left(\frac{g(r)}{P(r)}\right)\right) = c(r)\,. \tag{6.4.48}$$

where we defined

$$E(r) \equiv \exp\left\{\int a(r)dr\right\}\,. \tag{6.4.49}$$

Chapter 7

Quantum Chromodynamics on a Lattice

Lattice quantum chromodynamics is the main systematic nonperturbative framework of studying low-energy strong interactions. At the moment lattice QCD is successfully applied to the hadron spectroscopy, QCD phase diagram, hadron structure, flavor physics, etc. The basic idea of the approach is to put all QCD fields on a 4D hypercubic grid (lattice) of finite volume (usually, $V = L^3 \times T$, where L and T are the spatial box-length and Euclidean time extent, respectively) with lattice spacing a, and (anti-)periodic boundary conditions[1]. This step should be done in a clever way, such that the relevant symmetries (different for different problems) are preserved, which makes the lattice theory significant in its own right. In order to avoid infinities QCD as a field theory requires a regularization both in the ultraviolet (UV) and infrared (IR), which is naturally implemented in lattice QCD: the UV cut-off is provided through the lattice spacing a, and the IR cut-off through finite volume V that respects the gauge invariance of the QCD action. The path integral is rendered finite and reduces to a multidimensional integral over the fields at all grid sites,

$$\int \mathcal{D}\, A_\mu \mathcal{D}\psi \,...\, e^{-\int \mathcal{L}_E[A_\mu, \psi, ...]\mathrm{d}^4x} \to \int \prod_{x_i \,\in\, \mathrm{grid}} \mathrm{d}A_\mu(x_i)\, \mathrm{d}\psi(x_i) \,...\, e^{-a^4 \sum \mathcal{L}_i} \tag{7.0.1}$$

The numerical integration is generally done by means of Monte Carlo methods. We are not aiming to review all the methods of the theory, since they are very numerous and can be found in standard texts (for a general review read e.g. [180] and Refs. therein), and will focus only on some specific issues related to our simulations.

7.1 Improved action

In this section we describe a higher-accuracy lattice version of the Yang-Mills action, which we used in our computations (for a review and efficiency estimates read [181]). The continuum Euclidean Yang-Mills action is given by

$$S = \int d^4x \, \frac{1}{2} \sum_{\mu,\nu} \mathrm{Tr}\, F_{\mu\nu}^2(x)\,, \tag{7.1.1}$$

where $F_{\mu\nu}$ is the field stress tensor,

$$F_{\mu\nu} \equiv \partial_\mu A_\nu - \partial_\nu A_\mu + ig[A_\mu, A_\nu]\,. \tag{7.1.2}$$

[1] Due to the periodicity the Euclidean time extent plays a role of inverse temperature.

The main property of the theory (to be preserved after translating it to the lattice variables) is the invariance with respect to the gauge transformations[2],

$$F_{\mu\nu} \to \Omega(x)\, F_{\mu\nu}\, \Omega(x)^\dagger, \qquad \Omega(x) \in \mathrm{SU}(3)\,. \tag{7.1.3}$$

The naive version of the discretization with $A_\mu(x)$ defined at the sites violates the gauge invariance. Instead, the theory is usually formulated in terms of link variables $U_\mu(x)$,

$$U_\mu(x) \equiv \mathcal{P} \exp\left(-i \int_x^{x+a\hat{\mu}} gA \cdot \mathrm{d}y\right) \tag{7.1.4}$$

defined at a link between the sites x and $x + a\hat{\mu}$. The $\mathcal{P}$-operator denotes the path-ordering. The link variables transform under a gauge transformation in the way involving only its ends,

$$U_\mu(x) \to \Omega(x)\, U_\mu(x)\, \Omega(x + a\hat{\mu})^\dagger\,, \tag{7.1.5}$$

which holds also for an arbitrary path-ordered product of U_μ's. The conjugated variable $U_\mu^\dagger(x)$ is simply the one with integration going from $x + a\hat{\mu}$ to x. The property (7.1.5) leads to the gauge-invariance of the Wilson loop,

$$W(\mathcal{C}) \equiv \frac{1}{3}\mathrm{Tr}\, \mathcal{P} e^{-i \oint_{\mathcal{C}} gA\cdot \mathrm{d}x} = \frac{1}{3}\mathrm{Tr}\, \mathcal{P} \prod_{x\in\mathcal{C}} U_{\mu,\nu}(x), \tag{7.1.6}$$

where $\mathcal{C}$ is a closed path built of the lattice links. Using the Wilson loops one can introduce a discrete version of the Yang-Mills action obeying the locality, gauge-invariance and the symmetry with respect to the axis interchanges (left from the Lorentz invariance). The simplest one, the "Wilson action",

$$S_{\mathrm{W}} = \beta \sum_{x,\, \mu>\nu} (1 - P_{\mu\nu}(x)) \tag{7.1.7}$$

is defined via the sum over "plaquettes", the smallest Wilson loops,

$$P_{\mu\nu}(x) \equiv \frac{1}{3}\mathrm{Re}\,\mathrm{Tr}\left(U_\mu(x) U_\nu(x + a\hat{\mu}) U_\mu^\dagger(x + a\hat{\mu} + a\hat{\nu}) U_\nu^\dagger(x)\right) \equiv \frac{1}{3}\mathrm{Re}\,\mathrm{Tr}$$

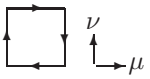

(7.1.8)

and involves the lattice coupling $\beta = 6/g^2$. Using the Tailor expansion,

$$\begin{aligned} P_{\mu\nu} &= \frac{1}{3}\mathrm{Re}\,\mathrm{Tr}\, \mathcal{P}\epsilon^{-i\oint_\Box gA\cdot\mathrm{d}x} \\ &= \frac{1}{3}\mathrm{Re}\,\mathrm{Tr}\left[1 - i\oint_\Box gA\cdot\mathrm{d}x - \frac{1}{2}\left(\oint_\Box gA\cdot\mathrm{d}x\right)^2 + \mathcal{O}(A^3)\right] \end{aligned} \tag{7.1.9}$$

and the Stoke's theorem,

$$\begin{aligned} \oint_\Box A\cdot\mathrm{d}x &= \int_{-a/2}^{a/2} \mathrm{d}x_\mu \mathrm{d}x_\nu \left[\partial_\mu A_\nu(x_0 + x) - \partial_\nu A_\mu(x_0 + x)\right] \\ &= \int_{-a/2}^{a/2} \mathrm{d}x_\mu \mathrm{d}x_\nu \left[F_{\mu\nu}(x_0) + (x_\mu \mathrm{D}_\mu + x_\nu \mathrm{D}_\mu) F_{\mu\nu}(x_0) + \cdots\right] \\ &= a^2\, F_{\mu\nu}(x_0) + \frac{a^4}{24}\,(\mathrm{D}_\mu^2 + \mathrm{D}_\nu^2) F_{\mu\nu}(x_0) + \mathcal{O}(a^6, A^2) \end{aligned} \tag{7.1.10}$$

[2] in this chapter we set the number of color to $N_c = 3$, which can be easily generalized to any number of colors.

one can show that the Wilson action (7.1.7) reproduces the Yang-Mills action (7.1.1) up to corrections of order a^2,

$$S_{\rm W} = \int d^4x \sum_{\mu,\nu} \left\{ \frac{1}{2}{\rm Tr}\, F_{\mu\nu}^2 + \frac{a^2}{24}{\rm Tr}\, F_{\mu\nu}(\mathrm{D}_\mu^2 + \mathrm{D}_\nu^2)F_{\mu\nu} + \cdots \right\}. \tag{7.1.11}$$

Here D_μ is the covariant derivative. One can cancel the a^2-terms by adding extended Wilson loops to the action. One of the choices can be the rectangular operator,

$$R_{\mu\nu} = \frac{1}{3}{\rm Re\,Tr} \quad \nu \;\uparrow \;\; \rightarrow \mu \tag{7.1.12}$$

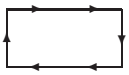

having the expansion

$$R_{\mu\nu} = 1 - \frac{4}{6}\, a^4 {\rm Tr}\,(gF_{\mu\nu})^2 - \frac{4}{72}\, a^6 {\rm Tr}\,\left(gF_{\mu\nu}(4\,\mathrm{D}_\mu^2 + \mathrm{D}_\nu^2)gF_{\mu\nu}\right) - \cdots . \tag{7.1.13}$$

With the help of this operator one can improve the action up to $\mathcal{O}(a^4)$ [182, 183],

$$S_{\rm rec.} \equiv -\beta \sum_{x,\mu>\nu} \left\{ \frac{5P_{\mu\nu}}{3} - \frac{R_{\mu\nu} + R_{\nu\mu}}{12} \right\} + {\rm const} \tag{7.1.14}$$

$$= \int d^4x \sum_{\mu,\nu} \frac{1}{2}{\rm Tr}\, F_{\mu\nu}^2 + \mathcal{O}(a^4)\,, \tag{7.1.15}$$

where we combined together two differently oriented rectangular loops, $R_{\mu\nu}$ and $R_{\nu\mu}$. The choice of the rectangular operator is not unique. One can consider, for instance, a twisted rectangle

$$T_{\mu\nu} = \frac{1}{3}{\rm Re\,Tr} \quad . \tag{7.1.16}$$

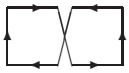

to build an alternative a^2-corrected action,

$$S_{\rm tw.rec.} \equiv -\beta \sum_{x,\mu>\nu} \left\{ P_{\mu\nu} + \frac{T_{\mu\nu} + T_{\nu\mu}}{12} \right\} + {\rm const} \tag{7.1.17}$$

$$= \int d^4x \sum_{\mu,\nu} \frac{1}{2}{\rm Tr}\, F_{\mu\nu}^2 + \mathcal{O}(a^4). \tag{7.1.18}$$

The above performed procedure improves the *classical* action for the gauge fields (gluons). However, the quantum effects is one more source of the error, which should be fixed. One example of such corrections (and the most relevant one) is the tadpole contribution. If we introduce fermions to the theory, then they will interact with gauge fields according to the term $\bar\psi U_\mu \gamma_\mu \psi \cdot a^{-1}$ in the Lagrangian. This term contains the usual vertex $\bar\psi g A \cdot \gamma \psi$ as well as ones with additional powers of $gA_\mu \cdot a$. These additional interactions are suppressed by powers of a in the classical theory, but not at the quantum level, since the contracted pairs of A_μ generate UV-factors $1/a^2$. One way how this contribution can be essentially cancelled out is to divide each link variable U_μ by the square root of the mean plaquette

$$U_\mu(x) \to \frac{U_\mu(x)}{u_0}, \qquad u_0 = \langle 0|P_{\mu\nu}|0\rangle^{1/4}, \tag{7.1.19}$$

since u_0 consists of only tadpoles. The average value u_0 is determined numerically in the following way. We start from some approximate guessed value, substitute it to the action, perform the Monte-Carlo simulation and find the mean plaquette from the ensemble of the generated configurations.

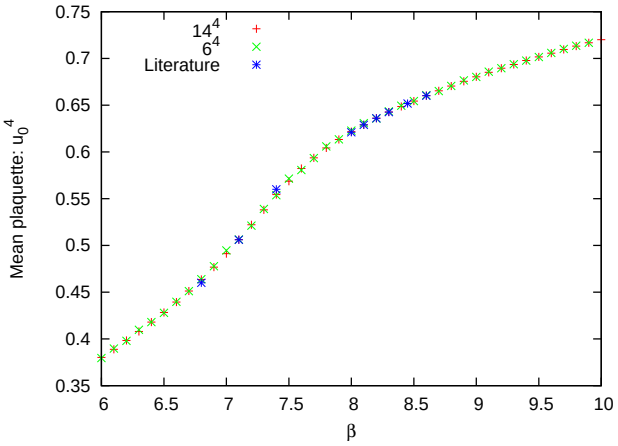

Figure 7.1: Mean plaquette versus coupling constant β obtained by our algorithm. Blue crosses correspond to the values from [184, 185].

This value is then should be taken as a new u_0, and the process is repeated until the input and output values of u_0 coincide. Result of our simulation with the action (7.1.23) above is shown in the Fig. 7.1.

The next step of the improvement is to perform renormalization due to contributions from momenta $k > \pi/a$. These renormalizations induce $a^2\,\alpha_s(\pi/a)$ corrections,

$$\begin{aligned}\delta\mathcal{L} &= \alpha_s\, r_1\, a^2 \sum_{\mu,\nu} \mathrm{Tr}(F_{\mu\nu} \mathrm{D}_\mu^2 F_{\mu\nu}) \\ &+ \alpha_s\, r_2\, a^2 \sum_{\mu,\nu} \mathrm{Tr}(\mathrm{D}_\mu F_{\nu\sigma} \mathrm{D}_\mu F_{\nu\sigma}) \\ &+ \alpha_s\, r_3\, a^2 \sum_{\mu,\nu} \mathrm{Tr}(\mathrm{D}_\mu F_{\mu\sigma} \mathrm{D}_\nu F_{\nu\sigma}) \\ &+ \cdots, \end{aligned} \tag{7.1.20}$$

that must be removed. The prefactor of the last term can be set to zero by a change of field variable (in the path integral) of the form

$$A_\mu \to A_\mu + a^2\,\alpha_s\, f(\alpha_s) \sum_\nu \mathrm{D}_\nu F_{\nu\mu}. \tag{7.1.21}$$

The other corrections are removed by renormalizing the coefficient of the rectangle operator $R_{\mu\nu}$ in the action, and by adding an additional operator. One choice for the extra operator is

$$C_{\mu\nu\sigma} \equiv \frac{1}{3}\mathrm{Re}\,\mathrm{Tr}$$ 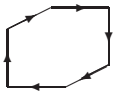 . (7.1.22)

Then the action, correct up to $\mathcal{O}(a^2\alpha_s^2, a^4)$ (used for the lattice calculations in the next chapters), is [186]

$$S = -\beta \sum_{x,\mu>\nu} \left\{ \frac{5}{3}\frac{P_{\mu\nu}}{u_0^4} - r_\mathrm{g}\,\frac{R_{\mu\nu}+R_{\nu\mu}}{12\,u_0^6} \right\} + c_\mathrm{g}\,\beta \sum_{x,\mu>\nu>\sigma} \frac{C_{\mu\nu\sigma}}{u_0^6}, \tag{7.1.23}$$

where

$$r_\mathrm{g} = 1 + .48\,\alpha_s(\pi/a) \tag{7.1.24}$$

$$c_\mathrm{g} = .055\,\alpha_s(\pi/a). \tag{7.1.25}$$

The coefficients $r_{\rm g}$ and $c_{\rm g}$ are computed by "matching" physical quantities, like low-energy scattering amplitudes, computed using perturbation theory in the lattice theory with the analogous quantity in the continuum theory.

7.2 Monte-Carlo algorithms

The next step is to generate an uncorrelated ensemble of gauge configurations with a given partition function

$$Z = \int \prod_{\mu} \mathrm{d}U_{\mu}(x) e^{-S[U]} \,. \tag{7.2.1}$$

The algorithm consists of a sequential updating for each link variable U_μ, such that the configuration approaches equilibrium. For the Wilson action the distribution of link variables has a simple form,

$$P_{eq}(U) \,\propto\, \exp\left\{ \frac{\beta}{N_c} \mathrm{Re}\,\mathrm{Tr}\, U \sum_{i=1}^{6} R_i \right\} \,, \tag{7.2.2}$$

where R_i is the product of three link variables at the i-th out of 6 "staples" connected to the considered link. For a general action built from Wilson loops UR_i is a product of all link variables at i-th Wilson loop contributing to the action and containing U.

In short, we use the Cabibbo-Marinari algorithm [187] for $SU(3)$ (based on the heat bath algorithm [188] for $SU(2)$) with overrelaxation [189]. There is one step of overrelaxation for each step of the heat bath algorithm. We describe the algorithms in the following sections.

Heat bath algorithm

At every step the algorithm replaces the current link variable by a random one, U', from the gauge group with the probability given by the Boltzmann distribution

$$\mathrm{d}P(U') \,\propto\, e^{-S[U']} \mathrm{d}U' \,. \tag{7.2.3}$$

The procedure is essentially equivalent to bringing the link in contact with a "heat bath" causing the fluctuations on a group manifold. This procedure is repeated until all link variables are updated. One can show [188] that many iterations of the updates move the configuration towards equilibrium. Let us consider how the algorithm works for $SU(2)$. A group element can be parameterized as

$$U(x) = a_0(x) \mathbb{1}_{2\times 2} + i\vec{\sigma}\vec{a}(x) \,, \tag{7.2.4}$$

where σ_i are the Pauli matrices. Elements of $SU(2)$ have a determinant equal to identity, therefore $a_\mu a^\mu = 1$, i.e. the group manifold is S^3. In this parametrization the Haar measure is given by

$$\mathrm{d}U = \frac{1}{2\pi^2} \delta(a^2 - 1) \mathrm{d}^4 a \,. \tag{7.2.5}$$

Let us recall a useful property of $SU(2)$: for any $a, b \in SU(2)$ there exist $k \in \mathbb{R}$ and $c \in SU(2)$ such that $a + b = kc$. This gives us

$$\sum_{i=1}^{n} R_i = k\bar{U}, \qquad k = \sqrt{\det \sum_{i=1}^{n} R_i} \tag{7.2.6}$$

and hence the distribution

$$\mathrm{d}P(U'\bar{U}^{-1}) \propto \exp\left\{\frac{\beta}{2}\mathrm{Re}\,\mathrm{Tr}\,U'\bar{U}^{-1}\sum_{i=1}^{n}R_i\right\}\mathrm{d}U' = \exp\left\{\frac{\beta}{2}k\mathrm{Tr}\,U'\right\}\mathrm{d}U'\,. \tag{7.2.7}$$

The latter with use of the invariant measure (7.2.5) and the group parametrization (7.2.4) can be transformed to

$$P(U'\bar{U}^{-1}) \propto \frac{1}{2\pi^2}\delta(a^2-1)\exp\{\beta k a_0\}\,\mathrm{d}^4a \sim \frac{1}{4\pi^2}\sqrt{1-a_0^2}\exp\{\beta k a_0\}\,\mathrm{d}a_0\mathrm{d}\Omega\,, \tag{7.2.8}$$

where $\mathrm{d}\Omega$ is the differential solid angle for the vector $\vec{a}$ and at the last step we integrated over the absolute value of $\vec{a}$. For large to moderate β the distribution (7.2.8) is dominated by the exponential factor. It is suitable to make a change of variables from a_0 to

$$z = \exp(\beta k a_0)\,, \tag{7.2.9}$$

and rewrite the probability distribution for z as

$$\mathrm{d}p(z) \sim \mathrm{d}z\sqrt{1-\left(\frac{\log z}{\beta k}\right)^2}\,. \tag{7.2.10}$$

The value of a trial z is generated by the pseudo-random generator within the allowed interval

$$e^{-2\beta k} \le z \le e^{2\beta k}\,, \tag{7.2.11}$$

and this is rejected with probability given by (7.2.10). This is repeated until some value is accepted. The last step of the algorithm is the choice of the orientation of $\vec{a}$. In our case this is done by a random choice of the spherical variables (polar and azimuthal angles).

Cabibbo-Marinari algorithm

In the previous section we used some specific properties of the $SU(2)$ group, which do not hold, in general, for $SU(N)$ with $N > 2$. To generalize the heat bath algorithm on the $SU(N)$ group we follow the approach proposed by Cabibbo and Marinari [187]. The approach essentially consists of selecting some $SU(2)$ subgroups $\{SU^{[k]}(2) : k = 1, ..., m\}$ of $SU(N)$ and applying the heat bath algorithm to each subgroup. Let us consider a simple choice of $m = N-1$ subgroups of $SU(N)$,

$$a_k = \begin{pmatrix} 1 & & & & & & \\ & \ldots & & & & & \\ & & 1 & & & & \\ & & & \alpha_k & & & \\ & & & & 1 & & \\ & & & & & \ldots & \\ & & & & & & 1 \end{pmatrix} \in SU^{[k]}(2), \qquad k = 1, ..., m\,, \tag{7.2.12}$$

where α_k is an $SU(2)$ matrix at the kth and $(k+1)$th row. Then the link variable is replaced by

$$U'_\mu = a_m a_{m-1} \ldots a_1 U_\mu\,. \tag{7.2.13}$$

We can introduce a definition $U_\mu^k \equiv a_k a_{k-1} \ldots a_1 U_\mu$ and denote by $\check{U}_\mu$ a link variable, which is not the one we consider (U_μ). Then the action splits in two parts, $S(U) \equiv S[U_\mu, \check{U}_\mu]$ and the random a_k is to be chosen according to the distribution

$$\mathrm{d}P(a_k) = \mathrm{d}^{(k)}a_k\, e^{-S[a_k U_\mu^{k-1}, \check{U}_\mu]}\, Z_k^{-1}[U_\mu^{k-1}]\,, \tag{7.2.14}$$

where $\mathrm{d}^{(k)}a_k$ is the Haar measure for $SU^{[k]}(2)$ and the normalization $Z_k[U_\mu^{k-1}]$ is given by

$$Z_k^{-1}[U_\mu^{k-1}] = \int\limits_{SU^{[k]}(2)} \mathrm{d}a\, e^{-S[aU_\mu, \check{U}_\mu]}\,. \tag{7.2.15}$$

Consequently generating the random $a_1 \ldots a_m$ we obtain the new link variable (7.2.13). Using the left-product invariance of the Haar measure,

$$Z_k[bU] = Z_k[U], \qquad b \in SU^{[k]}(2)\,, \tag{7.2.16}$$

one can demonstrate (by induction) that the algorithm leads to the thermalization. Let us assume that U^{k-1} are distributed by the Boltzmann law

$$\mathrm{d}P(U_\mu^{k-1}) = Z^{-1}\, e^{-S[U_\mu^{k-1}, U_\mu]}\, \mathrm{d}U_\mu^{k-1}\,. \tag{7.2.17}$$

By definition, $U_\mu^{k-1} = a_k^{-1}U_\mu^k$, so the distributes takes the form

$$\mathrm{d}P(U_\mu^{k-1}) = P(a_k^{-1}U_\mu^k) = Z^{-1}\, e^{-S[a_k^{-1}U_\mu^k, U_\mu]}\, \mathrm{d}U_\mu^{k-1}\,. \tag{7.2.18}$$

Taken that $\mathrm{d}P(U_\mu^k) = \mathrm{d}P(U_\mu^{k-1})\mathrm{d}P(a_k)$ for the measure, we get

$$\mathrm{d}P(U_\mu^k) = \int\limits_{SU^{[k]}(2)} \mathrm{d}^{(k)}a\, \frac{e^{-S[U_\mu^k, U_\mu]} \cdot e^{-S[a^{-1}U_\mu^k, U_\mu]}}{Z_k[a^{-1}U_\mu^k]Z}\, \mathrm{d}(a^{-1}U_\mu^k)\,. \tag{7.2.19}$$

Taking into account the invariance (7.2.16), i.e.

$$\mathrm{d}(a^{-1}U^k) = dU^k, \qquad \mathrm{d}^{(k)}a = \mathrm{d}^{(k)}a^{-1}, \tag{7.2.20}$$

we finally obtain the Boltzmann distribution

$$\mathrm{d}P(U_\mu^k) = Z^{-1}\, e^{-S[U_\mu^k, U_\mu]}\, \mathrm{d}(U_\mu^k)\,. \tag{7.2.21}$$

The latter means that the *thermalization of* $SU(2)$ *subgroups leads to the thermalization of the full* $SU(N)$.

At the next step we have to generate the random a_k with the distribution defined by (7.2.14). As before, we demonstrate it on a simple example with the Wilson action. The action can be rewritten as

$$S[U_\mu, \check{U}_\mu] = -\frac{\beta}{N}\sum_{\alpha=1}^{n} \mathrm{Re}\,\mathrm{Tr}\,(U_\mu \tilde{U}_\alpha) + \check{S}[\check{U}_\mu] = \frac{\beta}{N}\mathrm{Re}\,\mathrm{Tr}\,(U_\mu R_\mu) + \ldots\,, \tag{7.2.22}$$

where R_μ is a sum over all "staples" $\tilde{U}_\alpha$. One can note that

$$S[a_k U_\mu, \check{U}_\mu] = -\frac{\beta}{N}\mathrm{Re}\,\mathrm{Tr}\,(a_k U_\mu^{k-1} R_\mu) + \ldots \tag{7.2.23}$$

$$= -\frac{\beta}{N}\mathrm{Re}\,\mathrm{Tr}\,(\alpha_k \rho_k) + \text{terms independent of } \alpha_k\,, \tag{7.2.24}$$

where ρ_k is a $k \times (k+1)$ submatrix of $U_\mu^{k-1}R_\mu$. Now one can repeat the procedure from the previous section and generate the α_k matrices with the distribution

$$\mathrm{d}P(\alpha_k) = \delta(\alpha^2 - 1)\exp\left\{\frac{\beta}{N}\mathrm{Re}\,\mathrm{Tr}\,\alpha_k\rho_k\right\}\mathrm{d}^4\alpha_k\,. \tag{7.2.25}$$

For that purpose we can decompose ρ_k and α_k into

$$\rho_k = \rho_0 \mathbb{1} + i\vec{\sigma}\vec{\rho}, \qquad \alpha_k = \alpha_0 \mathbb{1} + i\vec{\sigma}\vec{\alpha} \tag{7.2.26}$$

and rewrite

$$\mathrm{Re}\,\mathrm{Tr}\,(\alpha_k \rho_k) = 2(\alpha_0 \mathrm{Re}\,\rho_0 - \vec{\alpha}\,\mathrm{Re}\,\vec{\rho})\,. \tag{7.2.27}$$

As a final remark let us comment on the case of the $SU(3)$ gauge group. According to (7.2.12) we need only two $SU(2)$ submatrices to apply the heat bath algorithm. Practically, it turns out to be not enough, because of the presence of UV-noise at the generated configurations. To avoid this problem we used three subgroups with the following structure

$$a_1 = \begin{pmatrix} \alpha_1 & \\ & 1 \end{pmatrix}, \quad a_2 = \begin{pmatrix} 1 & \\ & \alpha_2 \end{pmatrix}, \quad a_3 = \begin{pmatrix} \alpha_3^{11} & & \alpha_3^{12} \\ & 1 & \\ \alpha_3^{21} & & \alpha_3^{22} \end{pmatrix}, \tag{7.2.28}$$

where α_i are the $SU(2)$ matrices.

Overrelaxation

Now let us describe a complimentary method to the heat bath algorithm, the overrelaxation [189, 190]. The method is based on the "reflection" of a link variable with respect to the local minimum of the action. This accelerates the decorrelation of the gauge configurations. Usually, the method is alternated with the heat bath, which in case of the $SU(2)$ group results in a faster thermalization [191]. We apply the overrelaxation to the full $SU(3)$, following [190].

If $\hat{X} \in SU(N)$ is an element of the group minimizing the action, then the shift from U to $\hat{X}$ on the group manifold is represented by $\hat{X}U^{-1}$. The "reflection" with respect to $\hat{X}$ will then correspond to that action applied twice,

$$U' = (\hat{X}U^{-1})^2 U = \hat{X}U^{\dagger}\hat{X}\,. \tag{7.2.29}$$

The trial element U' is then accepted with the probability from the Metropolis algorithm [192],

$$P_A = \min\left[1, \exp\left(-S[U'] + S[U]\right)\right]. \tag{7.2.30}$$

This transformation is its own inverse and, hence, satisfies the detailed balance condition.

The algorithm is valid for any of the guessed $\hat{X}$. However its efficiently depends on a clever choice of $\hat{X}$. We use the one proposed in [193] based on the polar decomposition of the sum of "staples" R:

1. Perform the Singular Value Decomposition (SVD) of R: $R = W\Sigma V^{\dagger}$, where W and V are unitary matrices, and Σ is the diagonal matrix of singular values $\sqrt{\lambda_i}$, where $\{\lambda_i\}$ are the eigenvalues of the non-negative Hermitian matrix $R^{\dagger}R$.

2. Find $\det R \equiv \zeta \exp(i\varphi)$. Then find an approximate solution $\{\theta_i\}$ for the phases of the diagonal matrix $D = \mathrm{diag}(\exp i\theta_1, ..., \exp i\theta_N)$, $\sum_N \theta_i = 0 \bmod 2\pi$ to maximize

$$\mathrm{Re}\,\mathrm{Tr}\,\exp(-i\frac{\varphi}{N})WDV^{\dagger}R.$$

   We assume that all phases θ_i are small, and solve the linearized problem.

3. Accept the updated value $U' = \hat{X}U^{\dagger}\hat{X}$, where $\hat{X} = \exp(i\varphi/N)WDV^{\dagger}$, with the probability (7.2.30).

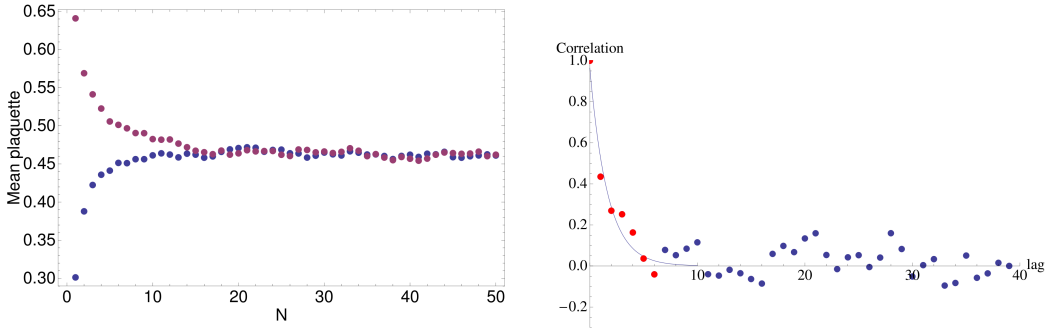

(a) (b)

Figure 7.2: (a) Thermalization for the cold (blue) and hot (magenta) initial configurations with $\beta = 6.8$ and $u_0 = 0.46$, see explanation in the text; (b) Autocorrelation for gauge configurations with the same parameters.

As mentioned above, we used a combination of one overrelaxed update with a heat bath (Cabibbo-Marinari) update. Fig. 7.2(a) presents typical runs of the algorithm with different initial conditions. The "cold" run is characterized by an ordered start, when all link matrices are set to the identity (i.e., if the initial temperature is zero). The "hot" run starts from a configuration with link variables were generated randomly, uniformly in the Haar measure (i.e., if the initial temperature is infinite). For both runs the thermalization occurs already after 20 iterations. Practically, we waited 50 iterations before starting saving the configurations. We made dumps after every 10 iterations, making sure of statistical independence of the configurations (see Fig. 7.2(b))

7.3 Overlap fermions

In the previous sections we considered a lattice formulation of the pure gluodynamics. A logical step towards the real QCD is to add fermions to the system. It turns out that the naive discretization of the Dirac operator

$$D = \frac{1}{2}\gamma^\mu\{\nabla_\mu + \nabla^*_\mu\} + m \equiv \frac{1}{2a}\gamma^\mu\left\{U_\mu(x)\psi(x+a\hat{\mu}) - U^\dagger_\mu(x-a\hat{\mu})\psi(x-a\hat{\mu})\right\} + m \qquad (7.3.1)$$

leads to the problem of doubling: instead of one fermion on a lattice in 4D one obtains $2^4 = 16$ copies [180]. One of the solutions of this problem proposed by Wilson [194] consists of adding an irrelevant operator to the fermion action, which modifies the dispersion relation for fermions, such that the doublers acquire a mass proportional to the inverse lattice spacing $m \sim 1/a$ and decouple in the continuum limit. The Wilson-Dirac operator has the following form

$$D_W(m) = \frac{1}{2}\left\{\gamma^\mu(\nabla_\mu + \nabla^*_\mu) - a\,r\nabla^2\right\} + m\,, \qquad (7.3.2)$$

where ∇_μ is the nearest-neighbor lattice derivative, r denotes the Wilson parameter, m is the bare fermion mass. However, the Wilson-Dirac operator explicitly violates the chiral symmetry. In general, no lattice fermion action can be undoubled, chiral (in the standard sense), and have couplings that extend over a finite number of lattice spacings (this is a folkloric version of the Nielsen-Ninomiya no-go theorem [195]). There is a way to avoid the Nielsen-Ninomiya theorem by modifying the chiral rotation with a local Dirac operator [196]

$$\psi \to e^{i\theta\gamma_5(1-\frac{aD}{2})}\psi, \qquad \bar{\psi} \to \bar{\psi}e^{i\theta(1-\frac{aD}{2})\gamma_5}\,, \qquad (7.3.3)$$

such that it coincides with the usual definition in the continuum limit $a \to 0$. It can be shown that the chiral symmetry is preserved in an undoubled lattice theory, if the Dirac operator D obeys the Ginsparg-Wilson relation [197],

$$\gamma_5 D + D\gamma_5 = aD\gamma_5 D\,. \tag{7.3.4}$$

A solution of this equation found by Neuberger [198] and named as the massless "overlap" operator (or Neuberger's operator) has the following form

$$D_{\rm ov}(0) = \frac{1}{a}\left(1 - \frac{A}{\sqrt{A^\dagger A}}\right)\,, \tag{7.3.5}$$

where A is a function of the massless Wilson Dirac operator (7.3.2),

$$A(0) = 1 - aD_W(0)\,. \tag{7.3.6}$$

The overlap operator is in general local [199] and can be generalized for the case of massive fermions,

$$D_{\rm ov}(m) = \left(1 - \frac{am}{2}\right) D_{\rm ov}(0) + m\,, \tag{7.3.7}$$

which we used in our simulations.

Though it has all suitable properties for the chiral symmetry studies, the overlap operator has a high computational cost compared to other lattice Dirac operators. This makes it important to develop effective methods for the practical realization of the overlap operator. The most expensive step is the computation of the square root of a sparse matrix in (7.3.5). There are many approaches to do that, namely the polynomial approximations, Lanczos based methods and partial fraction expansion [200, 201]. In our code we used the Chebyshev approximation [202], based on a construction of a polynomial $P_{n,\epsilon}(x)$ of degree n,

$$P_{n,\epsilon}(x) = \sum_{k=0}^{n} c_k T_k(z), \qquad z = \frac{2x - 1 - \epsilon}{1 - \epsilon}, \tag{7.3.8}$$

where $T_k(z)$ are Chebyshev polynomials defined in the range $z \in [-1, 1]$. Sufficient maximal degree of the polynomial n depends crucially on the parameter ϵ [201]. Usually, one computes the first $\mathcal{O}(10)$ lowest-lying eigenvalues of $A^\dagger A$ and their eigenfunctions, which are then projected out of $A^\dagger A$. The value of ϵ is then set to the minimal among remaining eigenvalues. The deflation leads to a substantial decrease of the order of the polynomial and the dimensionality of the Krylov subspace. Degree n is chosen such that the relative error does not exceed a bound ξ,

$$\max\left|\frac{(A^\dagger A)^{-1/2} - P_{n,\epsilon}(A^\dagger A)}{(A^\dagger A)^{-1/2}}\right| < \xi, \tag{7.3.9}$$

where ξ is a small number (in our code $\xi \sim 10^{-8}$). The lowest eigenvalues of the overlap operator are treated exactly and were computed with ARPACK [203] iterative solver (see also [204, 205] for the details of the algorithm and possible generalizations on a non-Hermitian A).

Chapter 8

SU(3) quenched lattice gauge theory in magnetic fields

In this chapter we study the effect of a strong magnetic field on the properties of the QCD vacuum. Due to the nonperturbative nature of the effects we perform the calculations in the lattice gauge theory. We use the quenched approximation (i.e. without dynamical quarks) and show that for our goals it provides rather reasonable values of the physical quantities. The list of considered effects induced by the magnetic field is the following.

The strong magnetic field can enhance the chiral symmetry breaking. There are various models (see Sec. 8.2) which predict the growing of the chiral condensate.

The second effect is the chiral magnetization of the QCD vacuum. This effect has a paramagnetic nature. The vacuum magnetization is related to the nucleon magnetic moments [206] and other nonperturbative effects of hadrons [207, 208]. We calculate the magnetic susceptibility and other quantities in Sec. 8.3.

The quarks develop an electric dipole moment along the field due to the local fluctuations of the topological charge [209]. We study this effect in Sec. 8.4.

Finally, the fluctuations of the topological charge can be a source of the asymmetry between numbers of quarks with different chiralities created in heavy-ion collisions. The so called "event-by-event P- and CP-violation" [30] can contribute to this asymmetry. Our aim is also to see some evidences of this effect in SU(3) lattice simulations, although they might be similar to the SU(2) lattice results [51].

The additional motivation for the study of the effects induced by a strong magnetic field could also come from the physics of the early Universe, where the strong fields ($B \sim 10^{16}$T, $\sqrt{eB} \sim 1$ GeV) might have been produced after the electroweak phase transition [210], and from the physics of compact dense stars, such as magnetars ($B \sim 10^{10}$T, $\sqrt{eB} \sim 1$ MeV) [211].

8.1 Technical details

We use the quenched $SU(3)$ lattice gauge theory with tadpole-improved Lüscher-Weisz action [183]. To generate the statistically independent gauge field configurations we use the Cabibbo-Marinari heat bath algorithm. The lattice size is 14^4, and lattice spacing $a = 0.105fm$. All observables we discuss later have a similar structure: $\langle\bar{\Psi}\mathcal{O}\Psi\rangle$ for VEV of a single quantity or $\langle\bar{\Psi}\mathcal{O}_1\Psi\ \ \bar{\Psi}\mathcal{O}_2\Psi\rangle$ for dispersions or correlators. Here $\mathcal{O}$, $\mathcal{O}_1$, $\mathcal{O}_2$ are some operators in spinor and color space. These expectation values can be expressed through the sum over M low-lying[1] but non-zero eigenvalues

[1] We believe that the IR quantities are insensitive to the UV cutoff realized by selecting some finite number of the eigenmodes [212]

$i\lambda_k$ of the chirally invariant Dirac operator D (Neuberger's overlap Dirac operator [198]):

$$\langle\bar{\Psi}\mathcal{O}\Psi\rangle = \sum_{|k|<M} \frac{\psi_k^\dagger \mathcal{O}\psi_k}{i\lambda_k + m} \tag{8.1.1}$$

and

$$\langle\bar{\Psi}\mathcal{O}_1\Psi\ \ \bar{\Psi}\mathcal{O}_2\Psi\rangle = \sum_{k,p} \frac{\langle k|\mathcal{O}_1|k\rangle\langle p|\mathcal{O}_2|p\rangle - \langle p|\mathcal{O}_1|k\rangle\langle k|\mathcal{O}_2|p\rangle}{(i\lambda_k + m)(i\lambda_p + m)}, \tag{8.1.2}$$

where all spinor and color indices are contracted and we omit them for simplicity. The λ_k are defined by the equation

$$D\psi_k = i\lambda_k\psi_k, \tag{8.1.3}$$

where ψ_k are the corresponding eigenfunctions. The uniform magnetic field $F_{12} = B_3 \equiv B$ is introduced by adding diagonal components to the vector potential ${A_\mu}^i_j$,

$${A_\mu}^i_j \to {A_\mu}^i_j + \frac{B}{2}(x_1\delta_{\mu,2} - x_2\delta_{\mu,1})\,\delta^i_j\,, \tag{8.1.4}$$

and introducing an additional x-dependent twist for fermions [213] in order to combine (8.1.4) with the periodic boundary conditions. The total magnetic flux is quantized, therefore the magnetic field can take only discrete values,

$$qB = \frac{2\pi k}{L^2}, \qquad k \in \mathbb{Z}\,, \tag{8.1.5}$$

where $q = \left|-\frac{e}{3}\right|$ is the d-quark charge, which we use in our simulations. To perform calculations in the chiral limit one calculates the expression (8.1.1) or (8.1.2) for some non-zero m and averages it over all configurations of the gauge fields. Then one repeats the procedure for other quark masses m and extrapolates the VEV to $m \to 0$ limit.

8.2 Chiral condensate

In this section we present our results for the chiral condensate

$$\Sigma \equiv -\langle 0|\bar{\Psi}\Psi|0\rangle, \tag{8.2.1}$$

as a function of the magnetic field B. The general tendency for Σ to grow with B at $T \ll T_c$ is usually referred to the magnetic catalysis of the chiral symmetry breaking [214, 215] and was already obtained in various models[2]: in the chiral perturbation theory [111, 112] ($\Sigma \propto B$ for weak fields, $\Sigma \propto B^{3/2}$ for strong fields); in the Nambu-Jona-Lasinio model [113] ($\Sigma \propto B^2$); in a confining deformation of the holographic Karch-Katz model [114] ($\Sigma \propto B^2$); in D3/D7 holographic system [1] ($\Sigma \propto B^{3/2}$ for low temperatures, $\Sigma \propto B$ for high temperatures); in SU(2) quenched lattice calculations [115]($\Sigma \propto B$); at larger than physical pion masses in $N_f = 2$ QCD [218,219] and in the $N_f = 4$ SU(2) theory [220]; and at physical quark masses in full $N_f = 2+1$ QCD [216,217]. Here our aim is to see how the chiral condensate behaves in the $SU(3)$ quenched gluodynamics.

We use the Banks-Casher formula [221], which relates the condensate (8.2.1) with the density $\rho(\lambda)$ of near-zero eigenvalues of the Dirac operator:

$$\Sigma = \lim_{\lambda\to 0} \frac{\pi\rho(\lambda)}{V}, \tag{8.2.2}$$

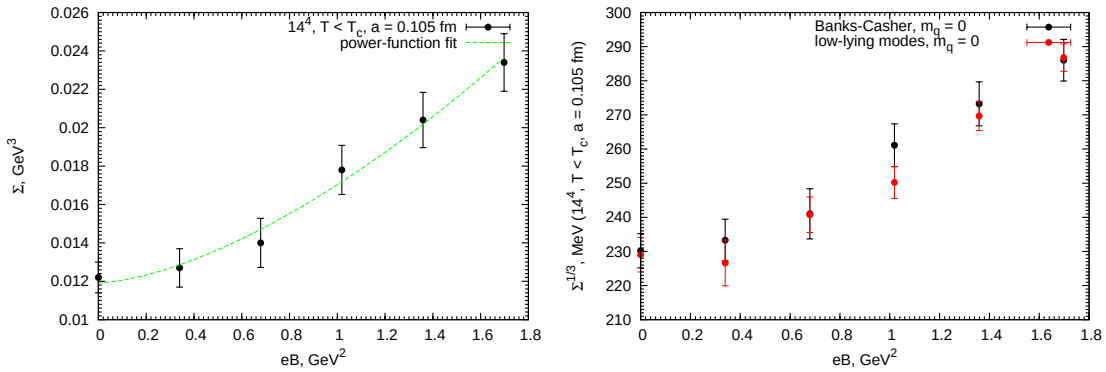

(a) (b)

Figure 8.1: Chiral condensate

where V is the four-volume of the Euclidean space-time. The result is shown in Fig. 8.1(a).

We perform the fit of the results by the following function:

$$\Sigma^{fit}(B) = \Sigma_0 \left[1 + \left(\frac{eB}{\Lambda_B^2}\right)^{\nu}\right], \tag{8.2.3}$$

where $\Sigma_0 \equiv \Sigma(0)$. The obtained fitting parameters are

$$\Sigma_0 = [(228 \pm 3)\,\mathrm{MeV}]^3\,, \qquad \Lambda_B = (1.31 \pm 0.04)\ \mathrm{GeV}, \qquad \nu = 1.57 \pm 0.23\,. \tag{8.2.4}$$

It is interesting to compare quantitatively the condensate obtained by the Banks-Casher formula and the one calculated by the expression (8.1.1) with $\mathcal{O} = \mathbb{1}$. The result is shown in Fig. 8.1(b). The value of the condensate in absence of the magnetic field equals $\Sigma(0) = [(230 \pm 5)\ \mathrm{MeV}]^3$ which is a reasonable value, compare with e.g. [222].

8.3 Chiral magnetization and susceptibility

In this section we calculate the quantity

$$\langle \bar{\Psi} \sigma_{\alpha\beta} \Psi \rangle = \chi(F) \langle \bar{\Psi} \Psi \rangle q F_{\alpha\beta}, \tag{8.3.1}$$

where $\sigma_{\alpha\beta} \equiv \dfrac{1}{2i}[\gamma_\alpha, \gamma_\beta]$ and $\chi(F)$ is a coefficient of proportionality (susceptibility), which depends on the field strength.

This quantity was introduced in [206] and can be used to estimate the spin polarization of the quarks in external magnetic field. The magnetization can be described by the dimensionless quantity $\mu = \chi \cdot qB$, so that

$$\langle \bar{\Psi} \sigma_{12} \Psi \rangle = \mu \langle \bar{\Psi} \Psi \rangle\,. \tag{8.3.2}$$

The expectation value (8.3.1) can be calculated on the lattice by (8.1.1) with $\mathcal{O} = \sigma_{\alpha\beta}$. The result is shown in Fig. 8.2(a) (here for comparison we also plot series for a finite quark mass). We can see, that the 12-component grows linearly with the field, which agrees with [206]. This allows

[2] A non-monotonic behavior in the vicinity of T_c has been recently observed [216, 217] and named as *inverse magnetic catalysis*.

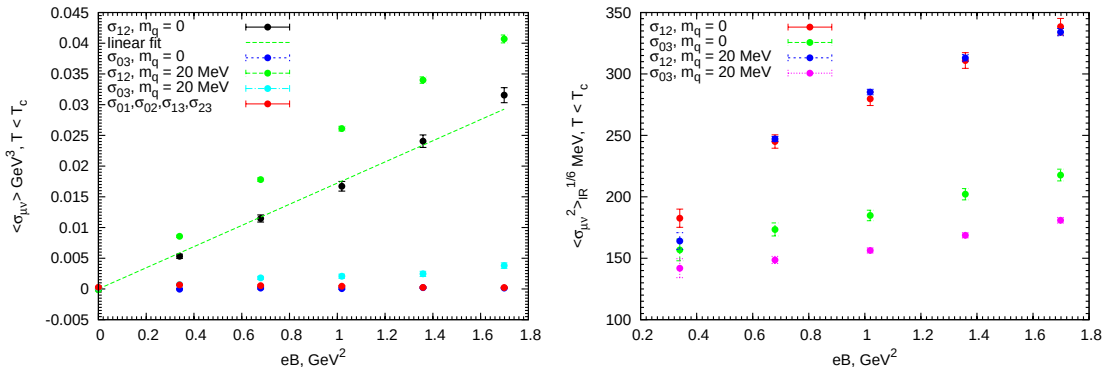

(a) (b)

Figure 8.2: Expectation values of $\bar{\Psi}\sigma_{\alpha\beta}\Psi$ and their square

us to find the chiral susceptibility $\chi(0) \equiv \chi_0$ from the slope of the curve. After making a linear approximation $\langle\bar{\Psi}\sigma_{12}\Psi\rangle = \Omega^{fit}eB$, where

$$\Omega^{fit} \equiv -\frac{1}{3}\chi_0^{fit}\Sigma_0\,, \tag{8.3.3}$$

we obtain $\Omega^{fit} = (172.3 \pm 0.5)\,\mathrm{MeV}$ and

$$\chi_0^{fit} = -4.24 \pm 0.18\,\mathrm{GeV}^{-2}\,, \tag{8.3.4}$$

showing that the QCD vacuum has a diamagnetic nature. This value fits well into the range of present theoretical estimations: the modern QCD sum rule calculations [223] ($\chi_0^{th} = -3.15 \pm 0.3\,\mathrm{GeV}^{-2}$) and [224] ($-2.85 \pm 0.5\,\mathrm{GeV}^{-2}$), the earlier ones [225] ($-5.7\,\mathrm{GeV}^{-2}$) and [226] ($-4.4 \pm 0.4\,\mathrm{GeV}^{-2}$), in the instanton vacuum model [227–229] ($-4.32\,\mathrm{GeV}^{-2}$), from the analysis of the Dirac zero-mode in an instanton background [230] ($-3.52\,\mathrm{GeV}^{-2}$), in dubbed quark-meson model [231] ($-4.3\,\mathrm{GeV}^{-2}$) and in the NJL model [231] ($-5.25\,\mathrm{GeV}^{-2}$). The value of the magnetic susceptibility can be measured in experiments on lepton pair photoproduction via the chiral-odd coupling of a photon to quarks [207, 208], and in radiative heavy meson decays [224].

Recently, the lattice calculations with full $N_f = 2+1$ QCD [232] provided the following values for the magnetic susceptibility

$$\chi_u = -(2.08 \pm 0.08)\,\mathrm{GeV}^{-2}\,, \quad \chi_d = -(2.02 \pm 0.09)\,\mathrm{GeV}^{-2}\,, \quad \chi_s = -(3.4 \pm 1.4)\,\mathrm{GeV}^{-2}\,. \tag{8.3.5}$$

We also have to mention a well known analytic result obtained by the OPE combined with the idea of pion dominance [233],

$$\chi^{OPE} = -\frac{N_c}{4\pi^2 F_\pi^2} \simeq -9.77\,\mathrm{GeV}^{-2}, \tag{8.3.6}$$

supported by two holographic studies [234, 235], but giving a too high value comparing to our result. This disagreement seems to be an important puzzle to solve, because it will lead to a better understanding of the pion dominance assumption and the large N_c limit.

Another interesting phenomenological quantity is the product of the chiral susceptibility χ and the condensate $\langle\bar{\Psi}\Psi\rangle$ [207, 208]. In our calculations it is equal to

$$-\chi_0^{fit}\langle\bar{\Psi}\Psi\rangle \simeq 52\,\mathrm{MeV}, \tag{8.3.7}$$

while from the QCD sum rules one can estimate this quantity as approximately 50 MeV [223, 225, 226], which is also close to our value.

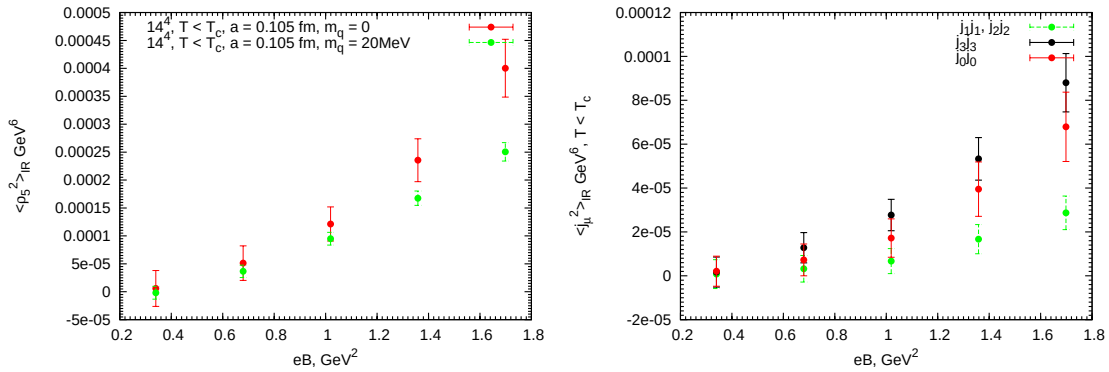

(a) (b)

Figure 8.3: Fluctuations of the chirality and electromagnetic current/charge

8.4 Electric dipole moment

Another interesting effect due to the magnetic field is a quark local electric dipole moment along the field [209]. This quantity corresponds to the $i0$-components of the (8.3.1):

$$d_i(x) \equiv \bar{\Psi}(x)\sigma_{i0}\Psi(x), \qquad i = \overline{1,3} \tag{8.4.1}$$

In the real CP-invariant vacuum the VEV of this quantity should be zero: $\langle d_i(x)\rangle = 0$, that we actually see in our results (Fig. 8.2(a)). At the same time the fluctuations of $d_i(x)$ can be sufficiently strong. We measure VEV's (8.1.2) with $\mathcal{O}_1 = \mathcal{O}_2 = \sigma_{\alpha\beta}$. In the case of $i0$-components it corresponds to dispersions of $\vec{d}$. The result is shown in Fig. 8.2(b). We see that the longitudinal fluctuations of the local dipole moment grow with the field strength, while transverse fluctuations are absent. Taking into account that the average dipole moment is zero, we may guess, that the QCD vacuum is divided into space-time domains, in which quarks have an anomalous electric dipole moment along $\vec{B}$.

Here and after we use the "IR" subscript to emphasize, that we subtract from the quantity its value at $B = 0$, removing also the leading order UV-divergences,

$$\langle Y\rangle_{IR}(B) = \frac{1}{V}\int\limits_V d^4x\langle Y(x)\rangle_B - \frac{1}{V}\int\limits_V d^4x\langle Y(x)\rangle_{B=0} \tag{8.4.2}$$

8.5 Some evidences of the chiral magnetic effect

One example of a new magnetic-field-induced effect mentioned in the Introduction is the chiral magnetic effect (CME), which generates an electric current along the magnetic field in the presence of a nontrivial gluonic background [30, 41–43]. This effect may naturally take place in heavy-ion collisions and is at the moment under active experimental search [37–40] (see also a review [177] on the interpretation of the experimental data). Lattice evidences of the effect can be found in [5–7,10, 51–54]. In [51] it has been found that the fluctuations of the electric current along the magnetic field are strongly enhanced as compared to the fluctuations of current in the perpendicular directions. This conclusion was also confirmed by an analytical calculation in the instanton gas model [236]. The result of [51] on the difference of longitudinal and transverse electric current susceptibilities has been reproduced later by an analytical calculation [237]; the frequency dependence of the conductivity has also been evaluated – for the weak coupling result, see [238]. Here we implement

the procedure from [51] for the $SU(3)$ case and study the local chirality

$$\rho_5(x) = \bar{\Psi}(x)\gamma_5\Psi(x) \equiv \rho_L(x) - \rho_R(x) \tag{8.5.1}$$

and the electromagnetic current

$$j_\mu(x) = \bar{\Psi}(x)\gamma_\mu\Psi(x). \tag{8.5.2}$$

The expectation value of the first quantity can be computed by (8.1.1) with $\mathcal{O} = \gamma_5$ and with $\mathcal{O} = \gamma_\mu$ for the second quantity. Both VEV's are zero, as expected from the Lorentz and parity invariance, but the corresponding fluctuations obtained from (8.1.2) are finite and grow with the field strength (see Fig. 8.3). One can interpret the enhancement of the current fluctuations either as short-living quantum fluctuations or as a charge flow. We measured the conductivity of the QCD vacuum in the next chapter and argue in support of the latter case.

Chapter 9

Magnetic-Field-Induced insulator-conductor transition

A natural question which one can ask concerning the results of the previous section is whether the enhancement of current fluctuations corresponds to a real flow of charge, or is just caused by short-lived quantum fluctuations. This question can be answered by studying the current-current correlation functions. The currents which correspond to a real transport of charged particles should have long-range correlations in time, while quantum fluctuations are typically characterized by a finite correlation time [239]. Recalling Green-Kubo relations, one can see that this property is intimately related to the electric conductivity - namely, the real transport of charged particles can occur only in conducting media. In this chapter we study the tensor of electric conductivity of the vacuum of quenched $SU(2)$ lattice gauge theory in external magnetic field. We find that the magnetic field induces nonzero electric conductivity along its direction, transforming the confining vacuum from an insulator into an anisotropic conductor.

Electric conductivity can be extracted from the correlator of two vector currents $j_i(x) = \bar{q}(x)\gamma_i q(x)$:

$$G_{ij}(\tau) = \int d^3\vec{x} \langle j_i(\vec{0},0) j_j(\vec{x},\tau) \rangle \tag{9.0.1}$$

Following [240], let us define the spectral function $\rho(w)$ which corresponds to the correlator (9.0.1)

$$G_{ij}(\tau) = \int_0^{+\infty} \frac{dw}{2\pi} K(w,\tau) \rho_{ij}(w), \tag{9.0.2}$$

$$K(w,\tau) = \frac{w}{2T} \frac{\cosh\left(w\left(\tau - \frac{1}{2T}\right)\right)}{\sinh\left(\frac{w}{2T}\right)}, \tag{9.0.3}$$

where T is the temperature. The Kubo formula for the electric conductivity then reads [239, 240]:

$$\sigma_{ij} = \lim_{\omega \to 0} \frac{\rho_{ij}(\omega)}{4T}. \tag{9.0.4}$$

In the limit of the weak time-independent *electric* field E_k, one has $\langle j_i \rangle = \sigma_{ik} E_k$. Thus electric conductivity is related to the behavior of the spectral function at small frequencies. If there is a gap in the spectrum so that $\rho_{ij}(w) = 0$ for $w < w_c$, electric conductivity is zero and $G_{ij}(\tau) \sim \cosh\left(w_c\left(\tau - \frac{1}{2T}\right)\right)$. On the other hand, if $\rho(w)$ is not zero near $w = 0$, one can expect slow nonexponential decay of $G_{ij}(\tau)$.

To measure the correlator (9.0.1), we perform lattice Monte-Carlo simulations of quenched $SU\,(2)$ lattice gauge theory. Since quark chirality is very important for magnetic effects in non-Abelian gauge theories [30, 41–43], we use the overlap lattice Dirac operator $\mathcal{D}$ with exact chiral symmetry [198] to measure the vector currents. We consider the two-current correlator in the meson channel, which is represented in terms of Dirac propagators in fixed Abelian and non-Abelian gauge fields and is then averaged over an equilibrium ensemble of non-Abelian gauge fields A_μ:

$$\langle\, \bar{q}\,(x)\,\gamma_i q\,(x)\;\bar{q}\,(y)\,\gamma_j q\,(y)\,\rangle = \int \mathcal{D}A_\mu\, e^{-S_{YM}[A_\mu]}\,\mathrm{Tr}\,\left(\frac{1}{\mathcal{D}+m}\,\gamma_i\,\frac{1}{\mathcal{D}+m}\,\gamma_j\right), \qquad (9.0.5)$$

where $S_{YM}\,[A_\mu]$ is the lattice action for gluons A_μ. A uniform magnetic field is added to the Dirac operator by substituting $su\,(2)$-valued vector potential A_μ with $u\,(2)$-valued one $A_{\mu\,ij} \to A_{\mu\,ij} + 1/2\;F_{\mu\nu}\;x_\nu \delta_{ij}$. In order to account for periodic boundary conditions we introduce an additional twist for fermions [51, 213]. The quark mass is fixed in lattice units at a small value $am = 0.01$. Previous studies of mesonic correlation functions with an overlap Dirac operator indicate that the vector current correlator depends very weakly on quark mass [212, 241].

Strictly speaking, the correlator (9.0.5) corresponds to the correlator of charged currents, for example $\bar{u}\gamma_\mu d$. The correlator of neutral currents $j_\mu = \bar{d}\gamma_\mu d$, should also contain the disconnected part. This part is quite intricate for an accurate numerical treatment. We have roughly estimated its contribution by inverting the Dirac operator on a subspace spanned on some small number $M \sim 30$ of the lowest Dirac eigenmodes, as in [242]. It turned out that this part of the full neutral current correlator behaves similarly to the connected one (9.0.5). We do not reproduce these estimates here due to uncontrollable systematic errors [242].

We use the tadpole-improved Wilson-Symanzik action (see, e.g., Eq. (1) in [243]). For inversion, we use a Gaussian source with radius $r = 1.0$ in lattice units in both spatial and time directions and a point sink (that is, quark position is smeared over a Gaussian profile). We have found that such smearing significantly improves the convergence of the maximal entropy method [240, 244, 245] at small lattice sizes, while the value of the conductivity is practically unaffected. Our lattice parameters are summarized in Table 9.0.1. A uniform magnetic field is introduced into the Dirac operator as described in [51]. In order to obtain the Dirac propagator, we implement the shifted unitary minimal residue method of Ref. [246, 247].

It is clear that since the magnetic field is parallel to the z axis, the principal axes of the tensor $\sigma_{ij}\,(\tau)$ will be the x, y and z axes and it is sufficient to consider only the diagonal components σ_{ii} (no summation over i=x, y, z).

We plot some correlators at different temperatures and magnetic fields on Fig. 9.1. The data are for the 14^4 lattice with spacing $a = 0.102\,\mathrm{fm}$ (left) and for the $16^3 \times 6$ lattice with spacing $a = 0.095\,\mathrm{fm}$ (right). For the latter lattice the temperature is $T = 350\,\mathrm{MeV} = 1.12\,T_c$ and the theory is in the deconfinement phase. In the quenched theory the critical temperature of the deconfinement transition is not affected by the magnetic field. The temperature $T = 1.12$ corresponds to the chirally restored phase.

One can see that without the magnetic field the correlators decay quickly in the confinement

β	a, fm	$N_s^3 \times N_t$	T/T_c	#conf
3.2810	0.102	$14^3 \times 14$	0.43	30
3.2810	0.102	$16^3 \times 16$	0.38	30
3.3555	0.089	$16^3 \times 16$	0.43	30
3.3250	0.095	$16^3 \times 6$	1.12	30

Table 9.0.1: Lattice parameters used in our simulations. The critical temperature of the deconfinement phase transition in quenched $SU\,(2)$ gauge theory is $T_c = 313.(3)\,\mathrm{MeV}$ [248].

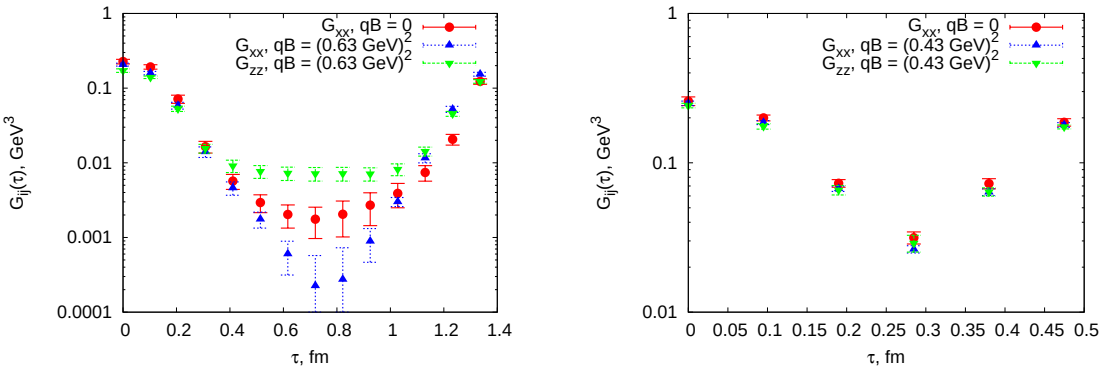

Figure 9.1: The correlator (9.0.1) in the confinement (left) and in the deconfinement phases (right) at $T = 350$ MeV.

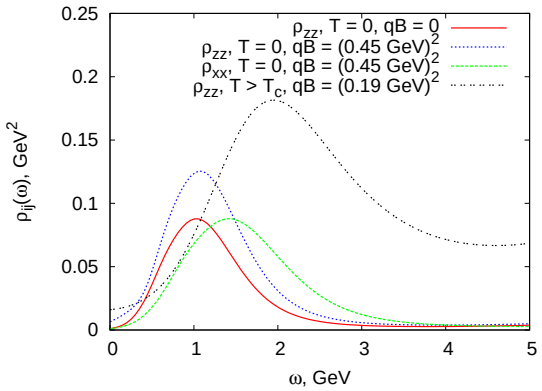

Figure 9.2: Spectral functions $\rho_{ij}(w)$ in the confinement and deconfinement phases.

phase. In the deconfinement phase the decay is significantly slower for all $G_{ii}(\tau)$. When we switch on a magnetic field with the strength $qB = (0.63\ \text{GeV})^2$, in the confinement phase the correlator $G_{zz}(\tau)$ decays much slower and is significantly larger than zero for all τ, much like in the deconfinement phase. In contrast, the correlators for the perpendicular components of the current $G_{xx}(\tau)$ and $G_{yy}(\tau)$ decay somewhat quicker than in the zero field case. In the deconfinement phase all the correlators are practically unaffected by the magnetic field.

We now apply the Maximal Entropy Method [240, 244, 245] to extract the spectral functions (9.0.2) from the correlators (9.0.1). Our analysis is similar to that of Refs. [240, 245]. We used the model with the default guess $\bar{m}(w) = \bar{m}_0(b + aw)$ [240]. Some spectral functions at different temperatures and magnetic fields are plotted on Fig. 9.2.

In the confinement phase and in the absence of magnetic field, the spectral function has a distinct peak near $w \approx 1\,\text{GeV}$, which corresponds to the mass of the ρ meson in quenched $SU(2)$ lattice gauge theory [242, 245]. The width of this peak in quenched approximation is a lattice artifact [245], and should decrease for finer and larger lattices. The spectral function in the limit of zero frequency, $\rho_{ij}(0)$, is equal to zero within error range. This indicates that in the absence of an external magnetic field the vacuum of quenched QCD is an insulator, in agreement with the results of [244, 245]. When the external magnetic field is applied, the peak grows and the spectral function becomes nonzero in the limit of zero frequency. For other components of $\rho_{ij}(w)$ nothing changes qualitatively, but the peak which corresponds to the ρ-meson becomes somewhat smaller and shifts slightly to larger w. The conductivity stays equal to zero within the error range. Thus when the external magnetic field is applied to the quenched vacuum of the $SU(2)$ lattice gauge

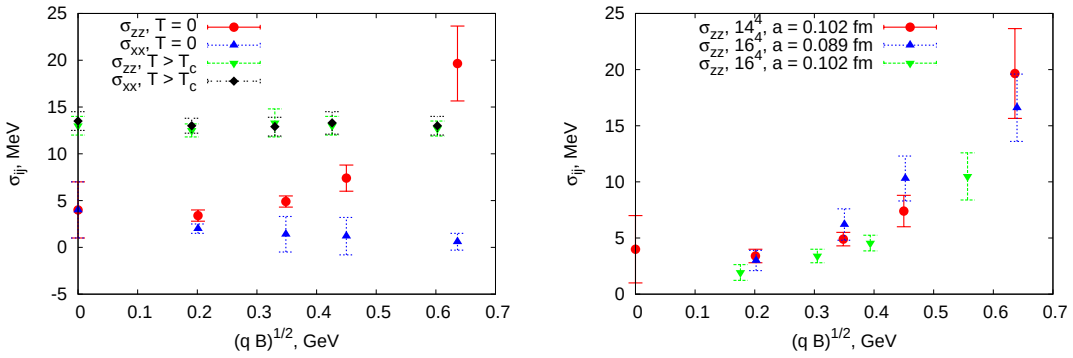

(a) (b)

Figure 9.3: (a) Electric conductivity of quenched QCD as a function of an external magnetic field at different temperatures. The points for σ_{zz} and σ_{xx} at $T>T_c$ coincide within the errors. (b) Electric conductivity in the direction of external magnetic field σ_{zz} for different lattice parameters.

theory, the vacuum acquires nonzero conductivity, but only in the direction of the magnetic field.

In the deconfinement phase at zero magnetic field, the spectral function is nonzero at $w = 0$ and has a smooth peak near $w \approx 2\,\text{GeV}$. Thus quenched $SU(2)$ lattice gauge theory is a conductor above the deconfinement phase transition [240, 244]. Since the shape of the correlator $G_{ij}(\tau)$ is practically unaffected by the magnetic field, the spectral function $\rho_{ij}(w)$ and the conductivity σ_{ij} do not depend on the magnetic field.

The electric conductivity σ_{ij} as a function of external magnetic field is plotted on Fig. 9.3(a) for the confinement and deconfinement phases. In the deconfinement phase the temperature is $T = 350\,\text{MeV}$. The value of the conductivity was extracted from the value of the spectral function at $w = 0$ using (9.0.4). In the confinement phase and at zero magnetic field the conductivity is zero within the error range. As the magnetic field is turned on, the conductivity σ_{zz} in the direction of the magnetic field grows, while all other components of σ_{ij} remain equal to zero within error range. In the deconfinement phase the conductivity is isotropic and is practically independent of the magnetic field. One can not exclude, of course, that there is a weak anisotropy, which cannot be seen at the small number of configurations that we have. It should be also noted that in our simulations the value of conductivity $\sigma = 15 \pm 2\,\text{MeV}$ at $T = 350\,\text{MeV} > T_c$ is still much smaller than the results obtained in [240, 244] in quenched $SU(3)$ lattice gauge theory with light staggered fermions. This difference is likely to be an artifact of a quenched theory, since in this case different probes of the confinement-deconfinement phase transition might give different transition temperatures. In particular, while in quenched $SU(2)$ lattice gauge theory the Polyakov loop goes to zero at $T_c = 313.(3)\,\text{MeV}$ [248], the chiral condensate is not zero above this temperature [249]. The situation might be similar for the insulator-conductor transition, which in the quenched case might be replaced by a soft crossover with much smaller conductivity at $T > T_c$.

The transport coefficients typically have rather strong dependence on lattice parameters. To ensure that the nonzero conductivity is not a finite-volume artifact, we have also performed the simulations at different lattice volumes and lattice spacings (see Table 9.0.1). The values of conductivity σ_{zz} for different lattice parameters are plotted on Fig. 9.3(b). One can see that as we go to finer and larger lattices, the conductivity does not change within statistical errors.

Strictly speaking, the expressions (9.0.1) and (9.0.4) are only valid at finite temperature, while we work with the 14^4 lattices which are symmetric in all space-time directions and hence correspond to zero temperature in the standard lattice lore. However, one can still apply the expressions (9.0.1), (9.0.4) with some small but finite temperature $T = (N_t a)^{-1}$, since real lattices have finite extent

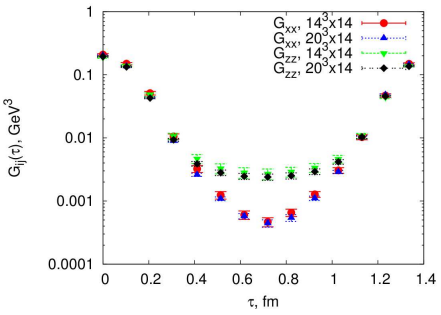

Figure 9.4: The current-current correlators (9.0.1) calculated on $14^3 \times 14$ and $20^3 \times 14$ lattices at magnetic field strength $\sqrt{qB} = 0.45\,\mathrm{GeV}$ with equal values of the lattice spacings.

N_t in time direction. In this case one should make sure that the effects of the finite spatial volume in the nonlocal observables such as the current-current correlator are insignificant. To this end, we plot the correlators (9.0.1) calculated on the $14^3 \times 14$ and $20^3 \times 14$ lattices at magnetic field strength $\sqrt{qB} = 0.45\,\mathrm{GeV}$ in Fig. 9.4. The correlators calculated on different lattices indeed agree within error bars for the currents both parallel and perpendicular to the magnetic field. Thus for the correlators under consideration finite-volume effects seem to be negligible. Correspondingly, the results presented here refer to the case of small but finite temperature (below the deconfinement phase transition) rather than to exactly zero temperature.

We conclude that a strong magnetic field can induce nonzero electric conductivity of the vacuum of quenched non-Abelian lattice gauge theory along the direction of the field, turning it into an anisotropic conductor[1]. This effect may be called "electric rupture facilitated by magnetic field"; it may originate from the interplay of gluon field topology and an increase in the quark zero mode density due to the presence of magnetic field. It can be interesting to investigate whether there is some critical value of the magnetic field at which the conductivity becomes nonzero. Transitions of this type are known in condensed-matter physics [253]. In contrast, in the deconfinement phase the vacuum is an isotropic conductor, and the value of the conductivity is practically independent of the magnetic field. Thus, if a strong magnetic field generates an electric current via the chiral magnetic effect in a CP-odd background, then the sufficiently strong field would guarantee that the charge will propagate through the media due to finite electric conductivity in the both phases.

Finally, let us comment on possible experimental consequences of the phenomenon described above. The expectation value $\langle\, j_k\,(x)\, j_l\,(y)\,\rangle$ is related to the polarization of soft photons and, hence, to the angular distribution of soft photons and dilepton pairs emitted in the process of collision [244, 254, 255]. According to the results presented above, the conductivity tensor can be represented as $\sigma_{ij} \propto B_i B_j$. The dilepton emission rate in the dilepton center of mass frame is [254, 255],

$$\frac{R}{V} \propto \int \frac{d^3p}{E(p)} \left(\vec{B}^2 - \left(\vec{B} \cdot \vec{n} \right)^2 \right) \propto \sin^2(\theta), \tag{9.0.6}$$

where $\vec{n}$ is the unit vector in the direction of the momentum of one of the leptons and θ is the angle between $\vec{n}$ and the direction of the magnetic field. Therefore, there should be more dileptons in the direction perpendicular to the magnetic field, which can be observed as an *additional elliptic flow* for soft photons and leptons[2].

[1] There are also models suggesting superconductivity of the QCD vacuum, if the magnetic field is above some critical value [250–252]

[2] There is a typo regarding the excess of the dileptons in [5, 10] corrected in [11, 256]

Chapter 10

Fractal dimension of the topological charge distribution

Topological charge density is an important characteristic of the QCD vacuum, recently involved in phenomenological studies of many new hypothetical effects [8, 41, 157, 158, 257, 258]. However, the spatial structure of the topological density distribution seems to be not well defined since the relevant properties of the underlying vacuum structure depend on the measuring procedure [259–261]. The classical instanton approach [262] assumes that the nonperturbative physics is governed by the scale of Λ_{QCD}, which means that the dimensionful quantities like volumes occupied by topological fermion modes should depend on Λ_{QCD} but not on the lattice spacing. On the contrary, the lattice measurements demonstrate that these volumes do depend on the spacing (i.e. on the measurement resolution) and shrink to zero in the continuum limit [263–267].

It turns out that the continuum definition of the topological charge density

$$q(x) = \frac{1}{32\pi^2}\epsilon^{\mu\nu\alpha\beta}\,\mathrm{Tr}\left(G^a_{\mu\nu}\,G^a_{\alpha\beta}\right) \tag{10.0.1}$$

cannot be directly applied to the lattice gauge theory, since the discretized version of (10.0.1) is no longer a full derivative. There are two widely used methods to study the topology of gauge fields on the lattice. First, one can apply a smearing procedure, which makes the gauge fields smoother and thus closer to the classical fields. Second, one can rely on the lattice version of the Atyah-Singer theorem and define the total topological charge of a gauge field configuration as the number of zero modes of the overlap Dirac operator [198] on this configuration. The corresponding local density of topological charge can be defined, for example, as follows [196, 268, 269]:

$$q(x) = -\mathrm{Tr}\left[\gamma_5\left(1-\frac{a}{2}D(x,x)\right)\right]\,, \tag{10.0.2}$$

where $D(x,x)$ is the zero-mass Neuberger operator and the trace is taken over spinor and color indices. Another attractive property of this definition is that it allows us to measure a *local* imbalance in the number of left- and right-handed quarks (chirality), which is important for lattice studies of the *local* CP-violation in strong interactions [30, 41–43]. A typical result of the lattice simulation for this quantity (without cooling) is shown in Fig. 1.1(b).

At the moment there are many investigations related to the spatial structure of the topological charge distribution [266, 267, 270–279], which use both of the alternative definitions. The measurements which rely on the cooling procedure mostly suggest an instanton-like picture of the QCD vacuum [280], while the definition (10.0.2) typically shows that the topological charge is localized at low-dimensional objects (defects) [266, 267, 273–279] and has a very-long-range structure of the

β	a [fm]	$L_s^3 \times L_t$	V [fm^4]	# conf
3.200	0.117	$12^3 \times 12$	3.93	50×13
3.295	0.100	$14^3 \times 14$	3.90	50×13
3.332	0.094	$15^3 \times 15$	3.89	50×13
3.365	0.088	$16^3 \times 16$	3.88	50×13
3.425	0.078	$18^3 \times 18$	3.87	50×13

Table 10.0.1: Lattice parameters used in the calculation: couplings β, lattice spacings a, lattice sizes $L_s^3 \times L_t$, physical volume V, and number of gauge field configurations.

distribution [274–279]. At the qualitative level it is known that both definitions yield the topological charge densities which are strongly correlated [270, 281, 282]. For an alternative filtering method based on adjoint fermions see Ref. [283].

The aim of this chapter is to fill the existing gap in the literature and to demonstrate in what way the cooling procedure affects the dimensionality of regions where the topological charge density is localized. We use the definition (10.0.2) based on zero modes of overlap Dirac operator and show that as the gauge field configurations are cooled the dimension of these regions gradually tends to 4, which is the total space dimension. The procedure makes the effective resolution of the measurement lower and thus provides a result close to the instanton picture. We verify our result using several measures of the localization [263, 265, 284].

10.1 Technical details

We work in the quenched $SU(2)$ lattice gauge theory with the tadpole-improved Wilson-Symanzik action [243]. Lattices we used are listed in Table 10.0.1. We also implement the cooling procedure described in Ref. [271] with coefficient $c = 0.5$ for the APE-smearing. For each lattice spacing we consider thirteen different stages of the cooling procedure: 0, 1, 2, 5 - 12, 20 and 50 iterations of the algorithm. For valence quarks we use the Neuberger's overlap Dirac operator [198]. Its eigenvalues and eigenfunctions are given by the following relation

$$D\psi_\lambda = \lambda\,\psi_\lambda\,. \tag{10.1.1}$$

The quantities we measure in the present work are functions of two basic ingredients: the "chiral condensate" computed on a mode with eigenvalue λ,

$$\rho_\lambda(x) = \psi_\lambda^{*\alpha}\,(x)\;\psi_{\lambda\alpha}(x) \tag{10.1.2}$$

and "chirality" computed on a mode with eigenvalue λ [in agreement with the definition (10.0.2)],

$$\rho_\lambda^5(x) = \left(1 - \frac{\lambda}{2}\right) \psi_\lambda^{*\alpha}\,(x)\gamma^5_{\alpha\beta}\,\psi_\lambda^\beta(x)\,. \tag{10.1.3}$$

Here we sum over spinor and (omitted) color indices. The total values of both chiral condensate and chirality are given by an infinite sum over all eigenvalues. Lattice studies [212,285] suggest that the long-distance properties of QCD can be treated with a finite cutoff of the fermionic spectrum. We hereby restrict our consideration to the IR part of the Dirac spectrum consisting of zero modes ($\lambda = 0$) and few low-lying modes ($\lambda \neq 0$).

Inverse participation ratio (IPR) for an arbitrary normalized distribution $\alpha(x)$ is usually defined in the following way

$$\mathrm{IPR} = \left\{ N \sum_x \alpha^2(x) \,\middle|\, \sum_x \alpha(x) = 1 \right\}, \tag{10.1.4}$$

where N is the total number of lattice sites x. From this definition one can clearly see that IPR $= N$ if $\alpha(x)$ is localized on a single site and IPR $= 1$ if $\alpha(x) = const$, i.e. the distribution is unlocalized. In general IPR is equal to the inverse fraction of sites occupied by the support of $\alpha(x)$. Since this fraction of sites can be thought of as a number of four-dimensional lattice hypercubes covering the support, the Hausdorff dimension d of these regions can be extracted from the asymptotic behavior of IPR at small lattice spacings a

$$\mathrm{IPR}(a) = \frac{c}{a^d}\,, \tag{10.1.5}$$

where c is a constant. It is also useful to mention, that in physical units IPR^{-1} is equal to the part of the total volume occupied by the distribution.

In the following sections we will modify the standard definition (10.1.4) to adapt it to our particular cases (i.e. unnormalized or non-normalizable distributions, etc.). The final result will show an equivalence of the chosen definitions.

10.1.1 Ordinary IPR for zero modes.

In this section we compute the inverse participation ratio for the fermionic zero modes according to the one defined in Ref. [265]:

$$\mathrm{IPR}_0 = N \left[\frac{\sum\limits_x \left(\rho_0(x)\right)^2}{\left(\sum\limits_x \rho_0(x)\right)^2} \right]_{\lambda=0}\,, \tag{10.1.6}$$

where the brackets $[...]_{\lambda=0}$ denote an averaging over all zero modes and further averaging over all gauge field configurations. Results are presented in Fig. 10.2.

The left-hand figure shows how the localization depends on the lattice spacing a - the finer the lattice, the larger the IPR. This fits very well to the idea of vanishing total volume occupied by fermionic zero modes in the continuum limit $a \to 0$ (see Ref. [259, 260] for a review). Using the fit (10.1.5) we recover the fractal (Hausdorff) dimension d of the volume. Results for the fits with fixed numbers of cooling steps are presented in the Table 10.1.1. Here, to minimize errors, we also prepared an alternative sample consisting only of those configurations which do not lose all the fermion zero modes during the cooling. We picked then the values with better (and also sufficient) statistical significance.

10.1.2 Chiral IPR for low-lying modes. First definition.

In this section we modify the IPR to measure localization properties of the topological charge distribution. The average chirality $\left[\sum\limits_x \rho^5_\lambda(x)\right]_\lambda$ is zero, therefore we have to use either the absolute value $|\rho^5_\lambda(x)|$ or the square $\left[\rho^5_\lambda(x)\right]^2$. Here we stick to the definition from [284], which in our terms has the following form

$$\mathrm{IPR}^5_0 = N \left[\frac{\sum\limits_x \left(\rho^5_0(x)\right)^2}{\left(\sum\limits_x \rho_0(x)\right)^2} \right]_{\lambda=0}\,. \tag{10.1.7}$$

Number of cooling steps	Fractal dimension	Standard error	P-value
0	2.84 ± 0.44	15%	0.008
1	2.66 ± 0.66	25%	0.027
2	2.49 ± 0.46	18%	0.013
5	2.17 ± 0.49	23%	0.021
6	2.75 ± 0.66	24%	0.025
7	3.17 ± 0.51	16%	0.009
9	3.71 ± 0.34	9%	0.001
12	3.88 ± 0.23	6%	$4 \cdot 10^{-4}$

Table 10.1.1: Fractal dimension of the fermionic zero modes and, equivalently, of the topological charge distribution.

Results are presented in Fig. 10.3. From the plots we conclude that the topological charge distribution behaves similar to the zero modes, tending to occupy a vanishing volume in the continuum limit. We can also compute the chiral IPR for small but nonzero eigenvalues (in our case we pick first 7 eigenvalues, $\lambda \lesssim 200\,\mathrm{MeV}$),

$$\mathrm{IPR}^5_{\lambda\neq 0} = N \left[\frac{\sum\limits_x \left(\rho^5_\lambda(x)\right)^2}{\left(\sum\limits_x \rho_\lambda(x)\right)^2} \right]_{\lambda\neq 0} . \tag{10.1.8}$$

Chiral IPR for these modes is small (Fig. 10.4) and thus the topological charge distribution at this part of the spectrum is delocalized.

10.1.3 Chiral IPR for zero modes. Second definition.

Finally we consider a second definition of the chiral IPR according to [263]:

$$\mathrm{IPR}^5_0 = N \left[\frac{\sum\limits_x \left|\rho^5_0(x)\right|^2}{\left(\sum\limits_x \left|\rho^5_0(x)\right|\right)^2} \right]_{\lambda=0} , \tag{10.1.9}$$

where, as before, $\rho^5_0(x)$ denotes the chirality on a zero mode (10.0.2). Results are presented in Fig. 10.5. As can be seen from Figs. 10.2, 10.3, and 10.5 the IPR for the zero modes and for the topological charge density on these modes are the same up to negligible deviations. Results of the fitting procedure coincide for these three cases and are shown in Table 10.1.1. The coincidence is not accidental, because for the zero modes $[D, \gamma^5] = 0$ and $\gamma^5|\psi_0\rangle = \pm|\psi_0\rangle$. This means that on a given mode $\rho_0(x)$ and $\rho^5_0(x)$ are equal to each other up to a sign.

10.1.4 Fractal dimension. Results and conclusions.

To conclude, we demonstrate that the topological charge is localized on low-dimensional fractal structures, whose fractal (Hausdorff) dimension depends on the number of cooling steps. The

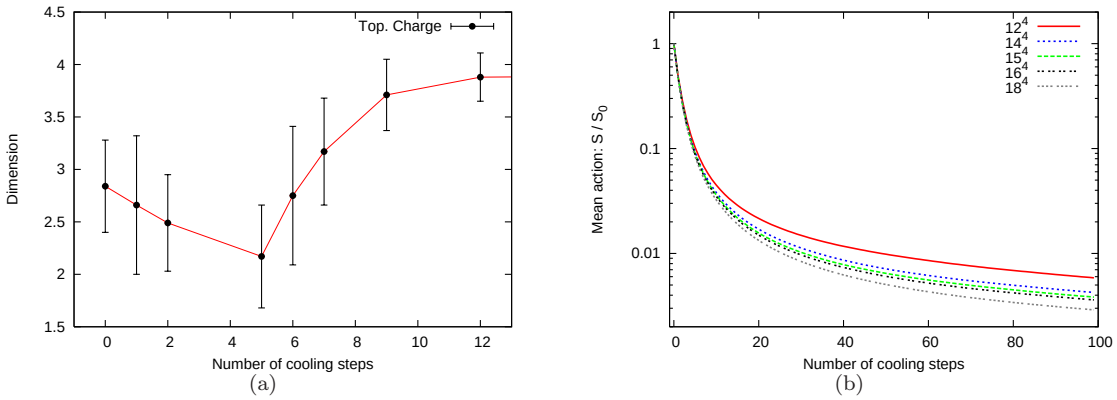

Figure 10.1: (a) Fractal dimensions at various cooling stages. The solid line is shown to guide the eye. (b) Mean action at various cooling stages.

obtained dimension is about $d = 2 \div 3$ for a few ($n < 6$) steps of the cooling, while it grows to $d = 4$ with further iterations (see Fig. 10.1(a)). For a long cooling ($n \gtrsim 20$) the result becomes insignificant, because the procedure leads to a delocalization of the distributions as can be seen in Figs. 10.2–10.5 (otherwise IPR remains consistent with a constant within error bars). We suppose that it can be caused by the annihilation of the instanton/anti-instanton pairs. Indeed, comparing the mean action evolution (Fig. 10.1(b)) with the one from e.g. Ref. [286] we see that the annihilation phase in our case could start already from $n \sim 20$. In Ref. [271], where the same cooling algorithm is used, the annihilation takes place even at a smaller number of steps.

The main conclusions of the chapter are the following:

(1) Fermionic zero modes and chirality are localized on structures with fractal dimension $d = 2 \div 3$, which is an argument in favor of the vortex/domain-wall nature of the localization [287–289].

(2) A long sequence of iterations of the cooling procedure provides a result close to the instanton picture, i.e. destroys the low-dimensional structure of the QCD vacuum.

The low dimensional structure of the vacuum, if true beyond the probe quark limit, may lead to a new phenomenology relevant for the heavy-ion experiments [8, 15, 143, 290]. One of the most promising effects appearing due to the nontrivial topology of the QCD vacuum is the so-called "chiral magnetic effect" (CME) [30, 41–43], which states the generation of an electric current in parallel to an external magnetic field. Topological charge density in this case can be understood as an imbalance in the number of left- and right-handed light quarks induced by a nontrivial gluonic background. At the current level of analytic studies CME is considered as an effect on the background of spatially homogeneous axial fields [30, 41–43], while the lattice simulations predict an irregular structure of the would-be axial field (see Fig. 1.1(b)). This spatial inhomogeneity can be treated within a chiral superfluid model [8], where the chirality is carried by an effective axion-like field. Knowledge of the nature of the topological charge localization can help us to translate lattice Euclidean properties of the chirality to the language of an effective Minkowski field theory [291].

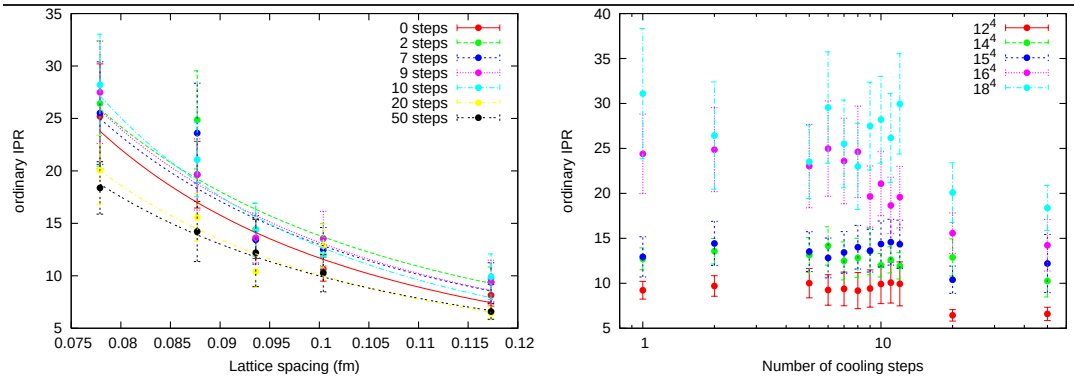

Figure 10.2: Ordinary IPR for zero modes (10.1.6).

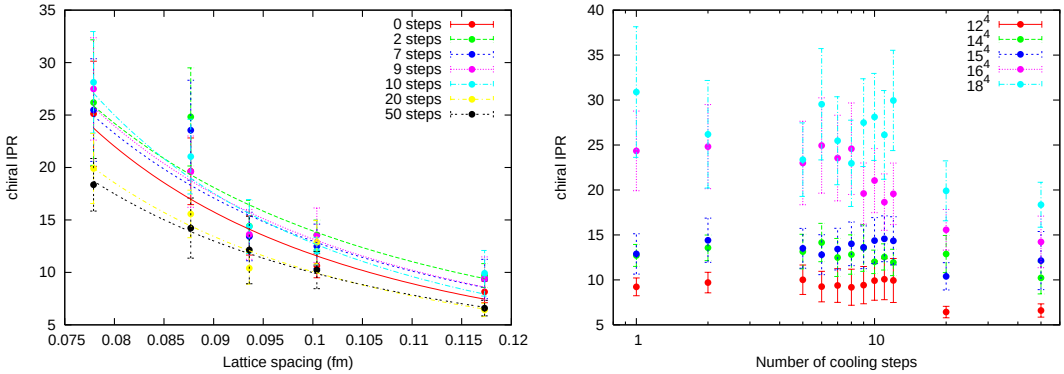

Figure 10.3: Chiral IPR for zero modes. First definition, Eq. (10.1.7).

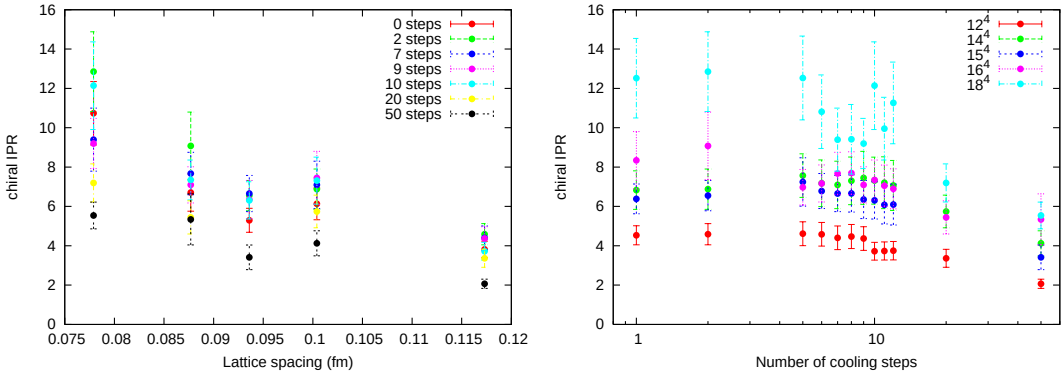

Figure 10.4: Chiral IPR for the lowest nonzero modes. First definition, Eq. (10.1.8).

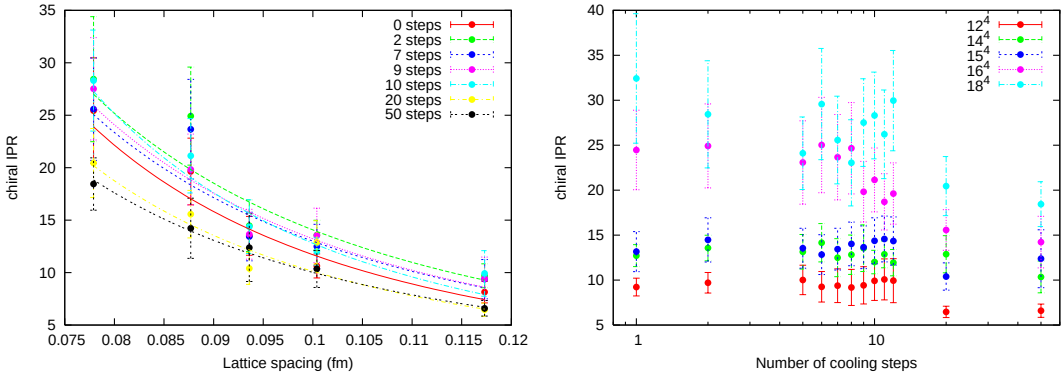

Figure 10.5: Chiral IPR for zero modes. Second definition, Eq. (10.1.9).

Chapter 11

Chiral superfluidity of the quark-gluon plasma

Chiral properties of the strongly coupled quark-gluon plasma (sQGP) have attracted much attention in light of recent measurements performed within the heavy-ion programs at RHIC and LHC. The analysis of charge-dependent azimuthal correlations by STAR [37, 38], PHENIX [39] and ALICE [40] collaborations suggests a possible local $\mathcal{P}$-violation in strong interactions, which manifests itself as an asymmetry in the charged particle production with respect to the reaction plane. One of the most popular theoretical approaches to study the observed phenomena is to seek for new electric currents of a specified direction in the QGP phase (see e.g. [30, 41, 42, 157]). Since the physics of sQGP is essentially nonperturbative, there is a lack of models based on the first-principle calculations, i.e. starting from the QCD Lagrangian. In this chapter we establish such a model for sQGP in the range of temperatures $T_c < T \lesssim 2\,T_c$, i.e. slightly above the deconfinement transition. We choose the range mainly because of two reasons: first, it is estimated to be typical for sQGP at RHIC [292]; and second, we can use hydrodynamic models to describe the system [16, 17, 293–297].

Lattice calculations [243, 249, 298] demonstrate that the Dirac spectrum for massless quarks at these temperatures contains a peak near zero virtuality separated by a gap from the bulk of the spectrum (Fig. 11.1(b) and Fig. 11.2). Therefore, it is natural to introduce a two-component fluid model for the sQGP: one component, carrying chiral properties of the fluid, and the rest, corresponding to the bulk of the spectrum. In our case it turns out that the fluid is described by a system of equations similar to ones of a relativistic superfluid [299, 300]. This fact, of course, does not directly lead to the conventional superfluidity, since the "normal" and "superfluid" components in our case carry different U(1) charges. We also do not assume any hidden symmetry spontaneously broken in the system. Instead, we treat the term "superfluidity" in a phenomenological sense traced back to the Landau's formulation [301], i.e. a combination of two independent (curl-free and "normal") motions of the fluid separated by an energy gap.

Before proceeding with a formal derivation let us provide a few hints supporting the existence of the "superfluid" component. In Refs. [274–279] it has been discovered and confirmed by [266, 267] that topological charge density forms long-range coherent global structures around a locally one-dimensional network of strong fields (so-called "skeleton"). Though the simulations were performed for low temperatures, the skeletons could very well survive slightly above the deconfinement transition, since there is a corresponding long-range order of gluonic fields [302] in the case of nonvanishing topological susceptibility. The extended character of the skeleton can be interpreted as a long-distance propagation of (quasi-) particles, carrying finite chirality and thus forming the chiral "superfluid" component.

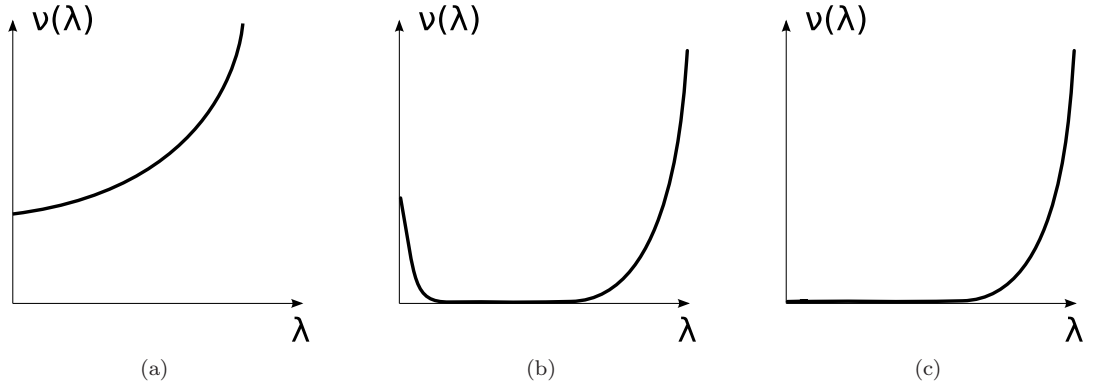

Figure 11.1: Fermionic spectrum of the chirally symmetric Dirac operator in a finite volume and quenched limit for $T < T_c$ (left), $T_c < T \lesssim 2\,T_c$ (center) and $T > 2\,T_c$ (right).

In addition, the lattice data [9, 266, 267, 273–279] suggest that the topological charge density itself (for uncooled configurations) is localized on low-dimensional defects with fractal dimension between 2 and 3, i.e. presumably on (percolating) central vortices (see also [263, 265] for a similar result based on the scalar density distribution and [303, 304] for a localization on vortex intersections). One can demonstrate [265, 304–306] that removal of the central vortices eliminates all zero and chiral near-zero modes from the fermionic spectrum. The converse statement is also true: small eigenvalues can be generated at separate center vortex configurations [305]. It seems natural to consider the vortices as spatially one-dimensional "guides" for light fermions. Since massless fermions propagate in (1+1) dimensions with the same speed (speed of light), we can consider their bilinear combinations as bosonic excitations, even without assuming their interaction with each other. A similar effect of binding for light fermions along 1D defects, without making use of the Goldstone theorem, was considered in [307,308] for non-Abelian fields and in [158,214,215] for a strong external magnetic field.

It is also known that monopole trajectories and central vortices populating QCD vacuum and leading to the confinement at low temperatures [309] become Euclidean-time oriented (static) at high temperatures [310]. Static nature of the vortices makes it possible to continue them to the Minkowski space-time by considering their intersections with planes of constant Euclidean time. These intersections are in general percolating strings, which, according to the polymer representation of the field theory [311–313], can be interpreted as a 3D scalar field with non-vanishing vacuum expectation value. If this field is complex, then its phase can describe a new Goldstone mode in the deconfinement forming the superfluid component of sQGP [291,314]. Taking into account the vortex picture of the topological charge generation [315, 316] it seems interesting to apply the arguments of [291, 314] to the chiral superfluidity (we do not implement it here).

Other arguments in favor of the superfluidity were presented in recent analysis in the framework of stringy models [317–319], where a new formulation of the superfluidity with vanishing chemical potential has been suggested.

In what follows we do not specify the way quarks are bound to each other and form a "superfluid" component, leaving the question open for the further studies (possible examples are given above and in the main text). Regardless of the nature of the "superfluid" component, we obtain the same universal phenomenological predictions, namely the chiral magnetic, chiral electric and dipole wave effects.

11.1 Derivation of the effective Lagrangian

It is known that many of the essential properties of the QCD vacuum (such as the value of the chiral condensate, electric and magnetic characteristics, etc.) can be determined from the IR part of the fermionic spectrum [6, 7, 51, 221, 266, 320, 321]. This makes it possible to introduce a finite cut-off Λ for the fermionic spectrum, without affecting the values of the observables (indeed, our phenomenological results do not depend on Λ, see Section 11.2.2). In this section we perform the bosonization procedure with a finite cut-off [322] for the $\mathrm{SU(N_c)} \times \mathrm{U_{em}(1)}$ theory and derive an effective Lagrangian. This procedure leads to appearance of a dynamical axion-like field $\theta(x)$, which we identify with the propagating chirality (i.e. local difference between numbers of left- and right-handed fermions) in the system.

11.1.1 The functional integral

The gauge fields of the theory are represented by

$$A_\mu = A_\mu^0 T^0 + g G_\mu^a T^a \equiv A_\mu^{\hat{a}} T^{\hat{a}}, \qquad A_{5\mu} = {A_5}_\mu^0 T^0 \,, \tag{11.1.1}$$

where $\left\{ T^a \;\middle|\; a = \overline{1, (N_c^2 - 1)} \right\}$ are the $SU(N_c)$ color matrices normalized by $\mathrm{Tr}(T^a T^b) = \delta^{ab}/2$ and $T^0 = \mathbb{1}$. Here A_μ^0 and ${A_5}_\mu^0$ play a role of Abelian fields, while G_μ^a are gluonic fields. The axial-vector field $A_{5\mu}$ is an auxiliary external field and will be turned off at the end of the procedure. The Euclidean functional integral for Dirac fermions ($N_f = 1$) in external vector $A_\mu(x)$ and axial-vector ${A_5}_\mu(x)$ fields is given by

$$\begin{aligned} Z(A, A_5) &= \int D\bar{\psi} D\psi \, \exp\left\{ - \int_V d^4x \, \bar{\psi} (\not{D} - im) \psi \right\} = \det(\not{D} - im) \,, \\ \not{D} &= -i(\not{\partial} + \not{A} + \gamma_5 \not{A}_5) \,. \end{aligned} \tag{11.1.2}$$

The eigenvectors of $\not{D}$ are defined by[1]

$$\not{D} \psi_n = \lambda_n \psi_n \,. \tag{11.1.3}$$

They form a complete orthonormal basis $\{\psi_n | n \in \mathbb{N}\}$ in the space of square-integrable spinors. According to the general prescription [322–324], we expand ψ and $\bar{\psi}$ into this basis and cut the summation after first N basis vectors:[2]

$$\psi(x) \to \sum_{n=1}^{N} a_n \psi_n(x) \,, \qquad \bar{\psi}(x) \to \sum_{n=1}^{N} \psi_n^\dagger(x) b_n \,. \tag{11.1.4}$$

Then the functional integral (11.1.2) can be rewritten as

$$\begin{aligned} Z_N &= \int \prod_{n=1}^{N} db_n \, da_n \, \exp\left\{ - \sum_{n,k=1}^{N} b_n \langle \psi_n | \not{D} - im | \psi_k \rangle a_k \right\} = \det(\not{D} - im)_N \,, \\ (\not{D} - im)_N &\equiv 1 - P_N + P_N (\not{D} - im) P_N, \qquad P_N \equiv \sum_{n=1}^{N} |\psi_n\rangle\langle\psi_n| \,. \end{aligned} \tag{11.1.5}$$

[1] The Dirac operator $\not{D}$ should be Hermitian, therefore formally the axial field has to be rotated $A_5 \to i A_5$ from the beginning and then rotated back $A_5 \to -i A_5$ in the final result. We stick to conventions of [322] and choose Hermitian gamma-matrices $\gamma^\dagger = \gamma$ and $\gamma_5 \equiv -\gamma_0\gamma_1\gamma_2\gamma_3$, while in Fujikawa's earlier works [323, 324] they are anti-Hermitian.

[2] We do not consider zero-modes, otherwise the functional integral (11.1.2) will vanish in the chiral limit. We are not interested in the *global* topological properties of the system.

From the gauge invariance of $(\not{D} - im)_N$ it follows that the projector P_N commutes with the Dirac operator $\left[\not{D}, P_N\right] = 0$, which will be used in the further calculations.

For the regularization we need to introduce a mass parameter Λ, to be discussed below. It will be defined via $|\lambda_N| < \Lambda < |\lambda_{N+2}|$. The projector P_N can then be replaced by

$$P_\Lambda \equiv \theta\left(1 - \frac{\not{D}^2}{\Lambda^2}\right) = \int\limits_{-\infty}^{+\infty} \frac{d\zeta}{2\pi i(\zeta - i\varepsilon)} \exp\left[i\zeta(1 - \not{D}^2/\Lambda^2)\right] , \tag{11.1.6}$$

where $\theta(x)$ is the Heaviside step function. We also replace all the indices N by Λ.

11.1.2 Vector currents conservation

The functional integral (11.1.2) is invariant under the gauge transformation

$$\left\{\begin{array}{lcl} A_\mu & \to & A_\mu + \partial_\mu\alpha + [A_\mu, \alpha] \,, \\ A_{5\mu} & \to & A_{5\mu} \,, \\ \psi & \to & (1-\alpha)\psi \,, \\ \bar\psi & \to & \bar\psi(1+\alpha) \,, \end{array}\right. \tag{11.1.7}$$

where $\alpha = \alpha^{\hat a} T^{\hat a}$. Therefore,

$$Z_\Lambda(A) = Z_\Lambda(A + \partial\alpha) \simeq Z_\Lambda(A) + \int d^4x \, \frac{\delta Z_\Lambda(A)}{\delta A^{\hat a}_\mu(x)} \cdot \partial_\mu \alpha^{\hat a}(x) \,. \tag{11.1.8}$$

After integration by parts we get

$$\partial_\mu \frac{\delta Z_\Lambda(A)}{\delta A^{\hat a}_\mu(x)} = 0, \tag{11.1.9}$$

which means that the vector currents

$$j^{\mu\,\hat a}_\Lambda(x) \equiv -\frac{1}{Z_\Lambda}\frac{\delta Z_\Lambda(A)}{\delta A^{\hat a}_\mu(x)} = i\,\mathrm{Tr}\left(\gamma^\mu T^{\hat a}\langle x|\frac{P_\Lambda}{(\not{D} - im)_\Lambda}|x\rangle\right) \tag{11.1.10}$$

are conserved. To derive the last expression one can use the equivalences $\exp\mathrm{Tr}\ln(\cdot) = \det(\cdot)$ and

$$\frac{1}{(\not{D} - im)_\Lambda} = 1 - P_\Lambda + \frac{P_\Lambda}{\not{D} - im} \tag{11.1.11}$$

as well as the general identity for projectors

$$PP'P = P(P^2)'P = 2PP'P = 0 \,, \tag{11.1.12}$$

where the prime denotes a derivative of P with respect to an arbitrary parameter.

11.1.3 Anomaly for the axial current

Let us perform the chiral transformation of the functional integral

$$\left\{\begin{array}{lcl} A_\mu & \to & A_\mu \,, \\ {A_5}^0_\mu & \to & {A_5}^0_\mu + \partial_\mu\epsilon \,, \\ \psi & \to & (1+\gamma_5\epsilon)\psi \,, \\ \bar\psi & \to & \bar\psi(1+\gamma_5\epsilon) \,, \end{array}\right. \tag{11.1.13}$$

with $\epsilon = \epsilon^0 T^0$. Then in analogy with the previous section we get

$$Z_\Lambda(A_5) = Z_\Lambda(A_5 + \partial\epsilon, \epsilon) \simeq Z_\Lambda(A_5) + \int d^4x \, \frac{\delta Z_\Lambda(A_5,\epsilon)}{\delta {A_5}^0_\mu(x)} \cdot \partial_\mu \epsilon(x) + \int d^4x \, \frac{\delta Z_\Lambda(A_5,\epsilon)}{\delta\epsilon(x)} \cdot \epsilon(x)\,. \tag{11.1.14}$$

The second term here is due to a nontrivial transformation of the integration measure of the functional integral, and was absent in the case of vector current. The projector P_Λ and combined operator $\not{D} - im$ also transform under the chiral rotations:

$$P_\Lambda \to (1+\gamma_5\epsilon)P_\Lambda(1+\gamma_5\epsilon)\,, \qquad (\not{D} - im) \to (1+\gamma_5\epsilon)(\not{D} - im)(1+\gamma_5\epsilon)\,. \tag{11.1.15}$$

$$\frac{\delta P_\Lambda(x)}{\delta\epsilon(x')} = \{\gamma_5, P_\Lambda(x)\}\,\delta(x-x')\,, \qquad \frac{\delta(\not{D} - im)(x)}{\delta\epsilon(x')} = -2im\gamma_5\delta(x-x')\,. \tag{11.1.16}$$

If we introduce the axial current as

$$j^{5\mu}_\Lambda(x) \equiv -\frac{1}{Z_\Lambda}\frac{\delta Z_\Lambda(A_5)}{\delta {A_5}^0_\mu(x)}\,, \tag{11.1.17}$$

then from (11.1.14) it follows that

$$\partial_\mu j^{5\,\mu}_\Lambda = -\frac{1}{Z_\Lambda}\frac{\delta Z_\Lambda(A_5)}{\delta\epsilon(x)}\,. \tag{11.1.18}$$

The latter is equal to

$$\begin{aligned} -\frac{1}{Z_\Lambda}\frac{\delta Z_\Lambda(A_5)}{\delta\epsilon(x)} &= -\operatorname{Tr}\left[\frac{1}{(\not{D} - im)_\Lambda}\left(-\frac{\delta P_\Lambda}{\delta\epsilon} + 2\frac{\delta P_\Lambda}{\delta\epsilon}(\not{D} - im)P_\Lambda + P_\Lambda\frac{\delta(\not{D} - im)}{\delta\epsilon}P_\Lambda\right)\right] \\ &= 2im\operatorname{Tr}\left(\gamma^5 T^0\langle x|\frac{P_\Lambda}{(\not{D} - im)_\Lambda}|x\rangle\right) + 2\operatorname{Tr}(\gamma^5\langle x|P_\Lambda|x\rangle)\,, \end{aligned} \tag{11.1.19}$$

where we used (11.1.11, 11.1.12, 11.1.15, 11.1.16) and the commutation properties of $\not{D}$. By means of (11.1.6), the second matrix element in this formula can be expressed as

$$\operatorname{Tr}(\gamma^5\langle x|P_\Lambda|x\rangle) = \operatorname{Tr}\left\{\gamma^5\int\frac{d^4k}{(2\pi)^4}\int\limits_{-\infty}^{+\infty}\frac{d\zeta}{2\pi i(\zeta - i\varepsilon)}\mathrm{e}^{-ikx}\mathrm{e}^{i\zeta(1-\not{D}^2/\Lambda^2)}\mathrm{e}^{ikx}\right\} \tag{11.1.20}$$

$$= \operatorname{Tr}\left\{\gamma^5\int\frac{d^4k}{(2\pi)^4}\int\limits_{-\infty}^{+\infty}\frac{d\zeta}{2\pi i(\zeta - i\varepsilon)}\exp\left[i\zeta\left(1 - \frac{k^2}{\Lambda^2} - \frac{2}{\Lambda^2}k^\mu D_\mu(x) - \frac{\not{D}^2}{\Lambda^2}\right)\right]\right\} \tag{11.1.21}$$

$$\begin{aligned} &= -\int\frac{d^4\tilde{k}}{(2\pi)^4}\int\limits_{-\infty}^{+\infty}\frac{\zeta^2 d\zeta}{4\pi i(\zeta - i\varepsilon)}\mathrm{e}^{i\zeta(1-\tilde{k}^2)}\operatorname{Tr}\left[\gamma_5(\not{D}^4 + 4\Lambda^2\,(\tilde{k}^\mu D_\mu)^2 + \Lambda^2\frac{2i}{\zeta}\not{D}^2)\right] \\ &\quad + O\left(\frac{1}{\Lambda^2}\right)\,, \end{aligned} \tag{11.1.22}$$

where $\tilde{k} \equiv k/\Lambda$. Using the algebra of the gamma-matrices, we write

$$\not{D}^2 = -D_V^2 - \frac{1}{2}\gamma^{[\mu}\gamma^{\nu]}A_{\mu\nu} + {A_5}^2_\mu - (\partial^\mu A_{5\mu})\gamma^5 - \gamma^{[\mu}\gamma^{\nu]}\left(D_{V\mu}A_{5\nu} - A_{5\mu}D_{V\nu}\right)\gamma^5\,, \tag{11.1.23}$$

where $D_V \equiv -i(\partial + A)$, and finally obtain

$$\partial_\mu j^{5\mu}_\Lambda = 2m\rho^5_\Lambda + \frac{1}{16\pi^2}\varepsilon^{\mu\nu\lambda\kappa}\mathrm{Tr}\left(A_{\mu\nu}A_{\lambda\kappa} + \frac{1}{3}A_{5\,\mu\nu}A_{5\,\lambda\kappa}\right)$$
$$+ \frac{1}{4\pi^2}\mathrm{Tr}\left(\partial_\mu\partial^\mu\partial^\nu A_{5\nu} + \frac{2}{3}\left\{\left\{\partial^\mu A_5{}^\nu, A_{5\nu}\right\}, A_{5\mu}\right\} + \frac{1}{3}\left\{\partial^\mu A_{5\mu}, A_5{}^\nu A_{5\nu}\right\} + \frac{2}{3}A_5{}^\mu\partial^\nu A_{5\nu}A_{5\mu}\right)$$
$$+ \frac{\Lambda^2}{2\pi^2}\mathrm{Tr}\left(\partial^\mu A_{5\mu}\right) + O\left(\frac{1}{\Lambda^2}\right), \tag{11.1.24}$$

where the chirality ρ^5_Λ is defined by

$$\rho^5_\Lambda \equiv i\,\mathrm{Tr}\left(\gamma^5 T^0\langle x|\frac{P_\Lambda}{(\not{D} - im)_\Lambda}|x\rangle\right) \tag{11.1.25}$$

and the field strengths are

$$A_{\mu\nu} = \partial_\mu A_\nu - \partial_\nu A_\mu + [A_\mu, A_\nu],$$
$$A_{5\,\mu\nu} = \partial_\mu A_{5\nu} - \partial_\nu A_{5\mu} + [A_\mu, A_{5\nu}] - \left[A_\nu, A_{5\mu}\right] = \partial_\mu A_{5\nu} - \partial_\nu A_{5\mu}.$$

The first line in (11.1.24) is the usual chiral anomaly with a mass-dependent term and the topological term. The rest of (11.1.24) can be subtracted away by adding to the Lagrangian the following gauge-invariant term:

$$\Delta\mathcal{L} = \frac{1}{12\pi^2}\mathrm{Tr}\left(3\Lambda^2\left(A_{5\mu}A_5{}^\mu\right) + \frac{1}{2}\left(\partial_\mu A_5{}^\mu\right)^2 - \left(A_{5\mu}A_5{}^\mu\right)^2\right). \tag{11.1.26}$$

11.1.4 Axionic Lagrangian

The external axial-vector field $A_{5\mu}$ should be now switched off, which is equivalent to considering the pure gauge $A^0_{5\mu} = \partial_\mu\theta$, since one can always generate a pseudoscalar field θ by the *local* chiral rotation $\not{A} \to \not{A} + \gamma^5\not{\partial}\theta$. In other words, the quadratic term in (11.1.26) is required by having the chiral transformation consistent with the correct form of the chiral anomaly. In the chiral limit $m \to 0$ the total effective Euclidean Lagrangian is given then by[3]

$$\begin{aligned}\mathcal{L}^{(4)}_E &= \Delta\mathcal{L} + \frac{1}{4}G^{a\mu\nu}G^a_{\mu\nu} + \frac{1}{4}F^{\mu\nu}F_{\mu\nu} - j^{\hat{a}\,\mu}A^{\hat{a}}_\mu - j^{5\mu}A^0_{5\mu}\\ &= \Delta\mathcal{L} + \frac{1}{4}G^{a\mu\nu}G^a_{\mu\nu} + \frac{1}{4}F^{\mu\nu}F_{\mu\nu} - j^{0\mu}A^0_\mu - gj^{a\,\mu}G^a_\mu - j^{5\mu}_\Lambda\partial_\mu\theta\\ &\sim \frac{1}{4}G^{a\mu\nu}G^a_{\mu\nu} + \frac{1}{4}F^{\mu\nu}F_{\mu\nu} - j^{0\mu}A^0_\mu - gj^{a\,\mu}G^a_\mu\\ &\quad + \frac{\Lambda^2 N_c}{4\pi^2}\partial^\mu\theta\partial_\mu\theta + \frac{g^2}{16\pi^2}\theta G^{a\mu\nu}\widetilde{G}^a_{\mu\nu} + \frac{N_c}{8\pi^2}\theta F^{\mu\nu}\widetilde{F}_{\mu\nu}\\ &\quad + \frac{N_c}{24\pi^2}\theta\Box^2\theta - \frac{N_c}{12\pi^2}\left(\partial^\mu\theta\partial_\mu\theta\right)^2,\end{aligned} \tag{11.1.27}$$

where we used the anomaly expression (11.1.24) and integrated by parts. Kinetic terms for the electromagnetic and gluonic fields could be introduced already in (11.1.2) and do not affect the derivation. As we see, the kinetic term for θ even being absent in (11.1.2) is generated dynamically[4],

[3] Currents $j^{\hat{a}\mu}$ can be sourced by fermions from the scales above Λ.

[4] The θ-field does not appear in the integration measure and hence should be treated as a classical low-energy excitation. It is possible due to the fact that the loop corrections by θ-fields are finite in 4D and depend on the powers of external momenta divided by Λ, i.e. such loop amplitudes are suppressed by powers of Λ.

see also [325,326] for similar examples. Appearance of the quartic terms in (11.1.27) is due to the fact that the bosonization procedure in 4D is not exact. One can in principle derive an infinite number of higher-order terms suppressed by powers of Λ, but we drop them for simplicity. If we drop quartic terms and replace conventions $A^0_\mu \to A_\mu$, $j^{0\mu} \to j^\mu$, then the effective Lagrangian is reduced to

$$\begin{aligned}\mathcal{L}_E^{(2)} =& \frac{1}{4}G^{a\mu\nu}G^a_{\mu\nu} + \frac{1}{4}F^{\mu\nu}F_{\mu\nu} - j^\mu A_\mu - g j^{a\,\mu} G^a_\mu \\ &+ \frac{\Lambda^2 N_c}{4\pi^2}\partial^\mu\theta\partial_\mu\theta \; + \frac{g^2}{16\pi^2}\theta G^{a\mu\nu}\widetilde{G}^a_{\mu\nu} + \frac{N_c}{8\pi^2}\theta F^{\mu\nu}\widetilde{F}_{\mu\nu}\,. \end{aligned} \tag{11.1.28}$$

This Lagrangian describes a generalization of the axion electrodynamics [327], where the new terms are due to gluonic fields. It seems interesting that the axionic field $\theta(x,t)$ appears within QCD coupled to QED, *without* any further assumptions as e.g. the Peccei-Quinn mechanism [328]. Similarly to the 'true' axion, $\theta(x,t)$ is a propagating dynamical field. However, the value of the decay constant $f = \dfrac{2\Lambda}{\pi}\sqrt{N_c}$ turns out to be of order of scales appearing in QCD (see below), while in cosmological scenarios this value is usually around $10^9 - 10^{12}$ GeV. The formal similarity of (11.1.28) to the axion Lagrangian allows us to derive an explicit expression for the mass of $\theta(x,t)$ [56,329,330],

$$m_\theta^2 f^2 = \chi(T)\,, \tag{11.1.29}$$

where $\chi = \lim_{V\to\infty}\frac{\langle Q^2\rangle}{V}$ is the topological susceptibility related to fluctuations of the topological charge Q. Lattice simulations demonstrate that χ goes (almost) to zero at temperatures above the deconfinement transition [243,298,331–333], this behaviour is also confirmed within the interacting instanton liquid model [330]. Meson masses in the deconfinement interpolate between their values at $T \lesssim T_c$ and approximately twice the lowest quark Matsubara frequency (i.e. $2\pi T$) [334]. These two facts allow us to consider the axion-like field $\theta(x,t)$ as a nearly-massless field, an essential requirement for a superfluid mode.

Instead of considering θ as a real particle we rather tend to interpret it as a collective excitation (quasi-particle) of the medium in the nonperturbative regime of QCD (e.g. combinations of chiral quarks). As will be shown in next sections, the excitation carries chirality and can be considered as a 4D generalization of the Chiral Magnetic Wave [158]. These excitations can also be exactly massless (compare with phonons or sound waves) and, at the same time, not necessarily consisting of massless quantum particles, appearing as Goldstone bosons of some broken (e.g. Peccei-Quinn-like) symmetry[5]. A straightforward derivation of this collective solution made out of quarks and gluons is not worked out at the moment. However, there are some evidences that it could exist, see e.g. comments on binary bound states in sQGP [336,337], lattice results on a screened attractive force in the color-singlet channel [338] and ideas mentioned already in the Introduction.

11.1.5 Interpretation of Λ

The scale Λ can be studied by considering $N_f = N_c = 1$ in the limit of a constant background $\mu = const$, $\mu_5 = const$ and negligible anomaly (i.e. slow varying $\theta = i\mu_5 t_E$). In this case, keeping also the quartic terms in (11.1.27) for generality, we get

$$\rho_5 = -\lim_{t_E\to 0}\frac{\delta\mathcal{L}_E^{(4)}}{\delta\mu_5} = \frac{1}{2}\left(\frac{\Lambda}{\pi}\right)^2\mu_5 + \frac{1}{3\pi^2}\mu_5^3\,. \tag{11.1.30}$$

In other words, the value of Λ can be read off from the dependence of chirality ρ_5 on the chiral chemical potential μ_5. We consider here three existing examples one can find in the literature.

[5]Even if we assume that $\mathrm{U(1)_A}$ symmetry is broken spontaneously, as suggested in [335], then the bosonization procedure does not describe η', since it is a spin-0 particle, which can not carry chirality as θ does.

(1) At high temperatures, neglecting effects of gluons and assuming equilibrium, one can define the thermodynamic grand potential as [41]

$$\Omega = \sum_{s=\pm} \int \frac{d^3p}{(2\pi)^3} \left[\omega_{p,s} + T \sum_{\pm} \log(1 + e^{-\frac{\omega_{p,s} \pm \mu}{T}}) \right] , \tag{11.1.31}$$

where $\omega_{p,s}^2 = (p + s\mu_5)^2 + m^2$ and one also assumes an approximate conservation of the axial charge. Differentiating the grand potential with respect to μ_5 and taking the massless limit one obtains [41]

$$\rho_5 = \frac{1}{3} \left(T^2 + \frac{\mu^2}{\pi^2} \right) \mu_5 + \frac{1}{3\pi^2} \mu_5^3 . \tag{11.1.32}$$

Comparing (11.1.32) with (11.1.30) we conclude

$$\Lambda = \pi \sqrt{\frac{2}{3}} \sqrt{T^2 + \frac{\mu^2}{\pi^2}} \qquad \text{(free quarks)} . \tag{11.1.33}$$

In [30,41] this scale is compared with the inverse radius of a typical sphaleron at given temperature. Notice, that in the high temperature limit $T \gg \mu$ and $T \gg \mu_5$ we get simplifications $\Lambda \propto T$ and $\rho_5 \propto \Lambda^2 \mu_5 \propto T^2 \mu_5$.

(2) In case of a strong external magnetic field ($eB > \mu_5^2/2$) one can construct the grand potential for fermions on the lowest Landau level [41]

$$\Omega = \frac{eB}{4\pi^2} \int_{-\infty}^{\infty} d^3p_{||} \left[\omega_p + T \sum_{\pm} \log(1 + e^{-\frac{\omega_p \pm \mu}{T}}) \right] , \tag{11.1.34}$$

where $\omega_p^2 = (p_{||} + \mu_5)^2 + m^2$ and $p_{||}$ denotes a component of momentum parallel to the magnetic field. This gives us $\rho_5 = \dfrac{eB}{2\pi^2} \mu_5$ and hence

$$\Lambda = 2\sqrt{eB} \qquad \text{(free quarks and strong } B) . \tag{11.1.35}$$

Upon the redefinition $\theta \to \dfrac{\pi}{\sqrt{2N_c eB}} \theta$ the kinetic term for θ in the effective Lagrangian (11.1.27) takes a canonical form $\dfrac{1}{2}(\partial_\mu \theta)^2$, while the quartic terms are suppressed by factors $1/B$ and $1/B^2$, respectively. Therefore, the bosonization procedure becomes exact in the limit $B \to \infty$ as in [158].

(3) To include effects of gluons one needs to perform a lattice calculation with finite μ_5, which has been done in [53,54]. Slope of the curve $\rho_5 = \rho_5(\mu_5)$ obtained in the paper[6] is approximately one (in lattice units), which being translated to physical units and compared with (11.1.30) gives us

$$\Lambda \simeq 3\,\text{GeV} \qquad \text{(dynamical lattice fermions, } N_f = 2, N_c = 3) . \tag{11.1.36}$$

Appearance of this scale (much larger than Λ_{QCD}) is not surprising, see e.g. [339, 340].

It is worth to mention that all three predictions even if being affected by either rough initial assumptions or lattice artifacts, still provide a *finite* and reasonable value of Λ.

[6] There is no *a priori* introduced UV-cutoff in the paper since the inversion of the Dirac operator is done by means of the BiCGstab solver

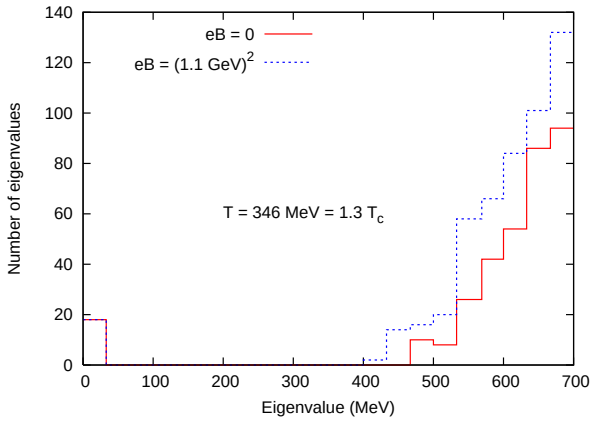

Figure 11.2: Typical fermionic spectrum in the deconfined phase as seen by a SU(3) quenched lattice simulation with tadpole-improved Lüscher-Weisz action and overlap fermions ($\beta = 8.45$, $a = 0.095\,\mathrm{fm}$, $V = 16^3 \times 6$, $N_f = 1, T_c \sim 260\,\mathrm{MeV}$).

11.1.6 Fermionic spectrum and chirality

The Dirac spectrum for massless fermions is schematically shown in Fig. 11.1.[7] Lattice studies can be found in [243,249,265,284,298]. Below the critical temperature T_c the spectrum is a continuously growing function in λ.

In contrast, at $T_c < T \lesssim 2\,T_c$ the spectrum consists of three parts: exact zero modes (and near-zero modes), followed by a gap for the low-lying modes and a continuous spectrum starting from a finite λ_B. Presence of the near-zero peak can be interpreted as a manifestation of a (small) remaining chiral condensate [249, 298], which is, however, not yet rigorously proven. Both the chiral condensate and topological susceptibility $\chi(T)$ are defined from the near-zero modes, since the exact zero modes do not survive in the thermodynamic limit [320, 332, 333]. It is important, that $\chi(T)$ is small enough (to keep m_θ small), but still not zero (otherwise θ itself does not exist). This forces us to choose the window of temperatures $T_c < T \lesssim 2\,T_c$. At higher temperatures $T \gtrsim 2\,T_c$ the peak disappears completely and all the correlations between quarks supposed to be washed out by thermal effects. The gap width seems to be temperature dependent and grows with the temperature [243]. The right bound λ_B is natural to identify with an effective quark mass, since on the corresponding fermionic mode

$$\lambda_B^2 \psi_B = \not{D}^2 \psi_B = \not{p}^2 \psi_B = m_{eff}^2 \psi_B \,. \tag{11.1.37}$$

A very strong external magnetic field can slightly shift the right bound of the spectrum to the left[8] (see Fig. 11.2), but for magnetic field strengths occurring in heavy-ion collisions [30] the principal shape of the spectrum remains the same.

[7] We show here only the non-negative part of the spectrum. In the chiral limit it is symmetric with respect to the reflection $\lambda \to -\lambda$.

[8] We are grateful to Victor Braguta for making this observation from our data

Let us demonstrate that chirality is determined by the first part of the spectrum.

$$\begin{aligned}\rho^5_\Lambda &= i\,\mathrm{Tr}\left(\gamma^5\langle x|\frac{P_\Lambda}{(\not{D}-im)_\Lambda}|x\rangle\right) = i\sum_{0<|\lambda|<\Lambda}\frac{{\psi_\lambda}^\dagger\gamma^5\psi_\lambda}{\lambda-im}\\ &= i\sum_{0<\lambda<\Lambda}\frac{{\psi_\lambda}^\dagger\gamma^5\psi_\lambda}{\lambda-im}+i\sum_{0<\lambda<\Lambda}\frac{{\psi_\lambda}^\dagger\gamma^5\gamma^5\gamma^5\psi_\lambda}{-\lambda-im}=-2m\sum_{0<\lambda<\Lambda}\frac{{\psi_\lambda}^\dagger\gamma^5\psi_\lambda}{\lambda^2+m^2}\\ &= -\int_0^\Lambda d\lambda\,\nu(\lambda)\frac{2m}{\lambda^2+m^2}{\psi_\lambda}^\dagger\gamma^5\psi_\lambda\,, \end{aligned}\tag{11.1.38}$$

where $\nu(\lambda)$ denotes the spectral density for an eigenvalue λ. Here, as before, we dropped the exact zero-modes. Then, using the identity

$$\lim_{m\to 0}\frac{m}{\lambda^2+m^2}=\pi\delta(\lambda)\tag{11.1.39}$$

we find the following expression for the chirality

$$\lim_{m\to 0}\rho^5_\Lambda=-2\pi\int_0^\Lambda d\lambda\,\nu(\lambda)\delta(\lambda){\psi_\lambda}^\dagger\gamma^5\psi_\lambda=-\pi\lim_{\lambda\to 0}\nu(\lambda)\,{\psi_\lambda}^\dagger\gamma^5\psi_\lambda\,.\tag{11.1.40}$$

From this expression we see that the chirality can be determined exclusively from the near-zero fermionic modes. It is suggested and tested on a lattice [298] that this part of the spectrum is originated from the zero modes of separate topological defects populating the vacuum, because interactions between the original zero modes break their degeneracy. So the exclusion of the *exact* zero modes from our analysis does not affect much the main results (for additional arguments see also [51]).

11.2 Quark-gluon plasma as a two-component fluid

We now consider Minkowski version of the effective Lagrangian (11.1.28) for the quark-gluon plasma with one quark flavor[9],

$$\begin{aligned}\mathcal{L}^{(2)} =& -\frac{1}{4}G^{a\mu\nu}G^a_{\mu\nu}-\frac{1}{4}F^{\mu\nu}F_{\mu\nu}-j^\mu A_\mu-gj^{a\,\mu}G^a_\mu\\ &-\frac{f^2}{2}\partial^\mu\theta\partial_\mu\theta\;+\frac{C_g}{4}\theta G^{a\mu\nu}\widetilde{G}^a_{\mu\nu}+\frac{C_\gamma}{4}\theta F^{\mu\nu}\widetilde{F}_{\mu\nu}\,,\end{aligned}\tag{11.2.1}$$

where, again, the decay constant is defined by $f=\dfrac{2\Lambda}{\pi}\sqrt{N_c}$ and the anomaly coefficients are given by $C_\gamma=\dfrac{N_c}{2\pi^2}$ and $C_g=\dfrac{g^2}{4\pi^2}$.

Varying the Lagrangian (11.2.1) with respect to θ and vector fields A_μ and G^a_μ, we obtain the following equations of motion:

$$\partial^\mu\partial_\mu\theta=-\frac{C_\gamma}{4f^2}F^{\mu\nu}\widetilde{F}_{\mu\nu}-\frac{C_g}{4f^2}G^{\mu\nu a}\widetilde{G}^a_{\mu\nu}\,,\tag{11.2.2}$$

$$\partial_\mu F^{\mu\nu}=-j^\nu+C_\gamma(\partial_\kappa\theta)\tilde{F}^{\kappa\nu}\,,\tag{11.2.3}$$

$$\partial_\mu G^{\mu\nu a}+gf^{abc}G^b_\mu G^{\mu\nu c}=-gj^{\nu a}+C_g(\partial_\kappa\theta)\widetilde{G}^{\kappa\nu a}\,,\tag{11.2.4}$$

[9]The metric we use has the signature $(-+++)$

where f^{abc} are the structure constants of $SU(N)$. Bianchi identities are given by

$$\partial_\mu \widetilde{F}^{\mu\nu} = 0\,, \tag{11.2.5}$$

$$\partial_\mu \widetilde{G}^{\mu\nu a} + g f^{abc} G^b_\mu \widetilde{G}^{\mu\nu c} = 0\,. \tag{11.2.6}$$

Interestingly, $\theta(\vec{x},t)$ obeys a wave equation which is sourced by the $U(1)_A$ chiral anomaly. This makes it a four-dimensional generalization of the so-called "Chiral Magnetic Wave" which has been recently proposed in [158].

11.2.1 Hydrodynamic equations

The hydrodynamic equations may now be derived from the effective Lagrangian (11.2.1) and the corresponding equations of motion (11.2.2)–(11.2.6). Taking the divergence of (11.2.3) and using the Bianchi identity (11.2.5), we obtain the conservation law for the electromagnetic current, $\partial_\nu j^\nu = 0$, provided that the topology of the θ-field is non-singular with[10]

$$[\partial_\mu, \partial_\nu]\theta = 0\,. \tag{11.2.7}$$

Varying $\mathcal{L}^{(2)}$ with respect to the axial-vector $-\partial_\mu\theta$, we obtain the axial current

$$j^\mu_5 = f^2 \partial^\mu \theta\,. \tag{11.2.8}$$

This current satisfies the anomaly equation

$$\partial_\mu j^\mu_5 = -\frac{C_\gamma}{4} F^{\mu\nu}\widetilde{F}_{\mu\nu} - \frac{C_g}{4} G^{\mu\nu a}\widetilde{G}^a_{\mu\nu}\,, \tag{11.2.9}$$

as can be seen by substituting the equations of motion (11.2.2) into the divergence of (11.2.8). Notice that $\mathrm{U(1)_A}$ is still broken in the deconfinement [332, 333].

The total energy-momentum tensor is a sum of both electromagnetic $\Theta^{\mu\nu}_\gamma$ and gluonic ones $\Theta^{\mu\nu}_{\mathrm{g}}$ and the stress-energy tensor of the fluid $T^{\mu\nu}$. The energy-momentum tensors of the free electromagnetic and gluonic fields are given by

$$\Theta^{\mu\nu}_\gamma = F^{\mu\lambda}F^\nu{}_\lambda - \frac{1}{4} g^{\mu\nu} F_{\alpha\beta}F^{\alpha\beta}\,, \tag{11.2.10}$$

$$\Theta^{\mu\nu}_{\mathrm{g}} = G^{\mu\lambda a}G^{\nu}_{\lambda\, a} - \frac{1}{4} g^{\mu\nu} G_{\alpha\beta}{}^a G^{\alpha\beta a}\,. \tag{11.2.11}$$

Their divergencies can be found by means of the equations of motion (11.2.3, 11.2.4),

$$\partial_\mu \Theta^{\mu\nu}_\gamma = -F^{\nu\lambda} j_\lambda - C_\gamma F^{\nu\lambda}\widetilde{F}_{\lambda\kappa}\partial^\kappa\theta\,, \tag{11.2.12}$$

$$\partial_\mu \Theta^{\mu\nu}_{\mathrm{g}} = -g G^{\nu\lambda a} j^a_\lambda - C_g G^{\nu\lambda a}\widetilde{G}_{\lambda\kappa}{}^a \partial^\kappa\theta\,. \tag{11.2.13}$$

Substituting this into the conservation law of the total energy-momentum,

$$\partial_\mu (T^{\mu\nu} + \Theta^{\mu\nu}_\gamma + \Theta^{\mu\nu}_{\mathrm{g}}) = 0\,, \tag{11.2.14}$$

we get (see also [343])

$$\partial_\mu T^{\mu\nu} = F^{\nu\lambda} j_\lambda + g G^{\nu\lambda a} j^a_\lambda + C_\gamma F^{\nu\lambda}\widetilde{F}_{\lambda\kappa}\partial^\kappa\theta + C_g G^{\nu\lambda a}\widetilde{G}^a_{\lambda\kappa}\partial^\kappa\theta\,. \tag{11.2.15}$$

[10] delta-function on the r.h.s. of (11.2.7) would generate an axionic string [341]. For relevant phenomenological consequences see [160, 342].

The first two terms on the right hand side are the standard terms for a work done by external fields. The last two terms is a work done by a Witten-like current [344]. Finally, keeping that $\rho_5 \equiv j_5^0 = f^2\partial^0\theta$, we obtain an expression for the axial chemical potential,

$$\mu_5 = \frac{\delta\mathcal{L}^{(2)}}{\delta\rho_5} = -\partial_0\theta\,. \tag{11.2.16}$$

When boosted this turns into the Josephson-type equation $\mu_5 = -u^\mu\partial_\mu\theta$, where u^μ will be chosen later as the velocity of the "normal" component, normalized by the condition $u_\mu u^\mu = -1$. We also should assume, that $\partial_t\theta$ is slow varying in time, i.e. $\partial_\mu\theta \sim O(p^0)$, so the changes in chiral (axial) charge are small at the scale of QGP lifetime [142, 345], otherwise the chiral chemical potential is not well-defined. Hydrodynamic and constitutive equations are then of order $O(p^2)$ and $O(p^1)$, respectively.

In summary, the system of hydrodynamic equations is given now by

$$\partial_\mu T^{\mu\nu} = F^{\nu\lambda}(j_\lambda + C_\gamma\widetilde{F}_{\lambda\kappa}\partial^\kappa\theta) + G^{\nu\lambda a}(g j^a_\lambda + C_g\widetilde{G}_{\lambda\kappa}{}^a\partial^\kappa\theta)\,, \tag{11.2.17}$$

$$\partial_\mu j_5^\mu = -\frac{C_\gamma}{4}F^{\mu\nu}\widetilde{F}_{\mu\nu} - \frac{C_g}{4}G^{\mu\nu\,a}\widetilde{G}^a_{\mu\nu}\,, \tag{11.2.18}$$

$$\partial_\mu j^\mu = \partial_\mu j^{\mu a} = 0\,, \tag{11.2.19}$$

$$u^\mu\partial_\mu\theta + \mu_5 = 0\,, \tag{11.2.20}$$

where the last one is the Josephson-type equation. Corresponding constitutive relations in gradient expansion, satisfying (11.2.2) and (11.2.17-11.2.18), can be represented by

$$T^{\mu\nu} = (\epsilon + P)\,u^\mu u^\nu + P g^{\mu\nu} + f^2\partial^\mu\theta\partial^\nu\theta + \tau^{\mu\nu}\,, \tag{11.2.21}$$

$$j^\mu = \rho u^\mu + \nu^\mu\,, \tag{11.2.22}$$

$$j^{\mu a} = \rho^a u^\mu + \nu^{\mu a}\,, \tag{11.2.23}$$

$$j_5^\mu = f^2\partial^\mu\theta + \nu_5^\mu\,, \tag{11.2.24}$$

where ϵ, P, ρ, ρ^a are the energy density, pressure, electric charge density and color charge density, respectively. Terms $\tau^{\mu\nu}$, ν^μ, $\nu^{\mu a}$ and ν_5^μ denote higher-order gradient corrections and obey the Landau conditions

$$u_\mu\tau^{\mu\nu} = 0\,, \qquad u_\mu\nu^\mu = 0\,, \qquad u_\mu\nu^{\mu a} = 0\,, \qquad u_\mu\nu_5^\mu = 0\,. \tag{11.2.25}$$

The stress-energy tensor $T^{\mu\nu}$ consists of two parts, an ordinary fluid component and a pseudoscalar "superfluid" component. This modifies the Gibbs relation

$$dP = sdT + \rho d\mu - f^2 d\left[\frac{1}{2}\partial^\mu\theta\,\partial_\mu\theta\right], \tag{11.2.26}$$

where s is the entropy density. Being additionally supported by the results of the Section 11.1.6, we can describe the fluid content as a mixture of two components, originated from different parts of the fermionic spectrum,

(1) Zero and near-zero fermionic modes, which are involved into a potential (curl-free) motion of the chirality described by $j_\mu^5 = f^2\,\partial_\mu\theta = \rho_5 u_{S\mu}$, where $u_{S\mu} \equiv \mu_5\,\partial_\mu\theta$ is the "superfluid" velocity.

(2) The rest forming an "axially-neutral" component described by an electric $j_\mu = \rho u_\mu$ and color $j^a_\mu = \rho^a u_\mu$ currents and separated from the curl-free component by a finite gap.

There are numerous studies (e.g. [30, 132, 346]) suggesting generation of a finite chirality in the processes of heavy-ion collisions, so we can assume $\langle\rho_5\rangle = f^2\langle\mu_5\rangle \neq 0$ within an event. Such kind of initial conditions is not captured by lattice simulations ($\langle\rho_5\rangle = 0$ after averaging over gauge configurations [6, 7, 51]), unless the finite $\langle\mu_5\rangle$ is introduced *ad hoc* [53, 54].

11.2.2 Phenomenological output, possible tests of the model

Electric and magnetic fields in the fluid rest frame are defined as

$$E^\mu = F^{\mu\nu}u_\nu, \qquad B^\mu = \tilde{F}^{\mu\nu}u_\nu \equiv \frac{1}{2}\epsilon^{\mu\nu\alpha\beta}u_\nu F_{\alpha\beta}. \tag{11.2.27}$$

One can also rewrite these definitions in the following way

$$F_{\mu\nu} = \epsilon_{\mu\nu\alpha\beta}u^\alpha B^\beta + u_\mu E_\nu - u_\nu E_\mu, \tag{11.2.28}$$

$$\tilde{F}_{\mu\nu} = \epsilon_{\mu\nu\alpha\beta}u^\alpha E^\beta + u_\mu B_\nu - u_\nu B_\mu\,, \tag{11.2.29}$$

which we will use later.

The second term in first brackets (11.2.17) or equivalently the second term on r.h.s. of (11.2.3) has an interesting phenomenological interpretation as an additional electric current, induced by θ-field, i.e. associated with the "superfluid" component. This current is conserved due to the Bianchi identity and vanishes in absence of either external electromagnetic fields or θ. Let us split this term in three pieces using (11.2.29):

$$\begin{aligned} j^S_\lambda &\equiv C_\gamma \widetilde{F}_{\lambda\kappa}\partial^\kappa\theta = C_\gamma\partial^\kappa\theta\left(u_\kappa B_\lambda + \epsilon_{\kappa\lambda\alpha\beta}u^\alpha E^\beta - u_\lambda B_\kappa\right) \\ &= -C_\gamma\mu_5 B_\lambda + C_\gamma\epsilon_{\lambda\alpha\kappa\beta}u^\alpha\partial^\kappa\theta E^\beta - C_\gamma u_\lambda(\partial\theta\cdot B)\,. \end{aligned} \tag{11.2.30}$$

The first term in the sum is nothing but the Chiral Magnetic Effect (CME) [41], i.e. generation of the electric current along the magnetic field. The second term is analogous to the Chiral Electric Effect (CEE) [258], i.e. generation of the electric current perpendicular to applied electric field and to both (normal and superfluid) four-velocities. The third term is a dynamical realization of the domain wall polarization [42, 43] or simply the fact that the "would-be" axions acquire an electric dipole moment in a magnetic field [327]. Keeping in mind a wave-like profile of the θ-field we could call this effect the "Chiral Dipole Wave" (CDW). First term contains μ_5 which is in our case *derived* within QCD in contrary to other CME models. Last two terms are specific for the two-component fluid model and can be considered as a possible experimental test of the model. A concrete quantitative prediction and comparison to the experimental data are beyond of the scope of this chapter and will be presented in a future publication. Some preliminary experimental ideas are presented in Section 11.2.4.

The same analysis can be applied to the color current

$$j^{S\,a}_\lambda \equiv \frac{C_g}{g}\widetilde{G}_{\lambda\kappa}{}^a\partial^\kappa\theta\,, \tag{11.2.31}$$

which is the second term on the r.h.s. of (11.2.4). The corresponding effects can be called "Color CME", "Color CEE" and "Color CDW", respectively. We are not focusing on these effects, since the color currents cannot be observed directly. It is also important to mention that both currents (11.2.30, 11.2.31) do not depend on the UV cutoff Λ introduced in the preceding sections.

11.2.3 Change in entropy and higher order gradient corrections

In previous sections we kept higher-order corrections $\tau^{\mu\nu}$, ν^μ, $\nu^{\mu a}$, ν^μ_5 undetermined. These corrections incorporate possible dissipative effects (in presence of e.g. viscosity or electrical resistivity) and can be found from the constraint $\partial_\mu s^\mu \geq 0$ on the entropy current s^μ [130]. A priori it is not obvious whether they can interfere with the result (11.2.30) or not. Indeed, within the ordinary hydrodynamics the chiral magnetic effect can be found as a part of the ν^μ term [3, 4, 140]. In this section we show that there are *no* higher order corrections to the electric current j_μ arising in our

case and affecting the phenomenological results of Section 11.2.2. Following [140], we transform the quantity

$$I \equiv u_\nu \partial_\mu T^{\mu\nu} + \mu \partial_\mu j^\mu + \mu_5 \partial_\mu j_5^\mu \tag{11.2.32}$$

using hydrodynamic and constitutive equations and equate both resulting expressions.

Constitutive equations

Using the second law of thermodynamics $\epsilon + P = Ts + \mu\rho$ and (11.2.21)-(11.2.24), we can rewrite this quantity as

$$\begin{aligned} I = & u_\nu \partial_\mu \left((Ts + \mu\rho) u^\mu \right) u^\nu + u_\nu \left(Ts + \mu\rho \right) u^\mu \partial_\mu u^\nu + u_\nu \partial_\mu P g^{\mu\nu} \\ & + u_\nu f^2 \partial^\nu \theta \, \partial_\mu \partial^\mu \theta + u_\nu f^2 \partial^\mu \theta \, \partial_\nu \partial^\mu \theta + u_\nu \partial_\mu \tau^{\mu\nu} \\ & + \mu \partial_\mu \left(\rho u^\mu + \nu^\mu \right) + \mu_5 f^2 \partial_\mu \partial^\mu \theta + \mu_5 \partial_\mu \nu_5^\mu \, . \end{aligned} \tag{11.2.33}$$

Using the normalization condition $u^\mu u_\mu = -1$, the Josephson equation $u^\mu \partial_\mu \theta + \mu_5 = 0$ and the following identities

$$\partial_\mu u^\mu = \text{inv} = \partial_0 u^0 = 0, \tag{11.2.34}$$

$$u_\nu u^\mu \partial_\mu u^\nu = \frac{1}{2} \left(u_\nu u^\mu \partial_\mu u^\nu + u^\nu u^\mu \partial_\mu u_\nu \right) = u^\mu \partial_\mu (u^\nu u_\nu) \equiv 0, \tag{11.2.35}$$

$$\partial_\mu (\rho u^\mu) = u^\mu \partial_\mu \rho + \rho \partial_\mu u^\mu = u^\mu \partial_\mu \rho = \text{inv} = u^0 \partial_0 \rho = 0 \tag{11.2.36}$$

we can simplify the expression for I to

$$\begin{aligned} I = & - T \partial_\mu \left(u^\mu s \right) - u^\mu \left\{ s \partial_\mu T + \rho \partial_\mu \mu - f^2 \partial_\nu \theta \, \partial_\mu \partial^\nu \theta - \partial_\mu P \right\} + u_\nu \partial_\mu \tau^{\mu\nu} \\ & + \mu \partial_\mu \nu^\mu + \mu_5 \partial_\mu \nu_5^\mu + 2 C_\gamma \mu_5 E^\lambda B_\lambda - \frac{C_g}{2} \mu_5 G^{\mu\nu a} \widetilde{G}^a_{\mu\nu} \, . \end{aligned} \tag{11.2.37}$$

The sum in the curly brackets is identically zero due to the thermodynamic relation (11.2.26). Also $u_\nu \partial_\mu \tau^{\mu\nu} = -\tau^{\mu\nu} \partial_\mu u_\nu$ because of the Landau frame condition (11.2.25). This leads to the further simplification,

$$I = -T \left(\partial_\mu \left(s u^\mu \right) - \frac{\mu}{T} \partial_\mu \nu^\mu - \frac{\mu_5}{T} \partial_\mu \nu_5^\mu \right) - \tau^{\mu\nu} \partial_\mu u_\nu + 2 C \mu_5 E^\lambda B_\lambda - \frac{C_g}{2} \mu_5 G^{\mu\nu a} \widetilde{G}^a_{\mu\nu} \, . \tag{11.2.38}$$

Hydrodynamic equations

Let us rewrite I again using the hydrodynamic equations (11.2.17-11.2.18). Then

$$\begin{aligned} I = & F^{\nu\lambda} u_\nu \rho \, u_\lambda + u_\nu F^{\nu\lambda} \nu_\lambda + g G^{\nu\lambda a} u_\nu \rho^a \, u_\lambda + g u_\nu G^{\nu\lambda a} \nu_\lambda^a \\ & + C_\gamma u_\nu F^{\nu\lambda} \widetilde{F}_{\lambda\kappa} \partial^\kappa \theta + C_g u_\nu G^{\nu\lambda a} \widetilde{G}^a_{\lambda\kappa} \partial^\kappa \theta \\ & + C_\gamma \mu_5 E^\lambda B_\lambda - \frac{C_g}{4} \mu_5 G^{\mu\nu a} \widetilde{G}^a_{\mu\nu} \\ = & - E_\lambda \nu^\lambda + 2 C_\gamma \mu_5 E^\lambda B_\lambda - \frac{C_g}{2} \mu_5 G^{\mu\nu a} \widetilde{G}^a_{\mu\nu} \, , \end{aligned} \tag{11.2.39}$$

where we used the Josephson equation, the definitions of the electric and magnetic fields (11.2.27) and the corresponding inversed relations (11.2.29).
Combining this result with (11.2.38) we obtain

$$-T \left(\partial_\mu \left(s u^\mu \right) - \frac{\mu}{T} \partial_\mu \nu^\mu - \frac{\mu_5}{T} \partial_\mu \nu_5^\mu \right) = \tau^{\mu\nu} \partial_\mu u_\nu - E_\lambda \nu^\lambda \, . \tag{11.2.40}$$

Then dividing by $-T$ and adding $-\nu^\mu \partial_\mu \frac{\mu}{T} - \nu_5^\mu \partial_\mu \frac{\mu_5}{T}$ to the both sides we can rewrite the result as

$$\partial_\mu \left(s u^\mu - \frac{\mu}{T}\nu^\mu - \frac{\mu_5}{T}\nu_5^\mu \right) = -\frac{1}{T}(\partial_\mu u_\nu)\tau^{\mu\nu} - \nu^\mu \left(\partial_\mu \frac{\mu}{T} - \frac{1}{T}E_\mu \right) - \nu_5^\mu \partial_\mu \frac{\mu_5}{T}\,. \tag{11.2.41}$$

Comparing this result with one of Son and Surowka [130], we see that the term proportional to C_γ is absent. This fact tells us that the divergence (11.2.41) is well defined, i.e. the entropy production is always nonnegative, and in contrary to [130] we do not need to add any additional terms to the entropy current. Therefore, there are no leading-order corrections to j_λ^S coming from the dissipative term ν^μ. So, all three anomalous effects are present already at the level of the hydrodynamic equations (11.2.17).

The expression for the entropy current remains unchanged also because the "superfluid" component itself has zero entropy. Indeed, considering (11.2.41) in absence of dissipative corrections we obtain

$$\partial_\mu (s u^\mu) = 0, \tag{11.2.42}$$

i.e. only the "normal" component contributes to the entropy current, which is a common property of a real superfluid. This fact would well agree with the long-range coherence of the chirality distribution [266,267,274–279,347,348], but should be studied more carefully, since the microscopic nature of θ is not known precisely.

11.2.4 Preliminary estimates for the CME

It was proposed [349] to use charge-dependent correlations $\gamma_{\alpha,\beta} = \langle \cos(\phi_\alpha + \phi_\beta) \rangle$ for the measurements of the local $\mathcal{P}$-violation in heavy-ion collisions (see Ref. [177] for a review). Here $\phi_{\alpha,\beta}$ with $\alpha, \beta = \pm$ are the azimuthal angles of the particles with respect to the reaction plane. The average is taken over all pairs within an event and then over the whole event ensemble. With use of reaction plane independent correlators $\delta_{\alpha,\beta} = \langle \cos(\phi_\alpha - \phi_\beta) \rangle$ and trigonometric identities one can split the initial correlation function into the "in-plane" $\langle \cos(\phi_\alpha)\cos(\phi_\beta) \rangle$ and "out-of plane" $\langle \sin(\phi_\alpha)\sin(\phi_\beta) \rangle$ components. The latter can be summarized in the following

STAR data [37, 38, 350] for $\sqrt{s} = 200\,\text{GeV}$ Au-Au collisions,

$$\langle \sin(\phi_\alpha)\sin(\phi_\beta) \rangle_{\text{same}} \simeq 0, \tag{11.2.43}$$

$$\langle \cos(\phi_\alpha)\cos(\phi_\beta) \rangle_{\text{same}} < 0, \tag{11.2.44}$$

$$\langle \sin(\phi_\alpha)\sin(\phi_\beta) \rangle_{\text{opp.}} \simeq \langle \cos(\phi_\alpha)\cos(\phi_\beta) \rangle_{\text{opp.}} > 0. \tag{11.2.45}$$

These relations can be interpreted as a mostly in-plane back-to-back emission of same-charged particles, while opposite-charge particles move together without a preferred direction. Equality in (11.2.45) can be qualitatively understood within the cluster model [34].

ALICE data [40] for $\sqrt{s} = 2.76\,\text{TeV}$ Pb-Pb collisions,

$$\langle \sin(\phi_\alpha)\sin(\phi_\beta) \rangle_{\text{same}} \gtrsim \langle \cos(\phi_\alpha)\cos(\phi_\beta) \rangle_{\text{same}} > 0, \tag{11.2.46}$$

$$\langle \sin(\phi_\alpha)\sin(\phi_\beta) \rangle_{\text{opp.}} \simeq \langle \cos(\phi_\alpha)\cos(\phi_\beta) \rangle_{\text{opp.}} > 0, \tag{11.2.47}$$

differ from the RHIC data, in particular by nonvanishing out-of plane same-charge correlations. One should also be aware of significant non-flow contributions to $\delta_{\alpha,\beta}$ in the ALICE data [40]. In both cases all nonzero correlators are growing in absolute value with centrality.

The data seems to be in contradiction with the predictions of CME. In fact, before drawing conclusions, one should take into account all possible contributions to the correlators, including ones coming from the parity-even effects, e.g. hydrodynamic flows. Let us assume, that in order

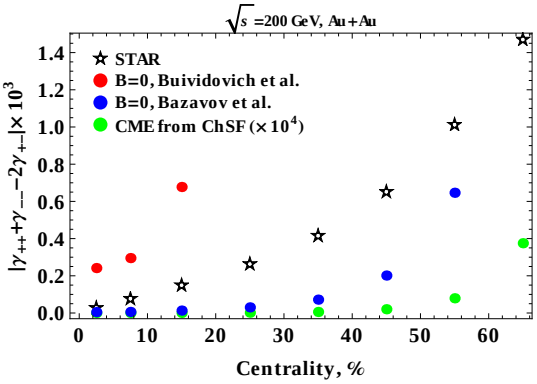

Figure 11.3: Absolute value of the charge separation (11.2.50). See explanation in the text.

to separate the elliptic flow contributions we can introduce the following decomposition, in spirit of [177],

$$\gamma_{\alpha,\beta} \sim v_2\, F_{\alpha,\beta} - H^{\rm out}_{\alpha,\beta} + H^{\rm in}_{\alpha,\beta}, \tag{11.2.48}$$

$$\delta_{\alpha,\beta} \sim F_{\alpha,\beta} + H^{\rm out}_{\alpha,\beta} + H^{\rm in}_{\alpha,\beta}, \tag{11.2.49}$$

where F's denote the flow-induced correlators (by e.g. the transverse momentum conservation, local charge conservation, etc.), and H's correspond to the flow-independent correlations in- and out-of-plane (induced by e.g. CME, CEE, dipole assymetry from fluctuations, etc.). Then, by considering an additional value $r_{\alpha,\beta} \equiv \frac{\gamma_{\alpha,\beta}(v_2\to 0)}{\gamma_{\alpha,\beta}}$ we can resolve (11.2.48,11.2.49) with respect to the shape-independent correlations. The criteria of completeness would be the symmetry of $F_{\rm same}, H_{\rm same}$ and $F_{\rm opp.}, H_{\rm opp.}$ with respect to zero, as a function of centrality.

As we concluded in Chapter 6, the CME contributes only to the v_2-independent part of the correlators, i.e. to H's, and, more precise, to $H^{\rm out}_{\alpha,\beta}$, since the magnetic field points in the direction out-of-plane. If there were no other $\mathcal{P}$-odd effects, then the $H^{\rm in}$ part would hold zero. However, lattice computations demonstrate the presence of temperature fluctuations of the chirality even for a vanishing magnetic field, which would result in an *isotropic* parity-violating effect. These fluctuations can be translated to the total charge asymmetry by means of a static fireball model [51],

$$H_{++} + H_{--} - 2H_{+-} \sim \frac{4\pi\tau^2\rho^2\mathcal{R}^2}{3N_q^2}\left(\langle j_\parallel^2\rangle + 2\langle j_\perp^2\rangle\right), \tag{11.2.50}$$

where $H_{\alpha,\beta}$ is the shape-independent part of $\gamma_{\alpha,\beta}$, τ is the emission time, $\rho \sim \dfrac{\hbar c}{1\,\text{GeV}}$ is a characteristic correlation length between particles, $\mathcal{R} \sim 5fm$ is the radius of the fireball [351], N_q is the number of particles of the same charge produced in one event (we took the data on the multiplicities from [352, 353]), and $j_\perp$, $j_\parallel$ are currents induced according to the geometry in Fig. 1.1(a). Results for the absolute value of (11.2.50) are shown in Fig. 11.3. Taken that $\langle j_\mu^2\rangle$ for different components are of the same order at $B = 0$ [51] we get red and blue points in Fig. 11.3 for the current/charge fluctuations taken from [51, 354]. These results are comparable by one-two orders of magnitude with the experimental values [37, 38], which is remarkable, taken that the lattice data [51] is for the quenched $SU(2)$ theory, and we did not subtract the flow contributions from the STAR data. The pattern of growth with the centrality is repeated even without magnetic fields, but because of multiplicity, which itself depends on the centrality.

We can use (11.2.50) to estimate the magnitude of CME alone. For RHIC the $\tau \sim 0.1fm/c$ is the lifetime of the electromagnetic fields (see Fig. 1.2), which makes the assumption of the static

fireball reasonable [25]. From (11.2.24) we get $\mu_5(x) = f^{-2}\rho_5(x)$ with $f \sim 1\,\mathrm{GeV}$ and hence

$$\langle \mu_5^2 \rangle = f^{-4}\langle \rho_5^2 \rangle \sim \frac{4N_f^2}{f^4} \cdot \frac{\langle \Delta Q_5^2 \rangle}{R^6}\,, \tag{11.2.51}$$

where the most optimistic estimate for the topological charge generated in a RHIC collision is $\sqrt{\langle \Delta Q_5^2 \rangle} \sim 40$ [346], $N_f = 2$ is the number of light flavors, $R = 1.2A^{1/3}$ fm is the radius of the nucleus. Using the estimate (11.2.51) we see that the root mean square of μ_5 is only of order of few MeVs. Taking the highest values of the magnetic field and $\mu_5 = 10\,\mathrm{MeV}$, we can find the upper bound on the CME which is $\mathrm{CME} < 10^{-9}$. Taking into account the response of QGP to the e.-m. fields and assuming the magnetic field to be approximately stationary during the QGP lifetime [28, 35], we would get a value, which is two orders of magnitude larger, i.e. $\mathrm{CME} < 10^{-7}$, see Fig. 11.3. The magnitude is too low to explain the charge asymmetry, while the temperature fluctuations fit better to the data.

11.3 Conclusion

In this chapter we provided a novel treatment of the sQGP dynamics for the temperatures typical for recent and ongoing heavy-ion experiments. The main feature of our studies is a combination of nonperturbative methods applied to a general form of the theory, namely, the QCD coupled to QED. Our conclusion is that there can exist a light (nearly massless) axion-like component of the quark-gluon plasma for the given range of temperatures. This component accommodates all the chiral and anomalous properties of the plasma and is responsible for a plenty of hypothetical effects leading to the *local* $\mathcal{P}$- and $\mathcal{CP}$-violation in the strong interaction. The rest of the matter content of QGP obeys the hydrodynamic equations of a nearly ideal fluid. Both of the components together form some kind of a superfluid, which we call the "chiral superfluid". This term should be understood in a relative sense as a two-component fluid with independent curl-free and normal motions. The separation between two motions is provided by a gap in the Dirac spectrum observed in lattice QCD simulations with massless quarks. It is worth to mention, that in our case we do not obtain the light "superfluid" component as a Goldstone field of a broken continuous symmetry. Instead, it appears as a consequence of a nontrivial underlying vacuum structure. At the same time, even not being a conventional superfluid, our system reproduces some usual properties, such as a (pseudo-)scalar nature of the "condensate", zero entropy of the "condensate", Josephson-type relation, etc. Taking into account only regular configurations of the "condensate" we reserve the vortex-like solutions for the further studies.

An important issue not covered in this Chapter is the probe limit (quenching) for the lattice fermions. It is not clear yet, whether the long-range structures survive in the full QCD or they are destroyed by dynamical fermions. As a crucial test of our model we propose some phenomenological effects (Section 11.2.2), which can be proven experimentally, i.e. a response of QGP to the presence of strong electromagnetic fields. A concrete description of the experimental consequences is currently in progress.

Chapter 12

On chromoelectric superconductivity of the Yang-Mills vacuum

The nonperturbative structure of the ground state of QCD vacuum is one of the most interesting unsolved problems in quantum field theory. At zero temperature the ground state exhibits a mass gap, breaks chiral symmetry and supports confinement of color sources, quarks and gluons. The confining properties of the QCD ground state were intensively studied last decades resulting in a number of phenomenological approaches to this problem.

One of the popular approaches is the "spaghetti vacuum" picture (the Copenhagen vacuum): the QCD vacuum is considered to be populated by evolving vortex tubes which carry a chromomagnetic flux [355–359]. An isolated color charge – for example, a quark – scatters off the vortices and develops an infinitely large free energy. As a result, the quarks may appear in the vacuum only in a form of colourless (hadronic) states bounded by a chromoelectric string [356].

The standard mechanism of formation of the chromomagnetic vortices is as follows. The perturbative vacuum of QCD – which is paramagnetic due to the asymptotic freedom – has an unstable mode towards formation of a chromomagnetic field [360]. However, in the background of a homogeneous chromomagnetic field the gluon part of the vacuum energy develops an imaginary part to large chromomagnetic moment of the gluon [355]. This implies that the homogeneous chromomagnetic field is also unstable towards squeezing of the chromomagnetic field into separate parallel flux tubes (vortices) [358], similarly to the Abrikosov vortex lattice in a mixed state of an ordinary type-II superconductor in an external magnetic field [361]. Finally, due to global rotational and Lorentz invariance of the QCD vacuum, the chromomagnetic field has locally a domain-like structure [357]: the field has different orientation in different domains. Due to the fact that the vortices follow the orientation of the chromomagnetic field, the vortex lines form an intertwining entangled structure, hence the name "spaghetti".

Thus, the Copenhagen confining mechanism has a tight relation to ideas from ordinary superconductivity such as condensation and flux tube (vortex) formation. However, in addition to the mentioned features there exists another, primary phenomenon which is associated with ordinary superconductivity which is the superconductivity itself (i.e., the perfect conductivity of an electric current). In this chapter we would like to show that the Copenhagen vacuum is not just "analogous" to an ordinary superconductivity: in this picture the Copenhagen vacuum *is* a chromoelectric superconductor from the point of view of the transport properties.

Why the Copenhagen vacuum should be a chromoelectric superconductor? A simple answer is because in this picture the chromomagnetic tubes are formed due to the gluon condensate while

the gluons are carrying a color charge. The condensation of the color charges should lead, naively, to the (chromo)superconducting phenomenon. However, our considerations may contain a caveat: in the ordinary superconductivity the Cooper-pair condensate has a macroscopic order over large distances and this property is the core reason why the electric current may be transported by the uniform condensate without dissipation. On the contrary, the QCD vacuum in the Copenhagen picture has a domain-like structure with each domain possessing its own orientation (both in color and coordinate spaces) of the gluon condensate so that the long-range order is absent. Nevertheless, we argue below that this property is not an obstacle due to the long-range order which is maintained *along* the chromomagnetic vortices. We arrive to the picture that in the spaghetti vacuum the chromoelectric current should be able to stream without dissipation along the chromomagnetic tubes. Basically, the chromomagnetic tubes work like specific, hollow wires which are able to carry the chromoelectric current without resistance.

As one of the possible consequences of the color superconductivity one can expect probe quarks to propagate along the flux tubes over arbitrary distances, so that the tubes can be considered as "fermionic guides" [143, 307, 308, 342]. From the phenomenological perspective the long-range propagation of quarks may lead to the phenomenon of chiral superfluidity of the quark-gluon plasma [8].

The Yang-Mills Lagrangian is

$$\mathcal{L} = -\frac{1}{4} F^a_{\mu\nu} F^{a\mu\nu} \,, \tag{12.0.1}$$

where $F^a_{\mu\nu} = \partial_\mu A^a_\nu - \partial_\nu A^a_\mu + g\epsilon^{abc} A^{b\mu} A^c_\nu$ is the strength tensor of the $SU(2)$ gluon field A^a_μ.

For simplicity, we consider the $SU(2)$ gauge field instead of more phenomenologically relevant $SU(3)$ fields since the latter solutions may be obtained – following the general construction of Ambjorn–Olesen [358] – by an imbedding the $SU(2)$ solutions into the $SU(3)$ color group.

The corresponding equations of motion are as follows

$$\partial^\mu F^a_{\mu\nu} + g\epsilon^{abc} A^{b\mu} F^c_{\mu\nu} = 0 \,. \tag{12.0.2}$$

Following Ambjorn and Olesen [358] we consider the state of the Yang-Mills theory in a uniform chromomagnetic field directed along the third spatial axis. In the color space the chromomagnetic field is assumed to be directed in the third axis as well:

$$F^{a,\mathrm{ext}}_{\mu\nu} \sim \delta^{a,3} \left(\delta_{\mu 1} \delta_{\nu 2} - \delta_{\mu 2} \delta_{\nu 1} \right) \,. \tag{12.0.3}$$

In order to obtain such a configuration, one can add a homogeneous Abelian magnetic flux in third direction in color space [358]:

$$A^3_1 = -x_2 \frac{B}{2}, \quad A^3_2 = x_1 \frac{B}{2} \,. \tag{12.0.4}$$

For definiteness we take $B > 0$.

The ground state solution to the equations of motion (12.0.2) has certain remarkable properties. The solution is a function of the transverse – with respect to the spatial direction of the external chromomagnetic field (12.0.3) – coordinates $x^\perp = (x_1, x_2)$ and it is independent on the longitudinal coordinates $x^\parallel = (x_0, x_3)$.

The longitudinal components of the vector fields are vanishing in the ground state, $A^a_0 = A^a_3 = 0$, so that the equations of motion (12.0.2) involve only the transversal components A^a_i with $i = 1, 2$. The latter can conveniently be rewritten in the complex notations by introducing the following combinations for all vector fields $\mathcal{O}_i$ with $i = 1, 2$: $\mathcal{O} = \mathcal{O}_1 + i\mathcal{O}_2$ and $\bar{\mathcal{O}} = \mathcal{O}_1 - i\mathcal{O}_2$. These relations imply $\bar{\mathcal{O}} = \mathcal{O}^*$ for all real vector fields $\mathcal{O}_i$. Defining the complex coordinate $z = x_1 + ix_2$ and complex derivative $\partial = \partial_1 + i\partial_2$, we find the non-canonical relations $\bar{\partial} z = \partial \bar{z} = 2$ and $\partial z = \bar{\partial} \bar{z} = 0$.

The off-diagonal gluonic fields $A_\mu^{1,2}$ can be combined into two complex-valued fields:

$$A_\mu^{\pm} = \frac{1}{\sqrt{2}} \left(A_\mu^1 \mp i A_\mu^2 \right), \tag{12.0.5}$$

These combinations are not independent, $A_\mu^{\pm} \equiv (A_\mu^{\mp})^\dagger$, so that below we will work with the A_μ^- field only.

The ground state can be described by two complex functions $A = A(x^\perp)$ and $A^3 = A^3(x^\perp)$ with

$$A \equiv A^- = A_1^- + i A_2^- , \tag{12.0.6}$$

$$A^3 = A_1^3 + i A_2^3 , \tag{12.0.7}$$

and their complex conjugates. The combinations (12.0.6) and (12.0.7) correspond to, respectively, the offdiagonal and diagonal components of the A_i^a fields. The color direction is defined by the background chromomagnetic field. The alternative (barred) combination of the off-diagonal A fields is zero in the ground state, $\bar{A}^- = A_1^- - i A_2^- = 0$. Notice that $A^+ \equiv (\bar{A}^-)^* = 0$ and $\bar{A}^+ = (A^-)^*$.

The constraints (12.0.3) for $a = 1, 2$ can now be rewritten as a single complex equation:

$$\bar{\partial} A = -\frac{gB}{2} \bar{z}\, A , \tag{12.0.8}$$

which is well known from the work of Abrikosov [361] to possess finite-energy solutions with a lattice symmetry.

The solution for this equation minimizing the remaining terms contributing to the energy integrated over the transversal plane

$$E_\perp = \int \frac{1}{2} \left(F_{12}^3 \right)^2 = \int \frac{1}{2} \left(B - \frac{g}{2} |A|^2 \right)^2 , \tag{12.0.9}$$

was constructed in terms of θ-functions. In the background of the strong chromomagnetic field the vacuum structure resembles the Abrikosov lattice in the mixed phase of the type-II superconductors [361]. In analogy with the lattice of the Abrikosov vortices in a superconductor, the chromomagnetic field in Yang–Mills theory organizes itself in similar periodic structures [358].

The ground state solution by Ambjorn and Olesen is given [up to a gauge factor due to a different parametrization of magnetic field (12.0.4)] by the following formula [358]:

$$A(x_1, x_2) = \phi_0\, e^{igBx_2 \frac{x_1 + i x_2}{2}} \theta_3 \left(\frac{(x_1 + i x_2)\nu}{L_B}, e^{\frac{2i\pi}{3}} \right), \tag{12.0.10}$$

$$\nu = \frac{\sqrt[4]{3}}{\sqrt{2}} , \qquad L_B = \sqrt{\frac{2\pi}{gB}}, \tag{12.0.11}$$

where θ_3 is the third Jacobi theta function and the overall factor $\phi_0 \approx 2.9\sqrt{B/g}$ is determined by minimization of the energy functional (12.0.9).

The global energy minimum is reached for the equilateral triangular lattice (which is also called the hexagonal lattice) solutions of Eq. (12.0.8). Another local minimum is found for a square lattice.

The geometrical pattern of the lattice structure in the Yang–Mills theory is determined by the Abrikosov ratio,

$$\beta_{\rm A} = \left(\int dx_\perp^2 |A|^4 \right) / \left(\int dx_\perp^2 |A|^2 \right)^2 , \tag{12.0.12}$$

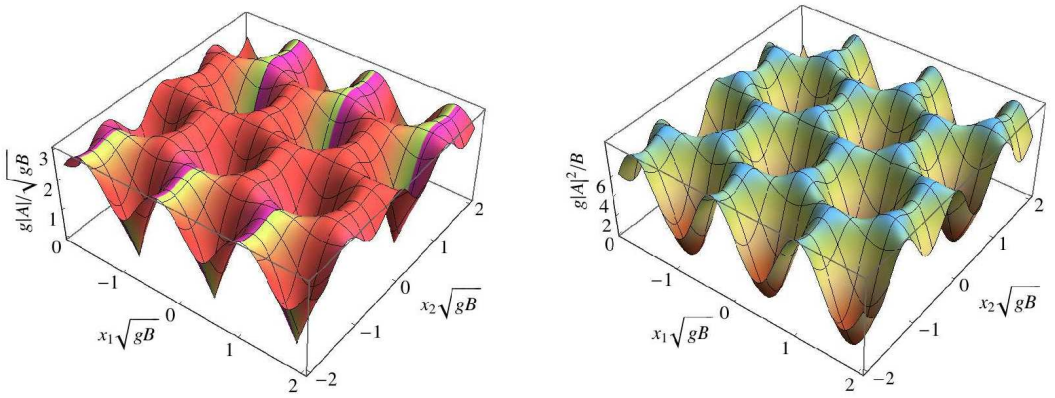

(a) (b)

Figure 12.1: (a) The amplitude of the gluon field (12.0.10) is shown by a density plot superimposed on the three dimensional plot of its absolute value. A few cells of the hexagonal periodic lattice are shown in the transverse (x_1, x_2) plane. All dimensional units are shown in terms of the only massive scale $\sqrt{gB}$. (b) The chromoelectric superconductivity coefficient in the London equation (12.0.16) in the transverse (x_1, x_2) plane.

which can be expressed in terms of generalized θ-functions [358]. The global minimum of the energy functional (12.0.9) is

$$E_{\perp,\min} = \frac{B^2}{2}\left(1 - \frac{1}{\beta_{\rm A}}\right), \tag{12.0.13}$$

where for the hexagonal structure the Abrikosov ratio is $\beta_{\rm A} \approx 1.16$ similarly to an ordinary type-II superconductor [362].

It is worth noting that even in models where the forth-order interaction terms are more complicated and, as a consequence, another definition of $\beta_{\rm A}$ is needed, one still finds that the global energy minimum still corresponds to the hexagonal lattice pattern [250–252, 362–364].

The gluon field (12.0.10) is shown in Fig. 12.1(a). The chromomagnetic vortices are arranged in the hexagonal structure. In the center of each vortex the gluon field (12.0.6) is vanishing and the phase of this field winds by the angle 2π, similarly to the usual Abrikosov vortex. The geometrical vortex pattern Fig. 12.1(a) is identical to the Abrikosov vortex lattice in an ordinary type-II superconductor.

Does the ground state (12.0.10) correspond to a chromoelectric superconductor? A simplest way to check an existence of the superconductivity is to calculate a relevant transport property: the superconducting nature of the ground state should reveal itself as an $\omega = 0$ (zero-frequency) δ-function peak in the real part of the complex (chromo)conductivity, $\sigma(\omega) = \sigma_1(\omega) + i\sigma_2(\omega)$. Alternatively, one can impose a weak external (chromo)electric field and then check that the ground state supports the London relation for the (chromo)electric currents. These two approaches are identical.

The London equations were used to argue in favor of existence of a magnetic-fields-induced electromagnetic superconductivity in QCD [250–252] and in electroweak model [363]. The former effect is mediated by the ρ–meson condensation while the latter one is caused by the condensation of the W mesons [365–367].

Following these approaches we impose a weak (test) chromoelectric field,

$$E_3 \equiv E_3^3 = F_{30}^3\,, \qquad |E_3| \ll B\,, \tag{12.0.14}$$

oriented along the background chromomagnetic field (12.0.3) both in the color and coordinate spaces in order to check possible validity of the London transport equation.

In order to define the relevant chromoelectric current we notice that the chromomagnetic field (12.0.3) plays a role of an object which identifies the Abelian $U(1)$ direction in the non-Abelian $SU(2)$ group. The chromoelectric current associated with this $U(1)$ gauge subgroup is defined as follows[1]:

$$J_\nu \equiv J^3_\nu = \partial^\mu(\partial_\mu A^3_\nu - \partial_\nu A^3_\mu)\,. \tag{12.0.15}$$

We utilize the equations of motion (12.0.2) in the background of the strong chromomagnetic (12.0.4) and weak chromoelectric (12.0.14) fields and we find the following analogue of the London equation:

$$\partial_{[0}J_{3]} = -g^2|A|^2E_3\,, \tag{12.0.16}$$

Equation (12.0.16) implies, that the chromoelectric current propagates ballistically (i.e., without dissipation) along the chromomagnetic flux tubes. In the transverse directions the chromoelectric superconductivity is absent, $\partial_{[0}J_{i]} \equiv 0$ with $i = 1, 2$.

The superconductivity coefficient of the London equation (12.0.16) is shown in Fig. 12.1(b). In the center of each flux tube the superconductivity is absent and the chromoelectric current may stream only at the regions in between the touching tubes. Therefore the chromomagnetic flux tube may be associated with a hollow (chromo)conducting "wire".

So far in our considerations we have followed the considerations of Refs. [358] where the regular solution was obtained in a homogeneous chromomagnetic background. In the real vacuum the flux tubes form an entangled spaghetti structure [357], so that the vacuum between two separated spatial points is, in general, disordered by the flux tubes. However, as we move along the tubes themselves they are supposed to keep their field structure in the transverse spatial directions [357]. In lattice gauge theory the thick chromomagnetic flux tubes can be associated with the so-called center vortices [368,369], which were indeed shown to exhibit the long-range correlations along the worldsheets of their flux tubes [370].

Interestingly, the chromoelectric currents (12.0.16) are induced by the chromoelectric field E^a_i provided it is parallel to the chromomagnetic field B^a_i both in color and coordinate spaces. Thus, the electric currents in the flux tubes are induced if the scalar product $(\vec{E}^a \cdot \vec{B}^a)$ of these fields is nonzero. Notice, however, that this scalar product is proportional to the topological charge density [371],

$$q(x) = \frac{1}{16\pi^2}\mathrm{Tr}\,[F_{\mu\nu}\tilde{F}^{\mu\nu}], \qquad \tilde{F}^{\mu\nu} = \frac{1}{2}\varepsilon^{\mu\nu\alpha\beta}F_{\alpha\beta}. \tag{12.0.17}$$

Thus, the topological charge density should induce the chromoelectric currents in the chromomagnetic flux tubes. We find it fascinating that the described mechanism links chromoelectric superconductivity with the topology in QCD.

According to the standard Copenhagen picture the chromomagnetic tubes form an entangled "spaghetti" structure in the real vacuum. In this chapter we have shown that this spaghetti is (chromo)superconducting.

[1]Notice that the chromoelectric current (12.0.15) is different from the full $SU(2)$ currents $\mathcal{D}^\mu F^a_{\mu\nu} \equiv 0$ since the Abelian and non-Abelian strengths are different: $\partial_\mu A^3_\nu - \partial_\nu A^3_\mu \neq F^3_{\mu\nu}$.

Chapter 13

Conclusions and Outlook

We developed several systematic approaches to study nonperturbative effects related to the chiral and electromagnetic properties of the quark-gluon plasma: the holographic framework based on the fluid-gravity duality; the quenched lattice simulation for two and three colors, and a two-component liquid model derived from the QCD Lagrangian. In addition, we also make certain predictions never mentioned before in the literature[1], which can be tested experimentally. Among them are the following: electric conductivity of the QGP induced by the magnetic field and modifying the elliptic flow for photons; magnitude of the chiral magnetic effect, its independence on the elliptic flow in QGP; charge separation in QGP induced by an electric field; color superconductivity of the QCD vacuum state, which may lead to the chiral superfluidity.

To conclude this thesis, we provide a list of open questions, which can be considered as a possible extension of our studies:

1) In holographic models of Chapter 5 we saw an equivalence between effects induced by a magnetic field (e.g. CME) and through the rotation of medium (e.g. CVE). This is not a coincidence, since the angular momentum $\vec{\omega}$ is in many respects similar to the magnetic field $\vec{B}$: rotating charged fluid produces a magnetic field, which is a well-known phenomenon in magnetohydrodynamics; rotating along a loop particle with mass m and charge e acquires the Aharonov-Bohm phase shift equal to the phase shift due to the Sagnac effect [372] along the same loop, if $\vec{B} = \frac{2m}{e}\vec{\omega}$; the same relation holds for a magnetic field generated by a rotating superconductor [373] and known to be present for any substance as well (Barnett effect [374]). It seems interesting to follow this equivalence from the holographic point of view. A strong magnetic field in QCD effectively reduces the dimensionality of problem to 2D, since the quarks tend to occupy the lowest Landau level and cannot move in directions transverse to the magnetic field. From the side of the bulk geometry this corresponds to the dimensional reduction of the black hole geometry to a BTZ-black hole background [375]. This leads to a natural question, whether the background of a uniformly rotating liquid (presumably, AdS-Kerr-Newmann BH) reduces to a low-dimensional black hole in limit of large angular momenta.

2) In light of various superfluid and superconducting properties of the QCD vacuum [8,15,250–252], Chapters 11-12, it is natural to investigate the spatial distribution of the CME-current in the transverse to $\vec{B}$ plane. Does the current density form any kind of honeycomb pattern? This question can be, perhaps, answered by applying the IPR methods from the Chapter 10.

3) The results of Chapter 3 and Section 8.2 on the chiral symmetry breaking rely on the fact that the quenched approximation is valid and reproduces the phenomenon of magnetic catal-

[1] Except our own articles.

ysis [214]. There are, however, recent unquenched lattice data [216, 217], demonstrating the inverse effect (chiral symmetry restoration by the magnetic field) in the vicinity of the conventional chiral transition. This leads to a conclusion that the back-reaction of the sea quarks on the gauge-field configuration can compete with the dynamical generation of the quark mass. Holographically, this means, that the backreaction of D7-branes is no longer negligible and one should choose a more suitable (unquenched) background. The mechanism can be also studied numerically, by analyzing the value of Polyakov loop in magnetic fields [376].

4) In Chapter 11 we suggested the gauge field defects as an important ingredient of the quark-gluon plasma. There is, unfortunately, a lack of analytic solutions of the Yang-Mills equations, which we could use in our studies. In Chapter 12 we used the "spaghetti" picture, which was originally established in a 1-loop approximation, and, generally speaking, is not proven beyond 1-loop. This makes it important to search for possible low-dimensional objects in Yang-Mills theories, as well as in holography [377]. Exact solutions can also shed light on the problem of confinement [309, 311] and the entropy in QCD [378].

5) In the same chapter we presented a spectrum of the overlap operator. It is not clear, whether the spectrum has the same form for the intermediate temperatures in the case of full QCD, and whether the remnant zero-modes survive in this case. For the phenomenological applications one should also study the Dirac spectrum in the presence of non-zero average chirality, which mimics initial conditions in the heavy-ion collisions. One can, perhaps, do that by selecting gauge-field configurations with a fixed topological charge.

6) Is there a consistent way to define the topological susceptibility in a finite volume? The same question can be posed, if we are dealing with vacuum condensates as well as with thermodynamic phenomena, e.g. superfluidity, in the case of real and hence finite systems.

7) Is the chiral magnetic effect saturated at some critical magnetic field? Such a conclusion can follow from Section 11.1.5, if considering large B limit,

$$j_{CME} = C\mu_5 B \propto \frac{\rho_5 B}{f^2} = \text{const.} \tag{13.0.1}$$

Here we used the approximation $f \propto \Lambda \propto \sqrt{eB}$ when B is much larger than all other scales under consideration.

8) Do we reproduce the the Chern-Simons diffusion rate [379] within the chiral superfluid model? One can use the axion Lagrangian (11.1.27) with higher-order terms and calculate the rate perturbatively in the limit $B \gg T^2$, which can be considered as an additional test of the model.

9) Do the lattice data coincide with the holographic results in the large N_c limit? Is $SU(3)$ close to $SU(\infty)$? One can answer these questions by changing our codes for three colors. The Cabibbo-Marinari heat-bath algorithm allows for such a modification, so one should only determine the couplings [380] and choose appropriate sizes of the lattices. There are already hints that the $SU(3)$ gauge theory is very similar to $SU(\infty)$ [381, 382].

For a list of general open questions related to our studies we refer the reader to an excellent review [65]. We hope that the ideas contained in this thesis will stimulate further advances in the intriguing and relatively modern subject of the quark-gluon plasma physics.

Acknowledgments

I wish to express my gratitude to Prof. Volker Schomerus for giving me the opportunity to do research at DESY. I am also grateful to him for supporting me during these years.

I would like to thank my supervisor Ingo Kirsch for his guidance and many discussions throughout my work, and my colleagues, Dmitri Kharzeev, Valentin Zakharov, Maxim Chernodub, Pavel Buividovich, Henri Verschelde, Mikhail Polikarpov, Nick Evans, Keun-young Kim, Jos Van Doorselaere, Ilmar Gahramanov and Victor Braguta for our excellent collaboration.

I am grateful to Alexander Polyakov, Mikhail Shifman, Arkady Vainstein, Igor Klebanov, Alexander Zhiboedov, Grigory Tarnopolsky, Mikhail Isachenkov, Edward Shuryak, Ismail Zahed, Andreas Ringwald, Mikhail Shaposhnikov, Kenji Fukushima, Vitaly Bornyakov, Guy Gur-Ari, Andreas Schmitt, Piotr Surowka, Arata Yamamoto, Ivan Horváth, Jan Pawlowski, Vladimir Shevchenko, David Dudal, Vladimir Skokov, Adam Bzdak, Jinfeng Liao, Ariel Zhitnitsky, Andrey Sadofyev, Eliezer Rabinovici, Andrew Strominger, Laurent Baulieu, Shiraz Minwalla, Ilya Selyuzhenkov, Keh-Fei Liu and Lincoln Carr for numerous discussions related to the works included in this thesis.

I am thankful to Alexey Shelaev, Pavel Buividovich, Victor Braguta, Fedor Gubarev, Sergey Morozov, Sergey Kuznetsov, Vitaly Bornyakov, Wei-Tian Deng and Xu-Guang Huang for providing numerical data and programming codes at various stages of the work. Numerical calculations were performed at the GSI batch farm, DESY BIRD cluster, DESY theory clusters, ITEP batch farm.

I am very much obliged to Valentin Zakharov, Valery Rubakov, Alexander Polyakov and Vladimir Arnold (1937 - 2010), who inspired me for the current research and gave me a feeling of the real science.

Bibliography

[1] N. Evans, T. Kalaydzhyan, K.-y. Kim, and I. Kirsch, JHEP **1101**, 050 (2011), arXiv:1011.2519.

[2] T. Kalaydzhyan and I. Kirsch, JHEP **1102**, 053 (2011), arXiv:1012.1966.

[3] T. Kalaydzhyan and I. Kirsch, Phys.Rev.Lett. **106**, 211601 (2011), arXiv:1102.4334.

[4] I. Gahramanov, T. Kalaydzhyan, and I. Kirsch, Phys.Rev. **D85**, 126013 (2012), arXiv:1203.4259.

[5] P. Buividovich *et al.*, Phys.Rev.Lett. **105**, 132001 (2010), arXiv:1003.2180.

[6] V. Braguta, P. Buividovich, T. Kalaydzhyan, S. Kuznetsov, and M. Polikarpov, PoS **LATTICE2010**, 190 (2010), arXiv:1011.3795.

[7] V. Braguta, P. Buividovich, T. Kalaydzhyan, S. Kuznetsov, and M. Polikarpov, Phys.Atom.Nucl. **75**, 488 (2012), arXiv:1011.3795.

[8] T. Kalaydzhyan, arXiv:1208.0012.

[9] P. Buividovich, T. Kalaydzhyan, and M. Polikarpov, Phys.Rev. **D86**, 074511 (2012), arXiv:1111.6733.

[10] P. Buividovich *et al.*, PoS **LATTICE2010**, 076 (2010).

[11] M. Polikarpov *et al.*, AIP Conf.Proc. **1343**, 630 (2011).

[12] I. Kirsch and T. Kalaydzhyan, PoS **CONFINEMENTX**, 262 (2013), arXiv:1301.6558.

[13] V. Braguta, P. Buividovich, T. Kalaydzhyan, and M. Polikarpov, PoS **CONFINEMENTX**, 085 (2013), 1302.6458.

[14] T. Kalaydzhyan, PoS **CONFINEMENTX**, 302 (2013), 1302.6510.

[15] M. Chernodub, J. Van Doorsselaere, T. Kalaydzhyan, and H. Verschelde, (2012), arXiv:1212.3168.

[16] STAR Collaboration, J. Adams *et al.*, Nucl.Phys. **A757**, 102 (2005), arXiv:nucl-ex/0501009.

[17] PHENIX Collaboration, K. Adcox *et al.*, Nucl.Phys. **A757**, 184 (2005), arXiv:nucl-ex/0410003.

[18] B. Muller, J. Schukraft, and B. Wyslouch, Ann.Rev.Nucl.Part.Sci. **62**, 361 (2012), arXiv:1202.3233.

[19] X. Zhao and R. Rapp, Nucl.Phys. **A859**, 114 (2011), arXiv:1102.2194.

[20] PHENIX Collaboration, A. Adare *et al.*, Phys.Rev.Lett. **104**, 132301 (2010), arXiv:0804.4168.

[21] CMS Collaboration, S. Chatrchyan *et al.*, Phys.Rev.Lett. **109**, 222301 (2012), arXiv:1208.2826.

[22] CMS Collaboration, S. Chatrchyan *et al.*, JHEP **1205**, 063 (2012), arXiv:1201.5069.

[23] A. Mocsy and P. Petreczky, Phys.Rev.Lett. **99**, 211602 (2007), arXiv:0706.2183.

[24] L. Landau, Izv.Akad.Nauk Ser.Fiz. **17**, 51 (1953).

[25] J. Bjorken, Phys.Rev. **D27**, 140 (1983).

[26] R. Snellings, New J.Phys. **13**, 055008 (2011), arXiv:1102.3010.

[27] http://www.lattice.itep.ru/img/QCDvacuum.gif .

[28] K. Tuchin, (2013), arXiv:1301.0099.

[29] STAR Collaboration, I. V. Selyuzhenkov, Rom.Rep.Phys. **58**, 049 (2006), arXiv:nucl-ex/0510069.

[30] D. E. Kharzeev, L. D. McLerran, and H. J. Warringa, Nucl.Phys. **A803**, 227 (2008), arXiv:0711.0950.

[31] V. Skokov, A. Y. Illarionov, and V. Toneev, Int.J.Mod.Phys. **A24**, 5925 (2009), arXiv:0907.1396.

[32] V. Voronyuk *et al.*, Phys.Rev. **C83**, 054911 (2011), arXiv:1103.4239.

[33] V. Toneev and V. Voronyuk, Phys.Atom.Nucl. **75**, 607 (2012), arXiv:1012.1508.

[34] K. Liu, Phys.Rev. **C85**, 014909 (2012), arXiv:1109.4883.

[35] W.-T. Deng and X.-G. Huang, Phys.Rev. **C85**, 044907 (2012), arXiv:1201.5108.

[36] A. Bzdak and V. Skokov, Phys.Lett. **B710**, 171 (2012), arXiv:1111.1949.

[37] STAR Collaboration, B. Abelev *et al.*, Phys.Rev.Lett. **103**, 251601 (2009), arXiv:0909.1739.

[38] STAR Collaboration, B. Abelev *et al.*, Phys.Rev. **C81**, 054908 (2010), arXiv:0909.1717.

[39] PHENIX Collaboration, N. Ajitanand, S. Esumi, and R. Lacey, Proc. of the RBRC Workshops **96** (2010), arXiv:0909.1717.

[40] ALICE Collaboration, B. Abelev *et al.*, Phys.Rev.Lett. **110**, 012301 (2013), arXiv:1207.0900.

[41] K. Fukushima, D. E. Kharzeev, and H. J. Warringa, Phys.Rev. **D78**, 074033 (2008), arXiv:0808.3382.

[42] D. E. Kharzeev, Annals Phys. **325**, 205 (2010), arXiv:0911.3715.

[43] D. Kharzeev and A. Zhitnitsky, Nucl.Phys. **A797**, 67 (2007), arXiv:0706.1026.

[44] A. Vilenkin, Phys.Rev. **D20**, 1807 (1979).

[45] A. Vilenkin, Phys.Rev. **D22**, 3080 (1980).

[46] A. Vilenkin, Phys.Rev. **D22**, 3067 (1980).

[47] M. Giovannini and M. Shaposhnikov, Phys.Rev.Lett. **80**, 22 (1998), arXiv:hep-ph/9708303.

[48] M. Giovannini and M. Shaposhnikov, Phys.Rev. **D57**, 2186 (1998), arXiv:hep-ph/9710234.

[49] A. Y. Alekseev, V. V. Cheianov, and J. Frohlich, Phys.Rev.Lett. **81**, 3503 (1998), arXiv:cond-mat/9803346.

[50] A. Vilenkin, Phys.Rev. **B25**, 4301 (1982).

[51] P. Buividovich, M. Chernodub, E. Luschevskaya, and M. Polikarpov, Phys.Rev. **D80**, 054503 (2009), arXiv:0907.0494.

[52] M. Abramczyk, T. Blum, G. Petropoulos, and R. Zhou, PoS **LAT2009**, 181 (2009), arXiv:0911.1348.

[53] A. Yamamoto, Phys.Rev.Lett. **107**, 031601 (2011), arXiv:1105.0385.

[54] A. Yamamoto, Phys.Rev. **D84**, 114504 (2011), arXiv:1111.4681.

[55] B. Muller and A. Schafer, Phys.Rev. **C82**, 057902 (2010), arXiv:1009.1053.

[56] L. D. McLerran, E. Mottola, and M. E. Shaposhnikov, Phys.Rev. **D43**, 2027 (1991).

[57] L. Csernai, V. Magas, and D. Wang, (2013), arXiv:1302.5310.

[58] A. M. Polyakov, Nucl.Phys.Proc.Suppl. **68**, 1 (1998), arXiv:hep-th/9711002.

[59] J. M. Maldacena, Adv.Theor.Math.Phys. **2**, 231 (1998), arXiv:hep-th/9711200.

[60] E. Witten, Adv.Theor.Math.Phys. **2**, 253 (1998), arXiv:hep-th/9802150.

[61] S. Gubser, I. R. Klebanov, and A. M. Polyakov, Phys.Lett. **B428**, 105 (1998), arXiv:hep-th/9802109.

[62] O. Aharony, S. S. Gubser, J. M. Maldacena, H. Ooguri, and Y. Oz, Phys.Rept. **323**, 183 (2000), arXiv:hep-th/9905111.

[63] E. D'Hoker and D. Z. Freedman, p. 3 (2002), arXiv:hep-th/0201253.

[64] J. Casalderrey-Solana, H. Liu, D. Mateos, K. Rajagopal, and U. A. Wiedemann, (2011), arXiv:1101.0618.

[65] A. Adams, L. D. Carr, T. Schaefer, P. Steinberg, and J. E. Thomas, New J.Phys. **14**, 115009 (2012), arXiv:1205.5180.

[66] E. T. Akhmedov, Phys.Usp. **44**, 955 (2001).

[67] G. 't Hooft, (1993), arXiv:gr-qc/9310026.

[68] L. Susskind, J.Math.Phys. **36**, 6377 (1995), arXiv:hep-th/9409089.

[69] G. 't Hooft, Nucl.Phys. **B72**, 461 (1974).

[70] S. de Haro, S. N. Solodukhin, and K. Skenderis, Commun.Math.Phys. **217**, 595 (2001), arXiv:hep-th/0002230.

[71] M. Bianchi, D. Z. Freedman, and K. Skenderis, Nucl.Phys. **B631**, 159 (2002), arXiv:hep-th/0112119.

[72] S. A. Hartnoll, Class.Quant.Grav. **26**, 224002 (2009), arXiv:0903.3246.

[73] A. Chamblin, R. Emparan, C. V. Johnson, and R. C. Myers, Phys.Rev. **D60**, 104026 (1999), arXiv:hep-th/9904197.

[74] R. A. Janik and R. B. Peschanski, Phys.Rev. **D73**, 045013 (2006), arXiv:hep-th/0512162.

[75] S. Bhattacharyya, V. E. Hubeny, S. Minwalla, and M. Rangamani, JHEP **0802**, 045 (2008), arXiv:0712.2456.

[76] J. Erdmenger, M. Haack, M. Kaminski, and A. Yarom, JHEP **0901**, 055 (2009), arXiv:0809.2488.

[77] N. Banerjee *et al.*, JHEP **1101**, 094 (2011), arXiv:0809.2596.

[78] M. P. Heller, R. A. Janik, and P. Witaszczyk, (2013), arXiv:1302.0697.

[79] M. Grana and J. Polchinski, Phys.Rev. **D65**, 126005 (2002), arXiv:hep-th/0106014.

[80] M. Bertolini, P. Di Vecchia, M. Frau, A. Lerda, and R. Marotta, Nucl.Phys. **B621**, 157 (2002), arXiv:hep-th/0107057.

[81] A. Karch and E. Katz, JHEP **0206**, 043 (2002), arXiv:hep-th/0205236.

[82] M. Kruczenski, D. Mateos, R. C. Myers, and D. J. Winters, JHEP **0307**, 049 (2003), arXiv:hep-th/0304032.

[83] J. Babington, J. Erdmenger, N. J. Evans, Z. Guralnik, and I. Kirsch, Phys.Rev. **D69**, 066007 (2004), arXiv:hep-th/0306018.

[84] J. Erdmenger, N. Evans, I. Kirsch, and E. Threlfall, Eur.Phys.J. **A35**, 81 (2008), arXiv:0711.4467.

[85] J. Erlich, E. Katz, D. T. Son, and M. A. Stephanov, Phys.Rev.Lett. **95**, 261602 (2005), arXiv:hep-ph/0501128.

[86] L. Da Rold and A. Pomarol, Nucl.Phys. **B721**, 79 (2005), arXiv:hep-ph/0501218.

[87] I. Kirsch, Fortsch.Phys. **52**, 727 (2004), arXiv:hep-th/0406274.

[88] D. Mateos, R. C. Myers, and R. M. Thomson, Phys.Rev.Lett. **97**, 091601 (2006), arXiv:hep-th/0605046.

[89] V. G. Filev, C. V. Johnson, R. Rashkov, and K. Viswanathan, JHEP **0710**, 019 (2007), arXiv:hep-th/0701001.

[90] V. G. Filev, JHEP **0804**, 088 (2008), arXiv:0706.3811.

[91] T. Albash, V. G. Filev, C. V. Johnson, and A. Kundu, JHEP **0807**, 080 (2008), arXiv:0709.1547.

[92] J. Erdmenger, R. Meyer, and J. P. Shock, JHEP **0712**, 091 (2007), arXiv:0709.1551.

[93] A. Gorsky, P. Kopnin, and A. Zayakin, Phys.Rev. **D83**, 014023 (2011), arXiv:1003.2293.

[94] V. G. Filev, C. V. Johnson, and J. P. Shock, JHEP **0908**, 013 (2009), arXiv:0903.5345.

[95] V. G. Filev, JHEP **0911**, 123 (2009), arXiv:0910.0554.

[96] N. Evans, A. Gebauer, K.-Y. Kim, and M. Magou, JHEP **1003**, 132 (2010), arXiv:1002.1885.

[97] N. Evans, A. Gebauer, K.-Y. Kim, and M. Magou, Phys.Lett. **B698**, 91 (2011), arXiv:1003.2694.

[98] K. Ghoroku and M. Yahiro, Phys.Lett. **B604**, 235 (2004), arXiv:hep-th/0408040.

[99] R. Alvares, N. Evans, A. Gebauer, and G. J. Weatherill, Phys.Rev. **D81**, 025013 (2010), arXiv:0910.3073.

[100] C. Hoyos-Badajoz, K. Landsteiner, and S. Montero, JHEP **0704**, 031 (2007), arXiv:hep-th/0612169.

[101] D. Mateos, R. C. Myers, and R. M. Thomson, JHEP **0705**, 067 (2007), arXiv:hep-th/0701132.

[102] K. Peeters, J. Sonnenschein, and M. Zamaklar, Phys.Rev. **D74**, 106008 (2006), arXiv:hep-th/0606195.

[103] K.-Y. Kim, S.-J. Sin, and I. Zahed, JHEP **0804**, 047 (2008), arXiv:0707.0601.

[104] G. Giecold, JHEP **0906**, 002 (2009), arXiv:0904.1874.

[105] J. Grosse, R. A. Janik, and P. Surowka, Phys.Rev. **D77**, 066010 (2008), arXiv:0709.3910.

[106] R. A. Janik, Lect.Notes Phys. **828**, 147 (2011), arXiv:1003.3291.

[107] S. Nakamura and S.-J. Sin, JHEP **0609**, 020 (2006), arXiv:hep-th/0607123.

[108] R. A. Janik, Phys.Rev.Lett. **98**, 022302 (2007), arXiv:hep-th/0610144.

[109] M. P. Heller, P. Surowka, R. Loganayagam, M. Spalinski, and S. E. Vazquez, Phys.Rev.Lett. **102**, 041601 (2009), arXiv:0805.3774.

[110] S. Kinoshita, S. Mukohyama, S. Nakamura, and K.-y. Oda, Prog.Theor.Phys. **121**, 121 (2009), arXiv:0807.3797.

[111] S. Schramm, B. Muller, and A. J. Schramm, Mod.Phys.Lett. **A7**, 973 (1992).

[112] I. Shushpanov and A. V. Smilga, Phys.Lett. **B402**, 351 (1997), arXiv:hep-ph/9703201.

[113] S. Klevansky and R. H. Lemmer, Phys.Rev. **D39**, 3478 (1989).

[114] A. Zayakin, JHEP **0807**, 116 (2008), arXiv:0807.2917.

[115] P. Buividovich, M. Chernodub, E. Luschevskaya, and M. Polikarpov, Phys.Lett. **B682**, 484 (2010), arXiv:0812.1740.

[116] A. J. Mizher, M. Chernodub, and E. S. Fraga, Phys.Rev. **D82**, 105016 (2010), arXiv:1004.2712.

[117] M. D'Elia, S. Mukherjee, and F. Sanfilippo, Phys.Rev. **D82**, 051501 (2010), arXiv:1005.5365.

[118] K. Rajagopal and F. Wilczek, Nucl.Phys. **B399**, 395 (1993), arXiv:hep-ph/9210253.

[119] K.-Y. Kim, S.-J. Sin, and I. Zahed, (2006), arXiv:hep-th/0608046.

[120] K.-Y. Kim, S.-J. Sin, and I. Zahed, JHEP **0801**, 002 (2008), arXiv:0708.1469.

[121] E. S. Fraga and A. J. Mizher, Phys.Rev. **D78**, 025016 (2008), arXiv:0804.1452.

[122] N. Agasian and S. Fedorov, Phys.Lett. **B663**, 445 (2008), arXiv:0803.3156.

[123] G. Beuf, M. P. Heller, R. A. Janik, and R. Peschanski, JHEP **0910**, 043 (2009), arXiv:0906.4423.

[124] P. M. Chesler and L. G. Yaffe, Phys.Rev. **D82**, 026006 (2010), arXiv:0906.4426.

[125] M. P. Heller and R. A. Janik, Phys.Rev. **D76**, 025027 (2007), arXiv:hep-th/0703243.

[126] P. Benincasa, A. Buchel, M. P. Heller, and R. A. Janik, Phys.Rev. **D77**, 046006 (2008), arXiv:0712.2025.

[127] M. P. Heller, PhD Thesis: "Various aspects of non-perturbative dynamics of gauge theory and the AdS/CFT correspondence", 2010.

[128] D. Bak and R. A. Janik, Phys.Lett. **B645**, 303 (2007), arXiv:hep-th/0611304.

[129] M. Torabian and H.-U. Yee, JHEP **0908**, 020 (2009), arXiv:0903.4894.

[130] D. T. Son and P. Surowka, Phys.Rev.Lett. **103**, 191601 (2009), arXiv:0906.5044.

[131] Y. Neiman and Y. Oz, JHEP **1103**, 023 (2011), arXiv:1011.5107.

[132] T. Lappi and L. McLerran, Nucl.Phys. **A772**, 200 (2006), arXiv:hep-ph/0602189.

[133] S. S. Gubser and I. Mitra, (2000), arXiv:hep-th/0009126.

[134] B. Sahoo and H.-U. Yee, JHEP **1011**, 095 (2010), arXiv:1004.3541.

[135] G. Policastro, D. Son, and A. Starinets, Phys.Rev.Lett. **87**, 081601 (2001), arXiv:hep-th/0104066.

[136] A. Buchel and J. T. Liu, Phys.Rev.Lett. **93**, 090602 (2004), arXiv:hep-th/0311175.

[137] P. Kovtun, D. Son, and A. Starinets, Phys.Rev.Lett. **94**, 111601 (2005), arXiv:hep-th/0405231.

[138] D. T. Son and A. O. Starinets, Ann.Rev.Nucl.Part.Sci. **57**, 95 (2007), arXiv:0704.0240.

[139] A. D. Polyanin and V. F. Zaitsev, Chapman & Hall/CRC Press, Boca Raton, 2003. ISBN 1-58488-297-2. .

[140] A. Sadofyev and M. Isachenkov, Phys.Lett. **B697**, 404 (2011), arXiv:1010.1550.

[141] S. Pu, J.-h. Gao, and Q. Wang, Phys.Rev. **D83**, 094017 (2011), arXiv:1008.2418.

[142] A. Sadofyev, V. Shevchenko, and V. Zakharov, Phys.Rev. **D83**, 105025 (2011), arXiv:1012.1958.

[143] V. I. Zakharov, (2012), arXiv:1210.2186.

[144] G. Lifschytz and M. Lippert, Phys.Rev. **D80**, 066005 (2009), arXiv:0904.4772.

[145] H.-U. Yee, JHEP **0911**, 085 (2009), arXiv:0908.4189.

[146] V. Rubakov, (2010), arXiv:1005.1888.

[147] A. Gynther, K. Landsteiner, F. Pena-Benitez, and A. Rebhan, JHEP **1102**, 110 (2011), arXiv:1005.2587.

[148] A. Rebhan, A. Schmitt, and S. A. Stricker, JHEP **1001**, 026 (2010), arXiv:0909.4782.

[149] L. Brits and J. Charbonneau, Phys.Rev. **D83**, 126013 (2011), arXiv:1009.4230.

[150] I. Amado, K. Landsteiner, and F. Pena-Benitez, JHEP **1105**, 081 (2011), arXiv:1102.4577.

[151] C. Hoyos, T. Nishioka, and A. O'Bannon, JHEP **1110**, 084 (2011), arXiv:1106.4030.

[152] J. Bhattacharya, S. Bhattacharyya, S. Minwalla, and A. Yarom, (2011), arXiv:1105.3733.

[153] Y.-P. Hu, P. Sun, and J.-H. Zhang, Phys.Rev. **D83**, 126003 (2011), arXiv:1103.3773.

[154] Y.-P. Hu and C. Park, Phys.Lett. **B714**, 324 (2012), arXiv:1112.4227.

[155] K. Behrndt, M. Cvetic, and W. Sabra, Nucl.Phys. **B553**, 317 (1999), arXiv:hep-th/9810227.

[156] M. Lublinsky and I. Zahed, Phys.Lett. **B684**, 119 (2010), arXiv:0910.1373.

[157] D. E. Kharzeev and D. T. Son, Phys.Rev.Lett. **106**, 062301 (2011), arXiv:1010.0038.

[158] D. E. Kharzeev and H.-U. Yee, Phys.Rev. **D83**, 085007 (2011), arXiv:1012.6026.

[159] D. Son and A. R. Zhitnitsky, Phys.Rev. **D70**, 074018 (2004), arXiv:hep-ph/0405216.

[160] M. A. Metlitski and A. R. Zhitnitsky, Phys.Rev. **D72**, 045011 (2005), arXiv:hep-ph/0505072.

[161] Q. Wang, PhD Thesis: "Charge Multiplicity Asymmetry Correlation Study Searching for Local Parity Violation at RHIC for STAR", 2012, arXiv:1205.4638.

[162] P. Huovinen and P. Petreczky, Nucl.Phys. **A837**, 26 (2010), arXiv:0912.2541.

[163] R. Ryblewski and W. Florkowski, Phys.Rev. **C77**, 064906 (2008), arXiv:0804.2427.

[164] W. Florkowski, Phys.Lett. **B668**, 32 (2008), arXiv:0806.2268.

[165] R. Ryblewski and W. Florkowski, Eur.Phys.J. **C71**, 1761 (2011), arXiv:1103.1260.

[166] P. F. Kolb, J. Sollfrank, and U. W. Heinz, Phys.Rev. **C62**, 054909 (2000), arXiv:hep-ph/0006129.

[167] M. Chernicoff, D. Fernandez, D. Mateos, and D. Trancanelli, JHEP **1208**, 100 (2012), arXiv:1202.3696.

[168] D. Mateos and D. Trancanelli, Phys.Rev.Lett. **107**, 101601 (2011), arXiv:1105.3472.

[169] D. Mateos and D. Trancanelli, JHEP **1107**, 054 (2011), arXiv:1106.1637.

[170] J. Erdmenger, P. Kerner, and H. Zeller, JHEP **1201**, 059 (2012), arXiv:1110.0007.

[171] R. A. Janik and P. Witaszczyk, JHEP **0809**, 026 (2008), arXiv:0806.2141.

[172] A. Rebhan and D. Steineder, JHEP **1108**, 153 (2011), arXiv:1106.3539.

[173] A. Rebhan and D. Steineder, Phys.Rev.Lett. **108**, 021601 (2012), arXiv:1110.6825.

[174] D. Giataganas, JHEP **1207**, 031 (2012), arXiv:1202.4436.

[175] K. Landsteiner, E. Megias, and F. Pena-Benitez, Phys.Rev.Lett. **107**, 021601 (2011), arXiv:1103.5006.

[176] A. Andronic, P. Braun-Munzinger, and J. Stachel, Nucl.Phys. **A772**, 167 (2006), arXiv:nucl-th/0511071.

[177] A. Bzdak, V. Koch, and J. Liao, (2012), arXiv:1207.7327.

[178] S. Kirkpatrick, C. Gelatt, and M. Vecchi, Science **220**, 671 (1983).

[179] V. Cerny, (1982).

[180] T. DeGrand and C. E. Detar, *Lattice methods for quantum chromodynamics* (New Jersey, USA: World Scientific, 2006).

[181] G. P. Lepage, (1996), arXiv:hep-lat/9607076.

[182] G. Curci, P. Menotti, and G. Paffuti, Phys.Lett. **B130**, 205 (1983).

[183] M. Luscher and P. Weisz, Commun.Math.Phys. **97**, 59 (1985).

[184] M. G. Alford, W. Dimm, G. Lepage, G. Hockney, and P. Mackenzie, Phys.Lett. **B361**, 87 (1995), arXiv:hep-lat/9507010.

[185] C. Gattringer, R. Hoffmann, and S. Schaefer, Phys.Rev. **D65**, 094503 (2002), arXiv:hep-lat/0112024.

[186] M. Luscher and P. Weisz, Phys.Lett. **B158**, 250 (1985).

[187] N. Cabibbo and E. Marinari, Phys.Lett. **B119**, 387 (1982).

[188] M. Creutz, *Quarks, gluons and lattices* (Cambridge, Uk: Univ. Pr., 1984).

[189] S. L. Adler, Phys.Rev. **D23**, 2901 (1981).

[190] M. Creutz, Phys.Rev. **D36**, 515 (1987).

[191] K. M. Decker and P. de Forcrand, Nucl.Phys.Proc.Suppl. **17**, 567 (1990).

[192] N. Metropolis, A. Rosenbluth, M. Rosenbluth, A. Teller, and E. Teller, J.Chem.Phys. **21**, 1087 (1953).

[193] P. de Forcrand and O. Jahn, p. 67 (2005), arXiv:hep-lat/0503041.

[194] K. Wilson, Subnucl.Ser. **13**, 13 (1977).

[195] H. B. Nielsen and M. Ninomiya, Phys.Lett. **B105**, 219 (1981).

[196] M. Luscher, Phys.Lett. **B428**, 342 (1998), arXiv:hep-lat/9802011.

[197] P. H. Ginsparg and K. G. Wilson, Phys.Rev. **D25**, 2649 (1982).

[198] H. Neuberger, Phys.Lett. **B417**, 141 (1998), arXiv:hep-lat/9707022.

[199] P. Hernandez, K. Jansen, and M. Luscher, Nucl.Phys. **B552**, 363 (1999), arXiv:hep-lat/9808010.

[200] J. van den Eshof, A. Frommer, T. Lippert, K. Schilling, and H. van der Vorst, Comput.Phys.Commun. **146**, 203 (2002), arXiv:hep-lat/0202025.

[201] e. Frommer, A., e. Lippert, T., e. Medeke, B., and e. Schilling, K., (2000).

[202] L. Giusti, C. Hoelbling, M. Luscher, and H. Wittig, Comput.Phys.Commun. **153**, 31 (2003), arXiv:hep-lat/0212012.

[203] http://www.caam.rice.edu/software/ARPACK/ .

[204] J. C. Bloch, A. Frommer, B. Lang, and T. Wettig, Comput.Phys.Commun. **177**, 933 (2007), arXiv:0704.3486.

[205] J. C. Bloch, T. Wettig, A. Frommer, and B. Lang, PoS **LAT2007**, 169 (2007), arXiv:0710.0341.

[206] B. Ioffe and A. V. Smilga, Nucl.Phys. **B232**, 109 (1984).

[207] B. Pire and L. Szymanowski, Phys.Rev.Lett. **103**, 072002 (2009), arXiv:0905.1258.

[208] V. Braun, S. Gottwald, D. Y. Ivanov, A. Schafer, and L. Szymanowski, Phys.Rev.Lett. **89**, 172001 (2002), arXiv:hep-ph/0206305.

[209] P. Buividovich, M. Chernodub, E. Luschevskaya, and M. Polikarpov, Phys.Rev. **D81**, 036007 (2010), arXiv:0909.2350.

[210] T. Vachaspati, Phys.Lett. **B265**, 258 (1991).

[211] R. C. Duncan and C. Thompson, Astrophys.J. **392**, L9 (1992).

[212] T. A. DeGrand and A. Hasenfratz, Phys.Rev. **D64**, 034512 (2001), arXiv:hep-lat/0012021.

[213] M. Al-Hashimi and U.-J. Wiese, Annals Phys. **324**, 343 (2009), arXiv:0807.0630.

[214] I. A. Shovkovy, (2012), arXiv:1207.5081.

[215] V. Gusynin, V. Miransky, and I. Shovkovy, Nucl.Phys. **B462**, 249 (1996), arXiv:hep-ph/9509320.

[216] G. Bali *et al.*, JHEP **1202**, 044 (2012), arXiv:1111.4956.

[217] G. Bali *et al.*, Phys.Rev. **D86**, 071502 (2012), arXiv:1206.4205.

[218] M. D'Elia, S. Mukherjee, and F. Sanfilippo, Phys.Rev. **D82**, 051501 (2010), arXiv:1005.5365.

[219] M. D'Elia and F. Negro, Phys.Rev. **D83**, 114028 (2011), arXiv:1103.2080.

[220] E.-M. Ilgenfritz, M. Kalinowski, M. Muller-Preussker, B. Petersson, and A. Schreiber, Phys.Rev. **D85**, 114504 (2012), arXiv:1203.3360.

[221] T. Banks and A. Casher, Nucl.Phys. **B169**, 103 (1980).

[222] P. Colangelo and A. Khodjamirian, (2000), arXiv:hep-ph/0010175.

[223] P. Ball, V. Braun, and N. Kivel, Nucl.Phys. **B649**, 263 (2003), arXiv:hep-ph/0207307.

[224] J. Rohrwild, JHEP **0709**, 073 (2007), arXiv:0708.1405.

[225] V. Belyaev and Y. Kogan, Yad.Fiz. **40**, 1035 (1984).

[226] I. Balitsky, A. Kolesnichenko, and A. Yung, Sov.J.Nucl.Phys. **41**, 178 (1985).

[227] V. Y. Petrov, M. V. Polyakov, R. Ruskov, C. Weiss, and K. Goeke, Phys.Rev. **D59**, 114018 (1999), arXiv:hep-ph/9807229.

[228] H.-C. Kim, M. Musakhanov, and M. Siddikov, Phys.Lett. **B608**, 95 (2005), arXiv:hep-ph/0411181.

[229] A. Dorokhov, Eur.Phys.J. **C42**, 309 (2005), arXiv:hep-ph/0505007.

[230] B. Ioffe, Phys.Lett. **B678**, 512 (2009), arXiv:0906.0283.

[231] M. Frasca and M. Ruggieri, Phys.Rev. **D83**, 094024 (2011), arXiv:1103.1194.

[232] G. Bali *et al.*, Phys.Rev. **D86**, 094512 (2012), arXiv:1209.6015.

[233] A. Vainshtein, Phys.Lett. **B569**, 187 (2003), arXiv:hep-ph/0212231.

[234] A. Gorsky and A. Krikun, Phys.Rev. **D79**, 086015 (2009), arXiv:0902.1832.

[235] D. T. Son and N. Yamamoto, (2010), arXiv:1010.0718.

[236] S.-i. Nam, Phys.Rev. **D80**, 114025 (2009), arXiv:0911.0509.

[237] K. Fukushima, D. E. Kharzeev, and H. J. Warringa, Nucl.Phys. **A836**, 311 (2010), arXiv:0912.2961.

[238] D. E. Kharzeev and H. J. Warringa, Phys.Rev. **D80**, 034028 (2009), arXiv:0907.5007.

[239] L. Kadanoff and P. Martin, Ann. Phys. **24**, 419 (1963).

[240] G. Aarts, C. Allton, J. Foley, S. Hands, and S. Kim, Phys.Rev.Lett. **99**, 022002 (2007), arXiv:hep-lat/0703008.

[241] R. Babich *et al.*, PoS **LAT2005**, 043 (2006), arXiv:hep-lat/0509182.

[242] P. Hasenfratz, S. Hauswirth, T. Jorg, F. Niedermayer, and K. Holland, Nucl.Phys. **B643**, 280 (2002), arXiv:hep-lat/0205010.

[243] V. Bornyakov *et al.*, Phys.Rev. **D79**, 054505 (2009), arXiv:0807.1980.

[244] S. Gupta, Phys.Lett. **B597**, 57 (2004), arXiv:hep-lat/0301006.

[245] M. Asakawa, T. Hatsuda, and Y. Nakahara, Prog.Part.Nucl.Phys. **46**, 459 (2001), arXiv:hep-lat/0011040.

[246] A. Borici and A. Allkoci, PoS **LAT2005**, 101 (2006), arXiv:hep-lat/0601031.

[247] A. Borici and A. Allkoci, (2006), arXiv:hep-lat/0602015.

[248] V. Bornyakov *et al.*, Phys.Rev. **D76**, 054505 (2007), arXiv:0706.4206.

[249] P. Buividovich, E. Luschevskaya, and M. Polikarpov, Phys.Rev. **D78**, 074505 (2008), arXiv:0809.3075.

[250] M. Chernodub, Phys.Rev. **D82**, 085011 (2010), arXiv:1008.1055.

[251] M. Chernodub, Phys.Rev.Lett. **106**, 142003 (2011), arXiv:1101.0117.

[252] M. Chernodub, J. Van Doorsselaere, and H. Verschelde, Phys.Rev. **D85**, 045002 (2012), arXiv:1111.4401.

[253] G. Jonker and J. van Santen, Physica **16**, 337 (1950).

[254] L. D. McLerran and T. Toimela, Phys.Rev. **D31**, 545 (1985).

[255] E. Bratkovskaya, O. Teryaev, and V. Toneev, Phys.Lett. **B348**, 283 (1995).

[256] P. Buividovich and M. Polikarpov, Phys.Rev. **D83**, 094508 (2011), arXiv:1011.3001.

[257] D. E. Kharzeev and H.-U. Yee, Phys.Rev. **D84**, 045025 (2011), arXiv:1105.6360.

[258] Y. Neiman and Y. Oz, JHEP **1109**, 011 (2011), arXiv:1106.3576.

[259] V. Zakharov, (2006), arXiv:hep-ph/0602141.

[260] V. Zakharov, (2006), arXiv:hep-ph/0612341.

[261] P. de Forcrand, AIP Conf.Proc. **892**, 29 (2007), arXiv:hep-lat/0611034.

[262] G. 't Hooft, Phys.Rev. **D14**, 3432 (1976).

[263] MILC Collaboration, C. Aubin *et al.*, Nucl.Phys.Proc.Suppl. **140**, 626 (2005), arXiv:hep-lat/0410024.

[264] C. Bernard *et al.*, PoS **LAT2005**, 299 (2006), arXiv:hep-lat/0510025.

[265] F. Gubarev, S. Morozov, M. Polikarpov, and V. Zakharov, (2005), arXiv:hep-lat/0505016.

[266] E.-M. Ilgenfritz *et al.*, Phys.Rev. **D76**, 034506 (2007), arXiv:0705.0018.

[267] E.-M. Ilgenfritz, K. Koller, Y. Koma, G. Schierholz, and V. Weinberg, (2009), arXiv:0912.2281.

[268] I. Horvath *et al.*, Phys.Rev. **D67**, 011501 (2003), arXiv:hep-lat/0203027.

[269] P. Hasenfratz, V. Laliena, and F. Niedermayer, Phys.Lett. **B427**, 125 (1998), arXiv:hep-lat/9801021.

[270] E.-M. Ilgenfritz *et al.*, Phys.Rev. **D77**, 074502 (2008), arXiv:0801.1725.

[271] T. A. DeGrand, A. Hasenfratz, and T. G. Kovacs, Nucl.Phys. **B520**, 301 (1998), arXiv:hep-lat/9711032.

[272] F. Bruckmann, F. Gruber, N. Cundy, A. Schafer, and T. Lippert, Phys.Lett. **B707**, 278 (2012), arXiv:1107.0897.

[273] A. Kovalenko, S. Morozov, M. Polikarpov, and V. Zakharov, Phys.Lett. **B648**, 383 (2007), arXiv:hep-lat/0512036.

[274] I. Horvath *et al.*, p. 312 (2002), arXiv:hep-lat/0212013.

[275] A. Alexandru, I. Horvath, and J.-b. Zhang, Phys.Rev. **D72**, 034506 (2005), arXiv:hep-lat/0506018.

[276] I. Horvath *et al.*, Phys.Rev. **D68**, 114505 (2003), arXiv:hep-lat/0302009.

[277] I. Horvath *et al.*, Nucl.Phys.Proc.Suppl. **129**, 677 (2004), arXiv:hep-lat/0308029.

[278] I. Horvath, Nucl.Phys. **B710**, 464 (2005), arXiv:hep-lat/0410046.

[279] I. Horvath *et al.*, Phys.Lett. **B612**, 21 (2005), arXiv:hep-lat/0501025.

[280] D. B. Leinweber, (1999), arXiv:hep-lat/0004025.

[281] J. Zhang *et al.*, Phys.Rev. **D65**, 074510 (2002), arXiv:hep-lat/0111060.

[282] F. Bruckmann *et al.*, Eur.Phys.J. **A33**, 333 (2007), arXiv:hep-lat/0612024.

[283] M. Garcia Perez, A. Gonzalez-Arroyo, and A. Sastre, JHEP **1107**, 034 (2011), arXiv:1103.5999.

[284] C. Gattringer, M. Gockeler, P. E. Rakow, S. Schaefer, and A. Schafer, Nucl.Phys. **B617**, 101 (2001), arXiv:hep-lat/0107016.

[285] T. A. DeGrand, Phys.Rev. **D64**, 094508 (2001), arXiv:hep-lat/0106001.

[286] M. Polikarpov and A. Veselov, Nucl.Phys. **B297**, 34 (1988).

[287] V. Zakharov, Phys.Atom.Nucl. **68**, 573 (2005), arXiv:hep-ph/0410034.

[288] A. Kovalenko, M. Polikarpov, S. Syritsyn, and V. Zakharov, Phys.Lett. **B613**, 52 (2005), arXiv:hep-lat/0408014.

[289] M. Polikarpov, S. Syritsyn, and V. Zakharov, JETP Lett. **81**, 143 (2005), arXiv:hep-lat/0402018.

[290] A. R. Zhitnitsky, (2013), 1301.7072.

[291] M. Chernodub, H. Verschelde, and V. Zakharov, Nucl.Phys.Proc.Suppl. **207-208**, 325 (2010), arXiv:0905.2520.

[292] PHENIX Collaboration, A. Adare *et al.*, Phys.Rev.Lett. **104**, 132301 (2010), arXiv:0804.4168.

[293] D. Teaney, J. Lauret, and E. Shuryak, (2001), arXiv:nucl-th/0110037.

[294] E. Shuryak, Prog.Part.Nucl.Phys. **62**, 48 (2009), arXiv:0807.3033.

[295] J. Liao and E. Shuryak, Phys.Rev.Lett. **101**, 162302 (2008), arXiv:0804.0255.

[296] M. Chernodub and V. Zakharov, Phys.Rev.Lett. **98**, 082002 (2007), arXiv:hep-ph/0611228.

[297] M. Chernodub and V. Zakharov, Phys.Atom.Nucl. **72**, 2136 (2009), arXiv:0806.2874.

[298] R. G. Edwards, U. M. Heller, J. E. Kiskis, and R. Narayanan, Phys.Rev. **D61**, 074504 (2000), arXiv:hep-lat/9910041.

[299] D. Son, Int.J.Mod.Phys. **A16S1C**, 1284 (2001), arXiv:hep-ph/0011246.

[300] C. Herzog, P. Kovtun, and D. Son, Phys.Rev. **D79**, 066002 (2009), arXiv:0809.4870.

[301] L. Landau, J. Phys. USSR **5**, 71 (1941).

[302] M. Luscher, Phys.Lett. **B78**, 465 (1978).

[303] H. Reinhardt, O. Schroeder, T. Tok, and V. Zhukovsky, Phys.Rev. **D66**, 085004 (2002), arXiv:hep-th/0203012.

[304] R. Hollwieser, M. Faber, J. Greensite, U. M. Heller, and S. Olejnik, Phys.Rev. **D78**, 054508 (2008), arXiv:0805.1846.

[305] J. Gattnar *et al.*, Nucl.Phys. **B716**, 105 (2005), arXiv:hep-lat/0412032.

[306] V. Bornyakov *et al.*, Phys.Rev. **D77**, 074507 (2008), arXiv:0708.3335.

[307] G. Tiktopoulos, Phys.Rev. **D35**, 732 (1987).

[308] V. Zhukovsky and O. Tarasov, Phys.Atom.Nucl. **67**, 2260 (2004).

[309] J. Greensite, Prog.Part.Nucl.Phys. **51**, 1 (2003), arXiv:hep-lat/0301023.

[310] M. Engelhardt, K. Langfeld, H. Reinhardt, and O. Tennert, Phys.Rev. **D61**, 054504 (2000), arXiv:hep-lat/9904004.

[311] A. M. Polyakov, *Gauge fields and strings* (Heidelberg: Springer-Verlag, 1987).

[312] M. Stone and P. R. Thomas, Phys.Rev.Lett. **41**, 351 (1978).

[313] S. Samuel, Nucl.Phys. **B154**, 62 (1979).

[314] M. Chernodub, H. Verschelde, and V. Zakharov, Theor.Math.Phys. **170**, 211 (2012), arXiv:1007.1879.

[315] M. Engelhardt, Nucl.Phys. **B585**, 614 (2000), arXiv:hep-lat/0004013.

[316] M. Engelhardt and H. Reinhardt, Nucl.Phys. **B567**, 249 (2000), arXiv:hep-th/9907139.

[317] H. Verschelde and V. Zakharov, (2011), arXiv:1106.4154.

[318] H. Verschelde and V. I. Zakharov, PoS **FACESQCD**, 006 (2010), arXiv:1107.1393.

[319] H. Verschelde and V. Zakharov, AIP Conf.Proc. **1343**, 137 (2011), arXiv:1012.4821.

[320] H. Leutwyler and A. V. Smilga, Phys.Rev. **D46**, 5607 (1992).

[321] P. Buividovich, M. Chernodub, E. Luschevskaya, and M. Polikarpov, Nucl.Phys. **B826**, 313 (2010), arXiv:0906.0488.

[322] A. A. Andrianov and L. Bonora, Nucl.Phys. **B233**, 232 (1984).

[323] K. Fujikawa, Phys.Rev.Lett. **42**, 1195 (1979).

[324] K. Fujikawa, Phys.Rev. **D21**, 2848 (1980).

[325] E. Rabinovici and M. Smolkin, JHEP **1107**, 040 (2011), arXiv:1102.5035.

[326] A. M. Polyakov, Phys.Lett. **B103**, 207 (1981).

[327] F. Wilczek, Phys.Rev.Lett. **58**, 1799 (1987).

[328] R. Peccei and H. R. Quinn, Phys.Rev.Lett. **38**, 1440 (1977).

[329] E. Witten, Nucl.Phys. **B156**, 269 (1979).

[330] O. Wantz and E. Shellard, Phys.Rev. **D82**, 123508 (2010), arXiv:0910.1066.

[331] B. Alles, M. D'Elia, and A. Di Giacomo, Nucl.Phys. **B494**, 281 (1997), arXiv:hep-lat/9605013.

[332] P. Hegde, PoS **LATTICE2011**, 014 (2011), arXiv:1112.0364.

[333] HotQCD Collaboration, A. Bazavov *et al.*, Phys.Rev. **D86**, 094503 (2012), arXiv:1205.3535.

[334] A. Gocksch, Phys.Rev.Lett. **67**, 1701 (1991).

[335] J. I. Kapusta, D. Kharzeev, and L. D. McLerran, Phys.Rev. **D53**, 5028 (1996), arXiv:hep-ph/9507343.

[336] E. V. Shuryak and I. Zahed, Phys.Rev. **C70**, 021901 (2004), arXiv:hep-ph/0307267.

[337] E. V. Shuryak and I. Zahed, Phys.Rev. **D70**, 054507 (2004), arXiv:hep-ph/0403127.

[338] WHOT-QCD Collaboration, Y. Maezawa *et al.*, Phys.Rev. **D75**, 074501 (2007), arXiv:hep-lat/0702004.

[339] V. Zakharov, (2002), arXiv:hep-ph/0202040.

[340] E. V. Shuryak, p. 210 (1999), arXiv:hep-ph/9911244.

[341] J. Callan, Curtis G. and J. A. Harvey, Nucl.Phys. **B250**, 427 (1985).

[342] V. Kirilin, A. Sadofyev, and V. Zakharov, Phys.Rev. **D86**, 025021 (2012), arXiv:1203.6312.

[343] S. Ozonder, Phys.Rev. **C81**, 062201 (2010), arXiv:1004.3883.

[344] P. Sikivie, Phys.Lett. **B137**, 353 (1984).

[345] A. Andrianov, V. Andrianov, D. Espriu, and X. Planells, Phys.Lett. **B710**, 230 (2012), arXiv:1201.3485.

[346] D. Kharzeev, A. Krasnitz, and R. Venugopalan, Phys.Lett. **B545**, 298 (2002), arXiv:hep-ph/0109253.

[347] S. Ahmad, J. T. Lenaghan, and H. Thacker, Phys.Rev. **D72**, 114511 (2005), arXiv:hep-lat/0509066.

[348] H. Thacker, PoS **LAT2006**, 025 (2006), arXiv:hep-lat/0610049.

[349] S. A. Voloshin, Phys.Rev. **C70**, 057901 (2004), arXiv:hep-ph/0406311.

[350] A. Bzdak, V. Koch, and J. Liao, Phys.Rev. **C81**, 031901 (2010), arXiv:0912.5050.

[351] ALICE Collaboration, K. Aamodt *et al.*, Phys.Lett. **B696**, 328 (2011), arXiv:1012.4035.

[352] PHOBOS Collaboration, R. Hollis *et al.*, Rom.Rep.Phys. **58**, 37 (2006).

[353] PHOBOS Collaboration, B. Back *et al.*, Phys.Rev. **C70**, 021902 (2004), arXiv:nucl-ex/0405027.

[354] HotQCD Collaboration, A. Bazavov *et al.*, Phys.Rev. **D86**, 034509 (2012), arXiv:1203.0784.

[355] N. Nielsen and P. Olesen, Nucl.Phys. **B144**, 376 (1978).

[356] N. Nielsen and P. Olesen, Phys.Lett. **B79**, 304 (1978).

[357] H. B. Nielsen and P. Olesen, Nucl.Phys. **B160**, 380 (1979).

[358] J. Ambjorn and P. Olesen, Nucl.Phys. **B170**, 60 (1980).

[359] J. Ambjorn and P. Olesen, Nucl.Phys. **B170**, 265 (1980).

[360] G. Savvidy, Phys.Lett. **B71**, 133 (1977).

[361] A. Abrikosov, Sov.Phys.JETP **5**, 1174 (1957).

[362] W. H. Kleiner, L. M. Roth, and S. H. Autler, Phys.Rev. **A133**, 1226 (1964).

[363] M. Chernodub, J. Van Doorsselaere, and H. Verschelde, (2012), arXiv:1203.5963.

[364] Y.-Y. Bu, J. Erdmenger, J. P. Shock, and M. Strydom, JHEP (2012), arXiv:1210.6669.

[365] J. Ambjorn and P. Olesen, Nucl.Phys. **B315**, 606 (1989).

[366] J. Ambjorn and P. Olesen, Phys.Lett. **B218**, 67 (1989).

[367] J. Ambjorn and P. Olesen, Int.J.Mod.Phys. **A5**, 4525 (1990).

[368] L. Del Debbio, M. Faber, J. Greensite, and S. Olejnik, Phys.Rev. **D55**, 2298 (1997), arXiv:hep-lat/9610005.

[369] L. Del Debbio, M. Faber, J. Giedt, J. Greensite, and S. Olejnik, Phys.Rev. **D58**, 094501 (1998), arXiv:hep-lat/9801027.

[370] V. Bornyakov, P. Y. Boyko, M. Polikarpov, and V. Zakharov, Nucl.Phys. **B672**, 222 (2003), arXiv:hep-lat/0305021.

[371] A. Belavin, A. M. Polyakov, A. Schwartz, and Y. Tyupkin, Phys.Lett. **B59**, 85 (1975).

[372] R. Anderson, H. Bilger, and G. E. Stedman, Am.J.Phys. **62**, 975 (1994).

[373] R. Becker, F. Sauter, and C. Heller, Z. Phys. **85**, 772 (1933).

[374] S. Barnett, Phys.Rev. **4**, No. 4 (1915).

[375] E. D'Hoker and P. Kraus, JHEP **0910**, 088 (2009), arXiv:0908.3875.

[376] F. Bruckmann, G. Endrodi, and T. Kovacs, (2013), arXiv:1303.3972.

[377] A. S. Gorsky, V. I. Zakharov, and A. R. Zhitnitsky, Phys.Rev. **D79**, 106003 (2009), arXiv:0902.1842.

[378] J. M. Cornwall, Mod.Phys.Lett. **A27**, 1230011 (2012), arXiv:1203.6618.

[379] G. Basar and D. E. Kharzeev, Phys.Rev. **D85**, 086012 (2012), arXiv:1202.2161.

[380] C. Allton, M. Teper, and A. Trivini, JHEP **0807**, 021 (2008), arXiv:0803.1092.

[381] M. Teper, PoS **LATTICE2008**, 022 (2008), arXiv:0812.0085.

[382] M. Panero, Phys.Rev.Lett. **103**, 232001 (2009), arXiv:0907.3719.